Functional characterisation of multiple sclerosis-associated genetic variant



Adam Patrick Gregory

St. Catherine's College, University of Oxford

Thesis submitted for the degree of Doctor of Philosophy

Trinity term, 2012

Functional characterisation of a multiple sclerosis-associated genetic variant

Adam P. Gregory, St. Catherine's College, University of Oxford

Thesis submitted for the degree of Doctor of Philosophy

Trinity term, 2012

Abstract

In recent years, Genome-wide association studies (GWAS) have identified several susceptibility-modifying genetic variants to complex diseases such as multiple sclerosis (MS). An association for one such single nucleotide polymorphism (SNP) in the gene encoding the principle receptor for the cytokine TNF (TNFR1), *TNFRSF1A*, has been replicated several times since its initial identification by De Jager *et al.*, 2009. This study demonstrates that the MS risk-associated G allele of this SNP, rs1800693, results in an alternative splicing event in which exon 6 is excluded from the mature *TNFRSF1A* transcript both in an *in vitro* splicing assay and *ex vivo* in several human immune cell types, and investigates the potential for creating an antisense-based mouse model for the effect of this SNP. Importantly, we show that the transcript lacking exon 6 is translated into protein, designated Δ6TNFR1, which can be detected in primary samples. Δ6TNFR1 is truncated in several important domains of the full-length receptor and is demonstrated to be unable to traffick to and anchor at the cell membrane, instead being constitutively secreted. Moreover, in contrast with the full-length receptor, the MS-associated splice isoform is unable to oligomerise either homotypically or with full-length receptors, or to engage the NF-κB-mediated or apoptosis signalling pathways *in vitro*. Δ6TNFR1 does, however, retain the ability to bind and neutralise TNF, albeit to a lesser extent than the full-length protein. This is striking in light of the results of clinical trials for the use of TNF antagonists in MS patients, in which neutralisation of TNF was associated with relapses and exacerbation of symptoms, and rare MS symptom-like side-effects in patients being treated with anti-TNF agents for the management of other inflammatory autoimmune diseases. In conclusion, this work provides a functional explanation for the association of an MS-risk SNP with the disease and provides support for a detrimental effect of broad-spectrum TNF inhibition in MS. Moreover, it reveals a novel use for GWAS; to inform clinical practice.

Acknowledgments

I would like to thank Professor Lars Fugger for the opportunity to work on such a fascinating project, for the freedom he has given me to think and work, and for his trust and generosity in making available the resources for this research.

Thank you to Professor Lars Fugger, Dr. Kate Attfield, Dr. Calliope Dendrou, Dr. Ruth Etzensperger, Dr. Gurman Kaur, Dr. Marco Baralle and Professor Finn Nielsen for giving up so much of their time to discuss ideas and data with me, and for considering even my most elementary questions with the utmost respect and patience. I would particularly like to thank Dr. Kate Attfield for her help in shaping my research and preparing this thesis, and Dr. Calliope Dendrou for her infectious enthusiasm, brilliant ideas and help in performing experiments.

It has been a real pleasure to work as part of the Fugger lab. They are a group of truly lovely people and wonderfully talented scientists. I could not have asked for a better environment, both in a professional and social sense, to carry-out my DPhil studies. In particular I would like to thank Sebastian and Karla for their friendship, and for making me want to stay in Oxford and the lab.

And thank you to Zoe, for putting up with me and giving me a reason to leave.

For my mother and father without whose love and support, in every sense, I would never have been able to complete this work.

And for my grandfathers, neither of whom are alive to read the end product of what they both, by their inspiration and encouragement, helped me to achieve.

Contents

Abstract	i
Acknowledgments	ii
Contents	iii
List of tables and figures	viii
List of abbreviations	xi
1.0 Introduction	1
1.1 Multiple sclerosis	1
1.1.1 Clinical course	1
1.1.2 Pathogenesis	2
1.1.2.1 Overview	2
1.1.2.2 The role of the adaptive immune system in MS	4
1.1.2.2.1 T cells	4
1.1.2.2.2 B cells	7
1.1.2.3 The role of the innate immune system in MS	8
1.1.3 Current treatments	9
1.1.4 The immune cell repertoire	11
1.1.4.1 Central tolerance	11
1.1.4.2 Peripheral tolerance	12
1.1.5 Initiation and propagation of autoimmunity	14
1.1.5.1 T cell degeneracy and molecular mimicry	14
1.1.5.2 Bystander activation	15
1.1.5.3 Exposure of cryptic epitopes	16
1.1.5.4 Epitope spreading	16
1.1.6 MS aetiology	17
1.1.6.1 Environmental factors	17
1.1.6.2 Genetics	19
1.1.6.2.1 MHC region	19
1.1.6.2.2 Non-MHC associations	20
1.2 SNPs and disease	23
1.3 Splicing	23
1.3.1 Alternative splicing	24
1.3.2 Alternative splicing in disease	26
1.4 Tumour Necrosis Factor (TNF) and its receptors	27
1.4.1 TNFR1	28
1.4.1.1 Structure and characteristics	28
1.4.1.2 Signalling	29
1.4.2 TNF and MS	33
1.5 Thesis aims	34
1.6 Hypothesis	35
2.0 General methods	36
2.1 Cloning	36

2.1.1 Overview 36
2.1.2 Vectors 37
2.1.3 DNA digestion by restriction enzymes 40
2.1.4 Ligation of vector and insert 41
2.1.5 Transformation of chemically competent bacteria 41
2.1.6 Preparation of LB Agar and LB Broth 42
2.1.7 Vector/construct propagation 44
2.1.7.1 Qiaprep Miniprep Kit 44
2.1.7.2 Qiagen HiSpeed Plasmid Midi Kit 45
2.1.8 DNA sequencing and analysis 45
2.1.9 Glycerol stocks of transformed bacteria 46
2.2 Molecular biological methods 46
2.2.1 Polymerase chain reaction 46
2.2.2 Overlap extension PCR 48
2.2.3 RNA extraction 48
2.2.4 Reverse transcription/cDNA synthesis 49
2.2.5 Quantitative Real-Time PCR (qRT-PCR) 49
2.2.6 Separation of DNA by electrophoresis 50
2.2.6.1 TBE agarose 50
2.2.6.2 TBE polyacrylamide 51
2.2.7 DNA purification 51
2.2.7.1 Qiagen MinElute PCR Purification Kit 52
2.2.7.2 Qiagen MinElute Gel Extraction Kit 52
2.2.8 Sodium Dioecyl Sulphate Polyacrylamide Gel Electrophoresis (SDS-PAGE) 53
2.2.9 Visualisation of resolved proteins 54
2.2.10 Quantification of proteins 54
2.2.11 Western blot 55
2.2.12 Enzyme-Linked Immunosorbent Assay (ELISA) 55
2.3 Cell biology 56
2.3.1 Mammalian cell culture 56
2.3.2 Thawing, counting, subculturing and freezing of cells 57
2.3.3 Transient transfection 58
2.3.4 Flow cytometry 59
2.3.5 Human blood sample work 60
2.3.5.1 Recruitment of donors and ethical approval 60
2.3.5.2 Isolation of plasma, peripheral blood mononuclear cells and polymorphonuclear cells 61
2.3.5.3 Magnetic sorting of human immune cell subsets 62
2.4 Replication and statistics 63
2.5 Intellectual contributions 63
3.0 Investigation of the influence of rs1800693 on the splicing of TNFRSF1A exon 6 64
3.1 Introduction 64
3.1.1 *In silico* investigation of alternative splicing 64
3.1.2 Functional assays of splicing 65
3.1.3 Identifying trans-acting factors 66

3.1.4 Models of MS-associated genetic variants 67
3.1.5 Splice-switching oligonucleotides 67
3.2 Methods 69
3.2.1 Construction of *TNFRSF1A* rs1800693 minigenes 69
3.2.2 Minigene assays 69
3.2.3 Analysis of *TNFRSF1A* transcripts in human immune cells 70
3.2.3.1 PCR using cDNA-specific primers flanking exon 6 70
3.2.3.2 qRT-PCR 71
3.2.3.3 Agilent DNA 1000 72
3.2.4 *In silico* splice site analysis 73
3.2.5 Rs1800693^{G} U1 complement vector construction 73
3.2.6 U1 complement minigene assay 74
3.2.7 *In silico* analysis of potential cis regulatory motifs and RNP binding partners for rs1800693 74
3.2.8 Pulldown of RNA binding proteins 74
3.2.8.1 *In vitro* transcription of RNA 74
3.2.8.2 Coating of RNA probes to Adipic Acid Dihydrazide Agarose 76
3.2.8.3 Pulldown 76
3.2.9 SR protein overexpression minigene assays 77
3.2.10 Locked Nucleic Acid Splice-Switching Oligonucleotides (LNA SSOs) 77
3.2.10.1 *In vitro* LNA SSO screens 78
3.2.10.2 *In vivo* LNA SSO studies 79
3.2.11 Murine TNFR1 constructs 80
3.2.12 Soluble murine FLTNFR1 and Δ6TNFR1 expression 81
3.3 Results 82
3.3.1 Characterisation of rs1800693-mediated alternative splicing of *TNFRSF1A* 82
3.3.2 Investigating the molecular basis of rs1800693^{G}-mediated skipping of *TNFRSF1A* exon 6 91
3.3.3 Developing antisense technology-based models to investigate the functional consequences of MS-associated alternative splicing 100
3.4 Discussion 111
3.4.1 Guanine at rs1800693 potentiates skipping of *TNFRSF1A* exon 6 111
3.4.2 The exon 6-intron 6 boundary of *TNFRSF1A* exon 6 is not weak and rs1800693^{G}-mediated alternative splicing likely involves members of the SR protein family of splicing factors 114
3.4.3 LNA SSOs targeted to murine *TNFRSF1A* exon 6 are able to durably induce skipping *in vitro*, and *in vivo* in several tissues 119
3.4.4 LNA SSOs targeted to murine *IL7RA* exon 6 are able to induce skipping of this exon *in vitro* 124
4.0 Expression and localisation of the protein translated from the TNFRSF1A transcript lacking exon 6 125
4.1 Introduction 125
4.1.1 Expression localisation of human TNFR1 125
4.1.2 *TNFRSF1A* folding and trafficking mutants 126
4.1.3 Analysis of protein translation 128

4.2 Methods 129
4.2.1 Lentivirus preparation, concentration and titre determination 129
4.2.2 qRT-PCR for *TNFRSF1A* exons and EmGFP in lentivirally-transduced cells 131
4.2.3 Constructs for transient transfection 131
4.2.3.1 Human TNFR1-EYFP and -ECFP fusion protein constructs 131
4.2.3.2 Organelle-resident fusion protein constructs 132
4.2.4 Transient transfection and expression 133
4.2.5 Flow cytometry 133
4.2.5.1 Transiently transfected/transduced cells 133
4.2.5.2 Whole blood multiplex immunostaining 134
4.2.6 ELISAs 136
4.2.7 Western blots 137
4.2.8 Confocal microscopy 137
4.2.9 Ribosome fractionation and analysis of associated RNA 138
4.2.9.1 Preparation of cells for fractionation 138
4.2.9.2 Cell lysis and sucrose density gradient fractionation by ultracentrifugation 138
4.2.9.3 RNA extraction and transcript analysis in ribosome fractions 139
4.3 Results 141
4.3.1 The protein translated from Δ6TNFR1 mRNA 141
4.3.2 Surface, intracellular and soluble *in vitro* expression of Δ6TNFR1 compared with FLTNFR1 142
4.3.3 Subcellular localisation of intracellular Δ6TNFR1 compared with FLTNFR1 151
4.3.4 Further analysis of soluble expression of Δ6TNFR1 compared with FLTNFR1 *in vitro* 154
4.3.5 Analysis Δ6_TNFR1 mRNA distribution across ribosome fractions 156
4.3.6 Developing an ELISA system for the analysis of soluble expression of Δ6TNFR1 in human samples 160
4.3.7 Surface, cellular and soluble expression of TNFR1 species in human immune cells by rs1800693 genotype 166
4.4 Discussion 170
4.4.1 Δ6TNFR1 is not detected at the cell surface, has diffuse intracellular expression and is a secreted protein 170
4.4.2 Transcripts lacking *TNFRSF1A* exon 6 are translated in cells homozygous for rs1800693^{G} 173
4.4.3 Δ6TNFR1 is detected in sera and is increased in MS patients compared to controls 174
4.4.4 No rs1800693 genotype-dependent differences are observed in surface TNFR1 levels 177
5.0 Functional characterisation of Δ6TNFR1 178
5.1 Introduction 178
5.1.1 Functional properties of TNFR1 178
5.1.2 ER stress responses 179
5.1.3 Assessing receptor oligomerisation by resonance energy transfer 180
5.1.4 Analysing TNF binding and neutralisation 182
5.2 Methods 184
5.2.1 Constructs for transient transfections 184
5.2.2 Analysis of apoptosis 184
5.2.2.1 DNA fragmentation 184

5.2.2.2 Mitochondrial membrane integrity 185
5.2.3 Analysis of NF-κB-mediated signalling 185
5.2.3.1 NF-κB induction 185
5.2.3.2 IL-8 production 186
5.2.4 Flow cytometry 187
5.2.5 Analysis of the UPR 188
5.2.5.1 XBP1 splicing 188
5.2.5.2 XBP1 induction 188
5.2.6 Analysis of association 189
5.2.6.1 Fluorescence resonance energy transfer 189
5.2.6.2 Bioluminescence resonance energy transfer 189
5.2.7 Recombinant Protein Expression and Purification 192
5.2.8 Co-immunoprecipitations 193
5.2.8.1 Using protein A Sepharose 193
5.2.8.2 Using anti-FLAG-M2 agarose 194
5.2.9 Cell-based TNF binding assay 194
5.2.10 Surface Plasmon Resonance 194
5.2.11 Constructs and concentrated cell culture supernatants for use in neutralisation assays 195
5.2.12 Comparison of HA-tagged protein expression by anti-HA ELISA 196
5.2.13 Neutralisation assays 196
5.3 Results 198
5.3.1 Analysis of the ability of Δ6TNFR1 to induce spontaneous apoptosis *in vitro* compared with FLTNFR1 198
5.3.2 Analysis of the ability of Δ6TNFR1 to induce spontaneous NF-κB-mediated signalling *in vitro* compared with FLTNFR1 201
5.3.3 Analysis of the ability of Δ6TNFR1 and FLTFNR1 to spontaneously induce ER stress responses *in vitro* 204
5.3.4 Analysis of the capacity of Δ6TNFR1 to interact and interfere with FLTFNR1 and signalling *in vitro* 207
5.3.5 Analysis of the capacity of Δ6TNFR1 to bind and neutralise TNF compared with TFNR1 *in vitro* 215
5.4 Discussion 225
5.4.1 Δ6TNFR1 is devoid of all signalling properties of the full-length receptor 225
5.4.2 *In vitro* expression of Δ6TNFR1 does not evoke ER stress responses 226
5.4.3 Δ6TNFR1 cannot associate with FLTNFR1 to influence signalling, nor can it self-associate 228
5.4.4 Δ6TNFR1 retains the ability to bind and neutralise TNF, but with a reduced affinity and capacity compared to TNFR1 231
6.0 Concluding remarks 234
7.0 References 240
8.0 Supplementary figures 254

List of tables and figures

1.0 Introduction
Figure 1.1: Diagram of TNFR1 signalling 33
2.0 General Methods
Table 2.1: Details of resistance encoded by vectors and concentrations of antibiotics used for selection 44
3.0 Investigation of the influence of rs1800693 on the splicing of *TNFRSF1A* exon
Table 3.1: Primers for generating rs1800693 'T' and 'C' allele minigene constructs 69
Table 3.2: Custom-designed primer-probes for qRT-PCR 72
Table 3.3: LNA SSO sequences 77
Table 3.4: Primers for amplification of spliced products of exons targeted by LNA SSOs 79
Table 3.5: Primers for amplification of murine TNFR1 cDNA inserts for cloning into pEYFP-N1 80
Figure 3.1: Analysis of *TNFRSF1A* splicing by rs1800693 allele 83
Figure 3.2: Analysis of *TNFRSF1A* exon 6 skipping in human PBMCs, based on rs1800693 genotype 84
Figure 3.3: Relative expression of TNFR1 transcripts lacking or containing *TNFRSF1A* exon 6 in the indicated immune cells isolated from healthy donors with different rs1800693 alleles 86
Figure 3.4: Analysis of *TNFRSF1A* exon 6 skipping in human immune cell subsets using the Agilent DNA 1000 assay system based on rs1800693 genotype 90
Figure 3.5: Analysis of splicing of RNA transcribed from rs1800693 'A' and 'G' minigenes co-transfected with wildtype (wt U1) or *TNFRSF1A* exon 6-intron 6 boundary complement U1 (U1 comp) snRNA constructs 92
Figure 3.6: SROOGLE Analysis of ISRs in *TNFRSF1A* intron 6 by rs1800693 allele predicted to disrupt recognition of the exon6-intron 6 boundary 93
Figure 3.7: RNA-binding proteins associated with RNA probes corresponding to rs1800693 'A' and 'G' alleles resolved by 12.5% SDS-PAGE 94
Figure 3.8: *in vitro* analysis of SR protein binding 96
Figure 3.9: Influence of SRp40 overexpression on splicing of rs1800693-mediated splicing of *TNFRSF1A* exon 6, and rs6897932-mediated splicing of *IL7RA* exon 6 98
Figure 3.10: Schematic representations of LNA SSOs targeted to exons 6 of murine (a) *TNFRSF1A* and (b) IL7RA sequences 100
Figure 3.11: Screen of ability of 10 LNA SSOs targeted to *TNFRSF1A* exon 6 to induce exon skipping 101
Figure 3.12: Screen of ability of LNA SSOs targeted to IL7RA exon 6 to induce exon skipping 103
Figure 3.13: analysis of splice-switching associated with LNA SSOs mtnfr1_06, 3274 and 5678 *in vitro* 105
Figure 3.14: LNA SSO mtnfr1_06 induces skipping of *TNFRSF1A in vivo* 106
Figure 3.15: Influence of mtnfr1_06 associated skipping of murine *TNFRSF1A* exon 6 on sTNFR1 production 108
Figure 3.16: Expression of EYFP tagged murine TNFR1 and Δ6TNFR1 109
4.0 Expression and localisation of the protein translated from the *TNFRSF1A* transcript lacking exon 6

Table 4.1: Primers to generate inserts for TNFR1 constructs 129
Table 4.2: Primers to generate inserts for organelle-resident fusion protein constructs 132
Table 4.3: Antibodies for whole blood multiplex immunostaining 135
Table 4.4: Antibody combinations for whole blood multiplex immunostainings 135
Table 4.5: Antibodies and concentrations used in ELISAs 136
Figure 4.1: Schematic of FLTNFR1 and Δ6TNFR1 proteins 140
Figure 4.2: Cellular Expression of FLTNFR1 and Δ6TNFR1 142
Figure 4.3: Soluble expression of FLTNFR1 and Δ6TNFR1 144
Figure 4.4: TNFR1 cDNA expression in FLTNFR1 and Δ6TNFR1 transduced cells 145
Figure 4.5: Expression and localisation FLTNFR1-EYFP and Δ6TNFR1-EYFP following transient transfection and expression 147
Figure 4.6: Expression and localisation HA-tagged FLTNFR1 and Δ6TNFR1 EYFP fusion proteins 149
Figure 4.7: Subcellular localisation of FLTNFR1 and Δ6TNFR1 fusion proteins by confocal microscopy 151
Figure 4.8: Soluble TNFR1 production from cells expressing HA-tagged FLTNFR1 and Δ6TNFR1 EYFP fusion proteins 155
Figure 4.9: qRT-PCR analysis of ribosome-associated *TNFRSF1A* transcripts 158
Figure 4.10: Analysis of ability of anti-TNFR1 ELISA antibody pairs to recognise FLTNFR1 and Δ6TNFR1 162
Figure 4.11: Analysis of soluble TNFR1 levels in cell culture supernatants and plasma 163
Figure 4.12: Serum Δ6TNFR1 levels in controls and MS patients 166
Figure 4.13: TNFR1 surface expression by donor genotype at rs1800693 in human peripheral blood immune cell subsets 168
5.0 Functional characterisation of Δ6TNFR1
Table 5.1: Primers for the construction of non-fluorescently-tagged receptor constructs in the pECFP-N1 vector backbone 187
Table 5.2: Primers for the generation of TNFR1 constructs for use in $BRET^2$ assays 190
Table 5.3: Ratios of GFP^2:RLuc constructs transfected into HEK 293T cells for Type I $BRET^2$ assays 191
Table 5.4: Primers for the generation of constructs for analysis of soluble receptor expression 195
Figure 5.1: Spontaneous apoptosis of HEK 293T cells expressing TNFR1 proteins following lentiviral transduction by DNA fragmentation analysis 199
Figure 5.2: Spontaneous apoptosis of HEK 293T cells expressing TNFR1-ECFP fusion proteins by analysis of mitochondrial integrity 200
Figure 5.3: Analysis of spontaneous NF-κB induction signaling in cells expressing FLTNFR1-EYFP and Δ6TNFR1-EYFP 202
Figure 5.4: Analysis of spontaneous NF-κB induction signaling in cells expressing FLTNFR1 and Δ6TNFR1 compared with EYFP fusion proteins 203
Figure 5.5: Analysis of IL-8 levels in cell culture supernatant of TNFR1-transduced cells 204
Figure 5.6: Analysis of the unfolded protein response in cells expressing FLTNFR1 and Δ6TNFR1 206
Figure 5.7: Analysis of spontaneous NF-κB induction signaling in cells co-expressing 210

FLTNFR1-EYFP and Δ6TNFR1-EYFP
Figure 5.8: Analysis of FLTNFR1 and Δ6TNFR1 associations by FRET 215
Figure 5.9: Analysis of hetero-association of FLTNFR1 with Δ6TNFR1 by Type II BRET^2 213
Figure 5.10: Analysis of homotypic associations of FLTNFR1 and Δ6TNFR1 by Type I BRET^2 215
Figure 5.11: Expressed receptor and ligand proteins for use in binding analysis assays 216
Figure 5.12: Immunoprecipitation of TNFR1-TNF complexes 217
Figure 5.13: TNF binding of cells expressing HA-FLTNFR1-EYFP and HA-Δ6TNFR1-EYFP 219
Figure 5.14: Analysis of TNFR1-Fc fusion protein binding to TNF by Surface Plasmon Resonance 221
Figure 5.15: Comparative analysis of TNF neutralisation by sTNFR1 and Δ6TNFR1 223
6.0 Concluding remarks 234
7.0 References 240
8.0 Supplementary figures
Supplementary Figure 1: *In silico* prediction of SR protein binding 254
Supplementary Figure 2: Alignment of human and mouse TNFR1 isoform amino acid sequences, and *in silico* analysis of hydrophobicity 256
Supplementary figure 3: Pfold prediction of RNA secondary structures based on rs1800693 allele 259
Supplementary Figure 4: Alignment of human and mouse IL7Rα isoform amino acid sequences, and *in silico* analysis of hydrophobicity 260
Supplementary figure 4: ELISA performed by AbD Serotec to verify the specificity of anti-Δ6TNFR1 monoclonal antibodies 262
Supplementary figure 6: Schematic of Δ6TNFR1 and the extracellular domain of TNFR1 263

List of Abbreviations

A	Adenosine
AIRE	autoimmune regulator
ALPS	Autoimmune lymphoproliferative syndrome
AP	Activator protein
APC	Antigen presenting cell
ASK	Apoptosis signal-regulating kinase
ATF	Activating transcription factor
BBB	Blood brain barrier
BIP	Binding immunoglobulin protein
BRET	Bioluminescence resonance energy transfer
BSA	Bovine serum albumin
C	Cytosine
CARP	Cardiac ankyrin repeat protein
CCL	CC chemokine ligand
CCR	CC chemokine receptor
CD	Cluster of differentiation
cDNA	Complimentary DNA
cFLIP	Cellular FLICE-like inhibitory protein
CHOP	CCAAT/enhancer binding protein
cIAP	Cyclic inhibitor of apoptosis protein
CIP	Calf intestinal phosphatase
CLEC16A	C type lectin domain family 16
CMV	Cytomegalovirus
CNS	Central nervous system
CRD	Cysteine rich domain
CSF	Cerebrospinal fluid

CT	Cycle threshold
CTL	Cytotoxic T lymphocyte
CTLA	cytotoxic T lymphocyte antigen
CXCL	CXC chemokine ligand
CYLD	Cylindromatosis
CYP27B1	Cytochrome P450 family 27 subfamily B polypeptide 1
DC	Dendritic cell
DD	Death domain
DISC	Death inducing signalling complex
DMEM	Dulbecco's modified essential medium
DNA	Deoxyribonucleic acid
DR	Death receptor
DUB	De-ubiquitinase
EAE	Experimental autoimmune encephalomyelitis
EBV	Epstein Barr virus
ECD	Extracellular domain
ECFP	Enhanced cyan fluorescent protein
EDAR	Ectodysplasin A receptor
EDTA	Ethylenediaminetetraacetic acid
EIF	Eukaryotic translation initiation factor
ELISA	Enzyme linked immunosorbent assay
EMAP	Endothelial monocyte activating polypeptide
EmGFP	Emerald green fluorescent protein
EOR	ER overload response
ER	Endoplasmic reticulum
ESE	Exonic splicing enhancer
ESS	Exonic splicing silencer
EtOH	Ethanol
EYFP	Enhanced yellow fluorescent protein

FADD	Fas associated death domain
FAM	Carboxyfluorescin
FBS	Foetal bovine serum
FLTNFR1	Full length TNFR1
FRET	Fluorescence resonance energy transfer
G	Guanine
GA	Glatiramer acetate
GADD	Growth arrest and DNA damage
GalNAc-T2	*N*-acetylgalactosamine transferase 2
GAPDH	Glyceraldehyde-3-phosphate dehydrogenase
gDNA	Genomic DNA
GFP	Green fluorescent protein
GM-CSF	Granulocyte macrophage colony stimulating factor
GRM	Golgi retention motif
GWAS	Genome wide association studies
HA	Haemagglutinin
HEK	Human embryonic kidney
HLA	Human leukocyte antigen
HPRT	Hypoxanthine-guanine phosphoribosyltransferase
HSV	Herpes simplex virus
IC50	Inhibitory concentration 50
ICAM	Intercellular adhesion molecule
IFN	Interferon
Ig	Immunoglobulin
IKKβ	Inhibitor of nuclear factor kappa-B kinase subunit β
IL	Interleukin
IL2RA	Interleukin receptor 2 alpha
IL7RA	Interleukin 7 receptor alpha
IRE	Insulin responsive element

ISE	Intronic splicing enhancer
ISS	Intronic splicing silencer
IκBα	Inhibitor of NF-κβ α
JNK	c-Jun N-terminal kinase
K	Lysine
LAR	Luciferase assay reagent
LB	Lysogeny broth
LNA	Locked nucleic acid
Luc2P	Firely luciferase
M	Molar
MAPK	p38 mitogen activated kinase
MBP	Myelin basic protein
MCP	Monocyte chemoattractant protein
MGB	Minor groove binder
MHC	Major histocompatability complex
mM	Millimolar
MOI	Multiplicity of infection
MS	Multiple sclerosis
mTEC	medullary thymic epithelial cell
NEMO	NF-κβ essential modulator
NES	Nuclear export signal
NF-κB	Nuclear factor κ B
NIH	National Institutes of Health
NK	Natural Killer
nm	Nanometre(s)
nM	Nanomolar
NO	Nitric Oxide
PBMC	Peripheral blood mononuclear cell
PBS	Phosphate buffered saline

PBST	PBS tween
PCR	Polymerase chain reaction
PERK	Protein kinase RNA-like endoplasmic reticulum kinase
PI	Propidium iodide
PLAD	Pre-ligand assembly domain
PLB	Passive lysis buffer
pM	Picomoles
PPMS	Primary progressive multiple sclerosis
PRMS	Progressive relapsing multiple sclerosis
qRT-PCR	Quantitative real-time PCR
RBC	Red blood cell
RIPK1	Receptor interacting serine/threonine kinase 1
RLuc	Renilla luciferase
RNA	Ribonucleic acid
RNF	RING finger
RNP	Ribonucleoprotein
ROS	Reactive oxygen species
RPMI	Roswell Park Memorial Institute
RRMS	Relapsing remitting multiple sclerosis
SA	Splice acceptor
SAS	Subarachnoid space
SD	Splice donor
SDS-PAGE	Sodium doecyl sulphate polyacrylamide gel electrophoresis
SEAP	Secreted embryonic alkaline phosphatase
SNP	Single nucleotide polymorphism
SODD	Silencer of death domain
SPMS	Secondary progressive multiple sclerosis
SRp	Serine arginine rich protein
SRβ	Signal recognition particle receptor β

SSO	Splice switching oligonucleotide
SV40	Simian vacuolating 40
T	Thymidine
TAB	TAK1 binding protein
TACE	TNF alpha cleaving metalloprotease enzyme
TACI	Transmembrane activator and CAML interactor
TAM	tetramethylrhodamine
TAX1BP	Tax1-binding protein
TBE	Tris Borate EDTA
TCR	T cell receptor
TGF-β	Transforming growth factor β
T_H	Helper T
TK	Thymidine kinase
TMD	Transmembrane domain
TMRM	Tetramethyl rhodamine methylester
TNF	Tumour necrosis factor
TNFR	Tumour necrosis factor receptor
TNFRSF1A	Tumour necrosis factor receptor superfamily member 1 a
TRADD	TNF receptor associated death domain
TRAF	TNF receptor associated factor
TRAPS	TNF receptor associated periodic syndrome
T_{reg}	Regulatory T
U	Uracil
U2AF	U2 auxiliary factor
UPR	Unfolded protein response
UTR	Untranslated region
µg	Microgram(s)
µl	Microlitre(s)
µm	Micrometre(s)

µM	Micromolar
VCAM	Vascular cellular adhesion molecule
VSV	Vesicular stomatis virus
WIMM	Weatherall Institute of Molecular Medicine
XBP	X box binding protein
zVAD.fmk	Carbobenzoxy-valyl-alanyl-aspartyl-[O-methyl]-fluoromethylketone

1.0 Introduction

1.1 Multiple sclerosis

Multiple sclerosis (MS) is an incurable, autoimmune, inflammatory and neurodegenerative disease of the central nervous system (CNS). MS affects over 2 million people worldwide, around 1 in 1,000 people in Europe, of which approximately two thirds are female (reviewed by (Compston and Coles, 2008)). The disease is characterised by inflammation and leukocyte infiltration into the CNS, demyelination, axonal and neuronal loss and gliosis, resulting in the formation of lesions within the white matter. Repeated cycles of demyelination, remyelination, and scar tissue deposition result in maturation of lesions to form the sclerotic plaques that are characteristic of the disease.

1.1.1 Clinical course

MS patients present one or several of a very diverse range of symptoms of varying severity, which affect the motor, sensory and autonomic nervous systems. Visual problems, incontinence, impaired balance and co-ordination and muscle weakness are some of the more commonly observed symptoms (Compston and Coles, 2008). The clinical course of MS can take several trajectories, which are broadly divided into four categories (Lublin and Reingold, 1996). Primary progressive MS (PPMS) is characterised by the steady worsening of neurological symptoms and accumulation of disability from the onset of clinically manifest disease, and approximately 20% of MS patients present with PPMS. Most MS patients present with Relapsing-Remitting MS (RRMS), in which erratic, acute periods of neurological disability are separated by periods of remission of clinical symptoms. Remission, however, is incomplete and persistent symptoms accumulate over time. Within 10 years of disease onset, ~ 50% of RRMS patients enter a progressive phase of disease progression; this disease course is termed Secondary Progressive MS (SPMS). Finally, in some cases PPMS can develop into progressive relapsing MS (PRMS), in which progressive disease is punctuated at erratic intervals by acute periods of severe symptoms.

In around 66% of cases, death of patients with MS is attributable to the disease, and on average MS patients have a reduced life expectancy of 5-10 years (Bronnum-Hansen *et al.*, 2004; Compston and Coles, 2008). This reflects an increased susceptibility to, for example, skin, bladder and chest infections associated with accumulation of disability.

1.1.2 Pathogenesis

1.1.2.1 Overview

MS is thought to occur as the result of an aberrant immune response being initiated to components of the myelin sheath that surrounds the neuronal axons of the brain and spinal cord and the oligodendrocytes that produce it. Axons are long, tubular projections from neurons that conduct electrical signals for receiving sensory stimuli and the transmission of motor responses. In CNS white matter axons are myelinated, with regular intervals known as nodes of Ranvier. The conduction of electrical impulses is more efficient in myelinated as opposed to unmyelinated axons due to increased electrical resistance across the cell membrane, decreased capacitance and faster transmission of the signal through saltatory conduction (leaping of the signal between consecutive nodes of Ranvier) (Kandel *et al.*, 2000). Destruction of the myelin sheath and myelinating oligodendrocytes therefore decreases the efficiency of signal transduction along axons and sensitises them to injury, resulting in axonal and neuronal degeneration and ultimately to the breakdown in communication between nerve cells of the brain and spinal cord.

In the absence of inflammation, brain endothelial cells do not express the adhesion molecules necessary for T cells adherence and extravasion into the CNS. Disease pathology is thought to be initiated by T cells that enter the sub-arachnoid space (SAS) at the choroid plexus, as part of normal immune surveillance, where adhesion molecules are constitutively expressed (Goverman, 2009). Re-

activation by APCs presenting myelin antigens in the SAS triggers the secretion of soluble inflammatory mediators, recruiting inflammatory cells and activating perivascular endothelial cells (Goverman, 2009). This results in the upregulation of the expression of adhesion molecules and allows T cells autoreactive for myelin self-antigen that have been activated by an environmental trigger in the periphery – and therefore express the appropriate chemokine receptors and integrins – to enter the CNS and cause disease (Steinman *et al.*, 2002). It is not known how myelin-specific T cells are activated in the periphery, but this could occur through molecular mimicry or through presentation of CNS antigens by APCs in the CNS-draining cervical lymph nodes (Fabriek *et al.*, 2005). Re-activated autoreactive T cells in the CNS recruit innate and adaptive immune cells that have key roles as amplifiers of inflammation and as effectors of demyelination and axonal damage (Glass *et al.*, 2010; Goverman, 2009). Active MS lesions contain perivascular infiltrates of mononuclear cells including $CD4^+$ and $CD8^+$ T cells, macrophages and some plasma B cells (Compston and Coles, 2008). Remyelination is most active in acute lesions, coinciding with the phagocytic removal of myelin debris, but often repeated cycles of demyelination and remyelination exhaust tissue repair mechanisms. As inflammatory, autoagressive cells accumulate and amplify the immune response, naive CNS-resident macrophages (microglia) are activated and deliver lethal signal to autoantibody- and complement-opsonised oligodendrocytes (Jack *et al.*, 2005). Over time lesions expand, giving rise to widespread activation of parenchymal microglia and diffuse and chronic inflammation.

Axonal loss can proceed through prolonged exposure to inflammatory mediators, which interfere with metabolism of reactive oxygen species (ROS) and ion exchange across membranes, and loss of trophic support provided by oligodendrocytes and other glia (Nave and Trapp, 2008). It has been proposed that clinical relapses are the result of activity at multifocal inflammatory and demyelinating lesions, with incomplete remission attributed to inadequacy or failure of repair mechanisms (Compston and Coles, 2008). However, studies have demonstrated that beyond a

threshold of disability the rate of disease progression is independent of relapse frequency (Leray *et al.*, 2010), suggesting that the mechanisms responsible for long-term symptoms and the development of severe disability may be independent of inflammatory processes (Trapp and Nave, 2008).

The pathogenesis of MS is incompletely understood and is an active area of scientific research (Fugger *et al.*, 2009), and the heterogeneity in the presentation, severity and clinical course of the disease reflects its complexity. It is thought to be most likely that the symptoms of MS occur as the result of cumulative axonal and neuronal loss resulting from and maintained in part by inflammatory immune responses, and that can subsequently proceed through independent neurodegenerative mechanisms (Compston and Coles, 2008).

1.1.2.2 The role of the adaptive immune system in MS

1.1.2.2.1 T cells

Cell-mediated adaptive immunity comprises two main types of T cell, $CD4^+$ helper T cells (T_H) and $CD8^+$ cytotoxic T lymphocytes (CTLs), which are activated when they recognise antigens derived from pathogens presented on major histocompatability complex (MHC) molecules through specific T cell receptors (TCRs), in the presence of appropriate co-stimulatory signals.

Extracellular pathogens and toxins are phagocytosed in tissues by antigen presenting cells (APCs) and processed to antigens that are then coupled to MHC Class II molecules and presented to T_H cells in peripheral lymphoid organs. Following activation T_H cells differentiate into subsets that secrete different cytokines to modulate the effector activity of cells of both the innate and adaptive immune systems (principally macrophages, CTLs and B cells) (reviewed by (Wan, 2010)). T_H cells have long

been implicated in MS pathology because of the very strong association of the MHC class II region with the disease (Hillert and Olerup, 1993). MS patients have similar frequencies of myelin-specific $CD4^+$ T cells to healthy controls, but show a more activated and proinflammatory phenotype (Bielekova *et al.*, 2004; Goverman, 2009). The T_H1 cell subset is thought to be important in MS pathology, as CNS and surrounding cerebrospinal fluid (CSF) IFN-γ and IL-12 levels, which are produced by these cells, correlate with disease activity in patients. Moreover, studies in the mouse model of MS, experimental autoimmune encephalomyelitis (EAE) have shown IFN-γ secretion by CNS-infiltrating T cells, IL-12 in inflammatory lesions, resistance to EAE in IL-12 knockout mice and initiation of EAE in naive mice upon adoptive transfer of T_H1 cells from mice with EAE (Compston and Coles, 2008; Fletcher *et al.*, 2010; Goverman, 2009). IFN-γ in turn induces macrophages to produce TNF and ROS which have effector roles in CNS pathology, whilst secretion of IL-2 by T_H1 cells is thought to contribute to uncontrolled proliferation of autoagressive lymphocytes. More recently a second T_H subset, T_H17, has been implicated in the pathogenesis of MS. Adoptively transferred T_H17 cells are also capable of initiating EAE, whilst mice deficient in IL-23 – a cytokine required for T_H17 differentiation – are resistant to EAE (Goverman, 2009). These cells produce proinflammatory cytokines IL-17, IL-21, IL-9, IL-22 and TNF, and are thought to facilitate leukocyte recruitment and CNS infiltration in MS through the production of GM-CSF, IL-6, matrix metalloproteases and chemokines (Fletcher *et al.*, 2010). Disease activity in MS patients is associated with increased IL-17 production by T cells and this cytokine is also detected in MS brain lesions (Fletcher *et al.*, 2010; Tzartos *et al.*, 2008). Furthermore, in EAE inflammation appears to be driven by IL-17 and IL-22 secretion by T_H17 cells which cause disruption of the blood-brain barrier (BBB) and allow T_H17 cells to infiltrate the CNS and initiate disease (Compston and Coles, 2008; Kebir *et al.*, 2007). However, as the mode of induction of EAE (through injection of myelin proteins with a bacterial adjuvant) favours the development of a $CD4^+$ T cell response, the relative contribution of $CD4^+$ T_H cells to MS pathology may be overestimated (Gold *et al.*, 2006).

CTLs induce death in cells that are recognised to be infected with viruses or other intracellular pathogens (reviewed by (Barry and Bleackley, 2002)). Alleles of the MHC Class I region have been associated with MS, and viral infections have long been proposed as candidates for triggering CNS autoimmunity (Gilden, 2005), suggesting a role for CTLs in MS. More cytotoxic $CD8^+$ T cells than $CD4^+$ T cells are found in MS lesions, and there is evidence of more clonal expansion of effector $CD8^+$ cells isolated from MS lesions and memory $CD8^+$ T cells isolated from CSF and peripheral blood of MS patients when compared to $CD4^+$ cells (Friese and Fugger, 2005; Goverman, 2009). CTLs might be important in the formation of new lesions, as this correlates with CCR5 and CXCR3 production from these cells rather than $CD4^+$ cells (Eikelenboom *et al.*, 2002). Moreover, whilst similar frequencies of CNS antigen-specific $CD4^+$ T cells are observed between MS patients and controls, a higher frequency of cytotoxic $CD8^+$ T cells specific for CNS antigens are found in MS patients and $CD8^+$ T cell numbers correlate with axonal injury and disability (Deb *et al.*, 2010; Friese and Fugger, 2009). CTLs may be activated in the periphery by APCs that take-up myelin and cross-present antigens on MHC class I molecules, a process that is upregulated by inflammation (Goverman, 2009). CTLs have the capacity to directly damage oligodendrocytes and axons directly through the production of IFN-γ, TNF and IL-17, through directed secretion of cytotoxic granules containing granzyme, through contact-mediated lysis via perforin or through Fas-FasL mediated induction of cell death (Friese and Fugger, 2005).

Certain T cell subsets may also serve to dampen the autoimmune response in MS. The suppressive function of IL-10 and TGF-β secreting $CD4^+$, $FoxP3^+$ Regulatory T cells (T_{reg}s) appears to be impaired in MS patients, whilst these cells have been demonstrated to suppress autoreactive $CD4^+$ T cells in EAE (Viglietta *et al.*, 2004; Zozulya and Wiendl, 2008). Furthermore, the frequency of T_{reg}s increases during remission of MS symptoms and decreases during relapses (Fletcher *et al.*, 2010). Regulatory $CD8^+$, $CD122^+$/$HLA\text{-}G^+$ T cells also produce IL-10, suppressing effector $CD8^+$ T cells, whilst $CD8^+$, $CD28^-$

T cells induce DCs to be tolerogenic and can directly kill autoreactive $CD4^+$ T cells (Zozulya and Wiendl, 2008). Anti-inflammatory cytokines such as IL-27 and IL-25 also serve to dampen the autoimmune response by inducing the production of IL-10 instead of IFN-γ and IL-13 respectively, thereby inhibiting the development of T_H17 cells (Goverman, 2009).

1.1.2.2.2 B cells

B cells require T_H help to be activated, and differentiate into plasma cells that produce antibodies to circulating antigens (reviewed in (Murphy *et al.*, 2008)). The success of Rituximab, an antibody to a surface marker for B cells, in trials for the treatment of MS implicates these cells in the pathogenesis of the disease (Hauser *et al.*, 2008). Moreover, MS patients have clonally-expanded memory B cells and plasma cells in the CSF, and antibodies make-up the oligoclonal bands found in the CSF of MS patients (Colombo *et al.*, 2000). Autoreactive B cells produce autoantibody reactive for CNS self-antigens such as myelin on oligodendrocytes and axons opsonising them for destruction and activating complement functions, targeting oligodendrocytes and neurons for lysis (Franciotta *et al.*, 2008). B cells also facilitate T cell mediated responses though their function as APCs, providing co-stimulatory signals, as well as by production of soluble mediators for recruitment and co-ordination of immune cells, propagating the autoimmune response and effector function of autoaggressive cells (Franciotta *et al.*, 2008). Furthermore, B cells may have a role in polarising T_H subsets in MS; in MOG-induced EAE B cells polarise a T_H1 and T_H17 response (Weber *et al.*, 2010). B cells capable of producing anti-inflammatory IL-10 may also dampen autoimmune responses directly and also indirectly by recruiting T_{reg}s, functions that may be impaired in MS patients (Duddy *et al.*, 2007; von Budingen *et al.*, 2011).

1.1.2.3 The role of the innate immune system in MS

In addition to their roles as APCs in promoting the activation and differentiation of naive autoreactive T lymphocytes, cells of the innate immune system also play an important part in regulating the balance of T cell subsets, their function and also exhibit their own effector functions in MS.

Dendritic cells (DCs) accumulate in the CNS during inflammation in EAE and based on their developmental or activation state can induce proliferation of and induction of disease by autoreactive T cells, or induce tolerance (Bailey *et al.*, 2007; Gandhi *et al.*, 2010). In MS patients DCs typically have a more activated phenotype and increased secretion of pro-inflammatory cytokines such as IFN-γ and TNF, both of which have effector functions as well as promoting T_H1 differentiation, and IL-23, promoting T_H17 differentiation (Huang *et al.*, 1999; Vaknin-Dembinsky *et al.*, 2006). CNS-resident macrophages termed microglia are quickly activated in response to injury, infection and inflammation. Similarly to DCs they contribute to MS pathology through antigen presentation and secretion of pro-inflammatory cytokines, and are more activated in MS patients compared to controls. Microglia are involved in demyelination and neurodegeneration, through the production of myeloperoxidases and ROS, respectively (Gandhi *et al.*, 2010; Gray *et al.*, 2008). However, they may also have a beneficial role, through the secretion of the anti-inflammatory cytokines IL-10 and TGF-β and neurotrophic factors (Napoli and Neumann, 2009); the contribution by microglia to MS pathology must therefore be considered as the net effect of these autoagressive and neuroprotective functions.

At the interface between innate and adaptive immune systems are the invariant NK-T cells and γδ T cells, both of which display invariant T cell receptors. NK-T cells produce immunoregulatory

cytokines and can induce T_{reg} differentiation, whilst γδ T cells increase in number during relapses and may be cytotoxic to oligodendrocytes.

Natural killer (NK) cells are found in the lesions of MS patients, and *in vitro* studies have demonstrated their cytotoxicity to oligodendrocytes and microglia under inflammatory conditions (Gandhi *et al.*, 2010). They have also been demonstrated to be able to modulate DC development and capacity to activate CTLs and so may also indirectly influence MS pathology (Della Chiesa *et al.*, 2006). Furthermore, NK cells can repress the expression of FoxP3 in T_{reg} precursors, inhibiting their differentiation (Zimmer *et al.*, 2008). As with microglia, however, NK cells can also produce neurotrophic factors and so may be involved in growth and repair during remission from MS symptoms, and certain NK cell populations may be able to negatively regulate the activation of autoreactive T cells (Takahashi *et al.*, 2004). The cytokines produced by mast cells can influence T_H differentiation (Christy and Brown, 2007), and *in vitro* can release myelin-degrading proteases, and these cells have been observed to accumulate in MS plaques of MS patients (Gandhi *et al.*, 2010).

Unresolved episodes of inflammation can result in chronic inflammation; the simultaneous destruction and healing of tissues by inflammatory processes, characterised by the ongoing production of proinflammatory cytokines, ROS and hydrolytic enzymes by monocytes, macrophages, lymphocytes and plasma cells and fibroblasts at the site of infection (Schmid-Schonbein, 2006), also contributing to MS pathology.

1.1.3 Current treatments

There are currently 6 licensed disease-modulating therapies for the treatment of MS. Interferons β-1a and β-1b are thought to be anti-inflammatory and may help to preserve the integrity of the BBB (Kraus *et al.*, 2008). Glatiramer acetate (GA) is a random polymer of four amino acids found in myelin basic protein, and may exert its beneficial effect by inducing tolerance or anergy of myelin-reactive T

cells (Compston and Coles, 2008). Studies have shown that treatment with GA skews T_H balance from the aggressive T_H1 to an immunomodulatory T_H2 phenotype (Vieira *et al.*, 2003). Mitoxantrone is a nucleic acid intercalating agent that inhibits DNA and RNA synthesis and works by inhibiting the proliferation and survival of immune cells (Fox, 2006). Natalizumab is a humanised antibody to the α4β1 integrin on the surface of lymphocytes, and is thought to act by reducing the capacity of these cells to adhere to the BBB and infiltrate the CNS (Rice *et al.*, 2005). The most-recently licensed MS therapy is Fingolimod, a sphingosine-1-phosphate receptor modulator. It works by sequestering lymphocytes in the lymph nodes, preventing migration to the CNS, and may also help promote remyelination and repair (Pelletier and Hafler, 2012).

Treatment with β interferons and GA typically reduces the frequency of MS relapses by ~ 20-35%, and can also reduce the relapse severity (Compston and Coles, 2008). Mitoxantrone, Natalizumab and Fingolimod have a more dramatic effect on relapse rate reduction, but are associated with severe side effects and so are often only prescribed to patients with advanced RRMS or SPMS (Compston and Coles, 2008). Crucially, none of the currently licensed therapies have a proven, long-term beneficial influence on the accumulation of disability, and serve to slow rather than stop the progression of the disease. However, Natalizumab does significantly reduce acquisition of disability in the short-term and may yet be demonstrated to have longer-term effects (Ransohoff, 2007). Finally, all existing MS therapies are associated varying percentages of non-responsive patients, which is ~ 30% in patients treated with β interferons (Compston and Coles, 2008).

The search for safe, efficacious and cost-effective MS therapies continues, with oral therapeutics such as Fumarate, and the surface molecule targeting Daclizumab (αIL2Rα), Rituximab (αCD20) and Alemtuzumab humanised antibodies (Compston and Coles, 2008). The currently licensed interventions and many of the drugs on the horizon for MS treatment target autoinflammatory

effectors of the adaptive immune system that predominate in relapses, with limited restorative activity on innate immune dysfunction and no significant impact on neurodegeneration (Lopez-Diego and Weiner, 2008). Future treatment for MS patients should be designed to provide early immunosuppression and to stabilise the cascade that leads to irreversible disability, through targeting chronic as well as acute immunological effector activity, providing neuroprotection and promoting remyelination and repair.

1.1.4 The immune cell repertoire

The processes that generate the enormous diversity of TCRs and antibodies that can recognise a vast array of pathogens inevitably gives rise to some that are specific for self-antigens, creating the potential for autoimmunity (Murphy *et al.*, 2008).

1.1.4.1 Central tolerance

During lymphocyte development, progenitor T and B cells are exposed to self antigens in the primary lymphoid organs, either through endogenous expression, importing of antigen from peripheral sites by circulation or additionally, in the case of T cells, through expression of peripheral tissue antigens under the control of the autoimmune regulator (AIRE) transcription factor (Kyewski and Klein, 2006). Developing lymphocytes that recognise self antigens without an appropriate co-stimulatory signal are negatively selected by being induced to undergo apoptosis, a process known as clonal deletion. Alternatively, developing lymphocytes expressing autoreactive TCRs and immunoglobulins can be induced to produce modified receptors that no longer recognise self antigen through a process called receptor editing, a permanently non-functional (anergic) state can be imparted on self-reactive lymphocytes, or they can be induced to become regulatory T cells (T_{reg}s) (Hogquist *et al.*, 2005).

Developing T cells undergo positive and negative selection, to produce mature, naive T cells that recognise self MHC molecules but do not recognise self-peptides presented by MHC, respectively. Positive selection is mediated by epithelial cells of the thymic cortex, which highly express MHC molecules. Negative selection is mediated by medullary thymic epithelial cells (mTECs) and DCs, and occurs in the cortico-medullary junction and medulla of the thymus (Kyewski and Klein, 2006). DCs present self-antigens captured from peripheral tissues, whilst mTECS ectopically express and display tissue-specific antigens under the control of AIRE; autoreactive T cells are deleted by being induced to undergo apoptosis (Hogquist *et al.*, 2005).

Negative selection occurs in developing B cells that express IgM molecules that recognise ubiquitous self cell-surface antigens present on cells in the bone marrow. A lag period before the induction of apoptosis allows the immature B cell to potentially be rescued through editing receptor specificity. Developing B cells expressing IgM capable of recognising soluble self-antigens have anergy induced by losing the ability to express IgM. In this way, only immature B cells that do not encounter antigen whilst maturing the bone marrow bear both IgM and IgD receptors as mature naive B cells, and can be activated in the periphery (Murphy *et al.*, 2008).

1.1.4.2 Peripheral tolerance

Clonal deletion of T and B cells in the thymus and B cells in the bone marrow cannot eliminate all potentially autoreactive lymphocytes, as self proteins expressed in some peripheral tissues or at certain periods of development are not expressed in the primary lymphoid organs during the establishment of central tolerance. Additionally, many self-reactive T cells have insufficient affinity for self-antigen to be deleted in the thymus. These 'escaped' self-reactive lymphocytes must be inactivated or suppressed in the periphery. This is achieved through deletion, induction of anergy

and suppression by T_{reg}s after maturation and migration to peripheral lymphoid organs (reviewed in (Murphy *et al.*, 2008) and by (Mueller, 2010)).

T cells that bind self-antigen presented by an APC that is not also expressing co-stimulatory CD80/CD86 (for example an immature DC) leads to induction of tolerance through deletion or inactivation, rather than activation; this is considered to be the most important mechanism of peripheral tolerance in T cells. Some potentially autoreactive T cells are not deleted or inactivated, and are instead prevented from responding to the self-antigen they are specific for by T_{reg}s, through production of immunosuppressive cytokines such as TGF-β and IL-10. T_{reg}s may be generated in the thymus (natural T_{reg}s) or in the periphery (induced T_{reg}s). B cells that are exposed to large amounts of soluble antigen in the periphery down-regulate surface IgM and become anergic, simultaneously upregulating surface Fas and so targeting themselves for apoptosis by Fas-L bearing T cells.

Immunological ignorance is an additional mechanism of peripheral tolerance; autoreactive T and B cells may mature and migrate to the periphery but never encounter their cognate antigen. This may be due to the antigen being in an immune-privileged area such as the brain, eyes, testis and foetus, which often have anatomical barriers to prevent immune cell entry and mechanisms to induce immune suppression. Additionally, B cells may never encounter the specific T cell required for activation. Split tolerance describes a related phenomenon relating to the interdependence of adaptive immune responses, so that not all autoreactive cells need to be tolerised. For example, tolerisation of the T_H required for activation of a self-reactive B cell prevents its activation and autoimmunity.

Further mechanisms of peripheral tolerance exist to control the immune response to an antigen and uncontrolled proliferation that can result in tissue destruction and autoimmunity. Negative

regulation of T cell activation occurs through binding of CTLA-4 to CD80/CD86 on APCs, which down-regulates IL-2 production and proliferation, whilst activated T cells are killed by activation-induced cell death (AICD) through Fas-FasL mediated apoptosis (Murphy *et al.*, 2008).

1.1.5 Initiation and propagation of autoimmunity

In the case of MS, CNS-autoantigen specific lymphocytes somehow escape central and peripheral tolerance mechanisms and following an environmental trigger are activated, proliferate and cause disease.

1.1.5.1 T cell degeneracy and molecular mimicry

TCRs of T cells in the periphery are often cross-reactive for both a pathogen-associated and self antigen. In this way an autoreactive T cell can be activated in response to a pathogen, as it receives the appropriate co-stimulatory signals (Benoist and Mathis, 2001). Activation upregulates the expression of adhesion molecules that allows migration into tissues that naive T cells are unable to migrate into, where they might subsequently encounter self-antigen and initiate an autoimmune response. For example, activated T cells cross-reactive for a CNS antigen may acquire the necessary receptor for a chemokine such as MCP-1, or upregulate expression of integrins that interact with adhesion molecules such as VCAM-1 and ICAM-1 expressed on blood-brain barrier (BBB) endothelial cells to be able to cross the BBB, enter the CNS and initiate disease (Lee and Imhof, 2008). Both virus-specific T cells and T cells specific for certain bacterial antigens have been demonstrated to cross-react with self-antigens and to have the capacity to initiate autoimmune disease (Benoist and Mathis, 2001). Molecular mimicry may occur due to shared amino acid sequences between self-proteins and those of pathogens. Alternatively, structural mimicry can occur when the processed, pathogenic antigen presented on MHC possesses a three-dimensional structure or MHC contact residues similar to that of a self-antigen, and may occur between proteins of dissimilar amino acid

sequence (Albert and Inman, 1999). For example, a microbial peptide expressed in several classes of bacteria, has been shown to cross-react with a TCR that also recognises a peptide from myelin basic protein (MBP) despite very little sequence similarity, and induces MS-like disease in humanised mice expressing the receptor (Harkiolaki *et al.*, 2009). Moreover, MS patients have more $CD4^+$ T cells with degenerate TCRs compared to control subjects, further implicating molecular mimicry as a disease mechanism in MS (Bielekova *et al.*, 2004; Goverman, 2009).

1.1.5.2 Bystander activation

Bystander activation is an alternative and complimentary explanation for how infection can initiate autoimmune disease (reviewed by (Fujinami *et al.*, 2006)), and may be important in the establishment of MS. The production of proinflammatory cytokines such as IFN-γ and IL-2 by T_H1 cells in response to viral infection can result in the significant activation of APCs, which can subsequently activate pre-primed autoreactive T cells, initiating autoimmune disease. Moreover, virus-specific CTLs may initiate autoimmune responses through bystander effects. Cytotoxic products such as NO and inflammatory cytokines such as TNF released from dying, virus-infected cells killed by CTLs non-specifically kill uninfected cells in their proximity. Bystander killing of uninfected cells has also been observed in response to proinflammatory cytokine production from T_H cells and T_H-activated macrophages in response to infections with other microbes. The dying non-infected cells release self-peptides that are processed and presented to autoreactive T cells, that in the context of an inflammatory cytokine milieu can be activated, either initiating or propagating an autoimmune response. Indeed, in the Theiler's virus infection model of EAE a virus-specific T cell response results in activation and recruitment of CNS resident APCs, which phagocytose and present myelin antigens to autoreactive T cells leading to induction of autoimmune responses against myelin (Katz-Levy *et al.*, 2000). In addition, B cells of MS patients have recently been demonstrated to

respond to non-CNS specific stimuli to produce cytokines that promote autoagressive T_H1 and T_H17 responses, further implicating bystander activation in MS pathology. (Bar-Or *et al.*, 2010).

1.1.5.3 Exposure of cryptic epitopes

Host tissue destruction associated with the innate and adaptive immune responses to an infection leads to the release of many otherwise cryptic self-antigens to which tolerance has not been conferred. These can be taken up by APCs at the site of injury and presented to autoreactive T and B cells, initiating autoimmunity (Lanzavecchia, 1995). This mechanism is particularly important in the initiation of autoimmune response to ordinarily immune-privileged areas such as the CNS, where injury can expose a vast array of previously 'unseen' self-antigens, and so may be involved in the development of MS.

1.1.5.4 Epitope spreading

'Epitope spreading' describes the spreading of an adaptive immune response after initiation to include new antigens, termed secondary epitopes (Vanderlugt and Miller, 2002). These may be intramolecular, where new epitopes of the same antigen are exposed as the immune response progresses, engaging T and B cell clones with specificity to the new epitopes to respond. Alternatively, intermolecular epitope spreading occurs when an immune response is mounted to new proteins adjacent to the site of the primary epitope. EAE is based on the principle of epitope spreading; upon immunisation with a defined myelin antigen the specificity of the immune response can be observed to change to other endogenous myelin epitopes as the disease progresses (Vanderlugt and Miller, 2002).

1.1.6 MS aetiology

The exact cause or causes of MS have not been identified, but it is thought to be initiated by an infectious environmental trigger in individuals that are inherently susceptible to the development of an autoimmune response against myelin self-antigens and neurodegeneration as the result of individuals with complex, polygenetic risk profiles.

1.1.6.1 Environmental factors

The concordance rate for MS between monozygotic and therefore identical twins is only 25-76% (Oksenberg and Baranzini, 2010), suggesting that in addition to genetic factors, environmental exposure is important in MS aetiology (Willer *et al.*, 2003). In terms of geographical distribution, MS is most common in the Northern hemisphere (Rosati, 2001). Migration from 'high-risk' to 'low-risk' areas in childhood is associated with decreased risk of developing the disease, whilst migration from 'low-risk' to 'high-risk' geographies is associated with an increased MS risk when compared to the population of origin (Compston and Coles, 2008). Several explanations involving both infectious and non-infectious factors have been invoked in an attempt to explain the geographical distribution of MS incidence.

Varying exposure to UV radiation and consequent differences in levels of vitamin D has been proposed as a non-infectious modifier of MS susceptibility, that might be able to explain the geographical distribution of the disease (Hart *et al.*, 2011). Vitamin D has been implicated in immune regulation, upregulating the expression of IL-4 and TGF-β and down-regulating expression of IL-2 in T cells, IL-12 in monocytes and IFN-γ and TNF in PBMCs (Hart *et al.*, 2011). Recently, a mutation that impairs the function of *CYP27B1*, an enzyme important in the synthesis of vitamin D, was found to be strongly associated with MS (Ramagopalan *et al.*, 2011). Several other non-infectious environmental

risk factors have been proposed, such as diet, geomagnetism, exposure to certain toxins and radioactivity (Compston and Coles, 2008).

In terms of infectious factors influencing MS risk, a variety of bacterial and viral pathogens have been suggested to initiate disease in genetically susceptible individuals. A commonly proposed mechanism for the triggering of MS has been through viral infection, and this is supported by several lines of evidence. The risk of relapse in patients with RRMS is doubled after exposure to a virus and many MS patients report infection with measles, mumps, rubella or EBV at later than average ages (Martyn *et al.*, 1993), providing some support for the hygiene hypothesis and explaining the observation that developed countries of a similar longitude have increased incidence of MS compared with less developed countries. MS patients also have a higher titre of measles virus than the control population (Hutchinson and Haire, 1976). EBV is the most study viral candidate for the triggering of MS, and infection as a young adult has been demonstrated to triple the risk of developing the disease (Levin *et al.*, 2003). Moreover, EBV-infected B cells have been observed to accumulate in chronic MS lesions (Serafini *et al.*, 2007), and higher titres of EBV-specific antibodies are associated with an increased risk of developing MS (Lunemann *et al.*, 2010). Structural molecular mimicry has been proposed as the mechanism by which EBV initiates an autoimmune response that results in MS; in their 2002 paper, Lang *et al.* isolated a T cell clone from the blood of an MS patient that was reactive to myelin basic protein (MBP), and were able to demonstrate that it was able to cross-react with a peptide in the polymerase of EBV, through four identical peptide contacts (Lang *et al.*, 2002).

A further mechanism has recently been proposed for a viral triggering of MS, by Ji *et al.* 2010. They found that infection with a virus not expressing myelin cross-reactive epitopes or resulting in

bystander activation could result in autoimmune disease by activating T cells expressing multiple TCRs, capable of recognising both myelin and viral antigens (Ji *et al.*, 2010). This mechanism would explain how a ubiquitous viral infection could initiate MS in only a subset of infected individuals, as is hypothesised to be the case for MS.

1.1.6.2 Genetics

1.1.6.2.1 MHC region

Susceptibility loci within the MHC (referred to as 'human leukocyte antigen' (HLA) in humans) encoding region on chromosome 6 were first identified in the early 1970s through case-control studies (Jersild *et al.*, 1972), and are the largest and most-replicated risk factor for developing the disease (Sawcer *et al.*, 2005). The MS-associated MHC molecules encoded are thought to confer risk by being able to present both a pathogenic antigen and a self-antigen for, for example, myelin to a cross-reactive T cell. Whilst several HLA class II MS-risk haplotypes have been identified, the best characterised of these associations is the DR-2 haplotype, which appears to have been positively selected in Northern Europeans (Gregersen *et al.*, 2006). This haplotype contains the *DRB5*0101*, *DRB1*1501*, and *DQB1*0602* genes, which encode HLA class II molecules DR2a, DR2b and DQ6 respectively, and has an odds ratio of 5.4 (Etzensperger *et al.*, 2008). Genetic studies and work in animal models has identified *DRB1*1501* as the primary MS risk gene in this region, whilst *DRB5*0101* has been demonstrated to be protective (Etzensperger *et al.*, 2008). Moreover, the TCR identified by Lang *et al.* to be cross-reactive for MBP and EBV polyermase has been demonstrated to recognise MBP presented in the context of *DRB1*1501* (Lang *et al.*, 2002). Associations of certain HLA class I molecules with MS have also been investigated; *HLA-A*0301* and *HLA-A*0201* have been shown to confer susceptibility and protection against the development of MS, respectively (Brynedal *et al.*, 2007). Moreover, *A*0201* has been shown, using a humanised transgenic mouse model, to exert its protective effect by modifying the risk conferred by *A*0301* in *trans*, which results in the negative selection of $CD8^+$ T cells recognising self-antigen presented by HLA-A3 and downregulation

of their TCR expression (Friese *et al.*, 2008). This decreases the likelihood of MS developing as there are fewer and less responsive T cells recognising self peptide presented in the context of HLA-A3 in the periphery (Friese *et al.*, 2008).

1.1.6.2.2 Non-MHC associations

MHC associations alone are thought to account for less than 20% of the total genetic risk in MS. Traditional small-scale case-control studies do not have the necessary power to unambiguously identify variants with smaller effect sizes (Hafler *et al.*, 2007), and so only since the advent of new and cost-effective high-throughput sequencing and bioinformatics technologies, and large, multi-centre collaborations has the typing of cohorts of thousands of case-controls been feasible. In recent years, genome-wide association studies (GWAS) have reproducibly identified associations of a number of single nucleotide polymorphisms (SNPs) in genes with immunological and neurological functions with MS, in various populations (Australia and New Zealand Multiple Sclerosis Genetics Consortium, 2009; Burton *et al.*, 2007; De Jager *et al.*, 2009b). The most recent and powerful GWAS for MS has confirmed many previously identified associations and newly identified others, totalling more than 50 SNPs (Sawcer *et al.*, 2011). Interestingly, several of these SNPs are in genes implicated in the differentiation of $CD4^+$ T_H cells, and specifically in the development and function of T_{reg}s, implicating a failure in this arm of peripheral tolerance in pre-disposition to the development of the disease (Sawcer *et al.*, 2011). Many of the associated regions have also been implicated by GWAS to be important in determining susceptibility to other autoimmune diseases, implicating common mechanisms leading to autoimmunity (Burton *et al.*, 2007; Zoledziewska *et al.*, 2009). As both the aetiology and pathogenesis of MS are complex and active areas of research, the demonstration of even a small contribution by a gene to its development or progression could dramatically alter the way in which we think about the disease (Oksenberg *et al.*, 2008). For example, a newly-implicated cellular signalling pathway might create new opportunities for therapy or prevention of the disease

(Fugger *et al.*, 2009; Oksenberg *et al.*, 2008). However, a barrier for translational research is the difficulty of determining which genetic variants, and therefore which genes, within an associated region are truly causal, due to the technical limitations of GWAS genotyping platforms and the haplotypic structure of the genome, which means that an associated SNP may simply tag a causal variant (Donnelly, 2008).

One approach to this problem is to use fine-mapping studies to more comprehensively catalogue genetic variation in associated regions, to facilitate the identification of potentially causal variants. For example, fine-mapping in the *IL2RA* gene region, which encodes the alpha chain of the IL-2 receptor (IL2Rα), has provided greater resolution to associated variants; whilst initial studies identified both rs12722489 and rs2104286 to be associated with MS (Hafler *et al.*, 2007), the signal from rs12722489 was subsequently demonstrated to be as a result of its linkage disequilibrium with rs2104286 (Perera *et al.*, 2009). Fine mapping can also identify additional associated variants in a putatively associated region; studies that initially identified rs6498169 in the *CLEC16A* gene region have been followed by others that have identified independent associations of other SNPs with MS susceptibility, such as rs725613 (Zoledziewska *et al.*, 2009).

Functional studies are a further and complementary means by which putatively associated SNPs can be confirmed to be disease pre-disposing variants. In their 2007 paper, Gregory *et al.* demonstrated the association of rs6897932^{C} in exon 6 of the IL-7 receptor alpha chain (IL7Rα) with MS, and further demonstrated this variant to result in increased skipping of this exon (Gregory *et al.*, 2007). This was predicted to result in an increase in the production of a soluble IL7Rα isoform at the expense of membrane-bound receptor, with the capacity to bind cognate cytokine and antagonise signalling (Gregory *et al.*, 2007). Similarly, the MS-risk associated rs2104286^{T} allele in *IL2RA* has been shown to

result in increased production of a soluble isoform of the protein, and is associated with reduced expression by stimulated $CD14^+$ and $CD16^+$ monocytes, and $CD4^+$ naïve T cells (Dendrou *et al.*, 2009). Both IL-7 and IL-2 have important roles in the growth, differentiation and maintenance of T cell populations. Kofler *et al.* 2011 investigated rs17824993 in CD6, a protein expressed on the surface of T cells with roles in activation and proliferation. They were able to demonstrate that the risk-associated G allele caused an alternative splicing event, resulting in exclusion of exon 5 from the mature transcript and truncation of the mature protein in $CD4^+$ and $CD8^+$ T cells (Kofler *et al.*, 2011). This decreased the proliferative capacity of $CD4^+$ T cells, and was proposed to predispose to the development of MS by potentially compromising T_{reg} populations. Furthermore, the protective G allele of rs2300747 in the gene encoding CD58, an important co-stimulatory molecule for TCR signalling, has been demonstrated to result in increased transcription in mononuclear cells of MS patients, and may influence T_H development towards a T_{reg} phenotype (De Jager *et al.*, 2009a). Functional effects of MS-associated SNPs have also been implicated in immune processes and cell populations other than T cells; the risk-associated rs2546133-rs2617822 haplotype of *VAV1*, which encodes a protein important for lymphocyte proliferation and differentiation, has been associated with increased expression of this gene, and correlates with increased TNF and IFN-γ expression in peripheral blood and CSF (Jagodic *et al.*, 2009). Also, activity of the JAK kinase TYK2, an important component of IL-6, IL-10, IL-12, IL-23 and IFN-λ signal transduction pathways, is compromised in individuals harbouring the risk-associated allele of rs34536443, who also display a relative increase in T_H2 responses (Couturier *et al.*, 2011).

A SNP that has achieved genome-wide significance in all GWAS studies in which it has been typed is rs1800693, located 10 bases into intron 6 of *TNFRSF1A*, which encodes the principle receptor for the proinflammatory cytokine TNF, TNF receptor 1 (TNFR1) (De Jager *et al.*, 2009b). The ancestral, protective allele is an Adenosine (A) at rs1800693, whilst the allele conferring disease susceptibility

is a Guanine (G). The association (P = 1.59 x 10^{-11}) was first identified by De Jager *et al.* in 2009, who found rs1800693 to be a common variant in US and UK populations (allele frequency = 0.44), conferring a small risk effect to the development of MS (odds ratio (OR) = 1.2) (De Jager *et al.*, 2009b). The SNP has subsequently been confirmed in several populations and more recently in highly-powered, large multi-centre studies (Patsopoulos *et al.*, 2011; Sawcer *et al.*, 2011).

1.2 SNPs and disease

Non-synonymous (amino acid altering) SNPs can predispose to the development of and/or cause disease by directly changing the functional properties of the protein translated from the mutant allele. Additionally, amino acid changes may alter normal processing of the translated protein, if the mutated residue is important for protein folding, formation of inter- or intra-molecular associations through hydrogen or disulphide bonds, glycosylation and phosphorylation or other post-translational modifications (Alberts, 2008). Both non-synonymous and synonymous SNPs can result in changes in the expression of genes in *cis* by altering normal transcription of the gene. They may perturb enhancer, insulator or promoter sequences of the gene in the mutant allele, so that the effect of the SNP is to alter the amount of mRNA transcribed and ultimately levels of the translated protein. Alternatively, these SNPs can influence gene expression at the mRNA level, through modifying post-transcriptional processing. SNPs may alter the nuclear export of the transcript to the cytoplasm for translation, mRNA stability and degradation properties, polyadenylation, translation, and splicing (Alberts, 2008).

1.3 Splicing

One of the most common ways for a SNP to exert a relatively large functional effect on the protein transcribed from a gene is through changing the normal pattern of splicing.

Following transcription, precursor messenger RNA (pre-mRNA) is modified to remove non-coding introns through splicing, and the protein is then translated from the resultant contiguous sequence of protein-encoding exons (reviewed by (Black, 2003). Splicing is performed by a series of transesterification reactions catalysed by the spliceosome, a complex of five (U1, U2, U4, U5 and U6) small, nuclear molecules of RNA complexed with protein, termed ribonucleoproteins (snRNPs).

Introns start with a 5' or donor splice site, which almost always has the sequence 'GU', within a larger more loosely conserved consensus region. This is followed by a branch point which contains a conserved 'A' nucleotide, and is followed by the polypyrimidine tract, rich in 'C' and 'U' nucleotides (Black, 2003). The intron ends with the 3' or acceptor splice site, which terminates the intron with the sequence 'AG'. The snRNPs of the spliceosome interact directly with the intronic motifs in the pre-mRNA through complementary base pairing.

1.3.1 Alternative splicing

Additional proteins and RNPs are also required for each splicing reaction, and have roles in definition and recognition of the key sites in the regulation of splicing by the spliceosome (Black, 2003; Matlin *et al.*, 2005). For example, members of the serine and arginine-rich protein family (SR proteins) are thought to bind pre-mRNA in conjunction with U1 and U2AF to help specify exon-intron boundaries, through recognition of loosely-conserved sequences (Graveley *et al.*, 1999).

This confers an additional level of complexity and plasticity to the proteins that can be produced from the eukaryotic genome (Blencowe, 2006; Brett *et al.*, 2002); rather than terminating splicing of an intron, if a mutation occurs in a nucleotide that is important for its splicing, a new pattern of splicing is typically created. This is known as alternative splicing, and most often results in skipping of

an exon from the mature transcript (Black, 2003). It is estimated that up to 80% of human genes are spliced in a variety of different ways through alternative splicing, allowing several different proteins to be produced from the same genetic sequence (Kampa *et al.*, 2004).

Trans-acting RNPs bind to *cis*-acting regulatory sites on the pre-mRNA, and through generation of permissive or restrictive RNA secondary structures, or through the recruitment or inhibition of the recruitment of further facilitator or inhibitory proteins and RNPs, promote or disrupt the recognition of the key splicing regulation sites respectively (reviewed by (Matlin *et al.*, 2005). Based on the net effect of the *trans*-acting factor to the splicing of a specific exon/intron these *cis*-acting motifs are defined exonic or intronic splicing enhancer or silencer elements (ESE/ISE/ESS/ISS). *Trans*- and *cis*-acting determinants of splicing work inter-dependently to regulate splicing, so that depending on context of the presence of other *cis*- and *trans*-acting factors, the same motif and associated factor can either promote or suppress the use of a nearby splice site.

As well as the evolutionary advantage afforded to eukaryotic organisms in the ability to produce several different isoforms of a protein from a single genetic sequence, alternative splicing has a further advantage. Through the manipulation of the relative abundance of the myriad of splice regulatory proteins, specific isoforms of proteins can be favoured at certain stages of development or cell types, in multicellular organisms (Matlin *et al.*, 2005). In some cases, however, alternative splicing can lead to the preferential production of aberrant, disadvantageous protein isoforms that, through either insufficient production of the correctly-spliced isoform or through a novel detrimental property of the splice variant, can pre-dispose to or cause disease. It is thought that more than 50% of human disease-causing mutations act through disrupting splicing (Lopez-Bigas *et al.*, 2005).

1.3.2 Alternative splicing in disease

Mutations that alter splicing in *cis* can either be considered gain or loss of splicing function mutations (Wang and Cooper, 2007). Gain of function splicing mutations may for example generate a cryptic (ordinarily ignored) splice site, or may create or strengthen a splice regulatory element. Conversely, if an element is removed or weakened the mutation is considered a loss of splicing function mutation. Both types of mutation can lead to abnormal exon definition, resulting in the inappropriate inclusion or exclusion of part or all of an intron or exon, respectively, in the mature transcript (Lukong *et al.*, 2008; Wang and Cooper, 2007).

The effects of alternative splicing in disease can be subtle, having a disease course- or susceptibility-modifying function. For example, two SNPs in the 3' UTR encoded by exon 4 of cytotoxic T lymphocyte antigen 4 (*CTLA4*) have been demonstrated to result in increased skipping of exon 3 and reduced production of a soluble isoform (Ueda *et al.*, 2003; Wang and Cooper, 2007). This increases susceptibility to the development of several autoimmune diseases, potentially through impaired T_{reg} function (Ueda *et al.*, 2003).

A more pertinent example is the effect of the rs6897932^{C} allele, in exon 6 of the gene encoding the IL-7 receptor alpha chain (*IL7RA*) (Gregory *et al.*, 2007), which has repeatedly and independently been demonstrated to be the most strongly-associated SNP conferring susceptibility to MS in the *IL7RA* gene region (Evsyukova *et al.*, 2010). Signalling through IL-7R is important for the survival, proliferation and differentiation of lymphocytes, particularly early in thymocyte development, and in the maintenance of naive and memory T cells in the periphery (Mazzucchelli and Durum, 2007). Rs6897932^{C} results in a 4-5 fold increase in the skipping of *IL7RA* exon 6, potentially by strengthening an ESS (Gregory *et al.*, 2007). This exon encodes the transmembrane domain of the

full-length, membrane-bound receptor, and skipping results in a frameshift mutation and formation of a soluble IL-7Rα isoform (Korte *et al.*, 2000). Furthermore, sIL-7Rα mRNA has been shown to be elevated in whole blood samples of MS patients when compared with controls (McKay *et al.*, 2008). Increased expression of sIL7Rα at the expense of membrane bound IL-7Rα might predispose to the development of MS by lowering IL-7-IL-7R signalling to below a threshold required for continued survival and proliferation of T cells, or certain T cell subsets, leading to an imbalance, dysregulation and potentially to autoimmunity (Evsyukova *et al.*, 2010; Mazzucchelli and Durum, 2007). Moreover, as sIL-7Rα retains the ability to bind IL-7 in solution, a significant proportion of the small pool of constitutively-expressed IL-7 may be sequestered by this isoform and be unable to bind membrane-bound, signalling-competent receptor (Evsyukova *et al.*, 2010; Mazzucchelli and Durum, 2007).

1.4 Tumour Necrosis Factor (TNF) and its receptors

TNF is a pleiotropic cytokine that is produced mainly by macrophages and is most often associated with proinflammatory properties and is considered a master regulator of innate and adaptive immunity. It is expressed as a 26 kDa transmembrane protein that associates into homotrimers at the cell surface, and can subsequently be cleaved by the TNF alpha cleaving metalloprotease enzyme (TACE) to be released into the extracellular space as a soluble 17 kDa form (Hehlgans and Pfeffer, 2005).

First described for its capacity to induce haemorrhagic necrosis in mouse tumours, TNF is most recognised now for its role in inflammation, particularly in the pathogenesis of diseases such as sepsis, RA, inflammatory bowel diseases, psoriasis and MS. TNF has also been demonstrated to have immunoregulatory properties, participating in the maintenance of immune homeostasis (Hehlgans and Pfeffer, 2005; Locksley *et al.*, 2001). The net effect of TNF is therefore a balance between its

proinflammatory and immunosuppressive functions, which is determined by the cellular microenvironment, and differs between phases of inflammation.

The cellular function of TNF is relayed by two structurally distinct receptors; TNF receptors 1 (TNFR1) and 2 (TNFR2) (Hehlgans and Pfeffer, 2005). They are both members of the death receptor superfamily, a group of type I transmembrane gylcoproteins with one or more conserved, cysteine-rich domains in the extracellular portion of the receptor (Locksley *et al.*, 2001). However, TNFR1 and TNFR2 share only 28% homology in their extracellular domains, and no homology in their intracellular regions (Locksley *et al.*, 2001). The two receptors have different affinity for soluble (sTNF) and membrane-bound TNF (tmTNF); TNFR1 has a higher affinity for sTNF whilst TNFR2 has a higher affinity for tmTNF (Hehlgans and Pfeffer, 2005). Furthermore, they have distinct expression patterns, with TNFR1 being expressed by almost every cell type, whilst TNFR2 expression is restricted to haematopoietic cells. Similarly to TNF, both TNFRs can be cleaved by TACE to a soluble form from membrane-bound receptor (Wallach *et al.*, 1991).

1.4.1 TNFR1

1.4.1.1 Structure and characteristics

TNFR1 is a type I, single-pass transmembrane glycoprotein, with an extracellular, ligand-binding N-terminal domain, a transmembrane domain and a C-terminal intracellular domain (Banner *et al.*, 1993). It has four characteristic cysteine-rich domains (CRDs), which determine receptor association and ligand specificity. CRD1 is also designated the pre-ligand assembly domain (PLAD), and TNFR1 monomers associate via non-covalent, homotypic interactions through this domain to form trimers at the cell surface (Banner *et al.*, 1993; Chan *et al.*, 2000). CRDs 2 and 3 have been demonstrated to be important for ligand binding by the receptor, and CRD4 may have a role in stabilising receptor-ligand interactions (Banner *et al.*, 1993; Marsters *et al.*, 1992). Immediately upstream of the

transmembrane region are major and minor metalloprotease cleavage domains, which are utilised by TACE to cleave the extracellular portion from membrane-bound receptor, to generate a soluble TNF-binding species (Reddy *et al.*, 2000). The death receptor family is characterised by a ~ 80 amino acid cytoplasmic region known as the death domain (DD) that is essential for the recruitment of cytosolic adaptor proteins for the transduction of both NF-κB and apoptotic signalling pathways (Brakebusch *et al.*, 1992; Rothe *et al.*, 1992). A short Golgi retention motif is found at the C-terminus, which localises the majority of cellular TNFR1 to this organelle under normal conditions (Storey *et al.*, 2002).

1.4.1.2 Signalling

At physiological levels of expression and in the absence of ligand, inhibitory silencer of death domain (SODD) protein associates with the homotypic DD of TNFR1, preventing self-association of DDs and spontaneous, ligand-independent signalling (Takada *et al.*, 2003). Upon binding of TNF, TNFR1s cluster, SODD dissociates and the scaffold adaptor protein TNF receptor associated death domain (TRADD) binds, facilitating the assembly of TNF receptor associated factors 2 and 5 (TRAF2/5) and receptor-interacting serine/threonine-protein kinase 1 (RIPK1) (Micheau and Tschopp, 2003). This is known as complex I, and initiates either pro-survival, NF-κB-mediated signalling, or matures to form a second complex known as the death inducing signalling complex (DISC) to bring about apoptosis (Kelliher *et al.*, 1998; Tartaglia *et al.*, 1993).

For NF-κB-mediated signalling, complexes I segregate into lipid rafts (D'Alessio *et al.*, 2010), and RIPK1 and TRAF2 are polyubiquitinated by the E3 ubiquitin ligases cyclic inhibitor of apoptosis proteins 1 and 2 (cIAP 1/2) and TRAF2 (Micheau and Tschopp, 2003). The resulting polyubiquitinated lysine 63 (K-63) chains recruit a complex containing TAK1 kinase, TAK1 binding protein (TAB) and NF-κB essential modulator (NEMO), which subsequently activates IKKβ, leading to the phosphorylation,

ubiquitination and consequent degradation of inhibitor of NF-κB (IκBα) (Bianchi and Meier, 2009). The release of NF-κB from inhibition by bound IκBα in the cytosol allows translocation to the nucleus where it can bind to NF-κB response elements in the enhancer regions of target genes, upregulating their transcription (Chen and Goeddel, 2002). NF-κB-mediated signalling through TNF-TNFR1 on immune cells typically upregulates genes involved in their activation, proliferation and maturation. Complex I also activates p38 mitogen-activated kinases (MAPKs) and c-Jun N-terminal kinases (JNKs), which phosphorylate and activate activating transcription factor 2 (ATF2) and activator protein 1 (AP-1) transcription factors, which similarly upregulate pro-survival and maturation genes (Wertz and Dixit, 2010).

Within minutes of ligand binding, complex I is internalised through clathrin-dependent endocytosis to form TNF-receptorsomes (Schutze *et al.*, 2008). Fas-associated death domain (FADD) is recruited to the complex containing RIP1K and TRAF2 in a non-polyubiquitinated state, along with initiator pro-cysteine-aspartic acid protease (caspase) enzymes 8 and 10 to form the DISC (Wertz and Dixit, 2010). Increased local concentration of pro-caspases induces their processing to functionally active forms, resulting in the initiation of a caspase cascade and ultimately to the cleavage and activation of executioner caspsases 3, 6 and 7. Executioner caspases cleave a broad spectrum of cellular proteins and DNA, bringing about apoptosis (Micheau and Tschopp, 2003).

NF-κB-mediated signalling is negatively regulated in a feedback loop by upregulation of IκBα expression along with A20 and cylindromatosis (CYLD). A20 interacts with Tax1-binding protein 1 (TAX1BP1), ITCH and RNF11 to form a complex that terminates NF-κB-mediated signalling by targeting RIP1K K-63 chains for deubiquitination whilst simultaneously promoting ubiquitination of RIP1K K-48, thereby targeting it for proteasomal degradation (Wertz and Dixit, 2010). CYLD exerts its inhibitory function through de-ubiquitinase (DUB) activity on K63 chains of RIPK1 and TRAF2 (Fujita

and Srinivasula, 2009). In addition, constitutively expressed cardiac ankyrin repeat proteins (CARP) 1 and 2 target RIP1K for degradation through poly K-48 ubiquitination (Bianchi and Meier, 2009).

Apoptotic signalling through TNF-TNFR1 is negatively regulated by the RING finger domain-containing cIAP 1/2 proteins, cFLIP and CARP1/2, and positively regulated by ITCH (Wertz and Dixit, 2010). IAPs act as inhibitors of executioner caspases by interfering with their activation or at the level of DISC complex formation, by interfering with recruitment of pro-caspases 8 and 10. cFLIP also interferes with recruitment of pro-caspase 8 to the DISC, through competitive inhibition due to its structural similarity, whilst CARP1/2 promotes pro-caspase 8 degradation. JNK signalling results in the negative feedback of pro-survival signalling and the upregulation of apoptosis through activation of ITCH, to promote K-48 linked polyubiquitination and subsequent degradation of cFLIP, releasing its inhibition of pro-caspase 8 (Fujita and Srinivasula, 2009).

How the balance between NF-κB-mediated, prosurvival and apoptotic signalling is determined is incompletely understood, but it is thought to complex and involve dynamic regulation of levels and functionality of adaptor and effector proteins involved in signalling processes through activating, K-63 linked and proteasome-targeting K-48 linked polyubiquitination (Wertz and Dixit, 2010). Furthermore, inhibition of NF-κB or upstream parts of the complex I signalling pathway has been demonstrated to sensitise cells to TNF-mediated apoptosis (Wang *et al.*, 1996).

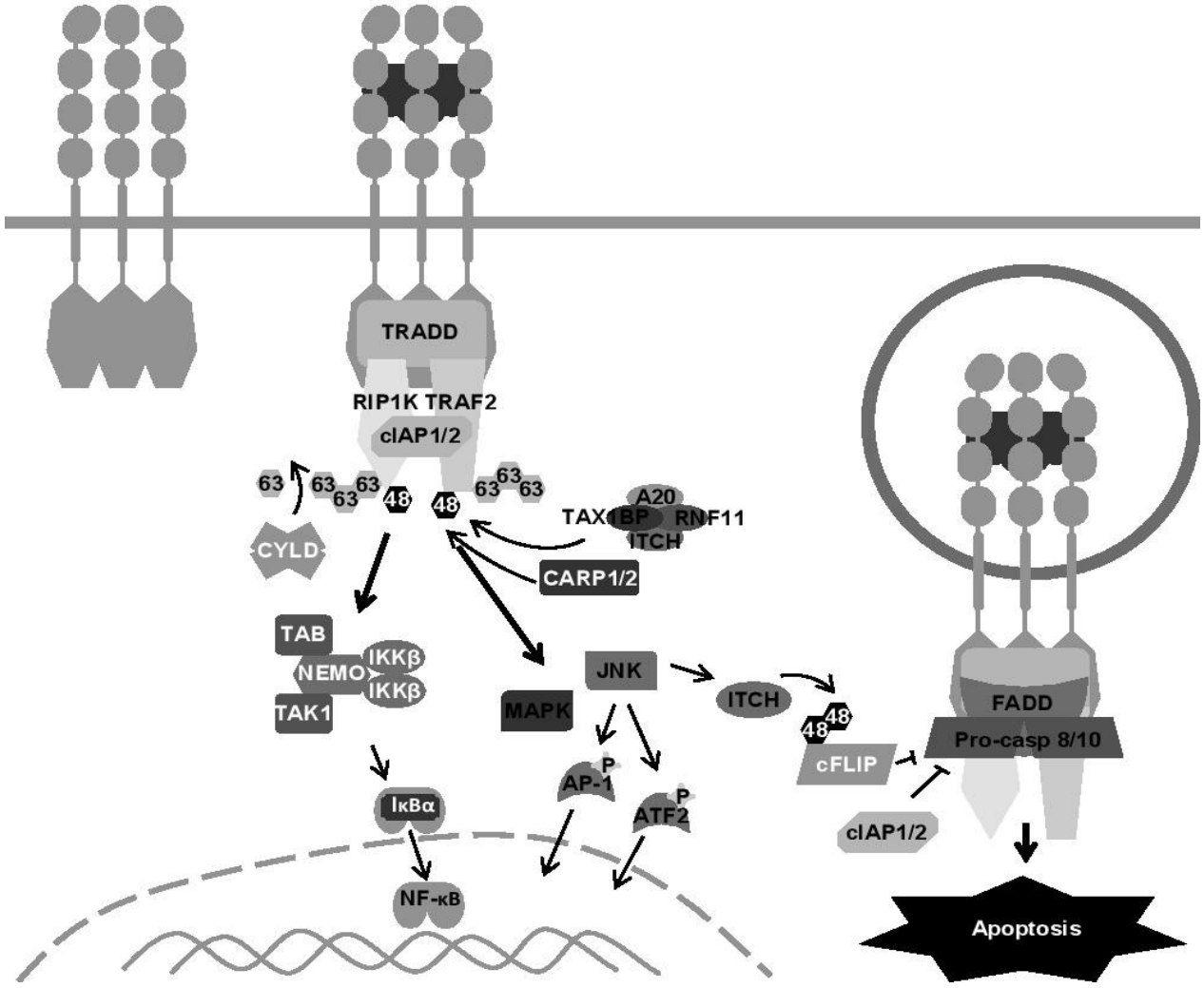


Figure 1.1: Diagram of TNFR1 signalling. Details are described in the text.

1.4.2 TNF and MS

TNF has been implicated in the pathogenesis of MS by several lines of evidence. High levels of TNF are detected in active MS lesions (Hofman *et al.*, 1989) and in their 1991 paper, Sharief and Hentges reported elevated levels of TNF in the CSF of chronic progressive MS patients compared with controls and that increased levels correlated with more severe disease, accelerated neurodegeneration and poorer long-term prognosis (Sharief and Hentges, 1991). Other studies have shown increased TNF secretion by PBMCs of MS patients immediately prior to relapses, further implicating the cytokine in disease pathology (Rieckmann *et al.*, 1995).

Studies from animal models have further implicated TNF in MS. Powell *et al.* found more severe EAE to be initiated upon adoptive transfer of T cells producing higher levels of TNF, and that TNF antagonism with soluble receptors or neutralising antibodies decreased disease severity (Powell *et al.*, 1990). Other studies reported complete inhibition of EAE transfer by treatment with monoclonal and polyclonal anti-TNF antibodies (Ruddle *et al.*, 1990; Selmaj *et al.*, 1991), or soluble TNF receptor-IgG fusion proteins (Korner *et al.*, 1997a; Selmaj *et al.*, 1995). Furthermore, transgenic mouse models have been used to investigate the role TNF in the pathogenesis of MS. TNF knockout mice have been demonstrated to display delayed EAE onset and less severe disease, potentially due to defective trafficking of inflammatory leukocytes into the CNS (Korner *et al.*, 1997b; Sean Riminton *et al.*, 1998). Indeed, subsequent studies shows the failure of TNF deficient mice to induce seven chemokines including MCP-1 early in the inflammatory processes of EAE, that are thought to play a role in leukocyte recruitment to the CNS (Murphy *et al.*, 2002). TNFR1 knockout and TNFR1 and TNFR2 double knockout mice were shown by Eugster *et al.* to have a similar disease course to TNF knockouts (Eugster *et al.*, 1999), but more recent studies have since demonstrated these mice to be resistant to EAE (Gimenez *et al.*, 2004; Suvannavejh *et al.*, 2000). This may be the result of the dependency of TNFR1 for the induction of VCAM-1 on astrocytes in the CNS parenchyma, for

lymphocytes to be able to effectively cross the BBB (Gimenez *et al.*, 2004). Conversely, TNFR2 single knockout mice display more severe EAE symptoms (Suvannavejh *et al.*, 2000), an intriguing aspect of TNF biology in MS that is discussed further in Chapter 6.

1.5 Thesis aims

In autumn 2009, Dr. Divya Punwani of Professor Lars Fugger's research group at the University of Oxford used an *in vitro* minigene system to demonstrate that the MS-associated rs1800693^{G} allele results in alternative splicing of *TNFRSF1A* pre-mRNA such that a novel transcript lacking exon 6 is produced (Dr. Divya Punwani and Professor Lars Fugger, unpublished data).

The Aims of this thesis are as follows:

- To better characterise the rs1800693^{G}-mediated skipping of *TNFRSF1A* exon 6, through investigating sequence-specific (*cis*) and interacting partner (*trans*) molecular determinants of this alternative splicing event.
- To investigate the potential for making a mouse model for this alternative splicing event, and that for another MS-associated alternative splicing event, rs6897932^{C}-mediated skipping of *IL7RA* exon 6, using antisense oligonucleotide technology.
- To study the cellular expression and distribution of the protein translated from the *TNFRSF1A* mRNA transcript lacking exon 6 (Δ6TNFR1) in comparison with that translated from the full-length *TNFRSF1A* mRNA (FLTNFR1).
- To study the functional behaviour of Δ6TNFR1 in relation to FLTNFR1 with reference to previously characterised functional properties (and determinants thereof) of FLTNFR1.
- To thereby provide an explanation for association of the rs1800693^{G} allele with MS, in relation to the current knowledge of the biology of the TNF-TNFR1/TNFR2 signalling axis, particularly in MS.

1.6 Hypothesis

We predict that the protein translated from the alternatively spliced *TNFRSF1A* transcript lacking exon 6 encodes a functionally altered isoform of TNFR1, that either through influencing the levels or functionality of the full-length receptor, or through a novel function of its own, predisposes individuals harbouring the rs1800693^{G} allele to the development of MS.

2.0 General methods

2.1 Cloning

2.1.1 Overview

Minigene and expression vector constructs were prepared according to standard laboratory protocols. The genomic DNA (gDNA) or complimentary DNA (cDNA) sequence of interest was amplified from purified gDNA in the case of the former, or from either reverse transcribed RNA or cDNA constructs in the case of the latter, using primers that incorporated appropriate restriction enzyme digestion sequences at the 5' and 3' ends of the amplified fragment. PCR amplification was performed (2.2.1), products were resolved in 1-2% agarose TBE and gel-purified (2.2.6.1 and 2.2.7.2). Amplified DNA was digested with the appropriate restriction enzymes for 1 h at 37°C (2.1.3), and digested products were purified (2.2.7.1). Target vector DNA was digested with the same restriction enzymes for 2 h at 37°C, dephosphorylated for 30 min at 37°C (2.1.3) to prevent re-ligation, resolved by electrophoresis (2.2.6.1) and gel-purified (2.2.7.2). Digested insert and vector were subsequently ligated (2.1.4) to yield a contiguous vector construct. Ligated constructs were then transformed into bacteria (2.1.5), and transformants were selected for by culture for 16 h on LB agar plates at 37°C in the presence of an antibiotic for which the vector encoded resistance (Table 2.1). Small preparations of antibiotic-resistant colonies were prepared by incubation with shaking for 16 h in 5 ml of LB broth containing the appropriate antibiotic and DNA was isolated (2.1.7.1). The appropriate region of the vector was subsequently sequenced at the WIMM sequencing facility and sequences were analysed to confirm integrity of the construct (2.1.8). Larger preparations of the verified vector constructs were then made for use in downstream applications (2.1.7.2).

2.1.2 Vectors

Features of the vectors used in this thesis are described below. Details of the antibiotic resistance they encode for their propagation can be found in Table 2.1.

pSPL3 was a kind gift from Finn Cilius Nielsen of the University of Copenhagen (Copenhagen, Denmark). It contains constitutively-spliced splice donor (SD) and splice acceptor (SA) exons to the 5' and 3' of a multiple cloning site, respectively. The splicing of a genomic region of interest can be analysed by its insertion at the multiple cloning site and analysis of the DNA sequence between SD and SA sequences amplified from cDNA by PCR.

pcDNA3.1 (Invitrogen) contains the human cytomegalovirus intermediate-early (CMV) promoter upstream of a multiple cloning site.

The **human U1 snRNA** construct was a kind gift from Dr. Marco Baralle of the International Centre for Genetic Engineering and Biotechnology (ICGEB; Trieste, Italy). It contains the coding sequence for the U1 snRNA component of the spliceosome under the control of the CMV promoter in pcDNA3.1.

pEYFP-N1 and **pECFP-N1** vectors were used to make fluorescent fusions of the receptors, for use in *in vitro* studies. It has a multiple cloning site at the N terminus of Enhanced Yellow Fluorescent Protein and Enhanced Cyan Fluorescent Protein (EYFP and ECFP respectively), which are spectral variants of the Green Fluorescent Protein (GFP), and are expressed under the control of the CMV promoter in the N1 reading frame.

TNFR2 leader-HA-EYFP was kindly donated by Professor Richard Siegel of the National Institutes of Health (NIH; Bethesda, MD, USA) and was used to create HA-tagged receptors. Derived from pEYFP-

N1, it contains the leader sequence for the TNF receptor 2 (TNFR2) in-frame with the Haemagglutinin (HA) tag (YPYDVPDYA), with a multiple cloning site in between the HA tag and the coding sequence for EYFP.

pGFP^2-N3 was used to create TNFR1-GFP^2 fusion proteins for use in BRET^2 assays to determine receptor association properties. It has a multiple cloning site at the N terminus of GFP^2, a variant of the green fluorescent protein (GFP), which allows cDNA sequences to be fused to the fluorophore in the N3 reading frame, expressed under the control of the CMV promoter.

pRluc-N3 was used to create TNFR1-Rluc fusion proteins for use in BRET^2 assays to determine receptor association properties. It is same as pGFP^2-N3, except that the luciferase gene from *Renilla reniformis* (Rluc) replaces the GFP^2 sequence. Rluc is an enzyme that catalyses the bioluminescent oxidation of luciferin to oxyluciferin, which can subsequently be quantified.

pGFP^2-Rluc was used as a positive control in BRET^2 assays. It encodes GFP^2 expressed in-frame with Rluc to yield a fusion protein.

pHRsinUbEm is a lentiviral expression plasmid that was kindly donated for this study by Prof. Paul J. Lehner (University of Cambridge; Cambridge, UK). It was used in conjunction with pMD2.G and psPAX2 to generate lentiviral particles empty, FLTNFR1 or Δ6TNFR1 lentiviral particles. The plasmid allows expression of cDNA cloned into downstream *BamHI* and *NotI* restriction sites under the control of the Spleen Focus Forming Virus (SFFV) promoter. Emerald GFP (EmGFP) expression is driven by the Ubiquitin promoter in *trans*.

psPAX2 is a second generation packaging plasmid that was used in the production of lentiviral particles and encodes the necessary enzymes and structural proteins. It expresses proteins from modified HIV-1 Gag and the HIV-1 Rev nuclear export signal (NES) under the control of the CAG promoter.

pMD2.G was used in the generation of lentivirus, and encodes the envelope protein; the G protein from the Vesicular Stomatis Virus (VSV), expressed under the control of the CMV promoter. The broad tropism of the VSV-G protein allows transduction of a wide variety of cell types.

sTNFR1-Fc and **DR5.CRD1-Fc** constructs were used for the production of Fc fusion proteins for use in immunoprecipitation, Surface Plasmon Resonance (SPR) and neutralisation assays. Constructs were kindly donated for this research by Prof. Richard Siegel, and use the pCDM7-Fc vector backbone. The CMV promoter drives expression of the CD5 leader sequence immediately upstream and in-frame with sTNFR1 and DR5.CRD1 proteins, ensuring their secretion. Proteins are fused at their N termini with human IgG1, yielding Fc-fusions. IgG1 has high affinity for protein A, facilitating purification and allowing use in pulldown experiments.

The **TNF-FLAG** construct was kindly donated by Prof. Richard Siegel and was used in the production of FLAG-tagged (DYKDDDDK) recombinant human TNF for use in immunoprecipitation and SPR studies. It encodes the sequence for human TNF under the control of the CMV promoter, in frame with the sequence for the FLAG tag at the C terminus.

pGL4.32[luc2P/NF-κB-RE/Hygro] (Promega) was used in NF-κB signalling reporter assays, and as the backbone for the generation of an XBP1 luciferase reporter construct. It has five, tandem copies of an NF-κB response element, that drive transcription of the firefly luciferase *luc2P* (*Photinus pyralis*) gene upon binding of when NF-κB.

pGL4.74[hRluc/TK] (Promega) was used as a transfection efficiency and viability control in luciferase reporter assays. It encodes the Rluc gene under the control of the minimal HSV-TK promoter, for constitutive, high expression.

2.1.3 DNA digestion by restriction enzymes

Purified DNA inserts and vectors were prepared for cloning by enzymatic cleavage at restriction sites using the appropriate restriction enzymes as follows:

Reagent	***Final Concentration/Volume***
10 X Digestion Buffer (NEB)	1 X
100 X BSA (NEB)	1 X
DNA template	X µl
Restriction enzymes (at 20 U/µl)	30 U each
dd H_2O	to 50 µl

Digestion reactions were performed in a heat block at 37°C for 2 h. In the case of vector digests, 1 µl of Calf Intestinal Phosphatase (CIP; NEB) was then added to digestion reactions and reactions were incubated for a further 30 min at 37°C. This removes 5' phosphate groups to minimise vector re-ligation during subsequent ligation reactions. The digested insert DNA was purified from restriction digest reactions using the Qiagen PCR purification kit (Qiagen), whilst digested vector DNA was resolved by electrophoresis in 1% TBE agarose. DNA bands at the correct molecular weight were excised and purified using the Qiagen Gel Extraction kit (Qiagen), to minimise contamination with non-digested vector in subsequent ligation reactions.

2.1.4 Ligation of vector and insert

Digested inserts and vectors were ligated together using the Rapid DNA Ligation Kit (Roche) as follows:

Reagent	*Final Concentration/Volume*
5 X DNA Dilution Buffer	1 X
Digested Insert and Digested Vector	Molar ratio of 3:1, X µl
2 X T4 DNA Ligation Buffer	1 X
T4 DNA Ligase (5 U/µl)	5 U
dd H_2O	to 20 µl

Ligation reactions were incubated at room temperature for 15 min. Control ligation reactions omitting either insert DNA or ligase were performed to test for vector re-ligation and/or incomplete vector digestion.

2.1.5 Transformation of chemically competent bacteria

Max Efficiency DH5α Competent Cells (Invitrogen) were transformed with vector DNA as follows. A vial containing 50 µl of cells was thawed on ice for 15 min. For transformation of ligations 2 µl of the reaction mixture was added to the thawed cells, and for supercoiled plasmids 10 ng of vector DNA was added. Following incubation on ice for 30 min, cells were heat-shocked in a water bath at 42°C for 30 s and then immediately incubated on ice for a further 2 min. 150 µl of room temperature SOC medium (Invitrogen) was added and then the vial was incubated at 37°C for 1 h with vigorous shaking. The contents of the vial were then pipette onto pre-warmed LB agar plates containing the appropriate selective antibiotic and spread using an ethanol-sterilised glass spreader. Plates were left to dry at room temperature for 1 h before being inverted and incubated for 16 h at 37°C.

2.1.6 Preparation of LB Agar and LB Broth

LB agar and LB broth were prepared from powder form (both Sigma-Aldrich) with ddH_2O according to the manufacturer's instructions and sterilised by autoclaving. Solutions were cooled to 50°C before the appropriate antibiotic was added to create selective LB agar and media. Media was stored at 4°C whilst LB agar was poured into 90 mm petri dishes (Sterilin) and allowed to set and dry before being stored at 4°C. The following final concentrations of antibiotic were used to select for bacteria transformed with the indicated vectors:

Antibiotic	*Concentration*	*Vectors/Constructs*
Ampicilin	100 µg/ml	pSPL3,TNFRSF1A_A, TNFRSF1A_G, TNFRSF1A_T, TNFRSF1A_C, pcDNA3.1, U1snRNA, pCG, SRp40, clone 3585060 (murine TNFR1 cDNA), clone 4131360 (human TNFR1 cDNA), clone 6172538 (human Fas cDNA) pHRsinUbEm, pMD2.G, psPAX2, clone 6146939 (human SRPRB cDNA), clone 5553465 (human GALNT cDNA), pGL4.32[luc2P/NF-kB-RE/Hygro], pGL4.74[hRluc/TK], luc2P/XBP1-RE
Kanamycin	50 µg/ml	pEYFP-N1, pECFP-N1, FLTNFR1-EYFP, Δ6TNFR1-EYFP, FLTNFR1-ECFP, Δ6TNFR1-ECFP, FAS180-EYFP, HA-FLTNFR1-EYFP, HA-sTNFR1-EYFP, HA-Δ6TNFR1-EYFP, HA-DR5.CRD1-EYFP, GalNAcT2-ECFP, SRβ-DSRED2, pRluc-N3, FLTNFR1-Rluc, Δ6TNFR1-Rluc
Zeocin	25 µg/ml	pGFP2-N3, pGFP2-Rluc, FLTNFR1-GFP2, Δ6TNFR1-GFP2
Ampicilin and Tetracycline	25 µg/ml and 7.5 µg/ml	sTNFR1-Fc, Δ6TNFR1-Fc, DR5.CRD1-Fc, TNF-FLAG

Table 2.1: Details of resistance encoded by vectors and concentrations of antibiotics used for selection.

2.1.7 Vector/construct propagation

The Qiaprep Miniprep Kit (Qiagen) and HiSpeed Plasmid Midi Kit (Qiagen) were used to yield quantities of vector or construct DNA necessary for downstream applications, according to the manufacturer's instructions:

2.1.7.1 Qiaprep Miniprep Kit

A single colony was selected from transformed bacteria that had been cultured on a selective antibiotic plate. This was used to inoculate a culture of 5 ml LB broth containing the appropriate antibiotic, and the culture was incubated for 16 h at 37°C with vigorous shaking. Bacterial cells were pelleted by centrifugation at 3,450 x *g* for 20 min at 4°C in a Heraeus Multifuge 3SR Plus (Thermo Scientific). Supernatant was discarded, the bacterial pellet was resuspended in 250 µl Buffer P1 and transferred to a 1.5 ml eppendorf tube. 250 µl of lysis Buffer P2 was added, the solution was mixed, incubated for 2 min at room temperature and 350 µl of neutralisation Buffer N3 was added. The solution was subsequently centrifuged for 10 min at 16,200 x *g* in a Heraeus Pico 17 Microcentrifuge (Thermo Scientific). The supernatant was subsequently applied to a QIAprep spin column over a collection tube and centrifuged at 16,200 x *g* for 1 min. Flowthrough was discarded and the column was washed with 750 µl Buffer PE by centrifugation at 16,200 x *g* for 1 min. After the flowthrough had been discarded, the column was centrifuged again empty at 16,200 x *g* for 1 min to remove residual Buffer PE. Finally, the 30-40 µl of ddH_2O was added to the column membrane, the column was left to stand for 1 min and then the vector DNA was eluted into a clean, new 1.5 ml eppendorf tube by centrifugation at 16,200 x *g* for 1 min.

2.1.7.2 Qiagen HiSpeed Plasmid Midi Kit

For larger preparations of vector DNA, 50 ml LB broth with selective antibiotic was inoculated and cultured at 37°C with vigorous shaking for 16 h. Bacterial cells were harvested by centrifugation at 3,450 x *g* for 20 min at 4°C in a Heraeus Multifuge 3SR Plus, and the supernatant was discarded. The bacterial pellet was resuspended in 6 ml of Buffer P1 by vortexing, 6 ml of Buffer P2 was added, the solution was mixed and left to lyse for 5 min at room temperature. 6 ml of chilled Buffer P3 was then added and mixed by inverting, before the lysate was applied to a QIAfilter Cartridge and incubated at room temperature for 10 min to allow precipitated cellular debris, proteins and genomic DNA to form a layer on top of the solution. A HiSpeed Midi Tip was then equilibrated with 4 ml of Buffer QBT and allowed to empty by gravity flow. The solution in the QIAfilter Cartridge was subsequently filtered into the equilibrated HiSpeed tip and allowed to pass through by gravity flow. The HiSpeed tip was then washed with 20 ml Buffer QC, before vector DNA was eluted from the HiSpeed tip with 5 ml of Buffer QF into a new, clean 50 ml falcon. DNA was precipitated by addition of 3.5 ml of isopropanol and incubation for 5 min at room temperature. The eluate/isopropanol mixture was then filtered through a QIAprecipitator Midi Module using a 20 ml syringe, and the Module was dried by forcing air through several times. Finally, vector DNA was eluted from the QIAprecipitator Midi Module using 500 µl of ddH2O and a 5 ml syringe. The eluate was passed through the Module a second time in the same way to increase the DNA yield.

Concentration and purity of isolated vector DNA was determined by measuring absorbance at 260nm and the 260nm/280nm ratio using a NanoDrop spectrophotometer (Thermo Scientific).

2.1.8 DNA sequencing and analysis

DNA sequencing was performed by the in-house WIMM DNA sequencing service, using the dideoxy termination method, an ABI Prism 377 DNA sequencer and the BigDye Terminator Cycle Sequencing

Reaction Kit (PE Biosystems). Sequence integrity was confirmed by analysis of automatically called base pairs from sequencing traces using BioEdit software, and sequence assembly and alignment was performed using Multalin ((Corpet, 1988); http://multalin.toulouse.inra.fr/multalin/) and DNA Baser (Heracle Biosoft) software.

2.1.9 Glycerol stocks of transformed bacteria

To store bacteria transformed with a plasmid vector, 500 µl of 80% (v/v with dd H_2O) filter-sterilised glycerol was added to 500 µl of an overnight bacterial culture and frozen at -80°C. Glycerol inhibits ice crystal formation that can damage the bacteria and compromise viability on thawing. Ethanol-sterilised loops were used to streak 10 µl of thawed culture on LB agar plates containing the appropriate selective antibiotic.

2.2 Molecular biological methods

2.2.1 Polymerase chain reaction

The polymerase chain reaction (PCR) was used to amplify target DNA sequences from reverse-transcribed cDNA, gDNA templates or vector DNA. The Expand High Fidelity^{PLUS} PCR System (Roche) was used, and reaction composition was as follows:

Reagent	***Final Concentration/Volume***
Forward Primer	0.3 µM
Reverse Primer	0.3 µM
PCR nucleotide mix (10 mM; Applied Biosystems)	0.2 mM
Expand High Fidelity^{PLUS} Buffer (5 X)	1 X
Expand High Fidelity^{PLUS} Enzyme Blend (5 U/µl)	2.5 U
DNA template	5-500 ng
PCR Grade H_2O	to 50 µl

Thermal cycling was performed on a DNA Engine Tetrad (MJ Research) as follows:

Step	***Temperature (°C)***	***Time (min)***
Enzyme Activation	94	2
Denaturation	94	0.5
Annealing	65, decreasing by 0.5 per cycle	0.5
Extension	68	1/Kb desired product
	Cycle to **step 2**, 10 times	
Denaturation	94	0.5
Annealing	60	0.5
Extension	68	1/Kb desired product
	Cycle to **step 5**, 20 times	
Final Extension	68	7
Cooling	4	∞

2.2.2 Overlap extension PCR

For the generation of chimeric or mutated DNA sequences, two separate PCR products ("A" and "B") were generated as in 2.2.1. The reverse primer of the A fragment and the forward primer of the B fragment were designed to have ~ 25 overlapping nucleotides at the point of junction or mutation. A and B fragments were then added in equal amount to a separate PCR reaction as template for the chimeric or mutated sequence.

2.2.3 RNA extraction

Total RNA was extracted from cells or tissues using the RNeasy Micro Kit (≤ 5 x 10^5 cells/≤ 5 mg starting tissue; Qiagen) or RNeasy Mini Kit (Qiagen). Cells or tissue were harvested and homogenised in the lysis Buffer RLT 1% β-ME using a blunt 20-gauge needle and an RNAse-free syringe or Dounce homogeniser (VWR) followed by a needle and syringe respectively. 1 volume of 70% Ethanol was added to lysates and mixed by pipetting before being applied to RNeasy Micro or Mini spin columns over collection tubes and centrifuged in a Heraeus Pico 17 Microcentrifuge at 16,200 x *g* for 30 s. The flowthrough was discarded and columns were washed with 700 µl of Buffer RW1 by centrifuging at 16,200 x *g* for 30 s. After the flowthrough had been discarded, the column was washed twice with 500 µl of Buffer RPE by centrifuging at 16,200 x *g* for 30 s, and then for 2 min. Flowthrough was discarded and residual buffer was removed by subsequently centrifuging at 16,200 x *g* for 5 min. 14 µl of RNAse-free H_2O was added to the centre of the spin column membrane over a clean, new 1.5 ml eppendorf, left to stand for 1 min and centrifuged at 16,200 x *g* for 1 min to elute the RNA. The quantity and quality of extracted RNA was determined by measuring the ratio of absorption obtained at 260 nm and 280 nm using a NanoDrop spectrophotometer.

2.2.4 Reverse transcription/cDNA synthesis

Reverse transcription of RNA to cDNA was performed using the High Capacity RNA-to-cDNA kit (Applied Biosystems). The reaction composition was as follows:

Reagent	***Final Concentration/Volume***
RT Buffer (2X)	1X
RT Enzyme (20X)	1X
RNA sample	up to 2 µg
RNAse-free H_2O	to 20 µl

Reverse transcription was performed on a DNA Engine Tetrad (MJ Research) as follows:

Step	***Temperature (°C)***	***Time (min)***
Amplification	37	60
Enzyme Inactivation	95	5
Cooling	4	∞

2.2.5 Quantitative Real-Time PCR (qRT-PCR)

Quantitative Real-Time PCR (qRT-PCR) analysis was performed using TaqMan Gene Expression Assays or custom-designed primer-probe mixes. TaqMan oligonucleotide probes were fluorescently labelled at the 5' with 6-carboxyfluorescin (6-FAM), and with either Minor Groove Binder (MGB) or tetramethylrhodamine (TAM) as a quencher at the 3', as indicated. For TaqMan Gene Expression Assays, reaction mixtures were as follows:

Reagent	*Final Concentration/Volume*
cDNA	2 µl
20 X TaqMan Gene Expression Assay	1 X
2 X TaqMan Mastermix	1 X
RNAse-free H_2O	to 20 µl

For custom-designed primer-probes:

Reagent	*Final Concentration/Volume*
cDNA	2 µl
Forward Primer	900 nM
Reverse Primer	900 nM
Probe	250 nM
2 X TaqMan Mastermix	1 X
RNAse-free H_2O	to 20 µl

Reactions were performed using the ABI Prism 7900HT Sequence Detection System and were analysed using SDS v. 2.4 software (Applied Biosystems), according to the manufacturer's instructions.

2.2.6 Separation of DNA by electrophoresis

2.2.6.1 TBE agarose

Tris-borate EDTA (TBE) agarose gels were used to resolve DNA fragments by size. Agarose (company details) was dissolved in TBE to make 1-2% (weight by volume) gels by melting using a microwave at 800W for 1 min 20 s. Gels were allowed to cool before Ethidium Bromide was added at a concentration of 0.5 µg/ml and the gel was poured into a casting tray supporting plastic combs, to create wells in the gel for sample loading. 4X Novex loading buffer (Invitrogen) was added to DNA

sample before gel loading and samples were subsequently electrophoresed in TBE using a Flowgen (company info) tank, at 75 V for 30-40 min depending on the size of the product and the percentage of the gel, using a PowerPac™ 300 (BioRad). DNA was visualised by ultra-violet (UV) irradiation in a GelDoc (BioRad). When excision of DNA bands was required for subsequent DNA extraction (2.2.7.2), a scalpel blade was used to cut a gel slice visualised under low intensity UV light.

2.2.6.2 TBE polyacrylamide

Pre-cast 5% Novex TBE polyacrylamide gels (Invitrogen) were used to resolve DNA fragments by electrophoresis in TBE in a Novex XCell SureLock™ Mini-Cell Electrophoresis System (Invitrogen), using a PowerPac™ 300 at 100 V for 30 min. 4X Novex loading buffer was added to samples prior to loading, and resolved DNA bands were visualised by gel staining with 1X SYBR® Gold Nucleic Acid Gel Stain (Invitrogen) in 1X TBE, with gentle rocking for 15 min in the dark at room temperature. DNA bands in stained gels were then imaged using a Biospectrum® 810 Imaging System (UVP) using the SYBR® Gold (485-655 nm) filter.

2.2.7 DNA purification

DNA was purified either directly from enzymatic reactions using the Qiagen MinElute PCR Purification Kit, or from agarose slices containing the DNA of interest using the Qiagen MinElute Gel Extraction Kit (both Qiagen). Purification was performed according to the manufacturer's instructions as follows:

2.2.7.1 Qiagen MinElute PCR Purification Kit

5 volumes of DNA binding Buffer PB were added to 1 volume of the enzymatic reaction, mixed and centrifuged in a MinElute column at 16,200 x *g* in a Heraeus Pico 17 Microcentrifuge for 1 min.

Flowthrough was discarded, and the column was washed with 750 µl of Buffer PE by centrifuging again at 16,200 x *g* for 1 min. Flowthrough was discarded and the column was centrifuged empty to remove residual Buffer PE. Finally, 20-40 µl of ddH_2O was added to the centre of the membrane in the column over a clean, new 1.5 ml eppendorf and left to stand for 1 min, before being centrifuged at 16,200 x *g* for 1 min to elute the DNA.

2.2.7.2 Qiagen MinElute Gel Extraction Kit

Excised gel slices were weighed and 3 volumes of agarose solubilisation Buffer QG was added to 1 volume of gel, and incubated at 50°C for 10 min. 1 gel volume of isopropanol was added to the sample, mixed by inverting and the sample was applied to a MinElute column over a collection tube and centrifuged at 16,200 x *g* in a Heraeus Pico 17 Microcentrifuge for 1 min. The flowthrough was discarded and the column was washed with 500 µl of Buffer QG to remove residual agarose from the column by centrifugation at 16,200 x *g* for 1 min. Flowthrough was discarded and the column was then washed with 750 µl of Buffer PE by centrifugation at 16,200 x *g* for 1 min. The flowthrough was discarded and the column was centrifuged empty to remove residual Buffer PE. Finally, DNA was eluted into a clean, new 1.5 ml eppendorf by addition of 20-40 µl of ddH_2O to the centre of the membrane which was left to stand for 1 min, before being centrifuged at 16,200 x *g* for 1 min.

Concentration and purity of DNA was determined as above (2.1.7) using a NanoDrop spectrophotometer.

2.2.8 Sodium Dioecyl Sulphate Polyacrylamide Gel Electrophoresis (SDS-PAGE)

SDS polyacrylamide gels were prepared in a laminar flow fume hood using Mini-Protean II protein gel apparatus (BioRad), with 1.5 mm glass spacer plates and combs. 12.5% polyacrylamide resolving gels were first cast as follows:

12.5% Separating gel

3.3 ml H_2O

4.2 ml Acrylamide/Bisacrylamide (30/0.8%)

2.5 ml 1.5 M Tris HCl, pH 8.8

100 µl 10 % SDS (w/v in ddH_2O)

40 µl 10 % Ammonium Persulphate (APS; w/v in ddH_2O; Sigma)

12 µl *N*,*N*,*N*',*N*'-tetramethyl-ethane-1,2-diamine (TEMED; Sigma)

After polymerisation had been initiated by addition of TEMED, the mixture was pipetted between the glass to form a gel 10 cm in length, overlayed with isopropanol to remove bubbles and allowed to set for 15 min. 4% polyacrylamide stacking gels were then prepared:

4% Stacking gel

6.2 ml H_2O

1.3 ml Acrylamide/Bisacrylamide (30/0.8%)

2.5 ml 0.5 M Tris HCl, pH 6.8

100 µl 10 % SDS

200 µl 10 % APS

15 µl TEMED

Isopropanol was removed and stacking gel was pipetted on top of the resolving gel to form a gel 1 cm in length. The gel comb was inserted immediately (before polymerisation) to create sample wells.

Protein samples to be resolved were prepared by 1:1 dilution with either non-reducing 2X Laemmli buffer (4% (w/v) SDS, 20% (v/v) glycerol, 0.004% (w/v) bromphenol blue and 125 mM Tris HCl, pH 6.8) or reducing Laemmli buffer (as for non-reducing but with 10% (v/v) β –mercaptoethanol) and boiled in a heat block at 95°C for 5 min.

Gels were submerged in Tris-Glycine running buffer (25 mM Tris-HCl, 192mM Glycine, 0.1% (w/v) SDS) in a BioRad gel tank and prepared samples were loaded to wells. The SeeBlue® Plus2 Pre-stained Standard (Invitrogen) was also loaded to monitor the progress of electrophoresis and for the inference of the molecular weights of resolved proteins. Electrophoresis was performed with a PowerPac™ 300 at 100 V for approximately 2 h, or until sufficient separation of proteins had been achieved.

2.2.9 Visualisation of resolved proteins

Resolved proteins were visualised using the SimplyBlue™ SafeStain Coomassie G-250 reagent (Invitrogen) according to the manufacturer's instructions. After electrophoresis, gels were placed in 100 ml of ddH_2O in a covered container and microwaved at 850 W for 1 min. Gels were then shaken on an orbital shaker for 1 min at room temperature and the water was discarded. This process was repeated a further two times, before 30 ml of SimplyBlue™ SafeStain was added to the gel and microwaved for 1 min. The gels were then shaken at room temperature for 5 min, before being washed with 100 ml ddH_2O for 10 min and with 120ml 33.3% (w/v) NaCl in ddH_2O to de-stain the gel and visualised protein bands.

2.2.10 Quantification of proteins

Protein concentrations were determined either by measuring the absorbance at 280 nm (A280) using a NanoDrop spectrophotometer, or using the BioRad Protein Assay (BioRad) according to the manufacturer's instructions. Briefly, 20 µl aliquots of concentrated supernatant were diluted and mixed into 500 µl aliquots of 1X Protein Assay Dye Reagent (BioRad) in triplicate, and optical density (OD) of samples was measured at 595 nm using a SmartSpec™ Plus spectrophotometer (BioRad). Concentrations of proteins in concentrated supernatants were determined by using an equation

derived from standard curve titrations performed using 10 point serial dilutions (triplicates of each point) of known amounts of BSA.

2.2.11 Western blot

Detection of specific proteins amongst those resolved by SDS-PAGE was achieved by fluorescent immunoblotting. Proteins were transferred to Amersham Hybond ECL Nitrocellulose Membranes (GE Healthcare) in 25 mM Tris-HCl, 190 mM Glycine using the Mini Trans-Blot System (BioRad) and a PowerPac™ 300 at 100 V for 1 h at 4°C. Following transfer, membranes were blocked at room temperature for 1 h with rocking using Odyssey Blocking Buffer (LI-COR Biotechnology). Membranes were subsequently probed with primary antibodies diluted in Odyssey Blocking Buffer at 4°C for 16 h. Following three, 10 min, room-temperature washes with PBS 0.1% Tween 20 (PBST), membranes were incubated for 1 h at room temperature with the appropriate IRDye®-conjugated secondary antibody (LI-COR Biotechnology) diluted in PBST with 0.01% SDS, at a final concentration of 0.1 µg/ml. Membranes were subsequently washed three times for 10 min with PBST, twice for 10 min with PBS and then were visualised by scanning membranes on an Odyssey Infrared Imaging System (software version 2.0; LI-COR Biotechnology).

2.2.12 Enzyme-Linked Immunosorbent Assay (ELISA)

Enzyme-Linked Immunosorbent Assay (ELISA) was used for absolute and relative quantification of proteins of interest in cell culture supernatants. For sandwich ELISAs, capture antibodies were diluted in PBS and added to wells of 96 well FluoroNunc plates (Thermo Scientific). Plates were sealed with adhesive film incubated for 16 h at room-temperature. Coating antibody solution was aspirated and wells were washed 6 times with 300 µl of PBST. Remaining protein binding sites of wells were blocked by addition of 200 µl of 1% BSA (Sigma) in PBST for 2 h at room temperature, with shaking on an orbital shaker. Blocking solution was then aspirated and wells were washed 6

times with PBST before replicates of serial dilutions of cell culture supernatants in PBS were applied to wells. Plates were sealed and incubated for 2 h at room temperature with shaking. Test samples were subsequently aspirated and wells were washed 6 times with PBST before biotinylated secondary antibodies diluted in PBS, 0.1% BSA were added, plates were sealed and incubated at room temperature for 1 h with shaking. After 6 PBST washes, wells were incubated with DELFIA Europium-conjugated Streptavidin (Perkin-Elmer; 0.1 µg/ml) diluted in DELFIA assay buffer (Perkin Elmer) for 1 h at room temperature with shaking. Europium-streptavidin solution was aspirated, and after a final 6 PBST washes 100 µl of DELFIA Enhancer Solution (Perkin Elmer) was added to each well, plates were incubated for 10 min at room temperature in the dark, and fluorescence was read at 340/612 nm (excitation/emission) using a Victor 1420 (Wallac). Values from serial dilutions of protein standards were used to plot titration curves and allowed absolute quantification of amounts of protein cell culture supernatant. Indirect ELISAs were performed as above, except that there was no coating antibody step and samples were captured directly to wells before blocking with PBS, 1% BSA, followed by capture with biotinylated antibody.

2.3 Cell biology

2.3.1 Mammalian cell culture

All procedures were performed in HEPA-filtered microbiological safety cabinets to maintain sterility, and all cell lines were cultured at 37°C in an atmosphere of 5% CO_2. HEK 293T, HeLa, HT1080, U937, Jurkat, RAW264.7 and L929 cells were all obtained from the American Type Culture Collection (ATCC). Adherent cell lines (HEK 293T, HeLa, HT1080, RAW264.7 and L929) were maintained in Dulbecco's Modified Essential Medium (DMEM; Sigma), whilst the Jurkat and U937cell lines were cultured in suspension, in Roswell Park Memorial Institute medium (RPMI 1640; Sigma). All cell culture media was supplemented with filter-sterilised 10% (v/v) Fetal Bovine Serum (FBS; Sigma), 100 U/ml Penicillin-Streptomycin Solution (Sigma) and 2 mM L-Glutamine (Sigma). HEK-Blue™ TNF-

α/IL-1β cells were obtained from Invivogen, and cultured in DMEM in the presence of 25 µg/ml Zeocin, for maintenance of the stably transfected SEAP reporter construct.

2.3.2 Thawing, counting, subculturing and freezing of cells

Cells that had been stored in liquid nitrogen or shipped on dry ice were thawed rapidly in a water bath at 37°C, washed by drop-wise addition of 30 ml growth medium warmed to 37°C, followed by centrifugation at 900 x *g* in a Heraeus Multifuge 3SR Plus for 6 min. Cells were resuspended and counted by dilution of a small aliquot with Trypan Blue solution (Sigma) counting of cells microscopically using a haemocytometer. Cells were then seeded in cell culture vessels at an appropriate density.

Cell lines were subcultured as follows. Confluency of adherent cells growing in a monolayer was assessed by microscopy. When cells were 70-80% confluent, cell culture supernatant was removed and discarded. Sterile PBS warmed to 37°C was used to wash residual medium and discarded, before enough pre-warmed trypsin-EDTA (Lonza) was added to cover the surface of the cell culture vessel. Cells were incubated in trypsin-EDTA for 5 min (HEK 293T, and HEK-Blue™ TNF-α/IL-1β cells) or 10 min (HeLa, HT1080, RAW264.7 and L929 cells) until they had become detached. An excess of 37°C culture medium was added to inactivate the protease activity of trypsin. The cell suspension was then centrifuged at 1000 x *g* in a Heraeus Multifuge 3SR Plus for 6 min and resuspended in an appropriate volume for counting. After counting, the appropriate volume of cell suspension was transferred to a new culture vessel, supplemented with an appropriate volume of culture medium and returned to the incubator at 37°C, 5% CO_2.

To Freeze cells for storage in liquid nitrogen, cells were harvested and counted as above, centrifuged at 1000 x *g* for 6 min and resuspended at a density of 3 x 10^6 cells/ml in filter-sterilised FBS

containing 10% (v/v) dimethyl sulphoxide (Sigma). 1 ml aliquots of the cell suspension were transferred to cryovials (Nunc) and placed in a Nalgene 'Mr. Frosty' freezing container cooled to 4°C, and placed in a -80°C for 48 h. The freezing container allows very gradual cooling of the cells, preserving viability on thawing. Finally, cells were transferred to liquid nitrogen for storage.

2.3.3 Transient transfection

HEK 293T, HT1080 and HeLa cells were transiently transfected using GeneJuice® Transfection Reagent (Novagen), a protein/polyamine-based method of transfection, according to the manufacturer's instructions. 16 h prior to transfection, cells were seeded in cell culture vessels as follows:

For HEK 293T cells:

Culture vessel	**Total number of cells**	**Volume of culture medium (ml)**
24 well plate	6.3×10^4	0.5
12 well plate	1.25×10^5	1
6 well plate	2.5×10^5	2
T75	2×10^6	17
T175	5×10^6	40

For HeLa, HT1080, L929 and RAW 264.7 cells:

Culture vessel	Total number of cells	Volume of culture medium (ml)
24 well plate	1×10^5	0.5
12 well plate	2×10^5	1
6 well plate	4×10^5	2
T75	3×10^6	17
T175	7×10^6	40

Complexes were prepared in Opti-MEM reduced-serum medium (Invitrogen) as follows. 3 µl of GeneJuice® was mixed with 100 µl of room-temperature Opti-MEM per µg of DNA to be transfected and incubated at room temperature for 5 min. DNA was then added, mixed and incubated at room temperature for 20 min. Complexes were then added drop-wise to wells, mixed by swirling and incubated at 37°C in 5% CO_2 for the desired amount of time before analysis or use in downstream applications.

2.3.4 Flow cytometry

Flow cytometry was used to analyse protein expression in transfected cells and primary human immune cells. Proteins of interest were immunostained using either fluorescently-conjugated primary antibodies, or with unconjugated primary antibodies followed by staining with fluorescently-conjugated secondary antibodies. Cells were pelleted by centrifugation in V-bottomed, 96-well plates (BD Falcon) in a Heraeus Multifuge 3SR Plus at 300 x *g* for 2 min at 4°C. Supernatants were discarded and cells were stained by resuspension in PBS, 2% FBS (v/v; Sigma) containing the appropriate antibody. Excess, unbound antibody was removed by centrifugation followed by resuspension in 200 µl of PBS, 2% FBS twice, to wash the cells. Finally, cells were re-suspended in

500 μL of PBS 2% FBS, samples were run using a FACS (fluorescence activated cell sorting) Calibur (BD Biosciences) and staining was analysed using a Summit 4.3 software.

2.3.5 Human blood sample work

2.3.5.1 Recruitment of donors and ethical approval

Healthy white European donors (without self-reported autoimmune disorders) were recruited under the Oxford Research Ethics Committee (REC) B approved study reference 10/H0605/5 (Studying molecular mechanisms of action of genes with relevance to multiple sclerosis in healthy controls). Ages ranged between 20 and 61 years (mean = 33.38 years) and 70% were female.

Rs1800693 was genotyped by Dr. Calliope Dendrou and Miss Lydia Lambert using a TaqMan® SNP Genotyping Assay according to the manufacturer's instructions. Genotyping data were scored independently by two operators to minimise error.

For the purposes of this study, individuals of known rs1800693 genotype were recruited for donation of 50 ml blood samples by venesection. Organisation and co-ordination of blood donations was performed by Dr. Calliope Dendrou with help from Dr. Kate Attfield, Miss Lydia Lambert and Miss Laura Millican.

All donor blood work – PBMC isolations, RNA preparation, qRT-PCR, whole-blood immunostainings, monocytes cultures and western blots – was performed with the help and under the guidance of Dr. Calliope Dendrou.

2.3.5.2 Isolation of plasma, peripheral blood mononuclear cells and polymorphonuclear cells

Before processing, all blood samples were mixed and allowed to equilibrate to room temperature by rotation at for 30 min. Samples were centrifuged in a Heraeus Multifuge 3SR Plus at 400 x *g* for 5 min and the supernatant was taken as plasma, and stored at -80°C for downstream analysis. Thereafter, blood samples were diluted 1:1 in RPMI 1640 (Sigma-Aldrich) and 25 ml aliquots were carefully layered onto 15 ml of Lymphoprep™ separation media (Axis-Shield) in 50 ml falcons. Samples were then centrifuged at 800 × *g* for 20 min without braking. Peripheral blood mononuclear cells (PBMCs) were recovered using disposable Pasteur pipettes from the interface between the Lymphoprep™ and plasma fractions, and transferred to pre-chilled 50 ml falcon tubes on ice. Isolated PBMCs were subsequently washed twice with 50 ml ice-cold PBS containing 2 mM EDTA and 10% human AB serum (PAA) with centrifugations at 400 x *g* for 10 min at 4°C. PBMCs from each donor were then pooled in ice-cold PBS containing 2 mM EDTA and 10% human AB serum, the volume of the cell suspension was adjusted to 5 ml and cells were counted using trypan blue and a haemocytometer as described in 2.3.2.

Polymorphonuclear cells (PMNs) were isolated from the erythrocyte/granulocyte fraction of the Lymphoprep™ gradient by removal of plasma and Lymphoprep phases, and lysis of erythrocytes. The pellet was resuspended in 20 ml 1 X RBC Lysis Buffer (BioLegend) and incubated at room temperature for 20 min. Cells were pelleted by centrifugation at 400 x *g* for 10 min, and the supernatant was discarded. The pellet was resuspended again in 20 ml 1 X RBC Lysis Buffer and incubated for 20 min at room temperature, the cells were pelleted by centrifugation at 400 x *g* for 10 min and supernatant was discarded, yielding polymorphonuclear leukocytes.

2.3.5.3 Magnetic sorting of human immune cell subsets

$CD14^+$ monocytes were isolated from PBMCs by positive selection using human CD14 MicroBeads (Miltenyi Biotec), and $CD3^+$ T cells were subsequently isolated from the $CD14^-$ population using human CD3 MicroBeads (Miltenyi Biotec). All isolations were performed on LS columns (Miltenyi Biotec) using a QuadraMACS™ magnet (Miltenyi Biotec) according to the manufacturer's instructions. After PBMCs had been counted (2.3.2) the volume was adjusted to 20 ml with ice-cold PBS, 2 mM EDTA, 10% human AB serum and cells were pelleted by centrifugation at 400 x *g* for 10 min at in a Heraeus Multifuge 3SR Plus 4°C. Cells were resuspended in PBS containing 2 mM EDTA and 10% human AB serum to 1.25 x 10^8 cells/ml. 20 µl of human CD14 MicroBeads were then added to samples per 1 x 10^7 cells and were then mixed gently by vortexing and incubated on ice for 15 min. Samples were subsequently washed by addition of 40 ml PBS, 2 mM EDTA, 10% human AB serum and centrifugation at 400 x *g* for 10 min at 4°C, and the pellet was resuspended in 500 µl PBS, 2 mM EDTA, 10% human AB serum and applied to LS columns in a QuadraMACS™ magnet, that had been equilibrated with 3 ml PBS, 2 mM EDTA, 10% human AB serum. Column flowthrough was collected in a 15 ml falcon, and LS columns were washed 3 times with 3 ml PBS, 2 mM EDTA, 10% human AB serum. Purified $CD14^+$ cells were subsequently eluted from LS columns by removal of the column from the QuadraMACS™ magnet, positioning over a clean, new 15 ml falcon, addition of 5 ml PBS, 2 mM EDTA, 10% human AB serum to the column and flushing of cells from the column using a plunger. Positively selected $CD14^+$ were subsequently counted as described in 2.3.2 before use in downstream applications. Negatively selected cells in the flowthrough of the CD14 MicroBead purification were pelleted by centrifugation at 400 x *g* for 10 min at 4°C, and CD3 positive cells were subsequently purified using human CD3 MicroBeads using LS columns and a QuadraMACS™ magnet as described above.

Cell subset purity was confirmed by staining aliquots of purified and non-purified and negatively selected populations with PerCP-Cy5.5-conjugated anti-CD14 (clone HCD14, BioLegend), FITC-conjugated Mouse Anti-Human CD3 (clone UCHT1, BD Pharmingen) and analysis by flow cytometry.

2.4 Replication and statistics

Apart from work with scarce and valuable donor samples, each individual experiment in this thesis was performed a minimum of three independent times, and figures and data sets shown are representative. The number of replicates for each condition within individual experiments was three unless otherwise stated. All statistical tests were performed using GraphPad Prism and the R statistical software package. Regression analysis to test for correlations between rs1800693 genotype and TNFR1 transcript levels in human immune cell subsets used a Bonferroni correction for multiple testing (taking a *P* value of 0.05 and considering three independent hypotheses for the three human immune cell subsets); the significance threshold estimated was $P = 0.017$. All other statistical analyses used a significance threshold of 5%. For statistical analysis of quantification of colocalisation in confocal microscopy studies, paired Student's T tests were used, whilst for all other statistical analyses, unpaired Student's T tests were performed.

2.5 Intellectual contributions

Inspiration for experiments performed in this thesis came from regular lab meetings and private discussions with members of the Fugger lab. My particular thanks go to Professor Lars Fugger, Dr. Calliope Dendrou and Dr. Kate Attfield for their suggestions for specific assays, help in their design and interpretation of the results.

3.0 Investigation of the influence of rs1800693 on the splicing of *TNFRSF1A* exon 6

3.1 Introduction

We first investigated the ability of the MS-associated rs1800693^{G} allele to influence the processing of mRNA transcribed from *TNFRSF1A*, and attempted to characterise the responsible molecular mechanisms. Furthermore, we attempted to establish a mouse model to mirror the splice-influencing effect of the SNP, for the investigation of potential functional, disease-level consequences.

3.1.1 *In silico* investigation of alternative splicing

Candidates for mutations altering normal pre-mRNA splicing are identified by their proximity to 5' and 3' splice sites, branch points, polypyrimidine tracts (such that they might interfere with sequence recognition of spliceosomal components, splice-regulatory proteins or create an RNA secondary structure non-permissive to the association of necessary RNPs) and by their immediate genetic context (such that they might generate a novel, cryptic splice site) (Chen and Manley, 2009; Majewski and Ott, 2002). A variety of informatics tools are available to help predict whether a particular variant will give rise to the above changes, that may ultimately result in an alternative splicing event to that produced by the ancestral allele (Baralle *et al.*, 2009). Donor site, acceptor site and branch point evaluation software are the most reliable programmes, as these are the most conserved sites influencing splicing. Splice regulatory element prediction software queries input sequences against databases of evolutionarily conserved putative and/or experimentally-validated RNP binding motifs, whilst RNA secondary structure programmes predict folding of a given sequence based on minimum energy of structures and pairing probabilities, but are biased by the length of the sequenced analysed. However, as discussed earlier, splicing makes use of loose consensus sequences and takes place in the context of both immediate and distal *cis* and *trans* factor

associations, and in the context of *trans* factor availability and RNA secondary structures. Moreover, the molecular mechanisms, associations, hierarchies and direction of splice factor bias of splicing (ie. promoting or disrupting exon definition) are incompletely understood and so the results of *in silico* analysis must be validated experimentally (Baralle *et al.*, 2009; Houdayer *et al.*, 2008).

3.1.2 Functional assays of splicing

Splicing can be analysed *in vitro* by transient transfection of minigene constructs and analysis of the products of splicing of RNA transcribed from minigenes corresponding to mutant compared with the ancestral allele of a SNP (Cooper, 2005). The SNP and its flanking genomic region of introns and exons are typically cloned into a mammalian expression vector and expressed in a human cell line by transient transfection. RNA is then harvested and reverse-transcribed into cDNA and PCR is performed with cDNA-specific primers flanking the region of interest to assay whether it has been alternatively spliced. Alternatively, minigene plasmids with constitutively spliced vector exons that flank the cloned genomic region of interest can be used, and the final PCR step is performed with primers specific to sequences in the vector exons. PCR products are then resolved in agarose gels and bands are sequenced to determine splicing. This is a quick, easy and reliable technique for identifying splice-influencing variants, but it has several caveats. Variation has been shown to effect the splicing of regions at a distance of up to ~ 10 kb, meaning an unfeasibly sized insert would be required for cloning into a minigene to detect this (Baralle *et al.*, 2009). Furthermore the system is artificial and relies on the relevant trans-acting RNP factors being expressed as they are in the tissue of interest for variant-associated changes in splicing to be observed (Baralle *et al.*, 2009). False negatives are therefore a problem associated with minigene analysis of splicing and in any case, putative splicing-influencing variants must be confirmed by RNA analysis from the appropriate tissue.

Splicing of a region of interest can also be analysed by PCR with cDNA-specific primers flanking the region, on cDNA transcribed from RNA isolated from the relevant tissues of individuals of each genotype for the variant (Johnson *et al.*, 2003). Products can be visualised and sequenced as above, and the relative abundance of splice variants can be determined. Quantitative Real-Time PCR (qRT-PCR) cDNA can also be used to quantify the exact amount of a defined RNA target (for example, an exon of interest) in tissues, allowing differential splicing by genotype to be detected (Vandenbroucke *et al.*, 2001). Furthermore, tissue samples can be taken at developmental/disease states of interest to see if these have an influence on splicing.

The influence of rs6897932 on the splicing of *IL7RA* exon 6 was analysed by Gregory *et al.* using minigenes corresponding to the ancestral 'T' or risk-associated 'C' allele. They found a ~ 2 fold increase in skipping of exon 6 associated with the rs6897932^{C} allele (Gregory *et al.*, 2007). This finding was subsequently verified *in vivo* by qRT-PCR analysis of the expression of exons 6-7 compared to control exons 3-4 and 9-10, in PBMCs isolated from TT homozygotes, TC heterozygotes and CC homozygotes for rs6897932; CC homozygotes were found to have a 4-5 fold increase in skipping of *IL7RA* exon 6 when compared with TT homozygotes (Gregory *et al.*, 2007).

3.1.3 Identifying *trans*-acting factors

The specific RNPs involved in an alternative splicing event can be identified through RNA pulldown experiments (Iioka *et al.*, 2011). In this technique, RNA fragments corresponding to the different alleles of the splice-mediating variant are transcribed *in vitro* and immobilised to beads. They are then incubated with nuclear protein extract, washed and proteins bound to RNA probes are eluted and analysed by SDS-PAGE followed by Coomassie staining for visualisation, and/or by western blot to probe for specific candidate proteins. Whilst this method is potentially informative, *in vitro*

transcribed RNA fragments are much shorter and are likely to fold differently to *in vivo* transcripts (Baralle and Baralle, 2005). Candidate RNPs identified using pulldown experiments must therefore be further investigated through analysing the effects of their overexpression, siRNA knockdown and knockdown followed by complementation in the splicing of the region of interest, either in tissues from donors with the relevant genotypes or using minigene systems (Cooper, 2005).

3.1.4 Models of MS-associated genetic variants

Experimental dissection of the molecular mechanisms by which MS-associated variants predispose to the development of the disease in humans is not possible. However, mouse models of MS-associated genetic variants have proven to be a useful surrogate. For example, humanised transgenic mice expressing HLA class II molecules and human MS patient-derived TCRs have been used to better understand the mechanisms underlying the association of the DR-2 haplotype with MS (Fugger *et al.*, 2009). Mice expressing the HLA-DR2b molecule as well as a TCR capable of recognising a myelin antigen develop a PPMS-like disease. However, mice that additionally express the HLA-DR2a develop milder, RRMS-like disease. The disease-modifying effect of DR2a was shown to be as a result of the deletion of T cells recognising myelin antigen presented in the context of DR2a in triply transgenic mice (Fugger *et al.*, 2009).

3.1.5 Splice-switching oligonucleotides

Splice-switching oligonucleotides (SSOs) are an antisense technology that can be used to artificially re-direct splicing to generate splice variant isoforms of a target protein (Aartsma-Rus and van Ommen, 2007; Hammond and Wood, 2011). SSOs bind to their complimentary RNA sequence, competing with the splice-mediating RNPs that usually bind to the target region, thereby disrupting the normal processing of pre-mRNA. SSOs are synthesised such that they have modified oligonucleotide backbones, preventing their digestion by cellular RNAse enzymes. In this way, rather

than invoking RNA interference mechanisms which would result in the degradation and consequent knockdown of the target RNA sequence, transcript processing is skewed, and so SSOs can be used to simultaneously downregulate the expression of certain protein isoforms and upregulate others (Aartsma-Rus and van Ommen, 2007; Bauman *et al.*, 2009).

SSOs have been used to successfully re-direct splicing *in vitro* in mammalian cell culture, and *in vivo* in both mice and humans (Cartegni and Krainer, 2003; Graziewicz *et al.*, 2008; Kalbfuss *et al.*, 2001; van Deutekom *et al.*, 2007). Most strikingly, an SSO for the treatment of Duchenne Muscular Dystrophy (DMD) has completed two Phase I clinical trials in humans and is set for a Phase II trial (Goyenvalle and Davies, 2011). The SSO is used to induce skipping of dystrophin exon 51 which in some DMD patients contains a mutation that results in a frameshift and the production of a non-functional isoform of the protein. Removal of exon 51 from the mature dystrophin transcript results in the production of a truncated but functional dystrophin isoform, slowing disease progression and improving muscle function of DMD patients (van Deutekom *et al.*, 2007; Wood *et al.*, 2010).

The penetrance, potency, stability and toxicity of SSOs varies with the nature of the modified oligonucleotide backbone selected and, along with modifications for improved uptake efficiency, delivery and targeting, are active and important areas of research in the development of SSO technologies for therapy in humans (Bauman *et al.*, 2009). For research purposes in animal models, several studies have shown that complimentary 16-mer alternating DNA and locked nucleic acid (LNA) oligonucleotides are potent inducers of splice-switching *in vitro* and are capable of effectively, stably and durably inducing splice variant production upon injection in mice *in vivo*, with minimal toxicity (Graziewicz *et al.*, 2008; Roberts *et al.*, 2006). LNA is similar to RNA, except that the ribose moiety is modified such that the 2’ oxygen and 4’ carbon atoms are linked by a methylene group, ‘locking’ the ribose in the 3’ *endo* conformation (Wengel *et al.*, 2001).

3.2 Methods

3.2.1 Construction of *TNFRSF1A* rs1800693 minigenes

TNFRSF1A 'A' and 'G' minigene constructs were made previously by Divya Punwani, DPhil under the supervision of Prof. Lars Fugger. 'T' and 'C' minigene constructs were made by overlap extension PCR as described in 2.2.2, using the following primers:

Name	***Sequence***
Afrag_F	5'-TACTGGATCCATGCTGACAACCAACTCCTCTCTGGC-3'
Bfrag_R	5'-TACTGCGGCCGCTTAGGAGAAACTCACTGTCTAGGCTCT-3'
Tallele_Afrag_R	5'-TGGGCACCAGGTCACATCTCCTCACCTGAGTCC-3'
Tallele_Bfrag_F	5'-GGACTCAGGTGAGGAGATGTGACCTGGTGCCCA-3'
Callele_Afrag_R	5'-TGGGCACCAGGTCACGTCTCCTCACCTGAGTCC-3'
Callele_Bfrag_F	5'-GGACTCAGGTGAGGAGACGTGACCTGGTGCCCA-3'

Table 3.1: Primers for generating rs1800693 'T' and 'C' allele minigene constructs.

The final inserts incorporated *XhoI* (CTCGAG) and *NotI* (GCGGCCGC) restriction enzyme sites at the 5' and 3' respectively. Inserts corresponding to *TNFRSF1A*'T' and 'C' alleles were then cloned (2.1.1) into the pSPL3 vector (2.1.2).

3.2.2 Minigene assays

Cos-7, HeLa and HEK 293T cells used in minigene assays were transfected with rs1800693 A, G T or C minigene constructs essentially as described in 2.3.3. Briefly, cells were seeded in wells of 6 well plates as in 2.3.3 and transfected with 1 µg of minigene construct DNA the 16 h later using the GeneJuice® Transfection Reagent (2.3.3) in triplicate. 24 h later, cell culture supernatant was

removed, cells were washed with 1 ml PBS warmed to 37°C and harvested by trypsinisation for 5-10 min at 37°C, then transferred to 1.5 ml eppendorfs (2.3.2). Cells were then pelleted by centrifugation in a Heraeus Pico 17 Microcentrifuge for 5 min at 1,500 x *g*, the supernatant was discarded and then total RNA was isolated using the RNeasy Micro Kit as described in 2.2.3, and quantified using a NanoDrop Spectrophotometer. cDNA was prepared from RNA using the High Capacity RNA-to-cDNA Kit (2.2.4), and 2 µl of the reaction products was used as DNA template in a PCR reaction (2.2.1) using the primers in SD_F (5'-GTGAACTGCACTGTGACAAGCTGC-3') and SA_R (5'-CACCTGAGGAGTGAATTGGTCG-3'), specific for sequence in the pSPL3 vector exons SD and SA, respectively.

The PCR reaction products were then resolved in 2% TBE agarose (2.2.6.1) or 5% TBE polyacrylamide gels (2.2.6.2) and resolved bands were visualised. Where appropriate, bands were excised from TBE agarose gels, DNA was purified (2.2.7.2) and sequenced using the primers in SD_F and SA_R as described in 2.1.8.

3.2.3 Analysis of *TNFRSF1A* transcripts in human immune cells

Blood samples were taken from healthy donors by venesection, and peripheral blood immune cell subsets were isolated as described in 2.3.5.2 and 2.3.5.3. Total RNA was isolated from cells using the RNeasy Mini Kit (2.2.3) and was reverse transcribed into cDNA as described in 2.2.4. Analysis of *TNFRSF1A* exon 6 splicing was performed using several techniques:

3.2.3.1 PCR using cDNA-specific primers flanking exon 6

PCR was performed (2.2.1) on 2 µl donor peripheral blood immune cell cDNA using a forward primer spanning the boundary between exons 4 and 5 (5'-ACCGTGTGCACCTGCCATGC-3') and a reverse primer spanning the boundary between exons 9 and 10 (5'-GGCACGTTCTCCACCACGGC-3'). PCR

products were resolved in agarose or TBE polyacrylamide gels and visualised as described in 2.2.6, respectively. Bands were excised from agarose gels, DNA was isolated using the Qiagen MinElute Gel Extraction Kit (2.2.7.2) and sequenced using the same primers as for PCR amplification, as described in 2.7.8. Percentage skipping of *TNFRSF1A* of exon 6 was determined by quantification of bands corresponding to the full-length transcript and that of transcripts lacking exon 6 (FL_TNFR1 and Δ6_TNFR1, respectively), adding these values together to give a value for the 'total' amount of *TNFRSF1A* transcripts, dividing this by the value obtained for the amount of Δ6_TNFR1 transcripts and then multiplying this number by 100.

3.2.3.2 qRT-PCR

Quantitative real-time PCR analysis was performed as described in 2.2.5. Expression levels of *TNFRSF1A* exons 3-4 and 6-7 were analysed using TaqMan® Gene Expression Assays Hs00533562_g1 and Hs00533565_g1 respectively (Applied Biosystems). A custom primer probe set spanning the exon 5-7 boundary was designed to allow the specific detection of *TNFRSF1A* transcripts lacking exon 6 (Table 3.2). Expression levels were measured relative to the housekeeping gene encoding Glyceraldehyde-3-Phosphate Dehydrogenase (*GAPDH*; Hs02758991_g1). Expression levels are given as ΔCT, calculated by subtracting the cycle threshold value (the cycle number at which signal is first detected) for GAPDH from the cycle threshold value for each transcript. Lower ΔCT values indicate higher expression. Cycle thresholds were in the exponential phase of amplification, so a 1 ΔCT difference is equivalent to a 2-fold change in RNA levels.

Name	*Sequence*
Δ6_TNFR1_F	5'-TACCGGCATTATTGGAGTGA-3'
Δ6_TNFR1_R	5'-CAACAGCACTGTGGTGCTTAC-3'
Δ6_TNFR1_probe	5'-6FAM-CGTGCACCTCTCCTGCCAGG-MGB-3'
EmGFP_F	5'-TACAACAGCCACAAGGTCTA-3'
EmGFP_R	5'-AATTGGTGCTAGGTAGTGGT-3'
EmGFP_probe	5'-6FAM-GCATCAAGGTGAACTTCAAGACCC-MGB-3'

Table 3.2: Custom-designed primer-probes for qRT-PCR.

Transcript copy numbers were determined by performing qRT-PCR analysis on preparations of known amounts of vector constructs containing FLTNFR1 or Δ6TNFR1 cDNA sequences. The percentage of transcripts lacking *TNFRSF1A* exon 6 was determined using by dividing the number of transcripts lacking exon six by the number of transcripts including exon 6 in addition to those lacking exon 6, and multiplying by 100 to give a percentage.

3.2.3.3 Agilent DNA 1000

PCR was performed on 2 µl donor peripheral blood immune cell cDNA using a forward primer spanning the boundary between exons 4 and 5 (5'-TGCACCTCTCCTGCCAGG-3') and a reverse primer spanning the boundary between exons 7 and 8 (5'- CCCACAAACAATGGAGTAGAGCTT-3'). PCR products were resolved and visualised using the Agilent DNA 1000 Kit and 2100 Bioanalyzer (Agilent) according to the manufacturer's instructions. Briefly, DNA dye concentrate and DNA gel matrix were allowed to equilibrate to room temperature for 30 min, and then 25 µl of the DNA dye was added to a DNA gel matrix vial, the contents were vortexed and then centrifuged at 2240 x g for 15 min through a spin filter, in a Heraeus Pico 17 Microcentrifuge. 9 µl of filtered gel-dye mix was pipetted into the appropriate well of an Agilent DNA 1000 chip in a chip priming station, and a 1 ml syringe

was used to distribute the gel-dye mix evenly throughout the chip. 5 µl of marker was pipetted into each well of the chip, and 1 µl of DNA ladder was pipetted into the appropriate well, before 1 µl of each PCR product sample was loaded to sample wells. The chip was then vortexed for 1 min before being run in the Agilent 2100 Bioanalyzer. The intensity of fluorescence of full-length and Δ6 bands was quantified using the Agilent 2100 expert software (Agilent). The percentage of transcripts lacking exon 6 was then calculated by dividing the value for the fluorescence of the band resolving at 213 bp, corresponding to TNFR1_Δ6, by the combined values for bands resolving at 213 bp and 287 bp (for FLTNFR1), and multiplying by 100.

3.2.4 *In silico* splice site analysis

Analysis of the strength of the *TNFRSF1A* exon6-intron 6 splice site was performed using the SplicePort tool for analysis of donor splice sites (http://spliceport.cs.umd.edu/don_browser.html). The 80 bases up and downstream of the last base of exon6 and the first base of intron 6 were queried.

3.2.5 Rs1800693^{G} U1 complement vector construction

The wildtype human U1 snRNA sequence was mutated to be the complement of the sequence at the exon 6-intron 6 boundary with the rs1800693^{G} allele by PCR using the wildtype U1 snRNA sequence as a DNA template as described in 2.2.1, integrating the rs1800693 complement sequence by using U1compF (5'-CCCAGCTGTGTGTCAGGGCTGGAAAGGGCTCGGGAGT-3') and U1compR (5'-TCGTGATCATGGTATCTCCCCTGCCAGGTGAGGAGGAGATCT-3'). The insert was designed to incorporate *BseYI* (CCCAGC) and *FatI* (CATG) restriction sites at the 5' and 3' respectively, and was cloned into the pcDNA3.1 vector (2.1.2) using the appropriate restriction sites (2.1.1).

3.2.6 U1 complement minigene assay

U1 complement minigene assays were performed as described in 3.2.2, except that at transfection 500 ng of DNA was the appropriate minigene construct DNA and 500 ng was the wildtype human U1 snRNA construct, or the rs1800693^{G} complement U1 snRNA construct.

3.2.7 *In silico* analysis of potential *cis* regulatory motifs and RNP binding partners for rs1800693

41 nucleotide genomic DNA sequences, with rs1800693 A, G, T and C alleles in the middle position (ie. with 20 nucleotides either side of the SNP) were analysed using web-based Splicing Regulation Online Graphical Engine (SROOGLE; http://sroogle.tau.ac.il/), ESEfinder (http://rulai.cshl.edu/cgi-bin/tools/ESE3/esefinder.cgi?process=home) and Splice Rainbow (http://www.ebi.ac.uk/asd-srv/wb.cgi?method=8) prediction programmes to identify potential *cis*-acting splice regulator motifs and potential *trans*-acting RNP binding partners that might be involved in rs1800693-mediated splicing of *TNFRSF1A* exon 6.

3.2.8 Pulldown of RNA binding proteins

3.2.8.1 *In vitro* transcription of RNA

DNA constructs integrating the T7 RNA polymerase promoter at the 5' end were PCR amplified from minigene constructs corresponding to rs1800693 'A' and 'G' alleles using the TNFR1pdF (5'-TACGTAATACGACTCACTATAGTTAAGGGCACTG-3') and TNFR1pdR (5'-GCAGGTGAGCATGGGCACC-3') primers to yield a DNA template for the transcription of 57 bp RNA probes incorporating rs1800693. PCR product DNA was ethanol precipitated as follows; 1 µl of glycogen (20 µg/µl, Invitrogen), 0.1 volumes of sodium acetate pH 5.0, and 2.5 volumes of 100% EtOH were added to four pooled 50 µl PCR reactions, vortexed and the mixture was incubated at -80°C for 1 hour. Precipitated DNA was pellet by centrifugation in a Heraeus Pico 17 Microcentrifuge at 10,000 x g for 30 min at 4°C. The supernatant was discarded and the DNA pellet was washed once in 1 ml of 70% EtOH by

centrifugation at 10,000 x g for 10 min at 4°C. Supernatant was discarded and the DNA was re-suspended in 20 µl of RNAse-free H_2O (Sigma).

In vitro transcription of RNA probes from DNA with an integrated 5' T7 RNA polyermase promoter sequence for use in pulldown experiments was performed using the SP6/T7 polymerase *in vitro* transcription kit (Roche). Reaction composition was as follows:

Reagent	***Final Concentration/Volume***
ATP, CTP, UTP, GTP	1 mM each
T7 RNA polymerase Buffer (10 X)	1 X
DNA template	1 µg
RNAse inhibitor (20 U/µl)	20 U
T7 RNA polymerase (20 U/µl)	40 U
RNAse-free H_2O	to 20 µl

Transcription reactions were performed on a DNA Engine Tetrad (MJ Research) as follows:

Step	***Temperature (°C)***	***Time (min)***
Transcription	37	120
	Add 20 U of RNAse-free DNAse I (Roche)	
DNA Digestion	37	20

The products of four transcription reactions per probe were pooled, DNAse treated, ethanol precipitated as above and resuspended in 40 µl RNAse-free H_2O.

3.2.8.2 Coating of RNA probes to Adipic Acid Dihydrazide Agarose

20 µg of RNA probe was diluted into 400 µl of 100mM sodium acetate pH 5.0 and 5mM sodium *m*-periodate, and incubated with rotation in the dark at room temperature for 1 h 20 min. The resultant periodated RNA was then ethanol precipitated (3.2.8.1) and resuspended in 200 µl of 0.1M sodium acetate pH 5.2. A 400 µl aliquot of Adipic Acid Dihydrazide Agarose Bead 50% Slurry (Sigma) was washed four times in 10 ml of 0.1M sodium acetate pH 5.2 with centrifugation at 3200 x *g* for 5 min in a Heraeus Multifuge 3SR Plus. After the final wash, 100 µl of 0.1M sodium acetate was added to the beads and the slurry was mixed with the periodated RNA by rotation overnight at 4°C. Beads with covalently linked RNA were then pelleted by centrifugation at 3200 x g for 4 min and washed two times in 1 ml of 2M NaCl and three times in 1 ml of a wash buffer containing 20mM HEPES-KOH, pH 7.5, 6% (v/v) glycerol, 0.1M KCl, 0.2mM EDTA and 0.5mM dithiothreitol (DTT).

3.2.8.3 Pulldown

RNA coated beads were then incubated in 400 µl of an *in vitro* splicing reaction mixture of 100 µl HeLa cell nuclear extract (Cilbiotech) and 200mM HEPES-KOH pH 7.5, 5mM DTT, 60% glycerol and 240 or 180 µg Heparin for 30 min at room temperature, with rotation. Beads were then pelleted by centrifugation at 3200 x g for 4 min and washed four times in 1 ml of wash buffer. After the final centrifugation, bound proteins were eluted by addition of 50 µl of 2 X Laemmli Buffer and denatured by boiling at 95°C for 5 min. Samples were allowed to cool, and were resolved by electrophoresis 12.5% SDS polyacrylamide as described in 2.2.8. Resolved proteins were subsequently visualised using SimplyBlue™ SafeStain Coomassie G-250 reagent as in 2.2.9, Brilliant Blue G-colloidal reagent (Sigma) or analysed by western blot (2.2.11) using the monoclonal mouse anti-SR protein antibody clone 1H4G7 (Invitrogen) at 1 µg/ml as a primary antibody, and the IRDye® 800CW goat-anti-mouse (LI-COR Biosciences) secondary antibody.

3.2.9 SR protein overexpression minigene assays

Co-transfection minigene assays in which SR proteins were over-expressed were performed as described in 2.3.3, except that at transfection 500 ng of DNA was the appropriate minigene construct DNA and 500 ng was either the empty pCG vector or SRp20, SC35 or SRp40 overexpression vectors.

3.2.10 Locked Nucleic Acid Splice-Switching Oligonucleotides (LNA SSOs)

The 16-mer LNA SSO sequences used in screens to identify inducers for splice switching of murine *TNFRSF1A* and *IL7RA* splicing to isoforms lacking exons 6 and *TNFRSF1B* exon 7 are listed in table 3.3.

LNA SSO	**Sequence**
mtnfr1_01	TcTtGcAgCtGaAaGa
mtnfr1_02	CtCaTtTtTcTtGcAg
mtnfr1_03	CtTcAtAcAcTcCtCa
mtnfr1_04	GaGtCcTgGgGgTtTg
mtnfr1_05	CtGaGtCcTgGgGgTt
mtnfr1_06	TcAcCtGaGtCcTgTg
mtnfr1_07	CcCcTcAcCtGaGtCc
mtnfr1_08	AcCcCcCcTcAcCtGa
mtnfr1_09	AgCcAcCcCcCcTcAc
mtnfr1_10	AcCaAgCcAcCcCcCc
mil7ra_01	CcAtCcTcCtGgAaTa
mil7ra_02	AcAgGaTcCcAtCcTc
mil7ra_03	AcAcTtGgCaAgAcAg
mil7ra_04	AaCaAaCtCaGaAtGg
mil7ra_05	GaCcAaCaAaAaCaCa
mil7ra_06	AaGaTgAcCaAcAaAa
mil7ra_07	GgCtAaGaTgAcCaAc
mil7ra_08	CaTgGgCtAaGaTgAc
mil7ra_09	AgCaCaTgGgCtAaGa

mil7ra_10	CcAtAgCaCaTgGgCt
mil7ra_11	CaAgAcAgGaTcCcAt
mil7ra_12	GgCaAgAcAgGaTcCc
mil7ra_13	TtGgCaAgAcAgGaTc
mil7ra_14	AcTtGgCaAgAcAgGa
mil7ra_15	TgAcAcTtGgCaAgAc
mil7ra_16	GgTgAcAcTtGgCaAg
mil7ra_17	AtGgTgAcAcTtGgCa
mil7ra_18	GaAtGgTgAcAcTtGg
mil7ra_19	CaGaAtGgTgAcAcTt
mil7ra_20	CtCaGaAtGgTgAcAC
3274	AgAgCaGaAcCtTaCt
5678	GgTgCtGtTgCcCcTg

Table 3.3: LNA SSO sequences. Capital and lowercase letters represent LNA and deoxyribonucleotides, respectively; all contain phosphorothioate internucleotide linkages throughout.

LNA oligonucleotides were made to order at Santaris Pharma A/S, through kind collaboration with Dr. Henrik Ørum. They were synthesised using the Äkta 100 platform, 2.5 eq. of monomers of both DNA and LNA, and purified on an EI-column Source^{TM} 30Q. LNA SSOs were subsequently desalted by ultrafiltration on a Millipore Pellicon 2 filter (MW 1000). They were received lyophilised, and were hydrated using PBS to a stock concentration of 100 µM.

3.2.10.1 *In vitro* LNA SSO screens

1 x 10^5 L929 or RAW 264.7 cells were seeded in 24 wells 12 h before LNA transfection. 5 µl of a 5 µM LNA SSO stock was diluted into 50 µl of OPTI-MEM (Invitrogen), and 2 µl of Lipofectamine 2000 was diluted into 50 µl of OPTI-MEM. The two mixtures were combined and allowed to form complexes

for 20 min, then applied to the cells in the 24-wells containing 400 µl of media (final SSO concentration 50 nM). After 24 h incubation at 37°C in a 5% CO_2 incubator, total RNA and cDNA was made (2.2.3 and 2.2.4) and PCR was performed (2.2.1) on 4 µl of the resultant cDNA with cDNA-specific primers flanking the target exon (Table 3.4). PCR products were subsequently resolved in 2% TBE agarose or polyacrylamide gels (2.2.6) to determine if exon skipping had been induced. To assay for LNA SSO interference with the reverse transcription of full-length amplicons, LNA SSOs were added directly to reverse transcription reactions at 0.5 nM, 5 nM and 500 nM concentrations. ImageJ software (National Institutes of Health) was used to quantify the relative intensity of full-length and bands lacking *IL7RA* or *TNFRSF1A* exon 6, and infer percentages.

Name	***Sequence***
mTNFRSF1Aexons5-7_F	5'-CCGTGACAATCCCCTGTAAGGAGACT-3'
mTNFRSF1Aexons5-7_R	5'-ACGGGATCCCTACAAATGATGGAGTAGACT-3'
mIL7RAexons5-7_R	5'-GGTGAAAGCAACTGGACGCATGTATCTTTATTCCACACAAG-3'
mIL7RAexons5-7_R	5'-ACTTTCGGGATTGAAACTCACATTCAGACTCGTTTTTGGCTTCTTACATAG-3'
mTNFRSF1Bexons6-8_F	5'-CCCAGCTGTGTGTCAGGGCTGGAAAGGGCTCGGGAGT-3'
mTNFRSF1Bexons6-8_R	5'-CGGGCCTTATCGGCAGGCAAGTGAGGCACCTTGGCTTCT-3'

Table 3.4: Primers for amplification of spliced products of exons targeted by LNA SSOs.

3.2.10.2 *In vivo* LNA SSO studies

For *in vivo* studies, C57BL/6 mice aged between 6 and 9 weeks were obtained from the Biomedical Services (BMS) at the University of Oxford, and were housed in specific pathogen-free conditions in accordance with Home Office regulations. All procedures were approved by the University of Oxford Clinical Medicine Ethical Review Committee, and were performed under personal and project licenses under the Animals Scientific Procedures Act.

Mice were injected with PBS or 200 µl of the indicated LNA SSO at 3.125 mg/ml dissolved in PBS intraperitoneally (IP) once daily for 5 consecutive days. Mice were considered to weigh approximately 25 g, giving a dosing regimen of 25 mg/kg/day. On days 5, 16 and 24, 50 µl blood samples were obtained from the tail vein and serum was obtained by centrifugation of the blood samples at 6,200 x *g* for 2 min in a Heraeus Pico 17 Microcentrifuge. At the indicated days, mice were sacrificed and the indicated internal organs were harvested for RNA preparation and analysis of splice-switching induction.

3.2.11 Murine TNFR1 constructs

The murine FLTNFR1 cDNA sequence was amplified by PCR (2.2.1) from a murine TNFR1 cDNA construct (clone 3585060, Open Biosystems, Thermo Scientific) using the primers indicated in Table 3.3 to yield an insert integrating *KpnI* (GGTACC) and *AgeI* (ACCGGT) restriction enzyme sites at the 5' and 3' ends, respectively. This was then cloned (2.1.1) into the pEYFP-N1 vector (2.1.2) in-frame with EYFP, to yield a murine FLTNFR1-EYFP fusion protein construct. An equivalent Δ6TNFR1 insert was generated by overlap extension PCR (2.2.2) using the indicated primers (Table 3.5), removing exon 6, the stop codon introduced by the frameshift associated with removal of exon 6 and the downstream nonsense nucleotide sequence. This was similarly cloned into pEYFP-N1 to allow the expression of a murine Δ6TNFR1-EYFP fusion protein.

Name	***Sequence***
mTNFR1_F	5'-TAGGTACCGCCACCATGGGTCTCCCCACCGT-3'
mFLTNFR1_R	5'-ATTACCGGTGTTCGCGGGAGGCGGGTCG-3'
mΔ6TNFR1_R	5'-CGGACCGGTAAATGATGGAGTAGACTTCGGGC-3'
mrem6_Afrag_R	5'-CGCAGTACTGGCTGCAAGGGACGCACTCACT-3'
mrem6_Bfrag_F	5'-TGCAGCCAGTACTGCGGTGCTGTTGCCCCT-3'

Table 3.5: Primers for amplification of murine TNFR1 cDNA inserts for cloning into pEYFP-N1.

3.2.12 Soluble murine FLTNFR1 and Δ6TNFR1 expression

ELISAs were performed as described in 2.2.12. sTNFR1 in mouse serum was analysed by sandwich ELISA using R&D Systems MAB425 as a capture antibody, and biotinylated BAF425 as a detection antibody.

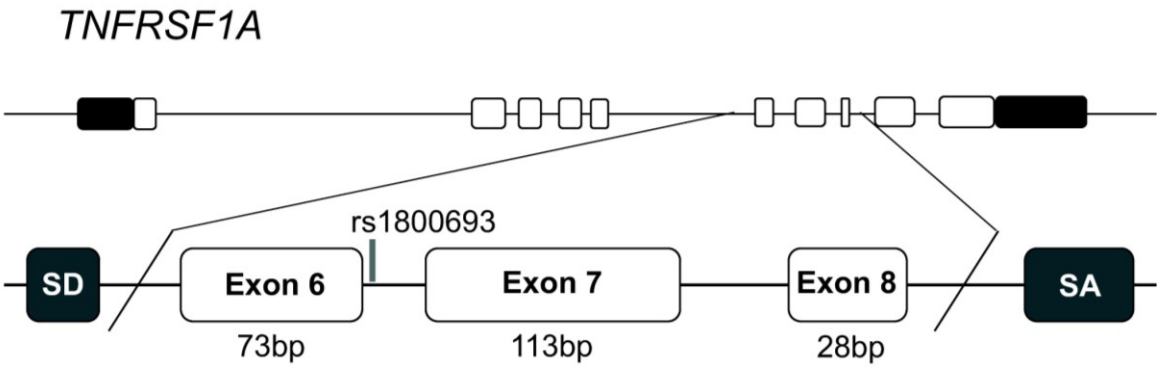
FLTNFR1-EYFP and Δ6TNFR1-EYFP fusion protein expression in cell culture supernatant was analysed as follows. HEK 293T cells were transiently transfected with the indicated constructs (2.3.3) and 24 h post-transfection, supernatant was removed, cells were washed with 1 ml of 37°C PBS and 1 ml of reduced-serum FreeStyle™ 293 Expression Medium (Gibco, Invitrogen). Cells were then incubated for a further 48 h at 37°C in an atmosphere of 5% CO_2. Supernatants were then harvested and centrifuged in 1.5 ml eppendorfs in a Heraeus Pico 17 Microcentrifuge, at 16,200 x *g* for 10 min to remove cells and debris. Supernatants were then concentrated 5 X using Amicon Ultra-0.5 Centrifugal Filter Units (Ultracel-10 membrane; Millipore) by centrifugation at 14,000 x *g* in a microcentrifuge for 7 min at 4°C. 20 µl of concentrated supernatants were then resolved by 12.5% SDS-PAGE (2.2.8) and immunoblotted (2.2.11) using the mouse anti-GFP primary antibody (Miltenyi Biotech), which is equally able to recognise the EYFP spectral variant of GFP, followed by incubation with the IRDye® 800CW goat-anti-mouse (LI-COR Biosciences) secondary antibody and scanning of membranes using the Odyssey Infrared Imaging System.

3.3 Results

3.3.1 Characterisation of rs1800693-mediated alternative splicing of *TNFRSF1A*

Rs1800693 is located 10 bp into *TNFRSF1A* exon 6 (De Jager *et al.*, 2009b). The recognition sequences for regulatory elements determining exon recognition and thereby splicing have been shown to cluster around exon-intron boundaries (Chen and Manley, 2009). We therefore tested whether rs1800693 allele could influence *TNFRSF1A* exon 6 splicing *in vitro* using a minigene assay system, with A, G, T or C at the SNP position (Figure 3.1a). The splicing products isolated from cells transfected with 'A', 'T' or 'C' minigene constructs were similar, with a 177 bp band containing vector exons only, a band at 250 bp comprising vector exons plus exon 6, and a band at 391 bp comprising the vector exons plus exons 6, 7 and 8 (Figure 3.1b). In cells transfected with the minigene with a 'G' at rs1800693, however, there was an additional 318 bp band comprising vector exons plus exons 7 and 8 only (Figure 3.1b). This suggested that rs1800693^{G} might result in an alternative splicing event, interfering in some way with the definition of the 5' splice site of exon 6 and resulting in its exclusion from the mature *TNFRSF1A* transcript. Furthermore, the fact that rs1800693 'A', 'T' and 'C' alleles have similar splicing profiles suggests that rs1800693^{G} either disrupts a splicing enhancer element, or generates a splicing silencer element.

a



b

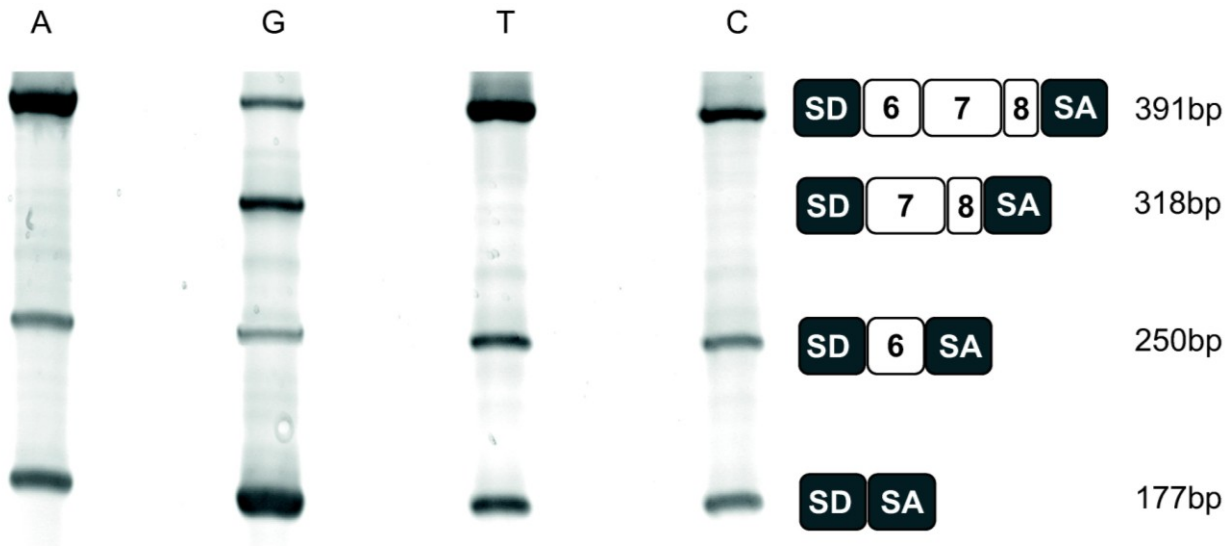


Figure 3.1: Analysis of *TNFRSF1A* splicing by rs1800693 allele. **(a)** Schematic representation of *TNFRSF1A* minigene for *in vitro* analysis of splicing in the region of rs1800693. **(b)** PCR products amplified from cDNA prepared from spliced RNA transcribed from minigenes corresponding to A, G, T and C alleles of rs1800693 resolved in 6% TBE polyacrylamide. Skipping of exon 6 is demonstrated by the presence of a band at 318bp, corresponding to vector exons plus exons 7 and 8. All bands were sequenced.

Having demonstrated rs1800693^{G}-mediated alternative splicing of *TNFRSF1A* exon 6 in an artificial minigene system, we next sought to investigate if skipping also occurred in healthy individuals harbouring this variant. Figure 3.2 shows analysis of spliced *TNFRSF1A* products isolated from PBMCs of donors of the indicated genotype. A 528 bp band comprising exons 5, 7, 8, 9 and 10 was visible at greatest intensity in G/G homozygotes, with lowest intensity in A/A individuals and with an intermediate intensity in A/G heterozygotes. A band at 602 bp containing exons 5-10 appeared with similar intensity in individuals of all genotypes and did not decrease with increasing intensity of the 528 bp band (Figure 3.2).

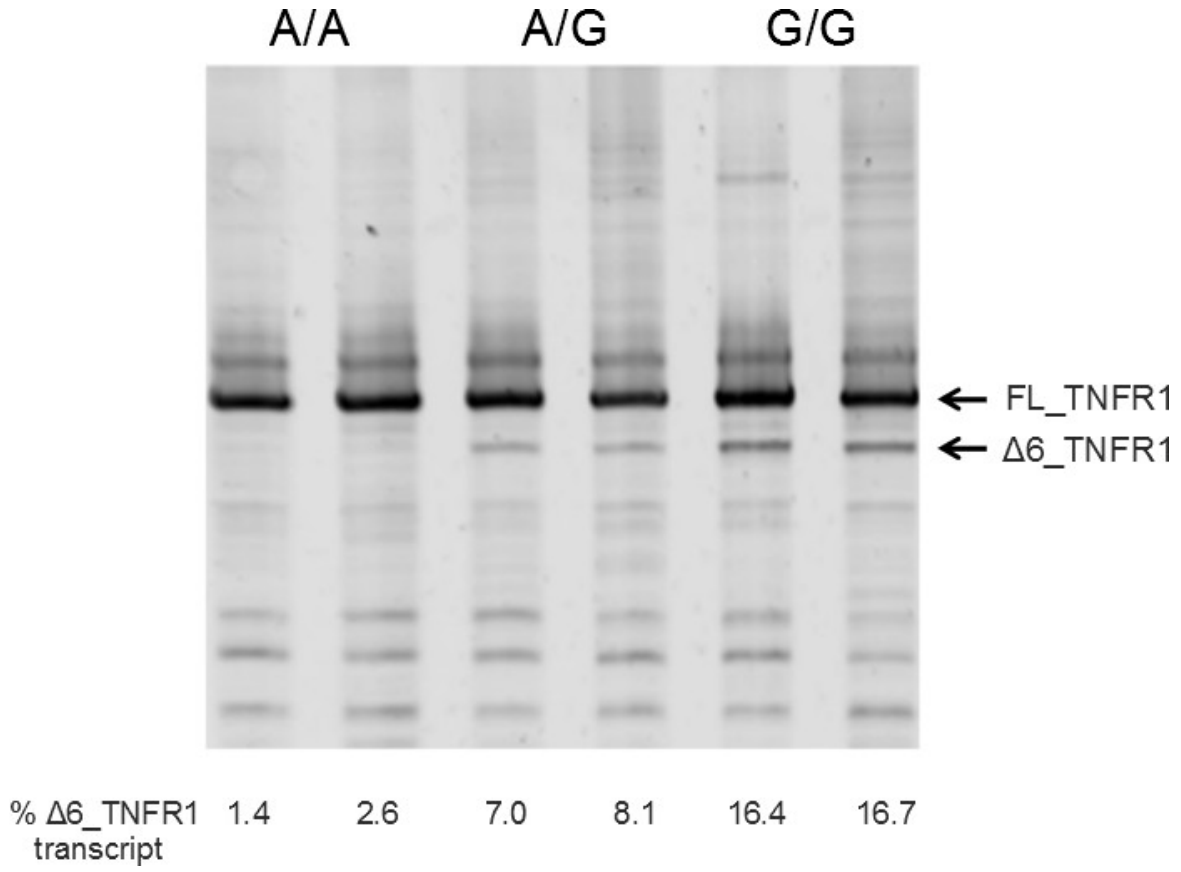
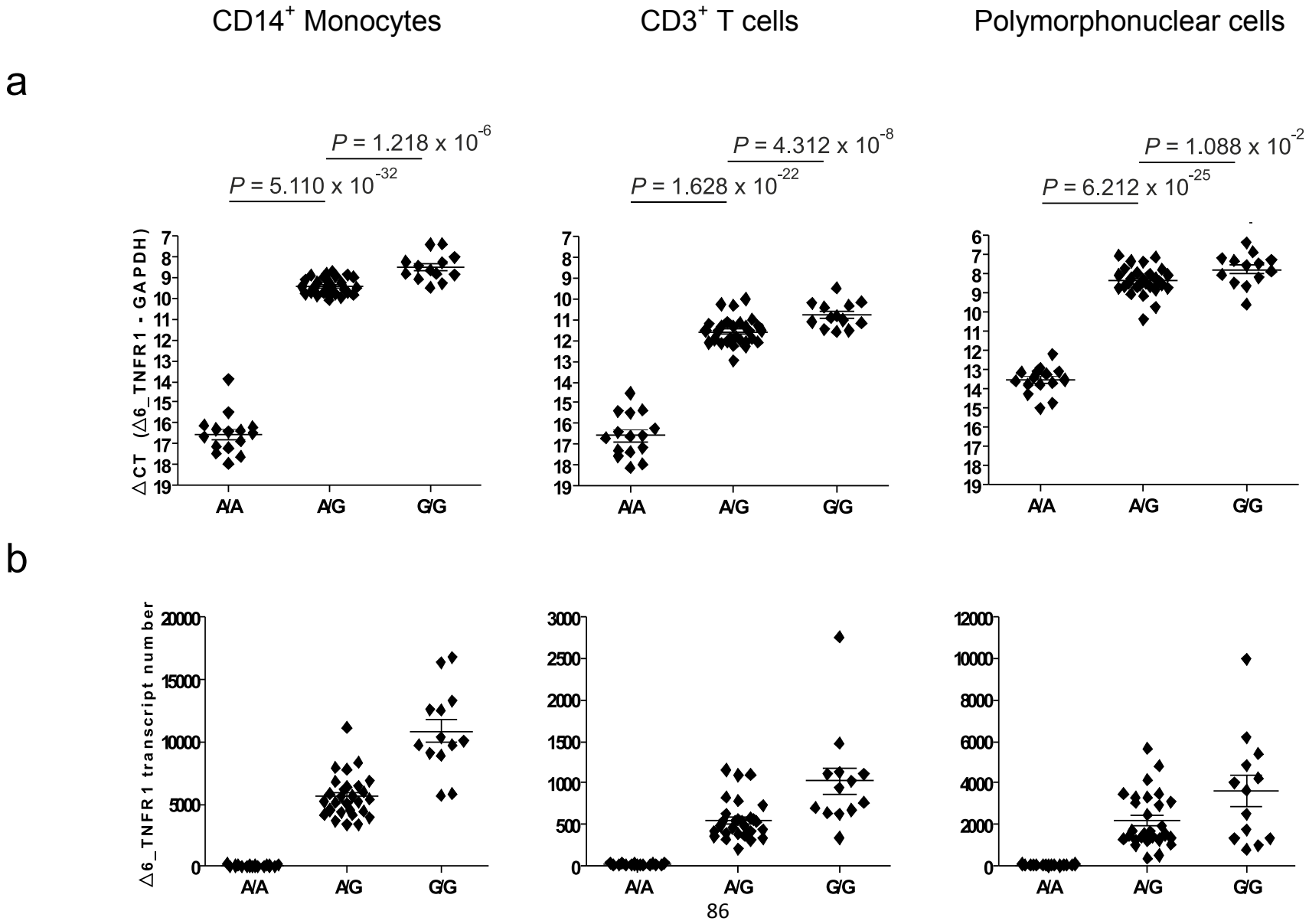
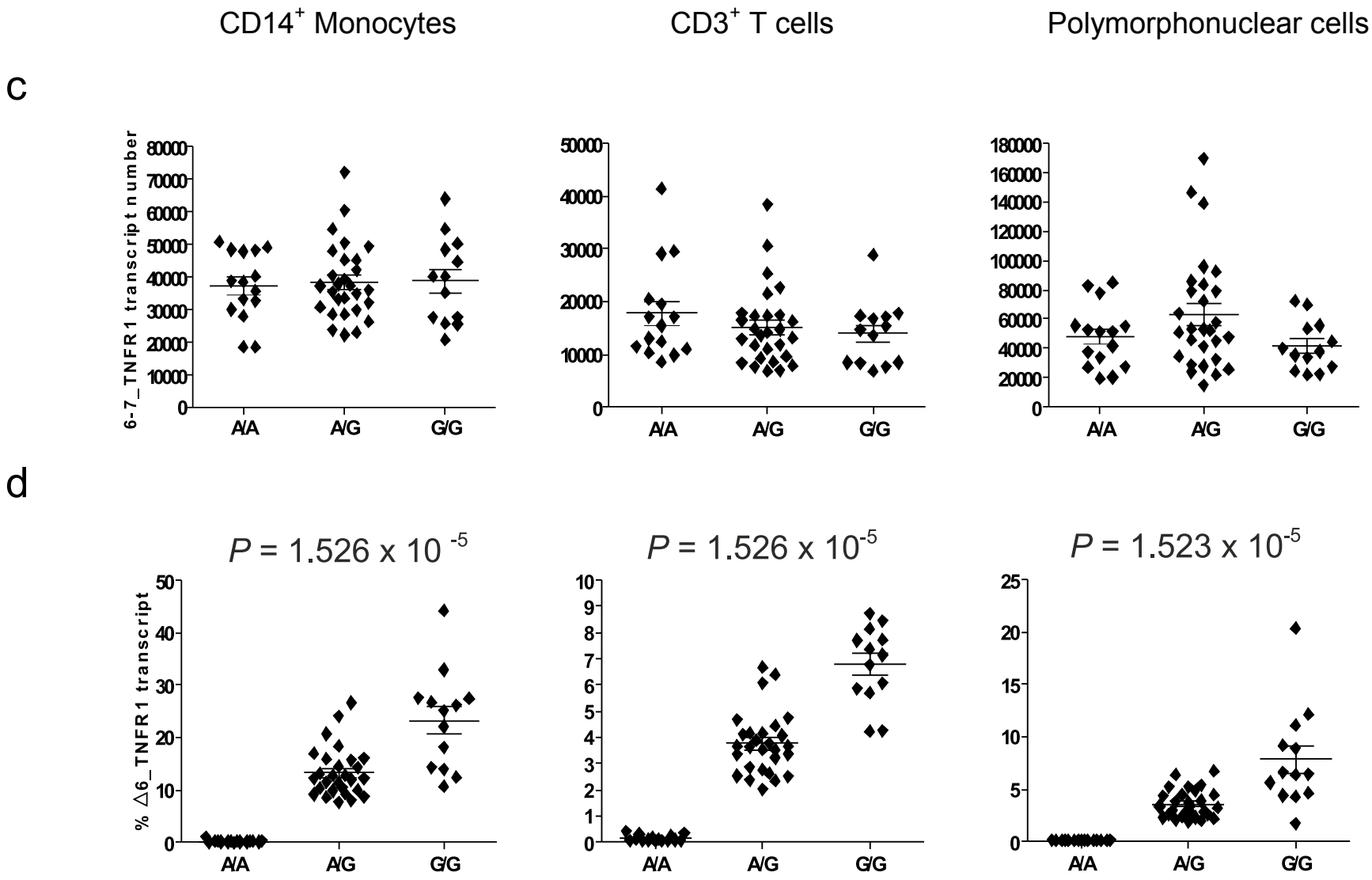


Figure 3.2: Analysis of *TNFRSF1A* exon 6 skipping in human PBMCs, based on rs1800693 genotype. Total RNA was made from donor PBMCs, reverse transcribed and PCR was performed with primers

in exons 5 and 10. Products were resolved in 6% TBE polyacrylamide. Bands corresponding to Full-length (FL; 602bp) and Δ6 (528bp) TNFR1 transcripts are indicated. Band quantification analysis was performed using ImageJ software. Genotypes; lanes 1 and 2 = rs1800693^{AA}, lanes 3 and 4 = rs1800693^{AG} and lanes 5 and 6 = rs1800693^{GG}.

These promising results led us to investigate *TNFRSF1A* exon 6 splicing by rs1800693 genotype in a larger sample size by examining the levels of transcripts lacking and containing exon 6 by quantitative real-time PCR (qRT-PCR). A probe designed to span the putative exon 5-7 junction was used for the specific detection of transcripts lacking exon 6 (Δ6_TNFR1). Figure 3.3a shows ΔCT values for Δ6_TNFR1 normalised to GAPDH in CD14^{+} monocytes, CD3^{+} T cells and Polymorphonuclear cells. In all cell types, the level of transcripts lacking *TNFRSF1A* exon 6 is lower in individuals with at least one copy of the rs1800693^{A} allele, and lower again in AA homozygotes than in heterozygotes. Furthermore, using qRT-PCR data for *TNFRSF1A* exons 3-4 as a control and by performing a standard curve titration with known amounts of target DNA we were able to determine the percentage of total *TNFRSF1A* mRNA transcripts lacking exon 6 (Figure 3.3d). In all cell types analysed, there was very little or no detectable Δ6_TNFR1 expression in AA homozygotes and a 'by-copy' increase was observed between heterozygotes and GG homozygotes, which fitted a linear regression. Figure 3.3e demonstrates that no significant difference was observed between levels of transcripts containing *TNFRSF1A* exon 6 by genotype, implying that in individuals of all genotypes the majority of *TNFRSF1A* transcripts contain exon 6, and that the main effect of rs1800693^{G}-mediated alternative splicing is not to downregulate the level of full-length TNFR1 mRNA, whilst Figure 3.3f shows similar levels of *TNFR1SF1A* control exons, indicating no significant difference in *TNFR1SF1A* transcription by rs1800693 allele.


CD14+ Monocytes
CD3+ T cells
Polymorphonuclear cells
a
P = 1.218 x 10-6
P = 5.110 x 10-32
P = 4.312 x 10-8
P = 1.628 x 10-22
P = 1.088 x 10-2
P = 6.212 x 10-25
ΔCT (Δ6_TNFR1 - GAPDH)
A/A
A/G
G/G
b
Δ6_TNFR1 transcript number


CD14+ Monocytes
CD3+ T cells
Polymorphonuclear cells
c
6-7_TNFR1 transcript number
A/A
A/G
G/G
d
P = 1.526 x 10 -5
P = 1.526 x 10-5
P = 1.523 x 10-5
% Δ6_TNFR1 transcript

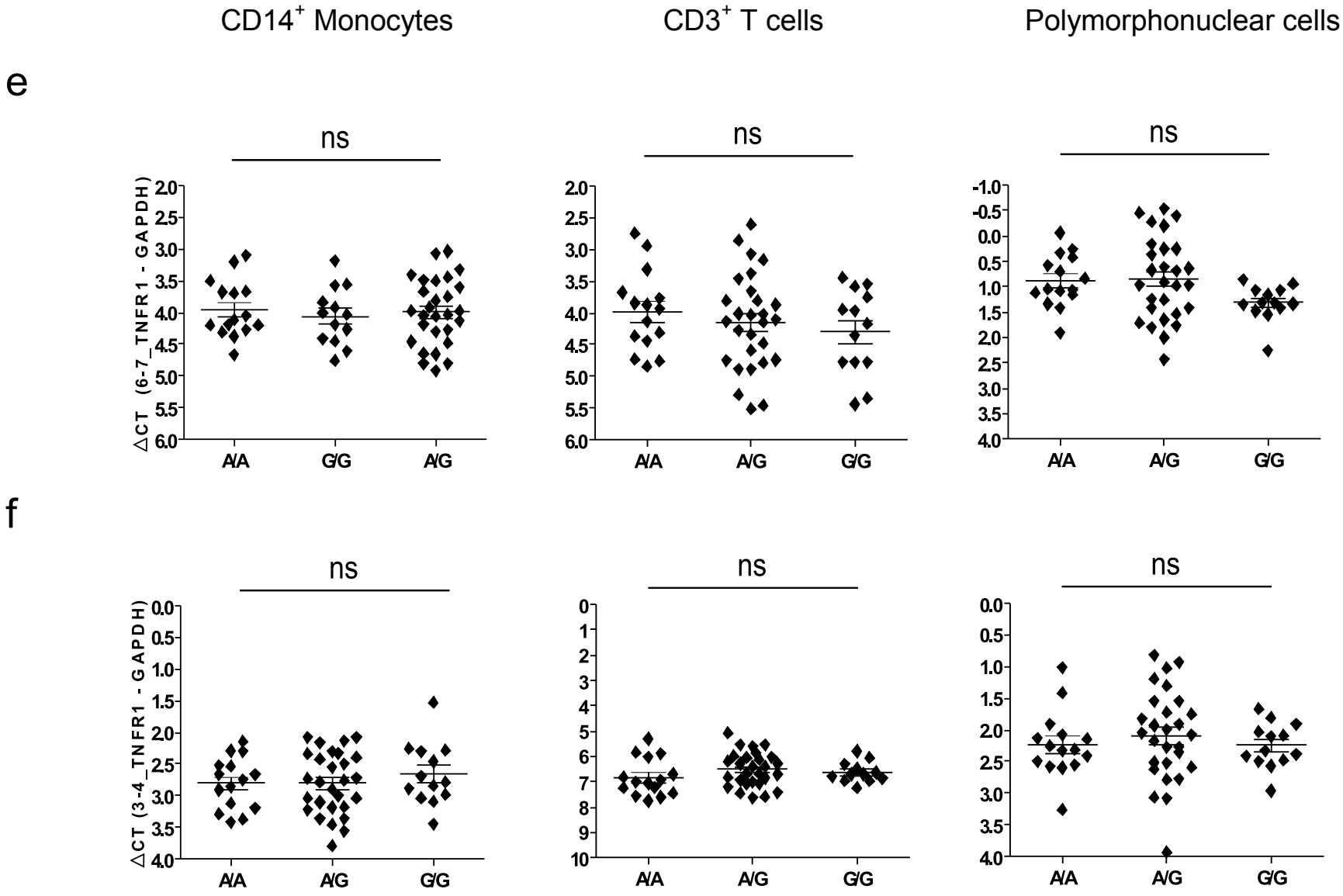
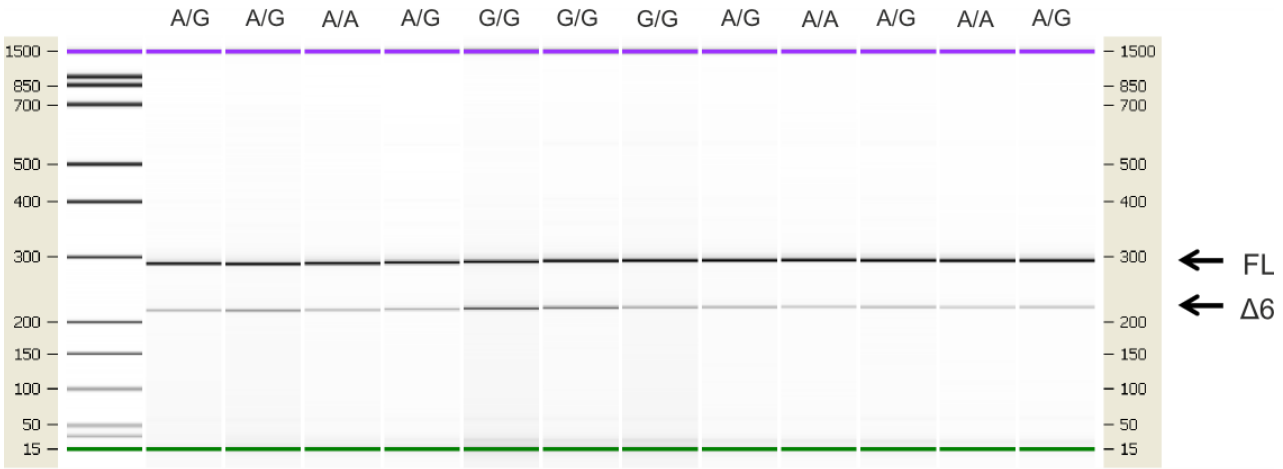

CD14+ Monocytes
CD3+ T cells
Polymorphonuclear cells
e
f
ns
ΔCT (6-7_TNFR1 - GAPDH)
ΔCT (3-4_TNFR1 - GAPDH)
A/A
A/G
G/G

Figure 3.3: Relative expression of TNFR1 transcripts lacking or containing *TNFRSF1A* exon 6 in the indicated immune cells isolated from healthy donors with different rs1800693 alleles. cDNA was made from RNA isolated from the indicated immune cell types isolated from donor blood samples and qPCR was performed with probes specific for the detection of *TNFRSF1A* exons. **(a)** Relative expression of TNFR1 mRNA lacking exon 6. **(b & c)** Absolute numbers of transcripts **(b)** lacking or **(c)** containing exon 6 were determined by performing titrations on cDNA constructs with known numbers of copies of the relevant exons. **(d)** Percentage of Δ6_TNFR1 transcripts from total Δ6_TNFR1 plus 6-7_TNFR1 transcripts in the indicated human immune cell subsets; 1 d.f., *P* values are indicated Percentages do not correlate with donor age or sex (for all subsets *P* = >0.05 for both age and sex). Relative expression of TNFR1 mRNA containing **(e)** exons 6 and 7 (6-7_TNFR1) and **(f)** exons 3 and 4 (3-4_TNFR1). Expression levels (ΔCT) were calculated by subtracting the cycle threshold (CT) value for the housekeeping gene GAPDH from values for the indicated TNFR1 transcripts. Error bars represent mean ± SEM; rs1800693^{GG} *n* = 13, rs1800693^{AG} *n* = 28, rs1800693^{AA} *n* = 15; *P* values are indicated; ns = non-significant.

Relative full-length and Δ6_TNFR1 transcript expression was also analysed by PCR amplification using a cDNA-specific primers flanking exon 6. Figure 3.4 demonstrates again that significantly less Δ6_TNFR1 transcript was detected in AA homozygotes than in GG homozygotes across the indicated cell types.

a


A/G
A/G
A/A
A/G
G/G
G/G
G/G
A/G
A/A
A/G
A/A
A/G
1500
850
700
500
400
300
200
150
100
50
15
FL
Δ6

b

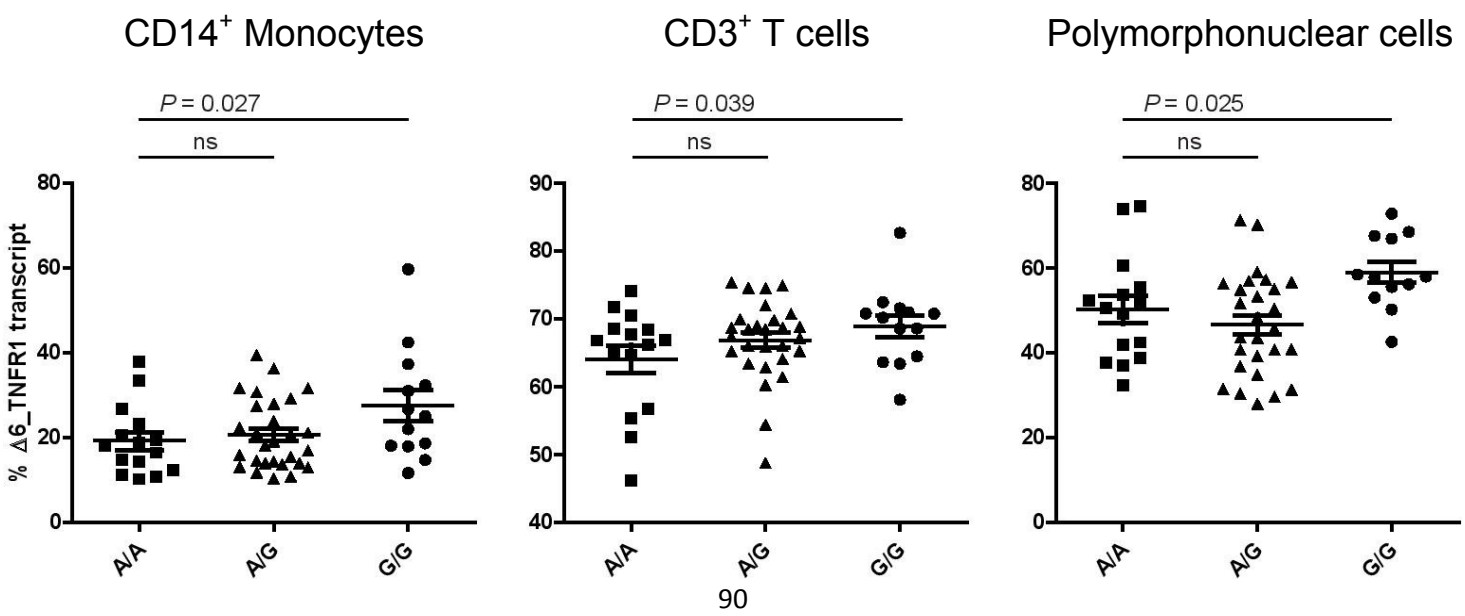

CD14+ Monocytes
CD3+ T cells
Polymorphonuclear cells
P = 0.027
ns
P = 0.039
ns
P = 0.025
ns
% Δ6_TNFR1 transcript
A/A
A/G
G/G

Figure 3.4: Analysis of *TNFRSF1A* exon 6 skipping in human immune cell subsets using the Agilent DNA 1000 assay system based on rs1800693 genotype. Products of PCR using primers spanning exon 6 on cDNA made from the indicated immune cell subsets were resolved and quantified using the Agilent DNA 1000 assay system. **(a)** A representative output from a single 12 sample Agilent DNA 1000 chip. Donor genotypes, bands corresponding to FL_TNFR1 (287 bp, FL) and Δ6_TNFR1 (213 bp, Δ6) transcripts and percentage of Δ6_TNFR1 transcripts from total Δ6_TNFR1 plus FL_TNFR1 transcripts are indicated. **(b)** Percentage of Δ6_TNFR1 transcripts from total Δ6_TNFR1 plus FL_TNFR1 transcripts in the indicated immune cell subsets by rs1800693 genotype. Error bars represent mean ± SEM; rs1800693^{GG} *n* = 13, rs1800693^{AG} *n* = 28, rs1800693^{AA} *n* = 15; *P* values are indicated; ns = non-significant.

3.3.2 Investigating the molecular basis of rs1800693^{G}-mediated skipping of *TNFRSF1A* exon 6

We next sought to better characterise the 5' splice site of *TNFRSF1A* exon 6 the molecular mechanism for rs1800693^{G}-mediated skipping. The 5' splice sites of certain exons are inherently weak due to having departures from the consensus binding sequence for U1 snRNA component of the spliceosome. This can mean that a small change in strength of binding of this or other ribonucleoprotein members of the splicing machinery can lead to improper definition of the 5' exon-intron boundary and result in exon skipping. *In silico* analysis revealed the 5' splice site for *TNFRSF1A* exon 6 to be very strong, with a consensus score of 0.99 (where 0 is the weakest and 1 is the strongest) (Dogan *et al.*, 2007). Nevertheless, at 10 bp into intron 6 the nucleotide at rs1800693 could potentially influence the binding of U1 snRNA and so we investigated if co-transfection of the 'G' minigene with a U1 snRNA construct exactly complementary to the *TNFRSF1A* rs1800693^{G} 5' splice site could result in increased inclusion of exon 6 in the mature transcript. Figure 3.5 shows that no difference was observed between products of splicing between cells co-transfected with the complementary U1 snRNA construct and the control, wildtype human U1 snRNA construct.

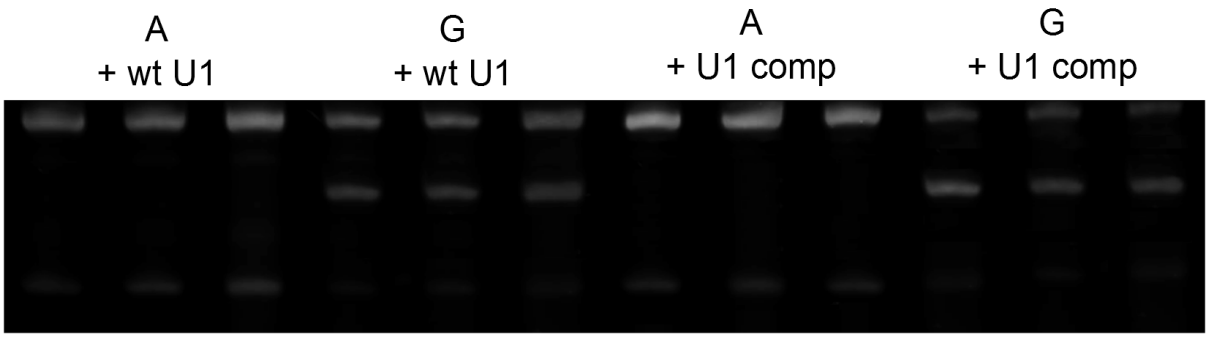


Figure 3.5: Analysis of splicing of RNA transcribed from rs1800693 A and G minigenes co-transfected with wildtype (wt U1) or *TNFRSF1A* exon 6-intron 6 boundary complement U1 (U1 comp) snRNA constructs. PCR products of cDNA made from transcribed RNA were resolved in 2% agarose. Skipping of exon 6 is demonstrated by the presence of a band at 318bp, corresponding to vector exons plus exons 7 and 8.

SROOGLE prediction software was used to identify putative intronic splice regulator sequences (ISRs) in the proximity of the *TNFRSF1A* exon 6-intron 6 boundary. Two overlapping motifs (AGGUG and AGGUGA) that are predicted to down-regulate the use of the 5' splice site immediately upstream were present only with G at rs1800693 position (Figure 3.6), reflecting the results from minigene assays (Figure 3.1b)

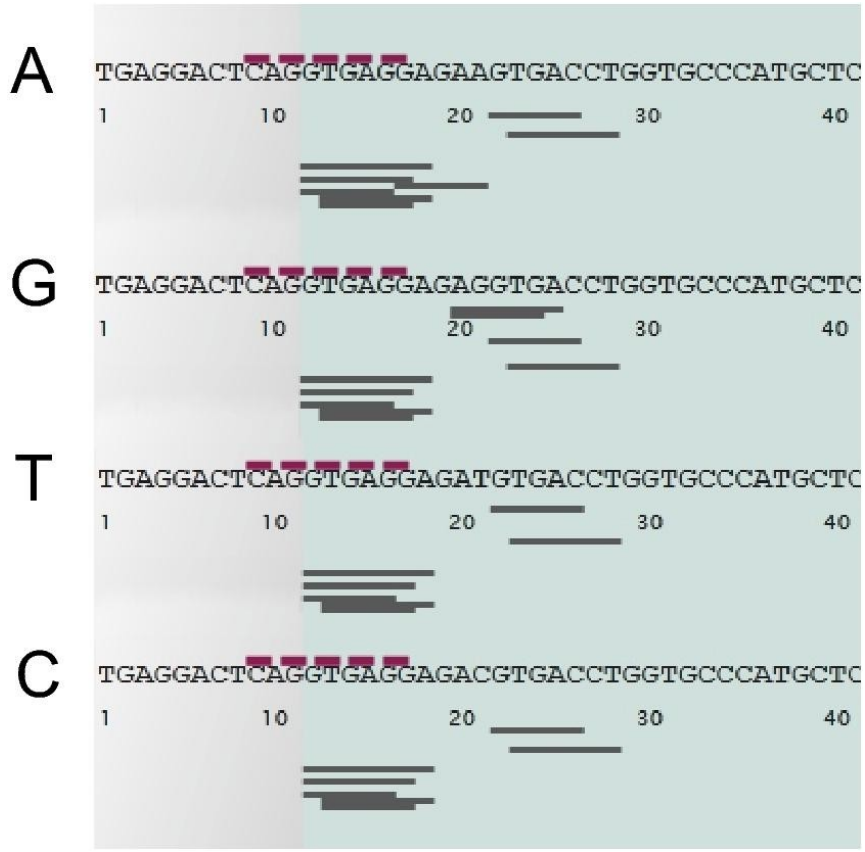


Figure 3.6: SROOGLE Analysis of ISRs in *TNFRSF1A* intron 6 by rs1800693 allele predicted to disrupt recognition of the exon6-intron 6 boundary. SROOGLE was queried with the indicated 41 bp sequences, corresponding to rs1800693 A, G, T and C alleles and their immediate genomic sequence. The exon 6-intron 6 boundary is shown (dotted line). Solid lines indicated ISRs predicted based on Voelker and Berguland 2007, and Yeo *et al.* 2007.

In an attempt to identify *trans*-acting factors that might bind this sequence or otherwise mediate the alternative splicing of exon 6, pulldown assays were performed with RNA probes corresponding to 'A' and 'G' alleles of the *TNFRSF1A* rs1800693 SNP. RNA probes for wildtype and +5G>C NF-1 exon 3 were included as a positive control for differential immunoprecipitation of splice-determining factors (the +5G>C mutant has impaired binding of the U1 spliceosome components U1-70K and U1-A (Buratti *et al.*, 2004)). No obvious difference in the profile of proteins eluted from rs1800693 'A' and

'G' probes was observed, even when pulldowns were performed using less non-specific competitor for protein binding, and a more sensitive Coomassie reagent (Figure 3.7).

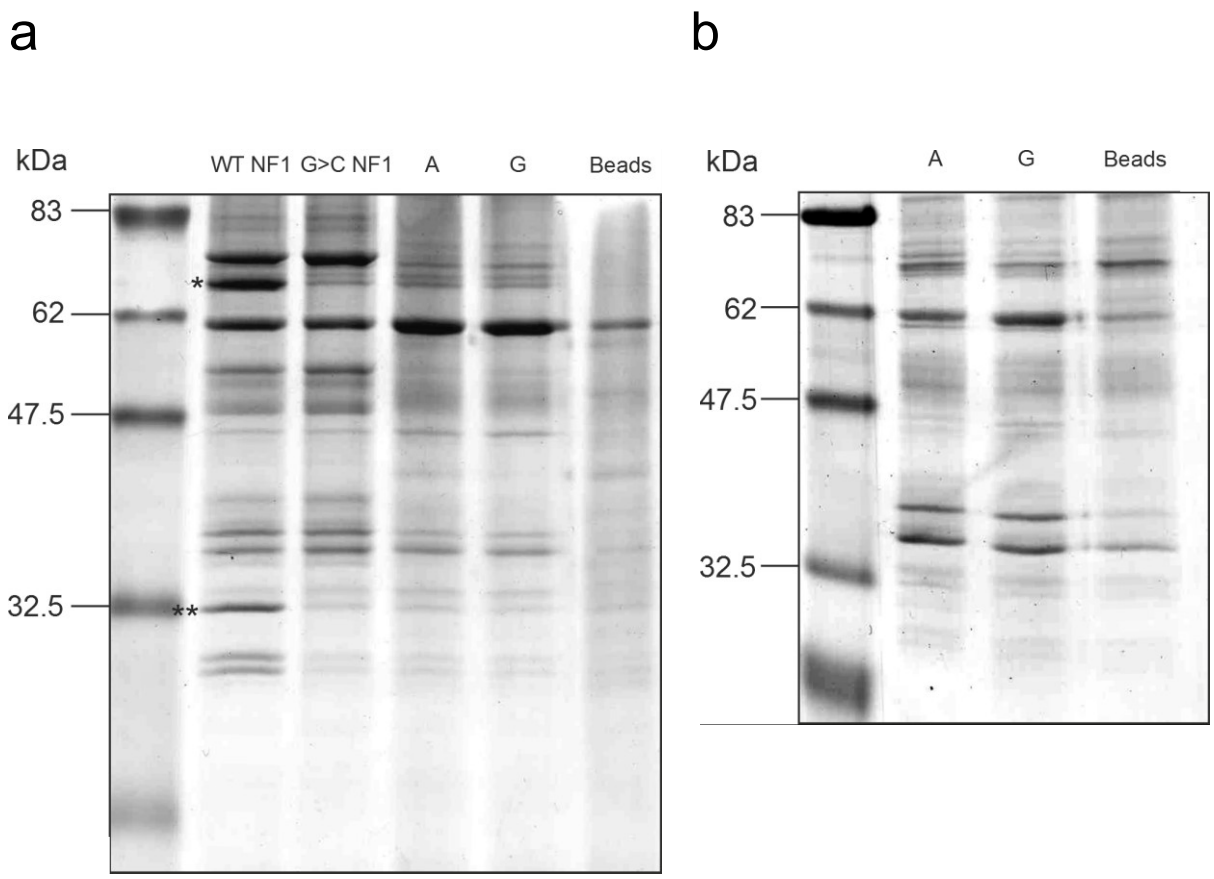


Figure 3.7: RNA-binding proteins associated with RNA probes corresponding to rs1800693 'A' and 'G' alleles resolved by 12.5% SDS-PAGE. Adipic acid dehydrazide beads were either coated with RNA probes corresponding to wildtype *NF-1* exon 3 (WT NF1), *NF-1* exon 3 +5G > C (G>C NF1), rs1800693^{A} (A) or rs1800693^{G} (G), or not coated (Beads) and incubated with HeLa nuclear extract. Associated proteins were resolved by 12.5% SDS-PAGE and gels were stained for visualisation. **(a)** 240 µg heparin in binding solution, gel stained with SimplyBlue™ SafeStain Coomassie G-250 reagent. **(b)**

180 µg heparin in binding solution, gel stained with Brilliant Blue G-colloidal reagent. *U1-70K and **U1-A bands are indicated.

In silico analysis was performed using SROOGLE, ESEfinder and Splice Rainbow programmes to identify potential regulatory motifs created or disrupted by an A>G transition at rs1800693 and potential trans-acting RNP binding partners. Supplementary Figure 1a, b and c show that there was no consensus between all three prediction programmes, and no pattern in the predicted binding of trans-acting factors by rs1800693 allele that would mirror the results of minigene experiments. However, as altered binding of several members of the serine/arginine (SR) protein and splicing factor family was predicted based on rs1800693 allele, further pulldown experiments were performed, followed by western blots using a monoclonal antibody recognising all members of the SR protein family (Figure 3.8). Whilst an SR protein was found to resolve at approximately 40 kDa in the lane for partners of the 'A' probe, no band is seen in the lane containing proteins immunoprecipitated with the 'G' probe. Based on its molecular weight this protein was predicted to be SRp40, a well-characterised splice-mediator protein (Long and Caceres, 2009).

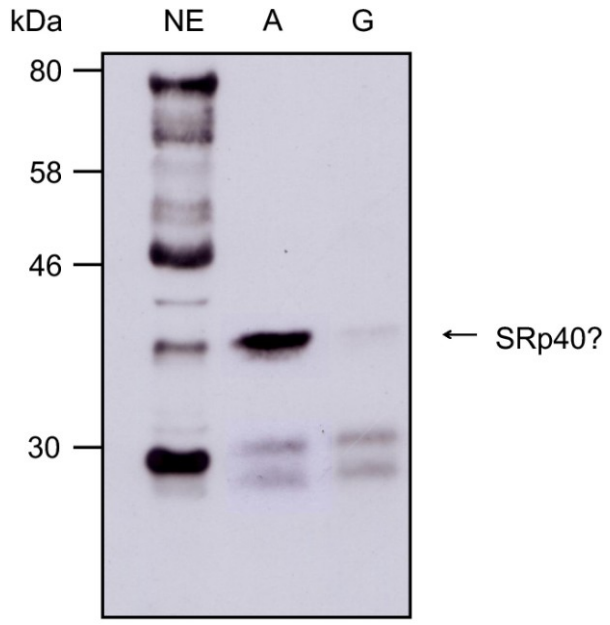
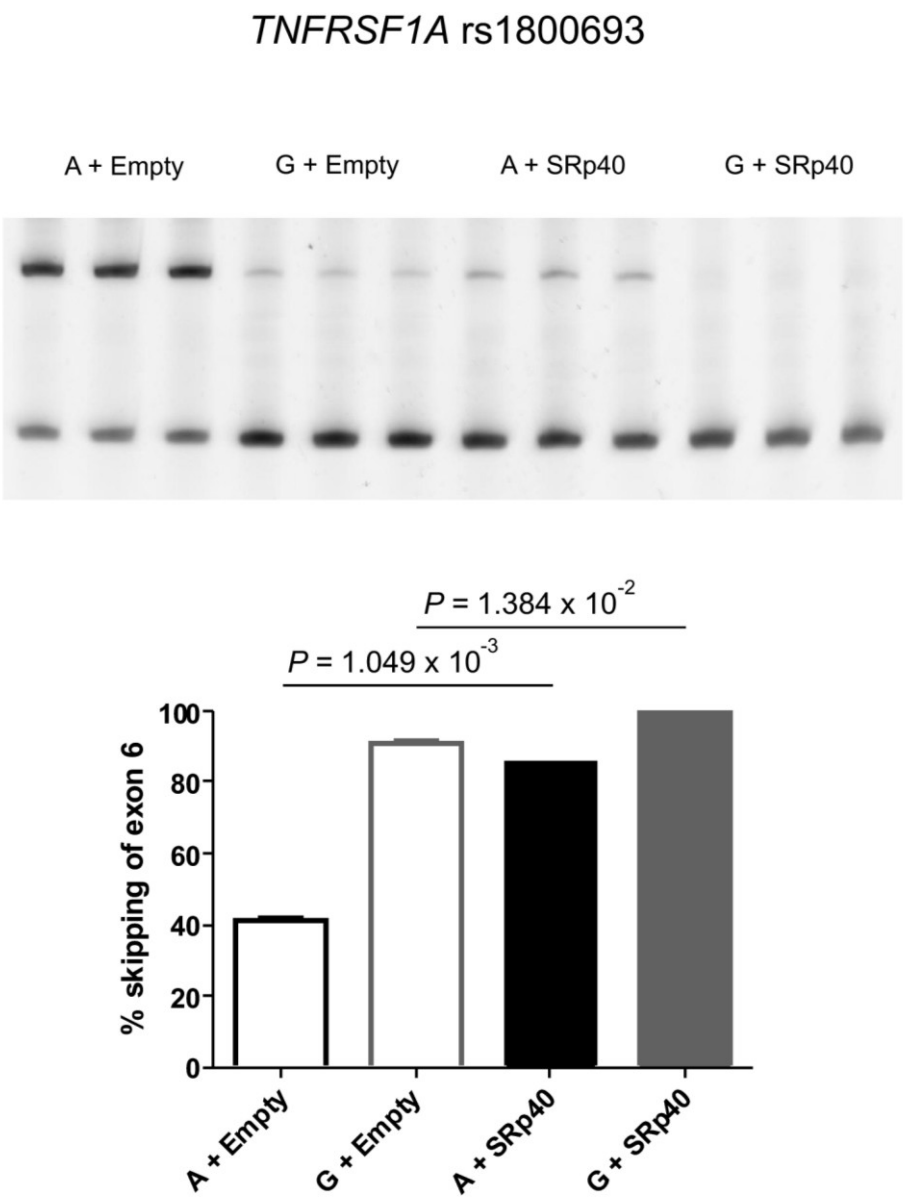


Figure 3.8: *in vitro* analysis of SR protein binding. Western blot using the monoclonal, anti-SR protein 1H4G7 antibody on the SDS-PAGE-resolved proteins of proteins immunoprecipitated with adipic acid dehydrazide beads coated with rs1800693^{A} (A) or rs1800693^{G} (G) RNA probes. NE = Nuclear Extract.

Splicing regulatory elements display weak consensus and splice-mediating proteins often bind many sequences in pre-mRNA with varying affinity (Matlin *et al.*, 2005). If the rs1800693^{G} allele weakens a recognition element for SRp40, the resulting loss in affinity may be compensated for by increasing the local concentration of SRp40, restoring normal splicing to *TNFRSF1A* exon 6. To investigate this simplified minigene constructs were made, using a 514 bp region from intron 5 to intron 6, allowing the comparison between two bands for the analysis of exon 6 skipping. The splicing products when 'A' and 'G' versions of this construct were co-transfected with a plasmid for the overexpression of SRp40 into HEK 293T cells are shown in Figure 3.9a. In contrast to our expectations from the results of the RNA pulldown experiments, rather than rescuing normal splicing of exon 6 SRp40 overexpression resulted in increased skipping of the exon, and was able to induce significantly more skipping of exon 6 in minigenes with an 'A' at rs1800693. Figure 3.9b shows the results of a control

experiment in which 'T' and 'C' minigenes for the MS-associated SNP in exon 6 of *IL7RA*, rs6897932 (Gregory *et al.*, 2007), were co-transfected with the SRp40 overexpression plasmid. The rs6897932^{C} allele has previously been demonstrated to increase skipping of *IL7RA* exon 6. In this instance, SRp40 overexpression appears to favour inclusion of exon 6 in the mature transcript (Figure 3.9b), suggesting that overexpression of this protein does not result in a constitutive increase in skipping of the middle exon in a three exon minigene system.

a


TNFRSF1A rs1800693
A + Empty
G + Empty
A + SRp40
G + SRp40
P = 1.384 x 10-2
P = 1.049 x 10-3
% skipping of exon 6
100
80
60
40
20
0
A + Empty
G + Empty
A + SRp40
G + SRp40

b

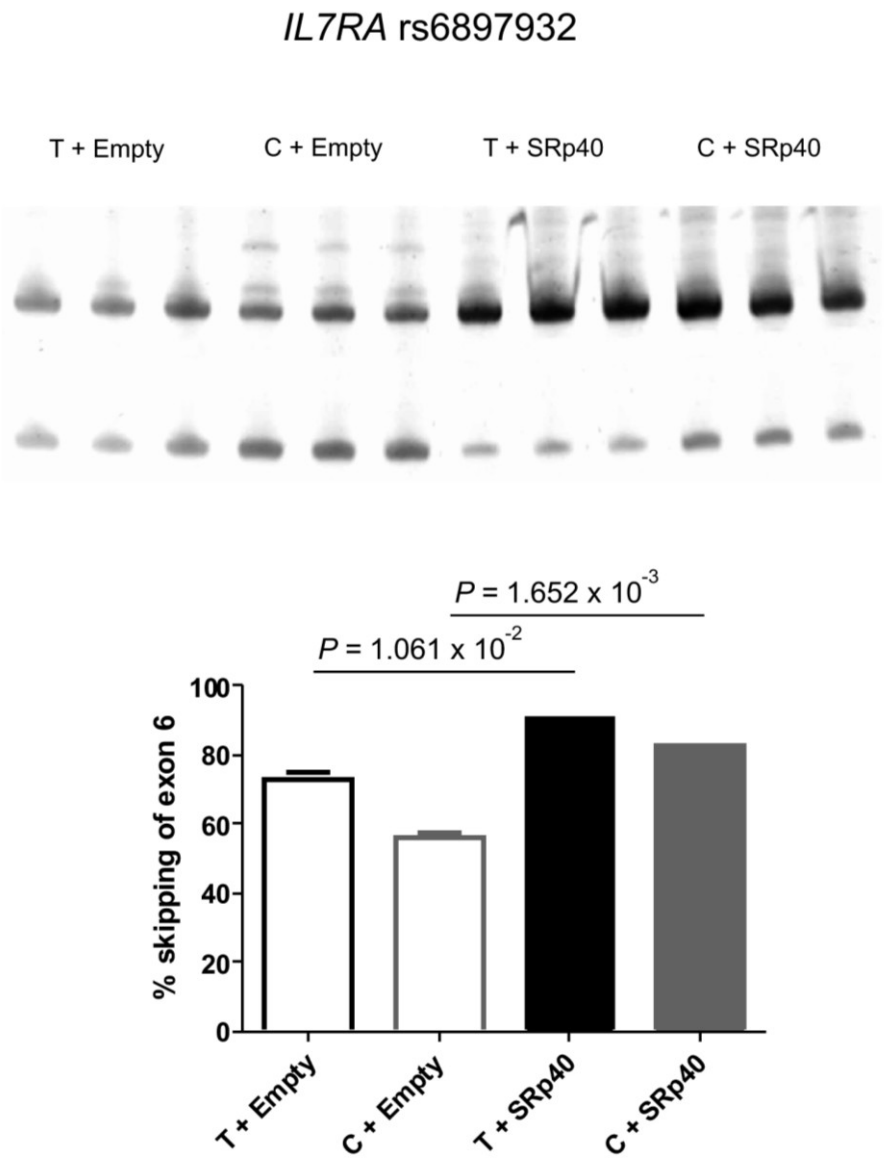


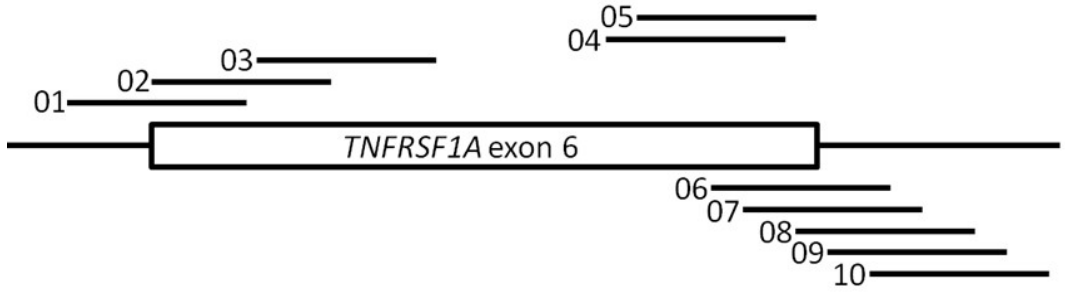
Figure 3.9: Influence of SRp40 overexpression on splicing of rs1800693-mediated splicing of *TNFRSF1A* exon 6, and rs6897932-mediated splicing of *IL7RA* exon 6. SRp40 over expression plasmid (SRp40) or empty pCG expression vector (Empty) were co-transfected with **(a)** rs1800693 A or G minigenes and **(b)** rs6897932 T or C minigenes. At 48 h post-transfection total RNA was made, cDNA was synthesised and PCR was performed with primers flanking the exon of interest. PCR products

were resolved in 6% TBE polyacrylamide and band intensities were quantified using ImageJ software. Error bars are mean ±SEM; *P* values are indicated.

3.3.3 Developing antisense technology-based models to investigate the functional consequences of MS-associated alternative splicing

In an attempt to indentify candidate SSOs for the development of *in vitro* and *in vivo* models for rs1800693^{G} and rs6897932^{C}-mediated skipping of *TNFRSF1A* and *IL7RA* exons 6 respectively, screens of 10, 16-mer LNA SSOs targeted to the 5' intron-exon junction were performed in L929 and RAW 264.7 cells (Figure 3.10). Figure 3.11b shows that the LNA SSOs mtnfr1_02 to mtnfr1_09 were found to induce skipping of *TNFRSF1A* exon 6. Of these, mtnfr1_02, mtnfr1_04, mtnfr1_05 and mtnfr1_06 were selected for further characterisation, as the most potent inducers of skipping. As mtnfr1_04 and mtnfr1_05 were found to interfere with reverse transcription (Figure 3.11b) and therefore detection of the full-length receptor at high concentrations, the next most potent inducer of exon 6 skipping, mtnfr1_06 was chosen to be taken forward into mouse studies.

a



b

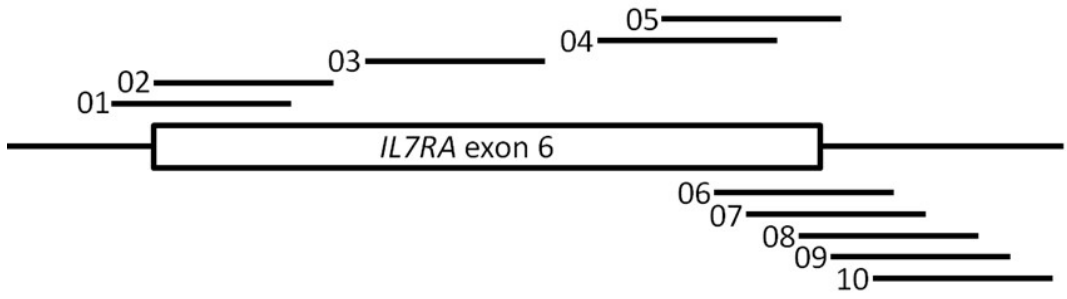
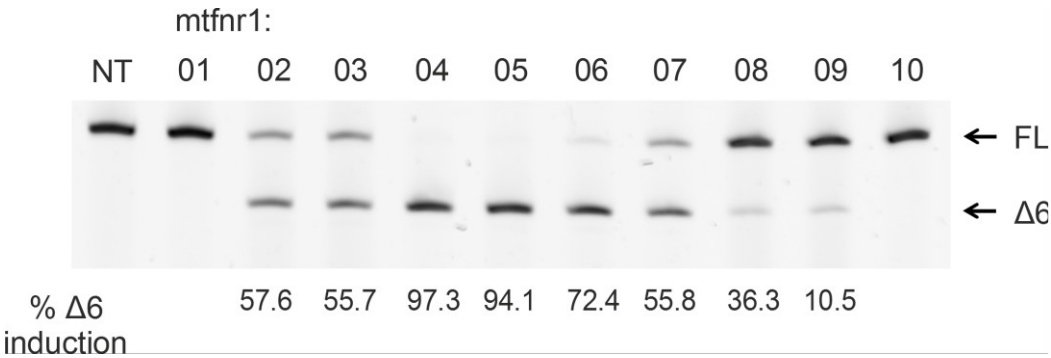


Figure 3.10: Schematic representations of LNA SSOs targeted to exons 6 of murine **(a)** *TNFRSF1A* and **(b)** *IL7RA* sequences.

a



b

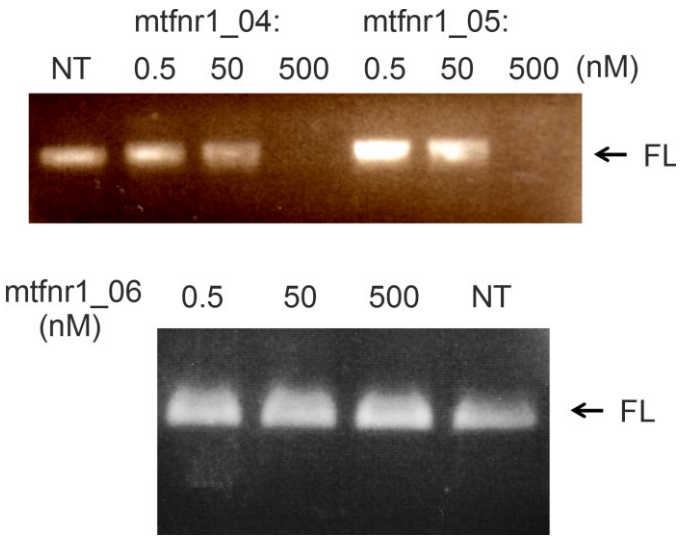
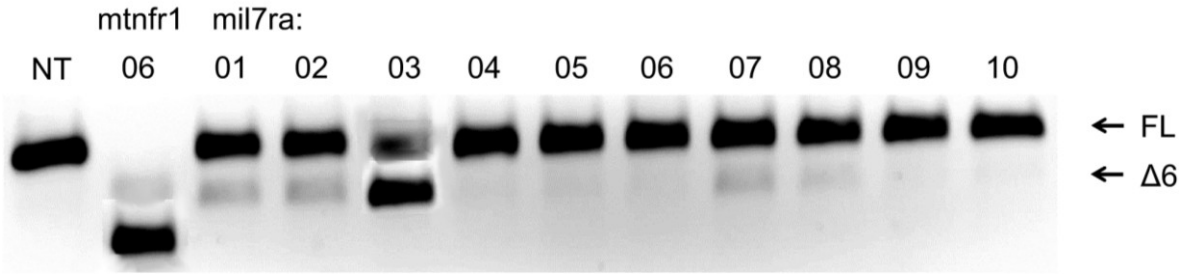


Figure 3.11: Screen of ability of 10 LNA SSOs targeted to *TNFRSF1A* exon 6 to induce exon skipping. **(a)** LNAs were transfected into L929 cells, after 24 h RNA and cDNA was made and PCR was performed with cDNA specific primers flanking exon 6 to assay for induction of skipping. Products were resolved by PAGE in a 6% TBE gel and bands were visualised with SYBR Gold Nucleic Acid Stain. Bands amplified from full-Length (FL) and Δ6TNFR1 (Δ6) transcripts are indicated. Band quantification analysis was performed using ImageJ software. **(b)** The indicated LNAs were added directly to reverse transcription reactions of RNA taken from non-transfected L929 cells at the indicated concentrations. PCR products amplified from cDNA were resolved in 2% agarose. NT = non-treated. All lanes shown are representative of triplicates.

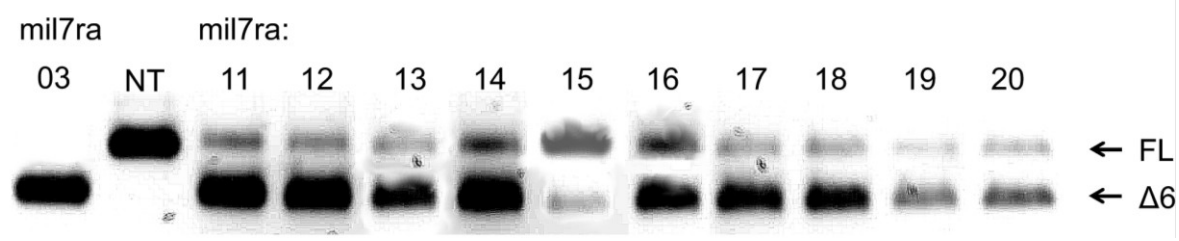
Skipping of *IL7RA* exon 6 was found to be inducible by transfection of RAW 264.7 cells with the LNA SSO mIL7Rα_03, and also to an extent with mIL7Rα_01, mIL7Rα_02, mIL7Rα_07 and mIL7Rα_08 (Figure 3.12a). mIL7Rα_03 was subsequently shown not to interfere with reverse transcription of the full-length amplicon even at high concentrations (Figure 3.12d). Ten further LNA SSOs targeted to *IL7RA* exon 6 were designed, concentrating specifically on the region targeted by mIL7Rα_03 (Figure

3.12c). As this LNA SSO induced the most skipping in the first screen, it was reasoned that this region might harbour the binding sites for the RNA-binding proteins that are most important for exon definition. Figure 3.12b shows that mIL7Rα_03 was still the most potent inducer of *IL7RA* exon 6 skipping and represents a promising candidate to be taken forward into *in vivo* mouse studies.

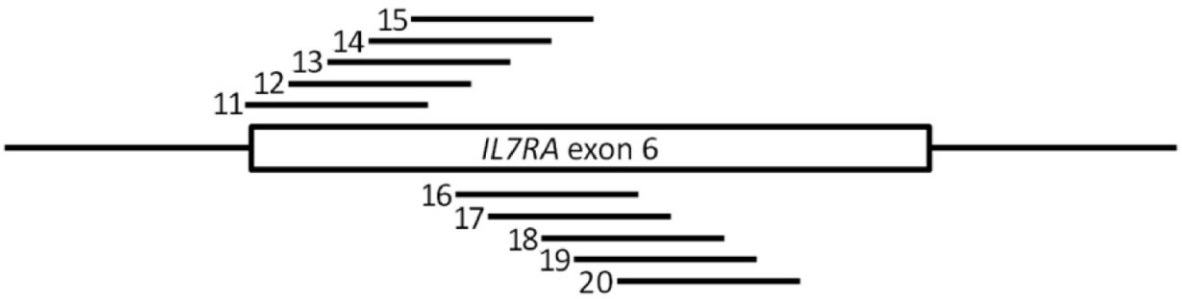
a



b



c



d

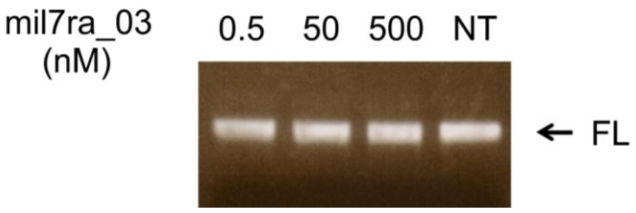


Figure 3.12: Screen of ability of LNA SSOs targeted to *IL7RA* exon 6 to induce exon skipping. PCR products amplified from cDNA were resolved in 2% agarose. **(a & b)** LNA SSOs mIL7Rα_01-10 **(a)** and mIL7Rα_011-20 **(b)** were transfected into RAW264.7 cells, after 24 h RNA and cDNA was made and PCR was performed with cDNA specific primers flanking exon 6 to assay for induction of skipping. mtnfr1_06 was included as a positive control. Bands amplified from full-Length (FL) and Δ6IL7RA (Δ6) transcripts are indicated. Band quantification analysis was performed using ImageJ software. **(c)** Schematic representation of the regions of murine *IL7RA* targeted by LNA SSOs mIL7Rα_11-20. **(d)** The indicated LNAs were added directly to reverse transcription reactions of RNA taken from non-transfected RAW264.7 cells at the indicated concentrations.

The ability of LNA SSOs mtnfr1_06 to induce skipping of murine *TNFRSF1A* exon 6 *in vivo* was investigated. As a positive control for the induction of splice switching, a control group of mice were treated with 3274, an LNA SSO capable of inducing of a splice isoform of TNFR2 lacking exon 7 following intraperitoneal injection (Graziewicz *et al.*, 2008). Figure 3.13 shows that 3274 induces no skipping of *TNFRSF1A* exon 6 and that mtnfr1_06 induces no skipping of *TNFRSF1B* exon 7, and that the negative control non-targeting LNA SSO 5678 induces skipping of neither.

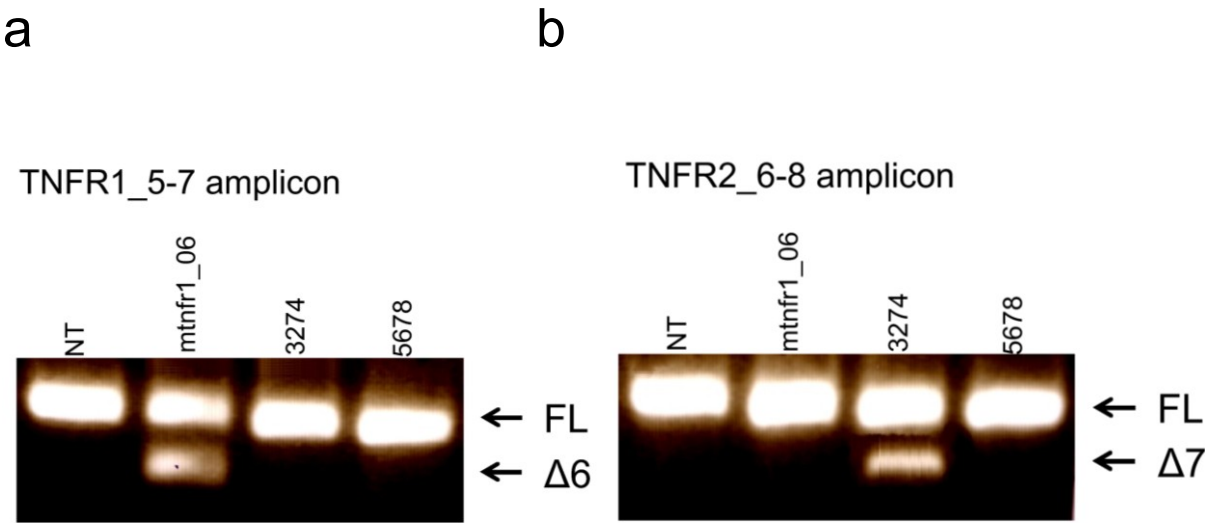
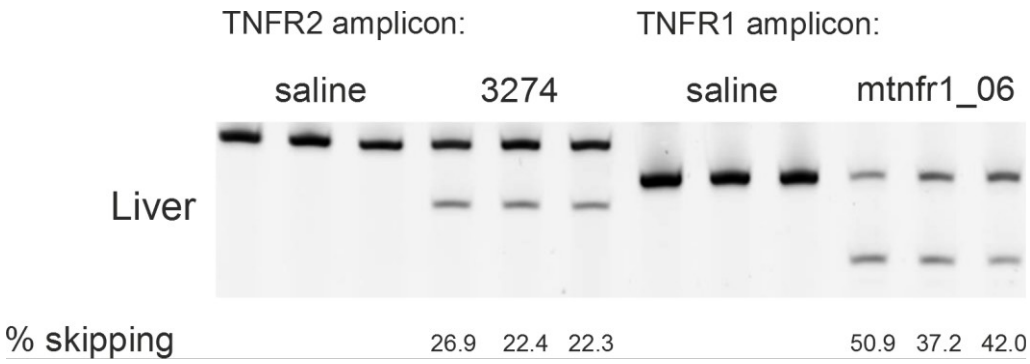


Figure 3.13: analysis of splice-switching associated with LNA SSOs mtnfr1_06, 3274 and 5678 *in vitro*. LNA SSOs were transfected into L929 cells and after 24 h RNA and cDNA was made and PCR was performed with cDNA specific primers flanking murine **(a)** *TNFRSF1A* exon 6 or **(b)** *TNFRSF1B* exon 7 to assay for induction of skipping. PCR products amplified from cDNA were resolved in 2% agarose. Bands amplified from full-Length (FL) TNFR1 and TNFR2, Δ6TNFR1 (Δ6) and Δ7TNFR2 transcripts are indicated.

Figure 3.14a shows that mtnfr1_06 had potently induced splice switching of *TNFR1SF1A* to a transcript lacking exon 6 in the liver of mice 15 days after the final injection, with even more potency than induction of the Δ7TNFR2 transcript by 3274. The ability of the mtnfr1_06 LNA SSO to be taken up by and induce splice switching in a variety of tissues was assayed 21 days after the final injection. As well as the liver, clear induction of the transcript lacking exon 6 was seen in spleens of mtnfr1_06-treated mice (Figure 3.14b).

a



b

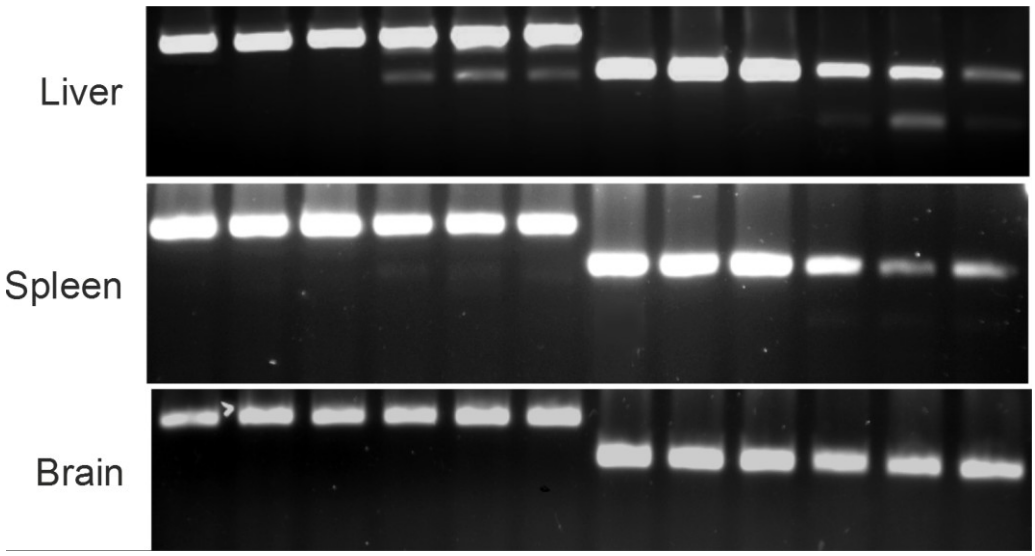
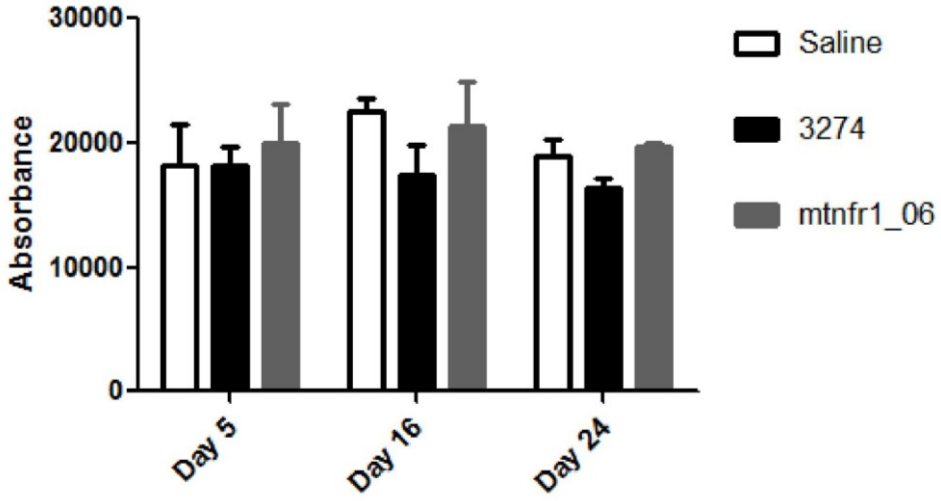


Figure 3.14: LNA SSO mtnfr1_06 induces skipping of *TNFRSF1A in vivo*. Mice were injected intraperitoneally with saline, SSO3274 or mtnfr1_06 at 25 mg/kg/day once daily for 5 days. Mice were taken at **(a)** day 15 or **(b)** day 21, and total RNA isolated from the indicated organ was analysed by RT-PCR for induction of splice switching of *TNFRSF1B* exon 7 (lanes 1-6) and *TNFRSF1A* exon 6 (lanes 7-12) pre-mRNA splice switching. PCR products from cDNA were resolved in **(a)** 6% TBE

polyacrylamide or **(b)** 2% agarose. Band quantification analysis was performed using ImageJ software. Each lane represents analysis of RNA isolated from the organ of a single treated mouse.

As mice produce soluble TNFR1 (sTNFR1) both by cleavage of the extracellular domain and by exosomal release of full-length receptor (Goodwin *et al.*, 1991), specific detection of a soluble isoform induced by splice switching was not possible simply by using an antibody specific to the ordinarily intracellular portion of the protein. No treatment group patterns were observed in levels of total sTNFR1 detectable by ELISA in the serum of mice collected at days 5, 16 and 24 (Figure 3.15a). To test sTNFR1 production in a more controlled setting, cell culture supernatant of L929 cells treated with mtnfr1_06 analysed. A more than 50% reduction in production of sTNFR1 was observed in mtnfr1_06 treated cells when compared with untreated cells (Figure 3.15b). To investigate this further, cellular and soluble expression of proteins from cDNA constructs encoding the full-length, full-length murine TNFR1 fused to EYFP, or an equivalent construct lacking exon 6 (Δ6TNFR1) was analysed *in vitro* (Figure 3.16). Whilst similar levels of EYFP were detected in cell lysates (Figure 3.16a), considerably less was detected in supernatants of cells transfected with murine Δ6TNFR1 (Figure 3.16b). Together, these results suggested that removal of exon 6 from the murine TNFR1 sequence does not result in the production of a protein equivalent to that of the human protein.

a



b

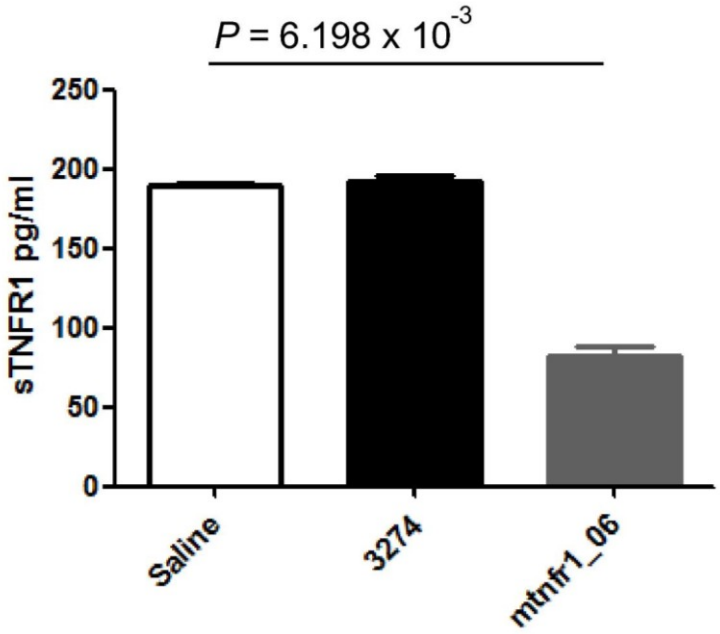


Figure 3.15: Influence of mtnfr1_06 associated skipping of murine *TNFRSF1A* exon 6 on sTNFR1 production. **(a)** ELISA for sTNFR1 in serum of mice injected intraperitoneally with saline, SSO3274 or mtnfr1_06 at 25 mg/kg/day once daily for 5 days, isolated on the indicated days. **(b)** ELISA for

sTNFR1 in cell culture supernatant of L929 cells 72 h after treatment with the indicated LNA SSO. Error bars represent mean ± SEM; *P* value is indicated.

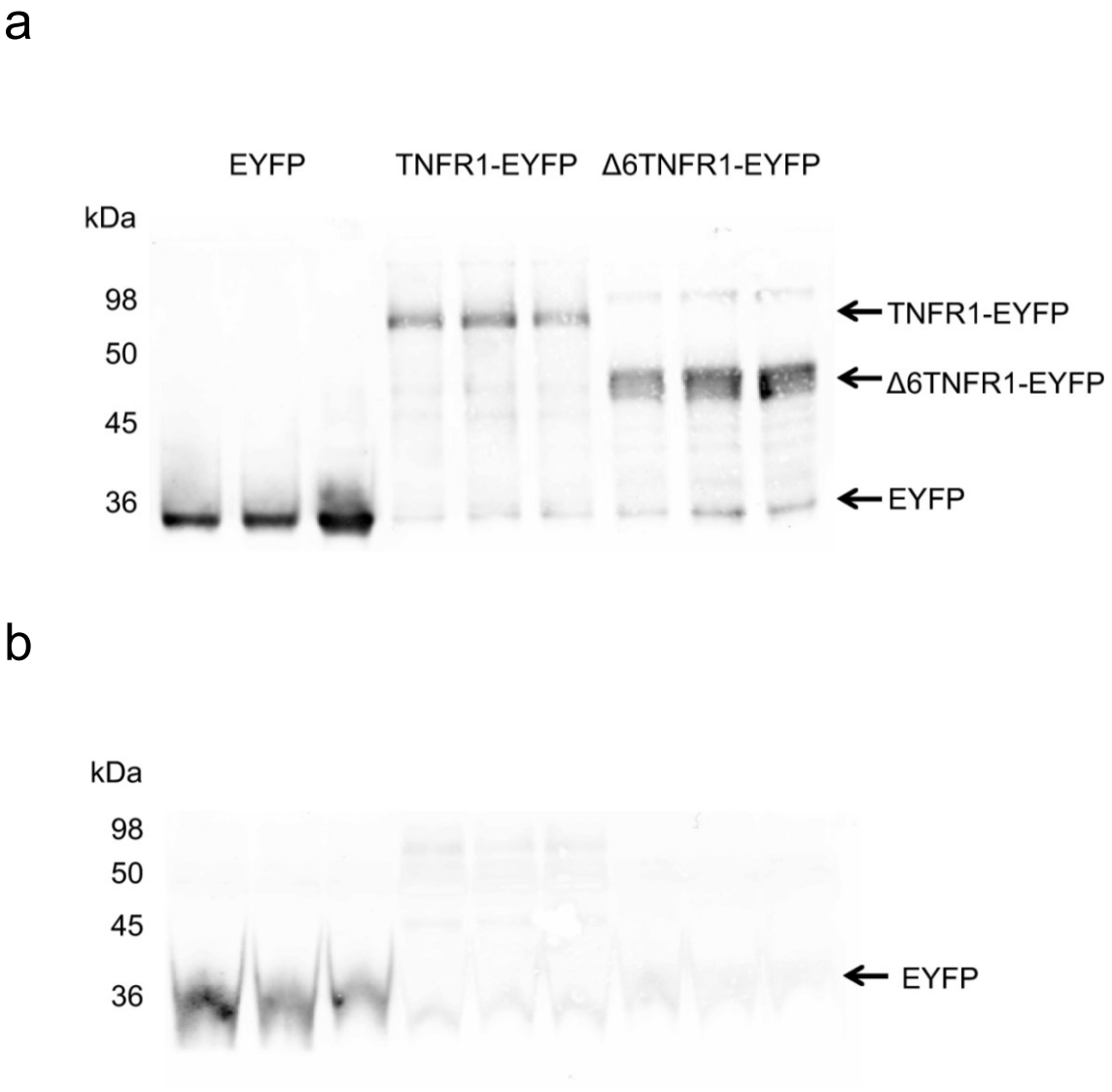


Figure 3.16: Expression of EYFP tagged murine TNFR1 and Δ6TNFR1. HEK 293T cells were transiently transfected with empty EYFP vector, TNFR1-EYFP or Δ6TNFR1-EYFP constructs and EYFP expression was analysed at 72 h in **(a)** lysates and **(b)** concentrated cell culture supernatant by western blot.

In an attempt to better understand the differences between the properties of human and murine Δ6TNFR1, *in silico* analysis of hydrophobicity and amino acid identity between full-length and Δ6 isoform receptor proteins, transcribed from mRNA lacking exon 6 were analysed using web-based ProtScale and Multalin software (Supplementary Figure 2). No regions of strikingly high or low hydrophobicity were observed such as to account for the differences in the ability of human and mouse Δ6TNFR1 to be secreted.

3.4 Discussion

3.4.1 Guanine at rs1800693 potentiates skipping of *TNFRSF1A* exon 6

In an *in vitro* minigene system containing the genomic region of *TNFRSF1A* from the last 299 bp of intron 5 to the end of exon 9, rs1800693^{G} potentiated the exclusion of exon 6 from the mature transcript (Figure 3.1). This pattern of splicing was observed in several mammalian cell types, suggesting that it is not a cell-type specific splicing phenomenon and is likely to involve changes in the interactions of ribonucleoproteins and RNA sequences that are conserved across species. Furthermore, a simplified minigene system in which the genomic insert was the 3' 299 bp of intron 5, exon 6 and intron 6 only similarly exhibited rs1800693^{G}-mediated skipping of exon 6 (Figure 3.9a), suggesting that this was not an artefact of minigene design.

We next sought to investigate splicing of *TNFRSF1A* exon 6 in cells isolated from humans based on rs1800693 genotype. Immune cells isolated from the peripheral blood of donors have previously been used in studies involving TNFR1 mutations (Bulua *et al.*, 2011; Simon *et al.*, 2010), and the relatively high expression of *TNFRSF1A* in these readily accessible cells makes them ideal for analysing the effects of rs1800693^{G}. Furthermore, *in vitro* studies had revealed alternative splicing of exon 6 to occur in multiple cell types and so it was likely that the *trans*-acting factors necessary for alternative splicing would also be present in peripheral blood immune cells (Watanuki *et al.*, 2008). Moreover, as MS is an autoimmune disease it is more appropriate to study the effects of the rs1800693^{G} allele in immunologically-relevant cell types. A small-scale pilot PCR on cDNA with primers in exons 5 and 10 and subsequent sequencing of bands revealed that skipping of exon 6 occurred in PBMCs, and appeared to correlate with the number of copies of the rs1800693^{G} allele (Figure 3.2). This was confirmed by qRT-PCR analysis of transcripts containing and lacking *TNFRSF1A* exon 6 (designated 6-7_TNFR1 and Δ6_TNFR1, respectively), compared with control *TNFRSF1A* exons (3-4_TNFR1) relative to a housekeeping gene in a powerful study, analysing a variety of immune cell

subsets from 15 AA homozygotes, 28 AG heterozygotes and 13 GG homozygotes (Figure 3.3). Graphs of ΔCT values do not represent as clearly as those displaying the percentage of Δ6_TNFR1 transcripts the by-rs1800693^{G} allele copy increase for two reasons. Firstly, it can be seen from percentage Δ6_TNFR1 data that there is no real expression of this transcript in AA homozygotes (Figure 3.3b and d), making the large difference between ΔCT values for Δ6_TNFR1 between AA homozygotes and heterozygotes misleading. Secondly, as ΔCT values are taken during the exponential phase of DNA target amplification, a single ΔCT difference corresponds to a two-fold difference in the amount of target DNA. For all cell types analysed, there is a single ΔCT difference between heterozygotes and GG homozygotes (Figure 3.3a), and so taken together this means that there is no Δ6_TNFR1 expression in AA homozygotes, and double the expression of Δ6_TNFR1 in GG homozygotes compared to heterozygotes, which is the pattern seen when the percentage of Δ6_TNFR1 transcripts amongst total TNFR1 transcripts is determined. Regression analysis confirmed this by-rs1800693^{G} allele copy increase in Δ6_TNFR1 transcripts to be highly significant (Figure 3.3d).

Skipping of exon 6 was found to be most pronounced in CD14^{+} monocytes, where transcripts lacking exon 6 made up almost 25% of *TNFRSF1A* transcripts in GG homozygotes, more than twice the percentage of transcripts found in PMNs and CD3^{+} T cells (Figure 3.3d). These cells have been demonstrated to have important roles in MS; monocyte-derived macrophages are found in MS lesions and are thought to be effectors of autoimmune inflammation, whilst monocyte-derived macrophages and DCs are thought to act as APCs for autoreactive T cells (Kouwenhoven *et al.*, 2001). Changes in the nature of signalling through TNFR1 in these cells may therefore have an important role in predisposition to the development of MS.

We were unable to detect a reciprocal decrease in transcripts containing exon 6 with increasing numbers of Δ6_TNFR1 transcripts (Figure 3.3). This may be because transcription of the *TNFRSF1A* gene is in some way regulated to ensure a constant level of full-length transcripts; in GG homozygotes increased transcription would compensate for an increase in transcripts lacking exon 6. However, qRT-PCR data for exons 3-4 revealed there to be no difference in *TNFRSF1A* transcription by genotype (Figure 3.3f). Alternatively, the commercial qRT-PCR primer-probe set used to detect transcripts containing exon 6 might not be specific enough. Applied Biosystems assert that the assay detects both exons 6 and 7, but depending on the design of the primers and probes it might be possible for transcripts with exon 7 but lacking exon 6 to still be detected. The most likely explanation is that a decrease in transcripts containing exon 6 cannot be detected because even in GG homozygotes, the transcript containing exon 6 is far more abundant, as evidenced by absolute copy numbers determined by qRT-PCR and titrations with plasmid standards (Figure 3.3b and 3.3c). In this instance the relatively small decrease in numbers of transcripts with exon 6 would take a very large sample size to be able to detect a significant difference by genotype. This is in agreement with the gel of the small-scale pilot, in which there appears to be no difference in intensity of bands containing exons 5-10 between individuals of each genotype (Figure 3.2). Our inability to detect a significant difference in the levels of transcripts containing exon 6 at the RNA level indicated that it was unlikely that we would be able to detect a change in the level of full-length TNFR1 at the protein-level, and furthermore that the functional effect by which rs1800693^{G} predisposes to the development of MS is less likely to be through down-regulating the full-length TNFR1 isoform, and is more likely to be the production of a novel TNFR1 isoform.

The difference observed between the percentages of Δ6_TNFR1 transcripts from 'G' minigenes and GG homozygotes are likely to be due to artefacts of the system, which involves very high levels of expression from a small genomic region of *TNFRSF1A* and splicing to exogenous vector exons.

Indeed, the minigene systems were used primarily to give an insight as to whether alternative splicing occurred, and the qRT-PCR data are much more likely to represent the *in vivo* proportions 6-7_TNFR1 and Δ6_TNFR1 transcripts. Nevertheless, as qRT-PCR makes use of two separate primer-probe assays to detect the different transcripts, we chose to investigate splicing of *TNFRSF1A* exon 6 using a single assay using the Agilent DNA 1000 system, which has previously been used to investigate alternative splicing by genotype ((Coulombe-Huntington *et al.*, 2009); Figure 3.4). Following PCR with cDNA-specific primers flanking exon 6 we were able to quantify skipping using Agilent DNA 2100 Bioanalyzer software. Whilst there was a significantly greater proportion of amplicons lacking exon 6 amplified from cDNA made from cells isolated from GG homozygotes than AA homozygotes, this was not as significant as the differences detected by qRT-PCR, and no significant difference was detected between homozygote groups versus heterozygotes (Figure 3.4b). This is likely to be due to this assay system not being as sensitive as qRT-PCR, and a larger sample size would likely have revealed an intermediate number of transcripts lacking exon 6 in heterozygotes.

3.4.2 The exon 6-intron 6 boundary of *TNFRSF1A* exon 6 is not weak and rs1800693^{G}-mediated alternative splicing likely involves members of the SR protein family of splicing factors

Co-transfection of cells with a construct expressing a U1 snRNA complementary to the *TNFRSF1A* exon 6-intron 6 boundary was unable to cause reversion of splicing to that of the ancestral rs1800693^{A} allele (Figure 3.5). This data was in agreement with *in silico* analysis of splice site strength, suggesting that *TNFRSF1A* exon 6 does not have a weak 5' splice site, and that the mechanism by which rs1800693^{G} disrupts proper recognition of the exon6-intron 6 boundary is not by generating a sequence for which the U1 component of the spliceosome has such affinity that it is below the threshold required for proper 5' splice site recognition and inclusion of exon 6 in the mature transcript.

Splicing of RNA transcribed from equivalent constructs with 'T' or 'C' at position rs1800693 was found to be similar to that transcribed from the rs1800693^{A} construct, in which exon 6 is present in the mature transcript. This observation is consistent with several possible molecular mechanisms for how a 'G' at position rs1800693 causes skipping of *TNFRSF1A* exon 6. It may generate a consensus binding sequence for a splice-mediating ribonucleoprotein that upon binding somehow impairs definition of the exon 6-intron 6 boundary or assembly of the necessary splice-regulator and effector proteins to bring about proper recognition of the 5' splice site of intron 6. Alternatively, rs1800693^{G} may disrupt an existing consensus binding site for a splice-mediator that is important for exon 6-intron 6 boundary definition, or that acts as an adaptor protein or binding partner for a crucial component of the 5' splice site complex. Of these two scenarios, the former is more likely, as 'T' or 'C' at rs1800693 do not result in alternative splicing of *TNFRSF1A* exon 6. It should be noted, however, that consensus sequences for splice-mediating ribonucleoproteins are weak (Wang and Cooper, 2007) and partial redundancy at this nucleotide in the putative regulatory element may explain why only a 'G' at this position results in exon skipping. Additionally, SROOGLE predicted the rs1800693^{G} allele only to result in the generation of two overlapping ISRs (AGGUG and AGGUGA) that were identified by Voelker and Berglund 2007 through computational analysis of conserved intronic sequences between eutherian mammals to potentially regulate the splicing of an exon immediately upstream (Voelker and Berglund, 2007) (Figure 3.6).

Another means by which rs1800693^{G} may induce skipping of exon 6 is through the creation of a unique local secondary structure to the RNA that is non-permissive to the assembly of necessary components for 5' splice site recognition, or conversely through disrupting a permissive secondary structure. However, *in silico* analyses of sequences of different of lengths using several web-based

programmes for predicting the secondary structure of RNA did not predict any rs1800693^{G}-specific changes (Supplementary Figure 3). Alterations to the secondary structure of RNA local to the exon 6-intron 6 boundary by rs1800693 genotype were therefore not explored experimentally.

The *trans*-acting factors mediating alternative splicing events can be identified through RNA pulldown studies (Baralle *et al.*, 2009). Common to all of the potential mechanisms by which rs1800693^{G} induces skipping of *TNFRSF1A* exon 6 is the differential binding of one or more splice-mediating ribonucleoproteins. Several SNP-mediated alternative splicing events result in subtle changes to the proportion of transcripts containing the affected exon in the mature transcript (Wang and Cooper, 2007). For example, the rs6897932^{C} allele has been demonstrated in a minigene system to result in 4-5 fold increase in skipping of *IL7RA* exon 6 (Gregory *et al.*, 2007). In such instances, it is more likely that a SNP results in a relative rather than an absolute change in the profile of ribonucleoprotein binding partners, which might be difficult to detect by RNA pulldown. We demonstrated the rs1800693 A>G transition to result in an increase of exon 6 skipping from ~ 30% to ~ 95% in an equivalent single exon minigene (Figure 3.9a); this is of the order of % changes in alternative splicing that relevant *trans*-acting factors have previously been identified by pulldown (Pagani *et al.*, 2003; Skoko *et al.*, 2008; Suzuki *et al.*, 2010). We therefore sought to identify binding partners involved in rs1800693^{G}-mediated alternative splicing using this technique.

There was no obvious difference observed between the profiles of Coomassie-stained, SDS-PAGE-resolved ribonucleoprotein binding partners of 'A' and 'G' RNA probes (Figure 3.7). This may be because the protein that was subsequently identified to bind the 'A' probe more than 'G' probe, SRp40, resolves at the same molecular weight as several abundant proteins that bind both probes (40 kDa; Figure 3.7). *In silico* prediction of binding protein partners for a given RNA sequence is

imperfect due to differences between the methods and conflicting results of studies used to identify splice regulatory elements, and the weak consensus of recognition elements (Baralle *et al.*, 2009). Nevertheless, several programmes predicted altered binding of one or several members of the SR protein family, a class of serine/arginine-rich proteins with important roles in both constitutive and alternative splicing; by modulating splice site recognition and spliceosome assembly (Supplementary Figure 1a-c). We therefore performed a speculative western blot with a monoclonal antibody recognising an epitope present in all SR proteins, 1H4G7 (Neugebauer *et al.*, 1995). As well as signal in both lanes at 20 and 30 kDa, thought to correspond to SRp20 and SRp30c respectively, signal at 40 kDa was detected specifically in lanes containing proteins pulled down with 'A' probes (Figure 3.8d). From comparison with previous western blots using this antibody and its inferred molecular weight, it was predicted that this band corresponded to SRp40, which has a well established role in promoting exon inclusion during splicing (Du *et al.*, 1997; Tacke *et al.*, 1997; Yan *et al.*, 2010), in stark contrast to ISR prediction by SROOGLE (Figure 3.6).

We hypothesised that the A>G transition at rs1800693 disrupts association of SRp40 through its RNA recognition motif (RRM) at the exon 6-intron 6 junction, causing improper definition of the 5' splice site of intron 6, consequent reversion to the previous 5' splice at the exon 5-intron 5 boundary, and skipping of exon 6. SR proteins also have a domain rich in arginine and serine repeats (RS), through which they interact with other splice mediators such as components of the spliceosome, the heterogeneous nuclear ribonucleoproteins (hnRNPs) and other SR proteins to regulate splicing (Long and Caceres, 2009). Therefore, whilst association of SRp40 in the proximity of rs1800693 may be important in *TNFRSF1A* intron 6 5' splice site definition directly, it may also act by associating with and increasing the local concentration of other components of the ribonucleoprotein complex that are the crucial splice modulators at this junction. Conversely, SRp40 might not bind directly, but may

be recruited by association through its RS domain to the RNA-binding protein, where it may have a functional role in exon 6-intron 6 boundary definition or may simply 'tag' the functional protein.

Knockdown and overexpression studies of putative *trans*-acting factors are typically performed to conclusively demonstrate their necessity or otherwise in a splicing event (Baralle and Baralle, 2005). From pulldown studies we predicted that overexpression of SRp40 would result in an increase in the local concentration of SRp40 at the exon 6-intron 6 boundary sufficient to overcome the decrease associated with reduced affinity for RNA transcribed from the rs1800693^{G} allele, rescuing exon 6 inclusion in the mature transcript. Overexpression of SRp40 in fact resulted in increased skipping of exon 6, in mature transcripts from both 'A' and 'G' minigenes (Figure 3.9a). Furthermore, overexpression of SRp40 in cells transfected with minigene constructs corresponding to 'T' and 'C' alleles of rs6897932 in *IL7RA* resulted in increased inclusion of exon 6, demonstrating that SRp40 overexpression does not constitutively result in increased exon skipping (Figure 3.9b).

The contradicting results of pulldown and overexpression studies can potentially be explained by a more complicated situation, in which there are multiple binding sites for SRp40 that act together to determine *TNFRSF1A* exon 6 splicing. The RNA pulldown technique necessitates the use of relatively short RNA probes for efficient immobilisation on beads and the ability to detect differences between probes despite the promiscuous binding of splice-mediators. The RNA sequence transcribed from the genomic region of *TNFRSF1A* in the exon 6 only minigene is almost ten times longer and may therefore harbour many more binding sites for SRp40. Furthermore, the secondary structure of the RNA transcribed from the minigene is predicted to be very different to that of the probes transcribed *in vitro* (Supplementary Figure 3), and this may also influence SRp40 binding.

3.4.3 LNA SSOs targeted to murine *TNFRSF1A* exon 6 are able to durably induce skipping *in vitro*, and *in vivo* in several tissues

As discussed earlier, mouse models have proven to be very useful in understanding both the pathogenesis of MS and the genetic component of MS risk, providing invaluable insights into molecular mechanisms and how they bring about organism- and disease-level consequences to predispose individuals harbouring these variants to developing the disease (reviewed by (Croxford *et al.*, 2010). However, the generation of transgenic mice is a time-consuming and expensive process, and there is no guarantee that the end-product will appropriately model the situation in humans. For example, the mouse *TNFRSF1A* gene sequence cannot simply be replaced with the human sequence lacking exon 6, as it might not interact appropriately with murine ligands and co-factors, making it impossible to distinguish between systemic artefacts and genuine mechanistic insights. An alternative approach would be to simply replace the murine *TNFRSF1A* sequence with the murine sequence lacking exon 6. Even using contemporary speed congenics techniques (Wong, 2002), it can still take years before mice are ready for experiments. We therefore decided to use an alternative, relatively much cheaper and quicker option and try to develop a mouse model for the effect of rs1800693^{G} using antisense technology to temporarily and sensitively induce skipping of exon 6 of murine *TNFRSF1A*.

For the induction of soluble protein isoforms, SSOs have several advantages over simple injection with recombinant soluble protein. Levels are titratable and durable, and come from an endogenous source, reducing adverse reactions (Graziewicz *et al.*, 2008). Furthermore, increased stability reduces the number of procedures for animals and avoids the physiological problems associated with fluctuating levels of the protein of interest associated with repeated cycles of injection and degradation that contribute noise to experimental results (Graziewicz *et al.*, 2008).

Previously, Graziewicz *et al.* used a 16-mer Locked Nucleic Acid (LNA) SSO to successfully, sustainably and non-toxically induce a TNFR2 splice variant in mice by IP injection and were thereafter able to study the effects of the induction of the novel protein transcribed from this splice variant in several inflammatory diseases (Graziewicz *et al.*, 2008). We therefore performed a screen of ten LNA SSOs targeted to *TNFRSF1A* exon 6 in L929 cells (Figure 3.11a). The exon6-intron 6 junction was targeted in particular in an attempt to competitively inhibit assembly of the 5' splice site complex and cause reversion to the upstream 5' splice site, which would result in exon skipping. Figure 3.11a shows that skipping of murine *TNFRSF1A* exon 6 was most potently induced by LNA SSOs mtnfr1_04-06, all of which were targeted to the 5' end of the exon. These three LNA SSOs all induced greater than 90% induction of the murine Δ6_TNFR1 splice isoform, and had a 10 nucleotide complementary target region in common, ACCAGGACTC, implying that this may harbour the binding site for a splice-mediating protein that has an important role in exon 6 definition. It is important that the SSOs used to induce exon skipping do not interfere with the detection of full-length transcripts, otherwise the potency with which skipping is induced will be over-estimated. It was for this reason that mtnfr1_06 was selected rather than mtnfr1_04 or m_tnfr1_05 to take forward into animal studies (Figure 3.11b).

The pilot study was designed by reference to Graziewicz *et al.* 2008, in which intraperitoneal injection of a 16-mer LNA SSO for 5 consecutive days at 25 mg/kg/day was able to potently and durably induce splice switching, particularly in the liver and kidneys of treated mice (Graziewicz *et al.*, 2008). Mice treated with the LNA used in this study, 3274, were included as a positive control group for induction of splice switching, along with a negative control LNA not targeted to any region of the mouse genome. Before initiating the study, we first ensured that each LNA used in the study

was only able to induce skipping of the target exon, that we were able to use LNA 3274 to induce skipping of murine *TNFRSF1B* exon 7 in the same way as Graziewicz *et al.*, and that the primers we had designed to detect this splice switching were appropriate (Figure 3.13). LNAs injected via the intraperitoneal route have previously been demonstrated to accumulate in the livers of treated mice (Roberts *et al.*, 2006), and so to assay the induction of splice switching total RNA was made from livers of three mice from each treatment group 15 days following the final injection with LNA. Despite some reports of high toxicity of LNAs due to their irreversible and promiscuous binding of cellular nucleic acids (Swayze *et al.*, 2007), no mice displayed abnormal behaviour or developed any clinical symptoms associated with LNA treatment throughout the duration of the study.

Using 3274, Graziewicz *et al.* were able to induce production of a soluble isoform of murine TNFR2 (Δ7TNFR2) by removing the exon encoding the transmembrane domain of the receptor, and demonstrated that circulating Δ7TNFR2 had disease-modifying properties in collagen induced arthritis (CIA) and TNF-induced hepatitis disease models (Graziewicz *et al.*, 2008). As splice switching was induced by mtnfr1_06 with even more potency than was observed in mice treated with 3274 (Figure 3.14a), we were optimistic that production of a Δ6TNFR1 isoform would be at sufficient levels such that any disease-modifying effects would be detectable in EAE. The high uptake and splice-switching potency of LNAs in hepatic cells was utilised by Graziewicz *et al.* to establish a 'protein factory', which thereafter would constantly seed Δ7TNFR2 into the circulating blood. For mtnfr1_06 to be able to act in the same way, Δ6TNFR1 would have to be a soluble protein. The exonic structure of TNFR1 is conserved between mice and humans, and removal of murine exon 6 is predicted to result in a frameshift, a premature stop codon and a truncated protein that is predicted to be soluble and secreted, as it retains the signal peptide of the full-length protein but, because of the frameshift induced by removal of exon 6, lacks the transmembrane domain encoded by exon 7.

Graziewicz *et al.* were able to develop an ELISA assay which allowed them to specifically detect Δ7TNFR2 in the serum of treated mice. Under physiological conditions, soluble murine TNFR2 is formed only by metalloprotease cleavage and consequent shedding of the extracellular domain of the receptor. The novel 3274-induced splice isoform could therefore be distinguished from endogenous soluble TNFR2 by using a capture antibody recognising the intracellular domain of the receptor, followed by a detection antibody recognising the extracellular domain (Graziewicz *et al.*, 2008). Murine soluble TNFR1 has been reported to be produced by two distinct mechanisms; metalloprotease-dependent cleavage and shedding of the extracellular domain and exosomal release of the full-length receptor (Goodwin *et al.*, 1991). It was therefore not possible to specifically detect mtnfr1_06-induced Δ6TNFR1 without the costly, lengthy and uncertain development of an antibody to the novel 40 amino acid sequence induced by the frameshift associated with skipping of murine *TNFRSF1A* exon 6. We therefore attempted to detect changes in levels of total sTNFR1 in serum isolated from blood samples taken from mice at days 5, 16 and 24 by treatment group, using an ELISA antibody pair recognising the extracellular domain of the protein and therefore capable of detecting cleaved, exosomally-released and mtnfr1_06-induced TNFR1 species. No significant difference was observed between treatment groups, and neither was any trend in sTNFR1 over time (Figure 3.15a). Serum samples often display high background in ELISA assays, and so we decided to investigate sTNFR1 production from cells induced to express murine Δ6TNFR1 in cell culture. Unexpectedly, 72 h cell culture supernatant from L929 cells confirmed to have had splice switching induced by mtnfr1_06 treatment contained significantly lower TNFR1 levels than untreated, saline and control treated cells (Figure 3.15b). Generation of murine TNFR1-EYFP and Δ6TNFR1-EYFP constructs and their transient transfection into HEK 293T cells and western blots on concentrated supernatants with an antibody with the ability to recognise EYFP confirmed that in contrast to *in silico* predictions, murine Δ6TNFR1 is not a secreted protein (Figure 3.16). As a mutant protein it is

possible that it is recognised by the cellular machinery to be imperfect or misfolded in some way, and therefore retained in the ER and ultimately targeted for degradation (Vembar and Brodsky, 2008).

If Δ6TNFR1 is not a secreted protein, for mtnfr1_06 to effectively model the effect of rs1800693^{G} the LNA SSO must have penetrance and potency in the relevant cell type(s) that Δ6TNFR1 exerts its disease-modifying effects in. Figure 3.13b shows that whilst the induction of Δ6TNFR1 mRNA was detectable in liver and spleens at 21 days following the final injection this only occurred at very low levels, and no skipping was induced in the brain. Previous studies have been better able to target LNA SSOs to immune cells by injecting intravenously. In this way, they have the opportunity to reach the lymph nodes and induce splice switching before being cleared by the liver and kidneys. In any case, experimental work on the human Δ6TNFR1 protein in parallel had emphatically demonstrated this to be a soluble and secreted protein. Therefore, even in an appropriate cell-type, induction of the production of a murine Δ6TNFR1 would not be able to accurately model the disease-modifying effects of the human protein, and so work with mtnfr1_06 was halted. Indeed, even if murine Δ6TNFR1 had been able to accurately represent the human Δ6TNFR1 protein conflicting data from studies using TNF antagonists in EAE (Selmaj and Raine, 1995), and clinical experience with anti-TNF therapy in MS patients (The Lenercept Multiple Sclerosis Study Group, 1999; van Oosten *et al.*, 1996), suggest that TNF may not play an identical role in EAE and MS, and therefore conclusions drawn from studies with a murine Δ6TNFR1 might be misleading.

Human and mouse TNFR1 share 64% amino acid identity (Milatovich *et al.*, 1991) and the exonic structure of the *TNFRSF1A* gene is conserved. The frameshift mutation associated with removal of exon 6 creates novel amino acid sequences, which whilst having similar hydrophobicity profiles have

only 44% identity (Supplementary Figure 2), which may explain why human and mouse Δ6TNFR1 have differ in their ability to be secreted.

3.4.4 LNA SSOs targeted to murine *IL7RA* exon 6 are able to induce skipping of this exon *in vitro*

LNA SSO screens in the mouse macrophage RAW264.7 cell line identified a promising candidate, mil7ra_03, for the development of a model for the effect of the rs6897932^{C} in human *IL7RA*. *IL7RA* exon 6 encodes the transmembrane domain of the IL-7 receptor alpha chain, and its exclusion from the mature transcript has previously been demonstrated to result in the production of a truncated, soluble IL7Rα isoform in humans. As mice do not naturally express a soluble, secreted version of this protein (Goodwin *et al.*, 1990), all sIL7Rα detected in cell culture supernatant of treated cells and in the peripheral blood of treated mice is likely to be the result of Δ6IL7Rα transcript induction by LNA SSO treatment. Exonic structure of *IL7RA* is conserved between mice and humans, identity between full-length proteins is 63%, and the novel amino acid sequences created by the frameshifts have 65% identity and similar hydrophobicity profiles (Supplementary Figure 4). These novel sequences are also much shorter than those generated by the frameshift in TNFR1 (26 amino acids) and their higher identity suggests that murine Δ6IL7Rα might also be a secreted protein, although transient transfection and expression studies will be used to confirm this before mil7ra_03 is trialled *in vivo*.

4.0 Expression and localisation of the protein translated from the *TNFRSF1A* transcript lacking exon 6

4.1 Introduction

Having demonstrated that rs1800693^{G} causes an alternative splicing event leading to the exclusion of *TNFRSF1A* exon 6 from the mature transcript, we next sought to characterise the splice isoform translated from this novel mRNA, comparing it to the full-length TNFR1 isoform.

4.1.1 Expression localisation of human TNFR1

TNFRSF1A expression occurs in almost all cell types, and significant surface TNFR1 levels are found on hepatocytes, monocytes, neutrophils, cardiac muscle cells, endothelial cells and hematopoietic progenitor cells (Wallach *et al.*, 1999), rendering them sensitive to TNF-mediated apoptosis. TNFR1 is translated in the ER as a 55 kDa, 455 amino acid, type I, single-pass transmembrane protein, anchored in the ER membrane by a 23 amino acid transmembrane domain and is N-glycosylated at three sites in the N-terminus of the protein before trafficking to the Golgi (Banner *et al.*, 1993; Zhang *et al.*, 2008). Under normal physiological conditions, the majority of cellular TNFR1 is localised to the Golgi through a 23 amino acid *trans*-Golgi-localisation sequence at the C-termius of the protein, with a smaller pool of TNFR1 expressed at the cell surface (Storey *et al.*, 2002). The Golgi-resident portion of cellular TNFR1 appears to be non-functional, acting only as a pool for cell surface TNFR1 (Wang *et al.*, 2003).

At the cell surface TNFR1 associates into trimers through homotypic, non-covalent, intermolecular associations between PLAD/CRD1 (Chan *et al.*, 2000; Lobito *et al.*, 2011). TNFR1 may be released in 20-50 nm exosome-like vesicles to form a full-length soluble TNFR1 pool, or its extracellular, ligand-binding domain may be cleaved at a site proximal to the transmembrane domain by the zinc

metalloprotease enzyme ADAM17/TACE to yield a 28-32 kDa soluble TNFR1 species, through receptor shedding (Hawari *et al.*, 2004; Reddy *et al.*, 2000). Shedding in this way allows dynamic and sensitive regulation of cell responsiveness to TNF, and also creates a pool of TNF-neutralising species, to dampen the inflammatory response. Upon binding of TNF, TNFR1 is also internalised through clathrin-mediated receptor endocytosis, a process that is required for the assembly of the DISC complex and induction of TNF-mediated apoptosis (Schneider-Brachert *et al.*, 2004).

In contrast to *TNFRSF1B*, *TNFRSF1A* mRNA expression is very stable and is not upregulated in response to soluble mediators; this is reflected in its comparatively simple promoter and enhancer regions (Vandenabeele *et al.*, 1995). Dynamic regulation of TNFR1 signalling is therefore achieved through a combination of controlled distribution of the receptor pool between the Golgi and cell surface, and TACE-mediated cleavage and shedding of the extracellular domain. The proinflammatory cytokine EMAP II has been demonstrated to cause redistribution of Golgi-resident TNFR1 to the cell surface (van Horssen *et al.*, 2006), whilst TNF and LPS have been shown to induce receptor shedding (Dri *et al.*, 2000) and histamine has been shown to potentiate both shedding and exosomal release of full-length receptor (Wang *et al.*, 2003).

4.1.2 *TNFRSF1A* folding and trafficking mutants

Mutations in the exons of *TNFRSF1A* that encode the CRDs in the extracellular portion of TNFR1 are associated with an autosomal dominant autoinflammatory disorder characterised by periodic fever, abdominal pain and inflammation termed tumour necrosis factor receptor associated periodic syndrome (TRAPS) (Kimberley *et al.*, 2007; Lobito *et al.*, 2011). Molecular modelling of TRAPS mutants revealed their potential to disrupt the overall structure of TNFR1 and *in vitro* studies have revealed abnormal intramolecular disulphide-bonding due to TRAPS mutations effecting cysteine

residues in CRDs 1, 2 and 3 (Lobito *et al.*, 2006; Rebelo *et al.*, 2006). This in turn has been observed to result in protein misfolding, defective trafficking and intracellular retention of TRAPS mutants, which are unable to traffick beyond the ER, where they accumulate (Lobito *et al.*, 2006; Siebert *et al.*, 2005; Todd *et al.*, 2007; Turner *et al.*, 2012).

The above observations were made by analysing TNFR1 expression in immune cell subsets isolated from TRAPS patient peripheral blood samples, and trafficking studies using transient transfection systems for the expression of wildtype TNFR1 and TRAPS mutants (Lobito *et al.*, 2006; Rebelo *et al.*, 2006; Siebert *et al.*, 2005; Simon *et al.*, 2010; Todd *et al.*, 2004). Short peptide sequence tags were used for *in vitro* immunolocalisation studies for the unbiased and equal detection of wildtype and mutant receptor proteins, whilst C-terminal fusions to variants of GFP allowed analysis of expression and association properties exclusively in cells expressing proteins of interest by flow cytometry (Chan *et al.*, 2000; Lobito *et al.*, 2006). In conjunction with fluorescent fusion proteins of endomembrane system organelle-resident proteins, fluorescently tagged wildtype and TRAPS mutant TNFR1 constructs have also been used to study intracellular receptor trafficking by confocal microscopy (Lobito *et al.*, 2006; Siebert *et al.*, 2005; Todd *et al.*, 2004).

A further consequence of defective trafficking of several TNFR1 mutants is an inability or reduced capacity to produce soluble TNFR1 (Kimberley *et al.*, 2007; Lobito *et al.*, 2006). Moreover, this has been demonstrated for TNFR1 mutants with an altered metalloprotease cleavage site which render the receptors insensitive to TACE (Kimberley *et al.*, 2007). This has been proposed to have a variety of functional implications, including defective downregulation of TNF-mediated inflammatory responses due to decreased production of soluble antagonist, to unregulated, constitutive signalling through uncleavable receptors (Kimberley *et al.*, 2007; Lobito *et al.*, 2011). The production of soluble TNFR1 species both *in vitro* and *in vivo* has typically been investigated using commercially available

and ELISA antibody pairs, capable of recognising both the cleaved, shed extracellular domain of TNFR1 and the full-length exosomally-released receptor (Churchman *et al.*, 2008; Manki *et al.*, 2006). Alternatively, *in vitro* studies have used antibodies to peptide or fluorescent protein tags for analysis by western blot (Lobito *et al.*, 2006; Simon *et al.*, 2010).

4.1.3 Analysis of protein translation

Mature mRNA molecules are translated into protein by the sequential addition of amino acids to form a polypeptide chain by ribonucleoprotein complexes termed ribosomes. During translation, a single mRNA molecule associates simultaneously with multiple ribosomes to increase the efficiency of protein synthesis; such structures are termed polyribosomes or polysomes (Alberts, 2008). As such, demonstrating the association of a given mRNA transcript with polysomes indicates that it is translated into protein (del Prete *et al.*, 2007). Density gradient separation of ribosomal complexes followed by analysis of fractionated RNA by northern blot and qRT-PCR has previously been used to investigate translational regulation at different stages of development and upon cell activation. (Garcia-Sanz and Lenig, 1996; Mikulits *et al.*, 2000). We therefore used this technique to investigate if the Δ6TNFR1 transcript was translated into protein.

4.2 Methods

4.2.1 Lentivirus preparation, concentration and titre determination

FLTNFR1 and Δ6TNFR1 lentiviral expression plasmids were generated from the empty pHRsinUbEm lentiviral expression plasmid using the primers indicated in Table 4.1 and 5' *BamHI* (GGATCC) and 3' *NotI* restriction sites by cloning (2.1.1). Lentivirus was prepared by follows. HEK 293T cells were seeded in T75 cell culture flasks to achieve a confluency of ~ 50% on the following day, for transfection. Per T75 flask of cells to be co-transfected, 1.6 ml of OPTI-MEM was mixed with 32 µl of TransIT®-293 Transfection Reagent (Mirus**,** Cambridge BioScience), mixed and incubated at room temperature for 5 min. 6 µg of the desired expression plasmid (empty pHRsinUbEm vector, FLTNFR1 or Δ6TNFR1) was mixed with 4 µg of the VSV-G envelope plasmid pMD2.G and 4 µg of the psPAX2 packaging plasmid in a separate tube, and then added drop-wise to the OPTI-MEM-TransIT®-293 mixture. The solution was then mixed and complexes were allowed to form for 15 min at room temperature. 12 ml of 37°C cell culture medium was then added, and the medium on the HEK 293T cells was replaced with this transfection medium. Cells were then incubated for 48 h at 37°C in 5% CO_2, after which time lentivirus-containing supernatants were harvested and stored at 4°C, and medium was replaced with 12 ml of cell culture medium. Supernatants were harvested again at 72 h post-transfection, pooled with 48 h supernatants and 0.2 µm filtered to remove cells and debris.

Name	***Sequence***
TNFR1lent_F	5'-AATTATTTAGGATCCGCCACCATGGGCCTCTCCACCGTGCC-3'
TNFR1lent_R	5'-GTATTACTTGCGGCCGCTCATCTGAGAAGACTGGG-3'
rem6_Afrag_R	5'-TCTAAGAAAACGAGTGTGTCTCCTGTAGTAAGCACCACAGT-3'
rem6_Bfrag_R	5'-GTCTCCTGTAGTAAGCACCACAGTGCTGTTG-3'
TNFR1fluor_F	5'-TAGGTACCGCCACCATGGGCCTCTCCACCGT-3'
FLTNFR1fluor_R	AGTGGATCCGTTCTGAGAAGACTGGGCGCGG-3'
Δ6TNFR1fluor_R	5'-AACTGGATCCGTGGTGTCGATTTCCCACAAACAAT-3'
HA-TNFR1_F	5'-ATACTCGAGATATACCCCTCAGGGGTTATTGG-3'

HA-FLTNFR1_R	5'-ATAGGTACCGTTCTGAGAAGACTGGGCGC-3'
HA-Δ6TNFR1_R	5'-ATAGGTACCGTGGTGTCGATTTCCCACAAACAAT-3'

Table 4.1: Primers to generate inserts for TNFR1 constructs.

Lentiviral particles were concentrated in sterile Beckman Coulter centrifuge tubes (Beckman Coulter) by ultracentrifugation at 22,000 x *g* for 2 h 30 min at 4°C using an Avanti JA 30.50 rotor. Supernatant from ultracentrifugation was discarded and the lentiviral pellet was resuspended in residual medium, aliquoted and stored at -80°C until further use.

Viral titre was determined by serial dilution and transduction of HEK 293T cells as follows. HEK 293T cells were seeded at a concentration of 1 x 10^5 cells/1 ml, in wells of a 12 well plate. Titration was performed by adding 10-fold serial dilutions (five dilution points) of the concentrated virus to wells containing HEK 293T cells. Cells and lentivirus were then cultured at 37°C in 5% CO_2 for 72 h. Transduction efficiency was assessed by flow cytometry by analysing the percentage of cells expressing Emerald GFP. The viral titre in transduction units (TU/µl) was calculated by multiplying the fraction of cells transduced by the number of cells (1 x 10^5), and then multiplying this to give the number of cells that would be transduced by 1 µl of concentrated virus, at a volume of lentivirus at which fewer than 10% of cells were transduced. For example, if 0.01 µl of concentrated lentivirus transduced 5% of 100,000 cells, the viral titre was 500,000 TU/µl.

For all experiments using the lentiviral expression system, HEK 293T cells were transduced at the time of seeding, at a multiplicity of infection (MOI) of 50; ie. 50 TUs per cell.

4.2.2 qRT-PCR for *TNFRSF1A* exons and EmGFP in lentivirally-transduced cells

Relative expression of *TNFRSF1A* exons in lentivirally-transduced HEK 293T cells expression FLTNFR1 or Δ6TNFR1 empty lentivirus was assayed by qRT-PCR on cDNA made from total RNA isolated from transduced cells at 72 h post transduction, as described in 2.2.3-2.2.5. Expression levels of human *TNFRSF1A* exons 3-4 and 6-7 were analysed using TaqMan® Gene Expression Assays Hs00533562_g1 and Hs00533565_g1 respectively. EmGFP expression was determined using a custom-designed primer-probe set, the details of which can be found in Table 3.2. Expression levels of TNFRSF1A exons are given as ΔCT, calculated by subtracting the CT for EmGFP from the CT value for each TNFRSF1A primer-probe assay.

4.2.3 Constructs for transient transfection

4.2.3.1 Human TNFR1-EYFP and -ECFP fusion protein constructs

HA-tagged, EYFP fusion protein constructs were generated as follows. The above fluorescent fusion protein constructs were used as templates in PCR reactions (2.2.1) with the primers detailed in Table 4.1 to generate FLTNFR1 and Δ6TNFR1 inserts lacking the TNFR1 signal peptide sequence. Inserts incorporated an *XhoI* site at the 5' end of the fragment, and a *KpnI* at the 3' end which were used to clone inserts in-frame with upstream TNFR2 leader and HA tag sequences, and the downstream EYFP sequence.

A human FLTNFR1 insert was amplified by PCR (2.2.1) using the primers indicated in Table 4.1 from a human TNFR1 cDNA construct (clone 4131360, Open Biosystems, Thermo Scientific) incorporating *KpnI* and *BamHI* restriction enzyme sites at the 3' and 5' ends of the insert respectively. This was cloned in-frame into pEYFP-N1 and pECFP-N1 vectors (2.1.2), and a Δ6TNFR1 insert was generated by overlap extension PCR using the primers indicated in Table 4.1 and cloned to generate equivalent fluorescent fusion protein constructs (2.1.1).

4.2.3.2 Organelle-resident fusion protein constructs

Human cDNA sequences for the endoplasmic reticulum (ER) resident beta subunit of the signal particle receptor (SRβ), and the stalk region (amino acids 1-114) of the *trans*-Golgi-resident protein *N*-acetylgalactosaminyltransferase-2 (GalNAc-T2) were amplified by PCR (2.2.1) from cDNA constructs (clones 6146939 and 5553465, respectively; Open Biosystems, Thermo Scientific) with the primers indicated in Table 4.2, to incorporate *KpnI* and *BamHI* sites at 5' and 3' ends of inserts, respectively. They were subsequently cloned (2.1.1) into pECFP-N1 using the appropriate restriction sites. An SRβ-DsRed2 fusion protein was subsequently constructed by amplifying the DsRed2 coding sequence from pIRES2-DsRed2 (Clontech) and cloning it in place of ECFP.

Name	***Sequence***
GalNAcT2_F	5'-TAGAATTCGCCACCATGCGGCGGCGCTCGCGGATGCTGC-3'
GalNAcT2_R	5'-CCGAGGATCCCGAAGCTTATCACTCTCCACCTGGTTGAACTTGTTGC-3'
SRbeta_F	5'-ATAGGTACCGCCACCATGGCTTCCGCGGACTCGCGCCG-3'
SRbeta_R	5'-CGCGGATCCGTGGCAATTTTAGCCAGCCATTTCTCCAAGTCCTGG-3'
DsRed2_F	5'-ATACCGGTCGCCACCATGGCCTCCTCCGAGAACGTCATCAC-3'
DsRed2_R	5'-ATGCGGCCGCTCTACAGGAACAGGTGGTGGCGGCCCTC-3'

Table 4.2: Primers to generate inserts for organelle-resident fusion protein constructs

4.2.4 Transient transfection and expression

The indicated TNFR1 constructs were transiently transfected into the indicated cell types as previously described (2.3.3), and incubated for the indicated amount of time at 37°C in 5% CO_2 before downstream analysis.

4.2.5 Flow cytometry

4.2.5.1 Transiently transfected/transduced cells

For analysis of surface expression of proteins in cells transfected or transduced *in vitro*, cells were analysed by flow cytometry on a FACS Calibur as described in 2.3.4. The Alexa-Fluor® 647-conjugated anti-CD120a antibody (clone H398, AbD Serotec) was incubated with cells to be stained at a final concentration of 2.5 µg/ml for 30 min at 4°C in the dark. For anti-HA stainings, cells were incubated with the monoclonal anti-HA.11 primary antibody (clone 16B12, Covance) at a final concentration of 10 µg/ml for 45 min, at room temperature. Cells were then washed twice with PBS, 2% FBS and incubated with APC-conjugated Goat-Anti-Mouse Ig (BD Bioscience) at a concentration of 0.4 µg/ml for 30 min at 4 in the dark.

For analysis of total expression (surface plus intracellular) of proteins in cells transfected or transduced *in vitro*, cells were first permeabilised by resuspension in 200 µl of ice-cold 70% EtOH in PBS and incubation at 4°C for 30 min. Cells were subsequently washed once with 200 µl PBS, 2% FBS before being stained and analysed by flow cytometry as above.

4.2.5.2 Whole blood multiplex immunostaining

Analysis of surface TNFR1 expression in the delineated immune cell subsets was performed by multiplex immunostaining. 50 ml blood samples were obtained from healthy donors recruited by genotype by venesection as described in 2.3.5.1, and 500 µl aliquots of whole blood were taken for immunostaining. Samples were first blocked with 100 µg of mouse IgG for 15 min at room temperature and then stained using the antibodies and combinations indicated in Table 4.4 and Table 4.6, for 30 min at room temperature in the dark. Red blood cells were then lysed by adding 2 ml of 1 X RBC lysis buffer (Biolegend) per tube and incubating for 10 min at room temperature. Cells were then pelleted by centrifugation at 400 x *g* for 5 min at 4°C, the supernatant was discarded and

cells were washed with 2 ml ice-cold PBS, 1% human AB serum, 2 mM EDTA. Finally, cells were fixed using 300 µl of 1 X CellFix (BD Biosciences) for 30 min at 4°C in the dark and subsequently analysed by flow cytometry.

Target/Name	*Clone*	*Conjugate*	*Company*
TNFR1	H398	Alexa-Fluor® 647	AbD Serotec
mIgG2a	-	Alexa-Fluor® 647	AbD Serotec
HLA-DR	L243	FITC	Biolegend
HLA-DR	L243	PE	Biolegend
Lin-1	-	FITC	BD Biosciences
CD14	HCD14	PerCP-Cy5.5	Biolegend
CD16	3G8	Pacific Blue™	Biolegend
CD123	6h6	e-Fluor® 450	eBioscience
CD11b	ICRF44	PE	eBioscience
CD11c	3.9	Alexa-Fluor® 700	eBioscience

Table 4.3: Antibodies for whole blood multiplex immunostaining.

	Alexa-Fluor® 647 (A647)	Fluorescein Isothiocyanate (FITC)	PerCP-Cy5.5	Pacific Blue™ (PB)/eFluor 450	Phycoerythrin (PE)
TNFR1 Monocytes & Neutrophils	TNFR1 H398-A647 (10)	HLA-DR-FITC (20)	CD14-PerCP-Cy5.5 (5)	CD16-PB (2)	CD11b-PE (5)
Isotype Control Monocytes & Neutrophils	mIgG2a-A647 (10)	HLA-DR-FITC (20)	CD14-PerCP-Cy5.5 (5)	CD16-PB (2)	CD11b-PE (5)
TNFR1 DCs	TNFR1 H398-A647 (10)	Lin-1-FITC (20)		CD123-e-Fluor® 450 (5)	HLA-DR-PE (20)
Isotype Control DCs	mIgG2a-A647 (10)	Lin-1-FITC (20)		CD123-e-Fluor® 450 (5)	HLA-DR-PE (20)

Table 4.4: Antibody combinations for whole blood multiplex immunostainings. (µl of antibody)

4.2.6 ELISAs

Soluble expression of transiently transfected or transduced cells were analysed in cell culture supernatants by ELISA as described in 2.2.12. For analysis of human sTNFR1 by sandwich ELISA, the indicated capture and detection antibody combinations were used at the indicated concentrations (Table 4.5). The anti-HA ELISA was performed as described in 2.2.12; cell culture supernatant was captured directly to ELISA plate wells, blocked and then incubated with biotinylated anti-HA.11 (clone 16B12, Covance) at the concentration indicated in Table 4.5. The indirect ELISA using clone 16805 was performed on 48 h cell culture supernatants and human donor plasma samples (2.3.5.2) as described in 2.2.12, with an additional step; following incubation with 16805 or mouse IgG1, samples were incubated with biotinylated anti-mouse IgG1 at the concentration indicated in Table 4.5, before subsequent incubation with Europium-labelled streptavidin incubation and development steps (2.2.12). The anti-Δ6TNFR1-specific monoclonal Fab antibody was generated using HuCAL® antibody technology by AbD Serotec that employs a human combinatorial antibody library and the CysDisplay® method of phage display.

Antibody	*Clone*	*Company*	*Final Concentration (µg/ml)*
anti-TNFR1	16805	R&D Systems	5
anti-TNFR1	H5	Santa Cruz	5
anti-TNFR1	H398	Hycult Biotech	5
mouse IgG1	MAB002	R&D Systems	5
biotinylated anti-HA.11	16B12	Covance	5
biotinylated anti-TNFR1	BAF225	R&D Systems	0.4
biotinylated anti-mouse IgG1	-	eBioscience	2
monoclonal anti-Δ6TNFR1	19050.1	AbD Serotec	2

Table 4.5: Antibodies and concentrations used in ELISAs.

Serum samples from RRMS patients and healthy controls were kindly donated for this study by Dr. Aiden Haghikia as part of a collaboration with Ruhr-University, Bochum.

4.2.7 Western blots

48 h cell culture supernatant of cells transiently transfected with HA-tagged constructs (or empty EYFP vector construct) (2.3.3) was harvested and concentrated 20 X using Amicon Ultra-0.5 Centrifugal Filter Units (Ultracel-10 membrane; Millipore) by centrifugation at 14,000 x *g* at 4°C for 7 min. 20 µl of concentrated supernatants were then resolved by 12.5% SDS-PAGE and immunoblotted using mouse anti-HA.11 as a primary antibody (clone 16B12, Covance) at a final concentration of 3 µg/ml, and IRDye® 800CW goat-anti-mouse (LI-COR Biosciences) as a secondary antibody, as described in 2.2.11.

4.2.8 Confocal microscopy

For analysis of subcellular localisation of fluorescent fusion proteins by confocal microscopy, HT1080 and HeLa were seeded in wells of a 24 well plate on Round Micro Cover Glasses (VWR) that had been sterilised with 100% EtOH. 24 h later, cells were co-transfected (2.3.3) with equal amounts of TNFR1 and organelle-resident protein fluorescent fusion constructs, to a total amount of 300 ng of DNA per well. 48 h post-transfection, cells were washed three times with 0.5 ml sterile PBS and fixed using 4% PFA dissolved in PBS, for 8 min at 4°C. After three more 0.5 ml PBS washes, cells were stained with 0.5 ml 1 µM TO-PRO®-3 iodide (Molecular Probes, Invitrogen) for 15 min in the dark at room temperature. Cells were washed two more times with 0.5 ml PBS, allowed to air-dry and were then mounted to SuperFrost™ Plus Micro Slides (VWR) using Dako Fluorescent Mounting Medium (Dako Cytomation). Slides were excited with the appropriate lasers for the visualisation of fluorescent proteins, and images were taken using an LSM510 confocal microscope (Zeiss, Oberochen, Germany) under oil immersion and using a 100 X objective. Images were minimally processed to optimise

signal:noise ratios using Zeiss LSM510 v. 3.2 and Image J software. Quantification of colocalisation was performed using MetaMorph® software (Molecular Devices), using the 'Colocalization' function plugin. This gave numerical values for the amount of a given colour colocalising with each other colour and the amount not colocalising with any other colour. Percentages were calculated by dividing these values by the total amount of the given colour and multiplying the fraction by 100.

4.2.9 Ribosome fractionation and analysis of associated RNA

4.2.9.1 Preparation of cells for fractionation

Primary human immune cells were prepared for fractionation as follows. PBMCs were isolated from peripheral blood samples as described in 2.3.5.2 and cultured at 1 x 10^6 cells/ml in RPMI containing 10% FBS, 4 ng/ml recombinant human IL-2 (PeproTech), 50 ng/ml recombinant human IL-4 (PeproTech) and 50 ng/ml recombinant human GM-CSF (PeproTech) for 72 h at 37°C, 5% CO_2. Cells were subsequently stimulated with 10 ng/ml PMA (PeproTech) and 100 ng/ml LPS (Sigma Aldrich) for 16 h before the addition of 10 µg/ml of cycloheximide for 15 min at room temperature. Cells were then harvested by scraping, pelleted by centrifugation at 400 x *g* for 10 min at 4°C, the supernatant was discarded and the cell pellet was snap-frozen in isopropanol cooled with dry ice.

U937 and Jurkat cells were cultured in RPMI medium containing 10% FBS at 37°C, 5% CO_2 at a density of ~ 1 x 10^6 cells/ml. Cells were harvested by centrifugation at 400 x *g* for 10 min and snap-frozen as described for PBMC samples.

4.2.9.2 Cell lysis and sucrose density gradient fractionation by ultracentrifugation

~ 1 x 10^7 cells were lysed by resuspension in 500 µl of ice-cold buffer containing 20 mM Tris-HCl pH 8.5, 1.5 mM $MgCl_2$, 140 mM KCl, 0.5 mM DTT, 0.1 mM cycloheximide, 0.5% NP-40 and 500 units/ml

RNasin® Ribonuclease inhibitor (Promega). Lysates were then centrifuged at 10,000 x g for 5 min at 4°C to obtain post-nuclear supernatants.

12 ml linear 20-47% sucrose gradients were prepared from 20% and 47% sucrose (w/v; Sigma Aldrich) in buffer containing 20 mM Tris-HCl pH 8.0, 5 mM $MgCl_2$, 140 mM KCl using a gradient mixer (Sigma) into 13.2 ml Thinwall Polyallomer Ultracentrifuge Tubes (Beckman Coulter). EDTA control gradients were prepared in buffer containing 20 mM Tris-HCl pH 8.0, 10 mM EDTA, 140 mM KCl.

Post-nuclear supernatants were layered carefully onto the top of gradients and centrifuged at 120,565 x *g* for 2 h 15 min at 4°C in a SW41Ti rotor (Beckman Coulter) using an Optima™ XE 90K Preparative Ultracentrifuge (Beckman Coulter).

A Gilson Fraction Collector coupled to a Gilson 112 UV/VIS detector (Gilson) were subsequently used to measure absorbance at 260 nm and collect 1 ml fractions from gradients. Absorbance profile traces were generated using Clarity software (Clarity). 80S, 60S and 40S monosome and polysome fractions were defined by reference to characteristic traces for ribosome fractionation experiments.

4.2.9.3 RNA extraction and transcript analysis in ribosome fractions

RNA was extracted from each fraction using TRIzol® reagent (Invitrogen) according to the manufacturer's instructions. 500 µl aliquots of each fraction were mixed with 1 ml of TRIzol® reagent and incubated for 2 min at room temperature. 200 µl of chloroform was then added and samples were vortexed vigorously for 15 s, followed by centrifugation at 10,000 x *g* for 15 min at 4°C. The upper aqueous phase was then mixed with 500 µl of isopropanol and incubated at room temperature for 10 min to precipitate the RNA. Samples were then centrifuged at 10,000 x *g* for 15 min at 4°C and the RNA pellet was washed once with 1 ml 75% EtOH by centrifugation at 7,500 x *g* for 5 min at 4°C. RNA pellets were allowed to dry, re-suspended in 20 µl of RNAse-free water and RNA purity and quantity was determined using a NanoDrop spectrophotometer.

cDNA synthesis was performed with 1 µg of RNA isolated from each fraction as described in 2.2.3 and 2 µl of the resultant cDNA was used in qRT-PCR analysis of transcript levels as described in 2.2.4, using the Hs00533565_g1 assay for *TNFRSF1A* exons 6-7, and the custom-designed primer-probe sets for Δ6_TNFR1 described in Table 3.2.

4.3 Results

4.3.1 Analysis of the protein translated from Δ6TNFR1 mRNA

At the protein-level, omission of the 72 bp *TNFRSF1A* exon 6 from the mature transcript is predicted to result in a frameshift in the translated protein, truncating it to the first 183 amino acids of the full-length protein followed by a novel 45 amino acid sequence before it reaches a premature stop codon. This truncation removes several well characterised domains of the full-length protein; the metalloprotease cleavage and transmembrane domains, required for shedding and membrane anchoring of the receptor respectively, as well as the Golgi retention motif and other localisation domains ((Gray *et al.*, 1990; Reddy *et al.*, 2000; Storey *et al.*, 2002); Figure 4.1). We therefore sought to investigate the trafficking and distribution of Δ6TNFR1 as compared to FLTNFR1.

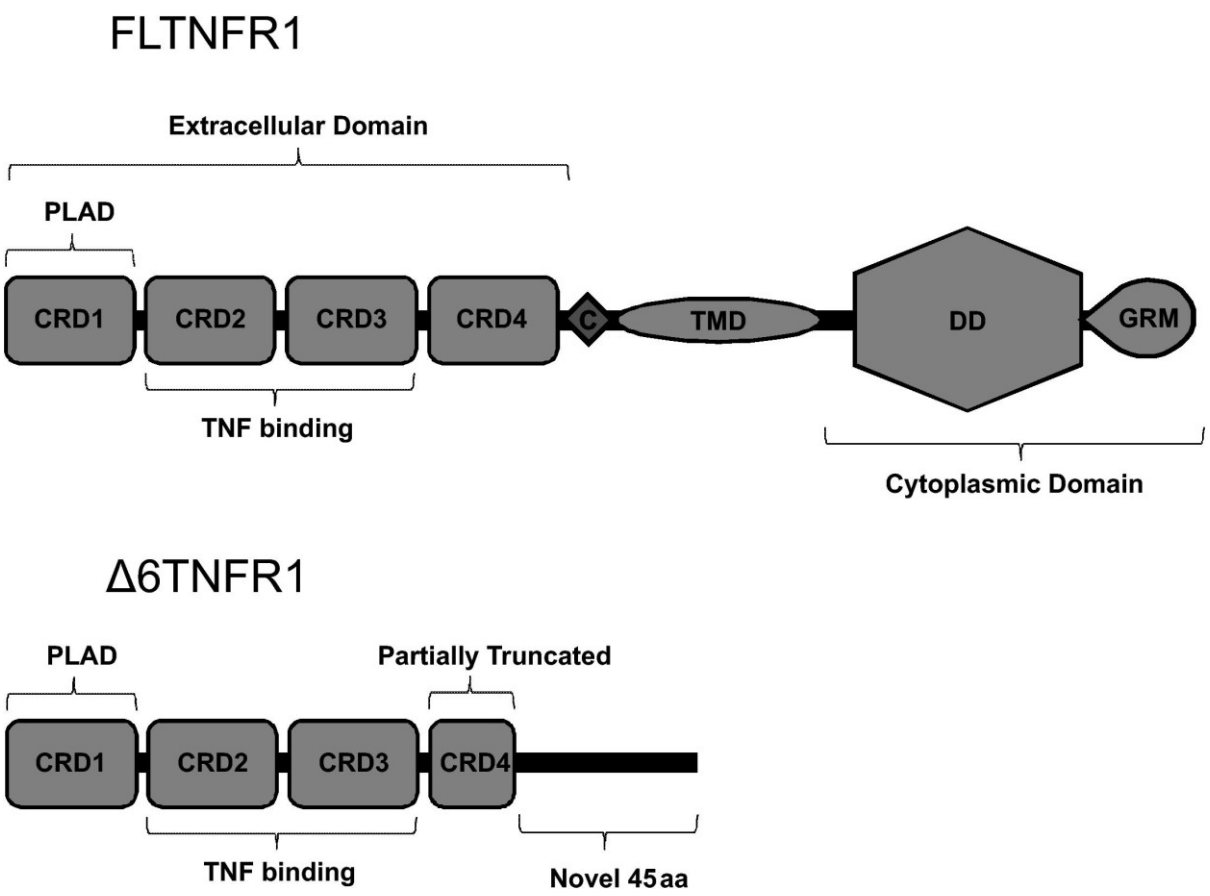


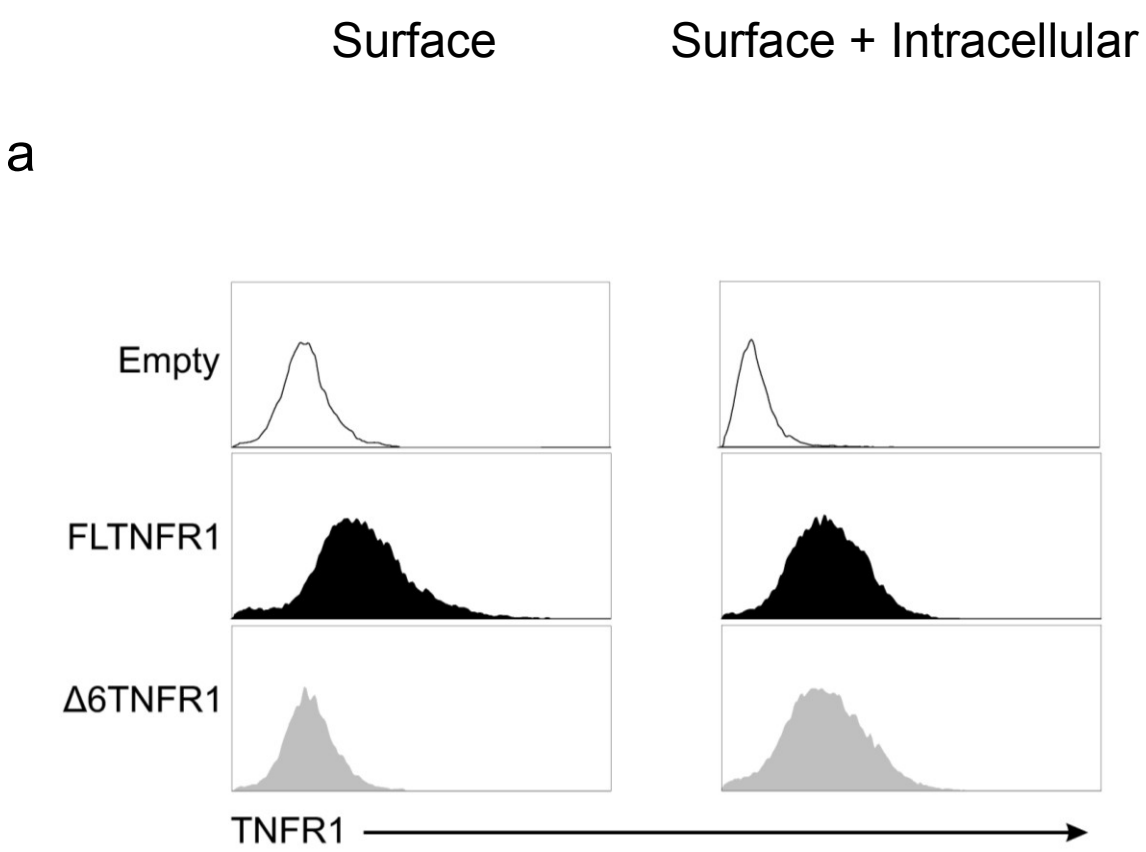
Figure 4.1: Schematic of FLTNFR1 and Δ6TNFR1 proteins. Known functional domains of FLTNFR1 are indicated. CRD = cysteine-rich domain; PLAD = Pre-Ligand Assembly Domain; C = Metalloprotease cleavage domain; TMD = Transmembrane Domain; DD = Death Domain; GRM = Golgi Retention Motif.

4.3.2 Surface, intracellular and soluble *in vitro* expression of Δ6TNFR1 compared with FLTNFR1

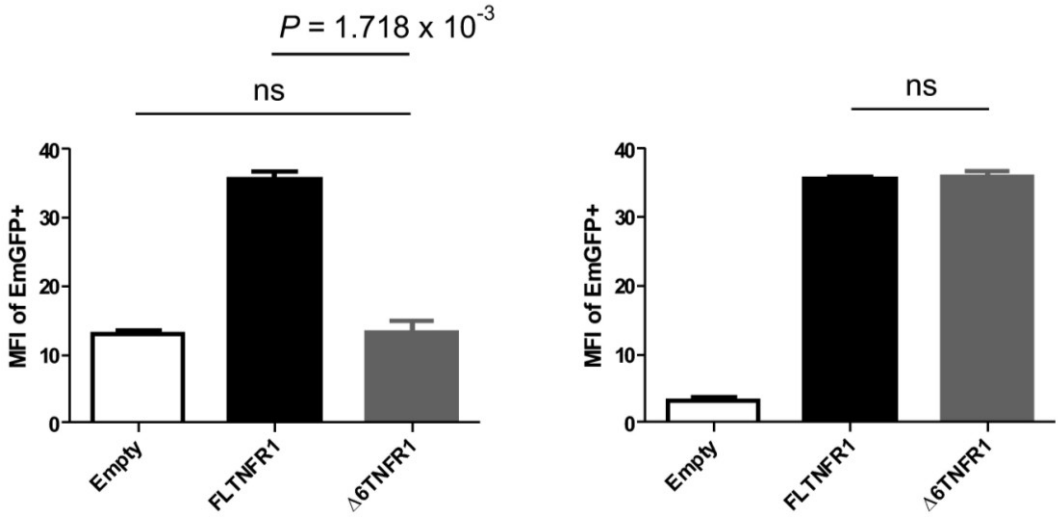
To study the protein translated from TNFRSF1A mRNA lacking exon 6, a lentiviral expression system was developed. This allowed the full-length (FLTNFR1) cDNA, and the sequence lacking exon 6 (Δ6TNFR1) to be introduced into cells with high efficiency and be expressed strongly. The lentiviral construct has an Emerald GFP (EmGFP) expressed under the control of an independent promoter, allowing transduction efficiency to be determined irrespective of TNFR1 protein expression.

Surface and intracellular expression of HEK 293T cells transduced with the indicated TNFR1 lentiviruses was analysed by flow cytometry, using an antibody recognising the extracellular domain of the protein. Whilst similar levels of total expression were observed between FLTNFR1 and Δ6TNFR1 transduced cells (Figure 4.2, right panels), considerably less TNFR1 was detectable at the cell surface of non-permeabilised cells transduced with Δ6TNFR1 lentivirus, and that this was not significantly more than the background amounts detected in cells transduced with the empty lentivirus (Figure 4.3, left panels). An ELISA performed using the R&D systems kit for detection of soluble TNFR1 showed there to be significantly less detectable TNFR1 in the supernatant of Δ6TNFR1 compared to FLTNFR1 transduced cells (Figure 4.3a). Subsequent ELISAs performed on supernatants taken at 16, 24, 48 and 72 h post-transduction revealed that the decreased sTNFR1 levels detected at 72 h in the supernatant of cells transduced with Δ6TNFR1 lentivirus were not the result of instability of this protein in the cell culture supernatant (Figure 4.3c). Similar levels of expression of

TNFR1 cDNA in cells transduced with different lentiviruses, and the appropriateness of normalisation to EmGFP expression was confirmed by performing qRT-PCR on cDNA using primer-probes sets specific for the detection of *TNFRSF1A* exons 3-4 and 6-7, as well as a custom-made primer-probe set for the detection of EmGFP expression (Figure 4.4).



b



c

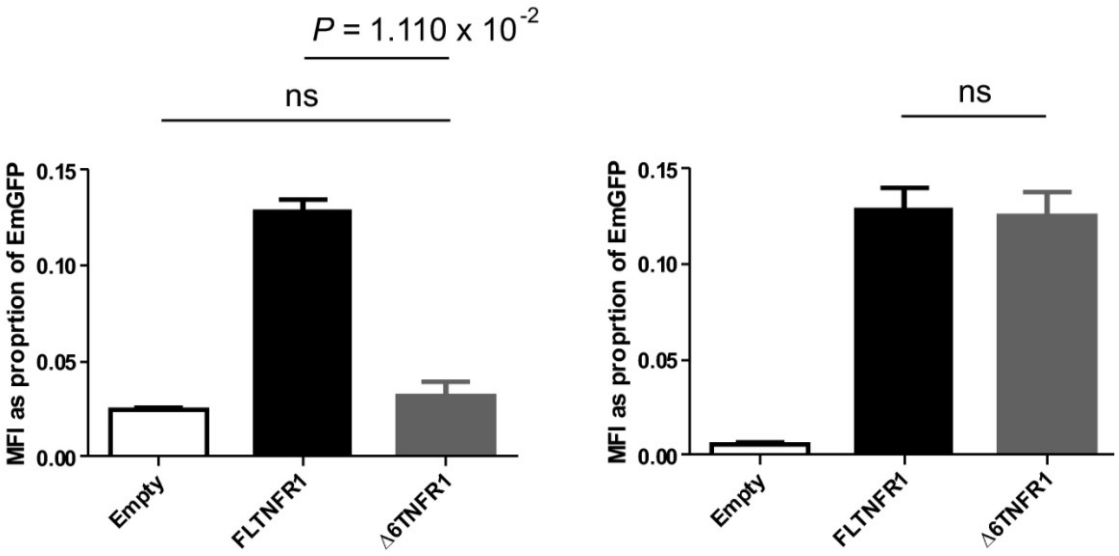


Figure 4.2: Cellular Expression of FLTNFR1 and Δ6TNFR1. Anti-TNFR1 staining of HEK 293T cells expressing FLTNFR1 and Δ6TNFR1. Cells were transduced with the indicated TNFR1 lentivirus or empty lentivirus (Empty) at an MOI of 50 and at 72 h post-transduction, anti-TNFR1 staining was analysed in EmGFP^{+} (ie. transduced) cells. **(a)** Histograms of **(left panels)** surface staining of non-

permeabilised cells and **(right panels)** Surface and intracellular staining of permeabilised cells. **(b)** Graphs of Mean Fluorescence Intensity (MFI) of anti-TNFR1 staining in EmGFP^{+} cells. **(c)** Graphs of MFI of anti-TNFR1 staining normalised to EmGFP expression. Error bars represent mean ± SEM; *P* values are indicated; ns = non-significant.

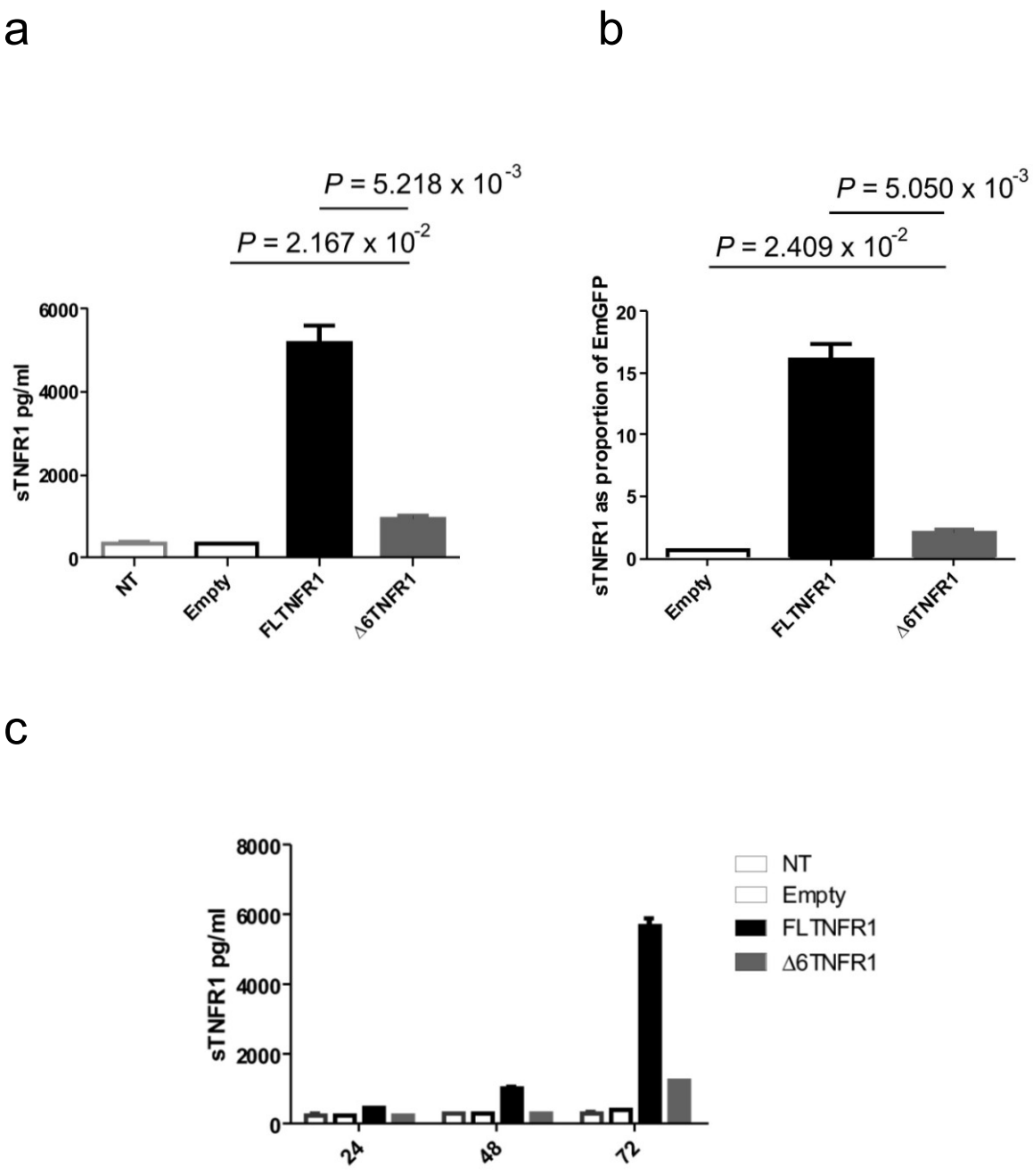


Figure 4.3: Soluble expression of FLTNFR1 and Δ6TNFR1. Analysis of sTNFR1 production in cell culture supernatants of HEK 293T cells transduced with the indicated TNFR1 lentivirus or empty

lentivirus (Empty) by R&D systems sTNFR1 ELISA. **(a&b)** 72 h cell culture supernatants; **(b)** normalised to EmGFP expression. **(c)** 24, 48 and 72 h cell culture supernatants. Error bars represent mean ± SEM; *P* values are indicated. NT = non-transduced.

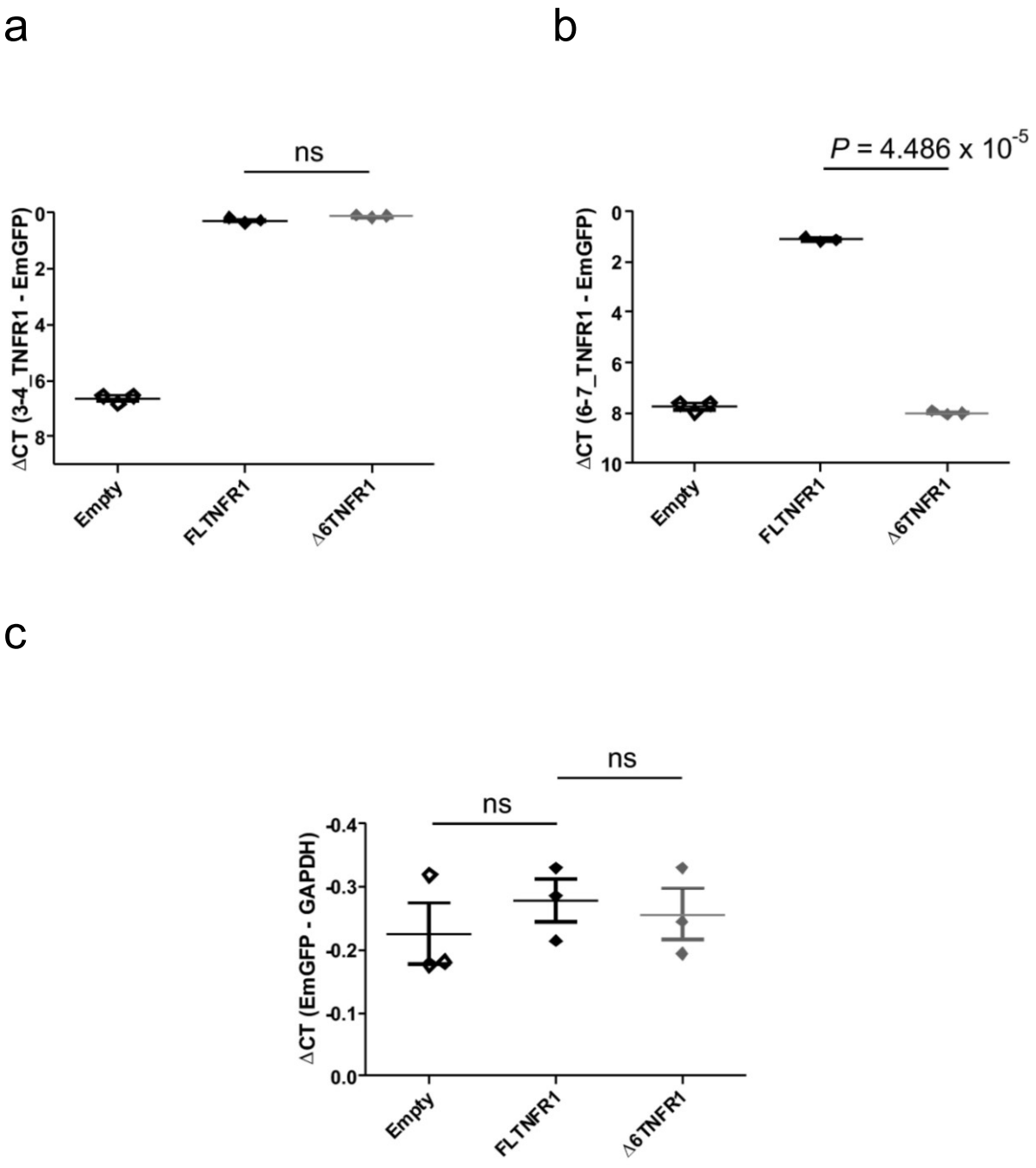
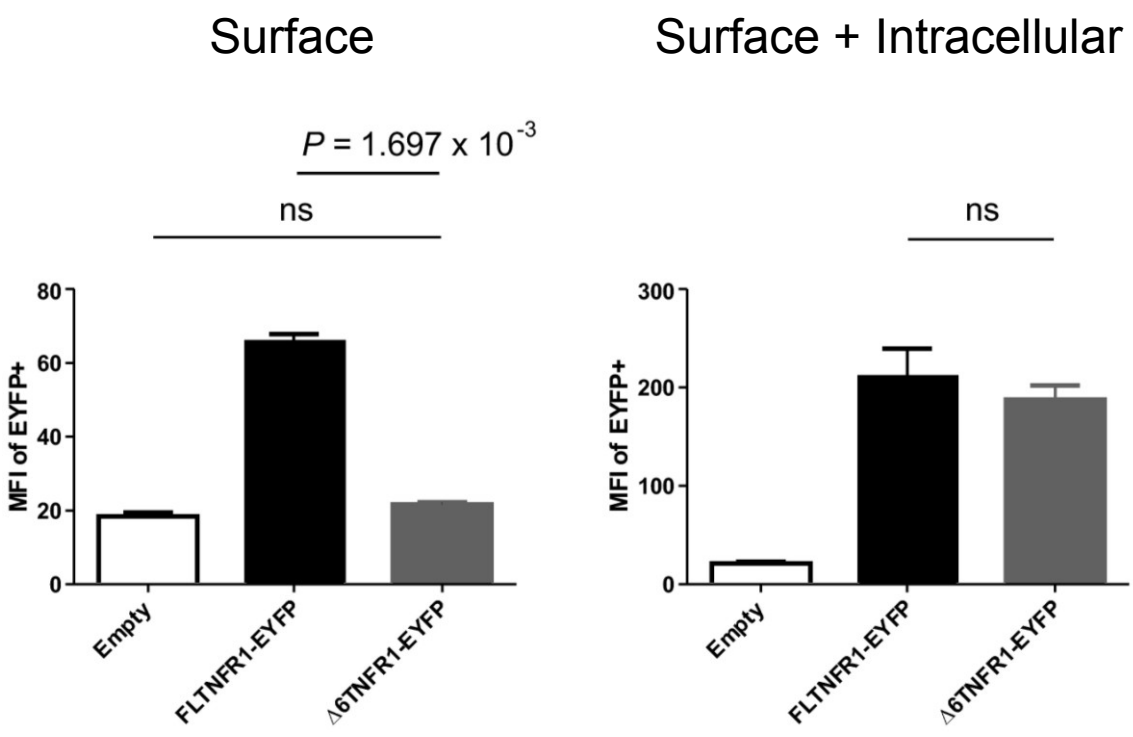


Figure 4.4: TNFR1 cDNA expression in FLTNFR1 and Δ6TNFR1 transduced cells. RNA was isolated and cDNA was made from HEK 293T cells transduced with the indicated TNFR1 lentivirus or empty lentivirus, and qRT-PCR was performed with TaqMan® primer-probe sets for the detection of GAPDH, EmGFP, and *TNFRSF1A* exons 3-4 and 6-7. **(a &b)** Expression levels (ΔCT) were calculated by subtracting the cycle threshold (CT) value for EmGFP from values for the indicated *TNFRSF1A* exons. **(c)** Expression levels (ΔCT) were calculated by subtracting the cycle threshold (CT) value for GAPDH from values for EmGFP. Error bars represent mean ± SEM; P value is indicated; ns = non-significant.

To provide further support for our observation that Δ6TNFR1 was not expressed at the cell surface or to the same extent in cell culture supernatant as cells expressing FLTNFR1 we used an expression system in which constructs expressing FLTNFR1 and Δ6TNFR1 fused at the C-terminus to EYFP were transiently transfected into cells. Figure 4.5 shows the same pattern of expression as observed in the lentiviral expression system.

a



b

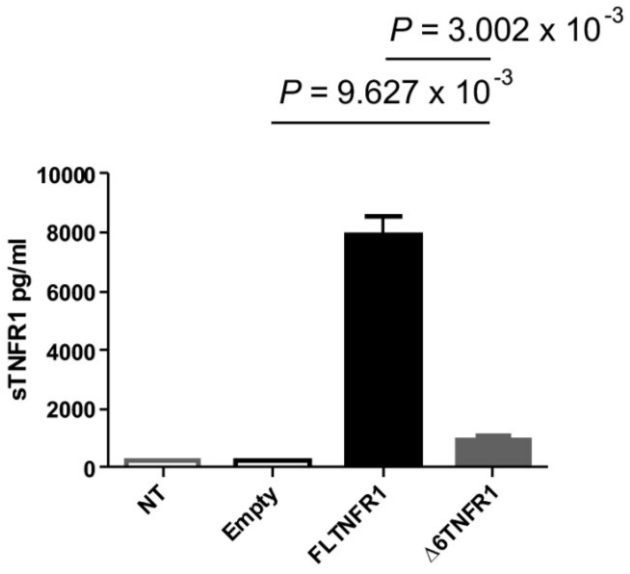
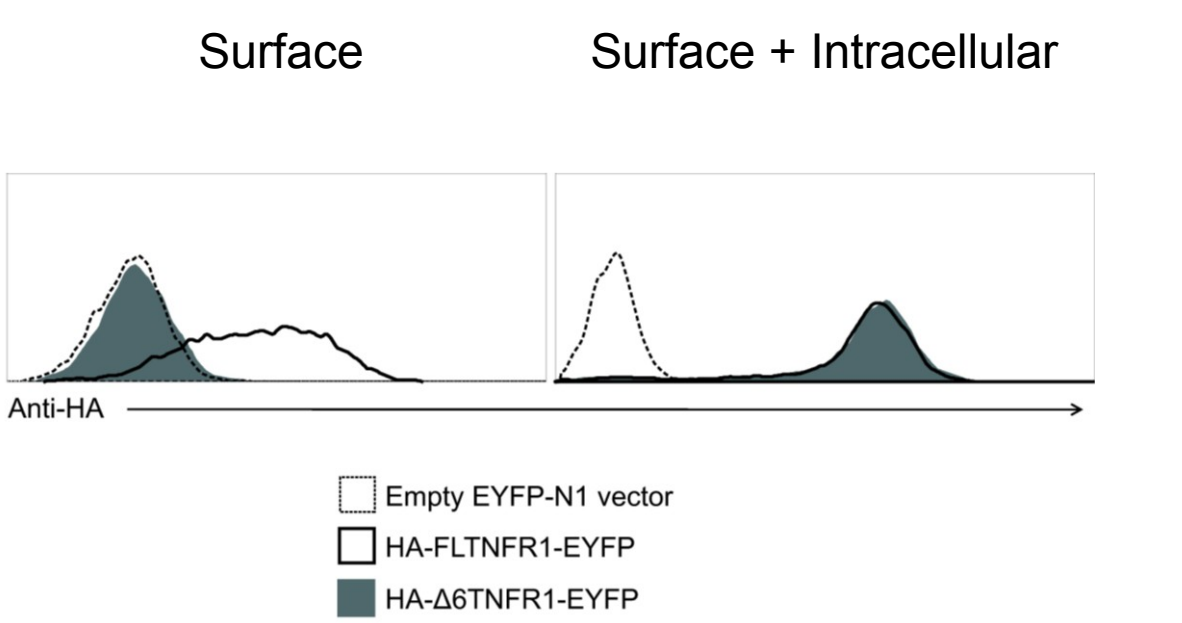


Figure 4.5: Expression and localisation FLTNFR1-EYFP and Δ6TNFR1-EYFP following transient transfection and expression. Cells were transfected with the indicated TNFR1-EYFP fusion protein

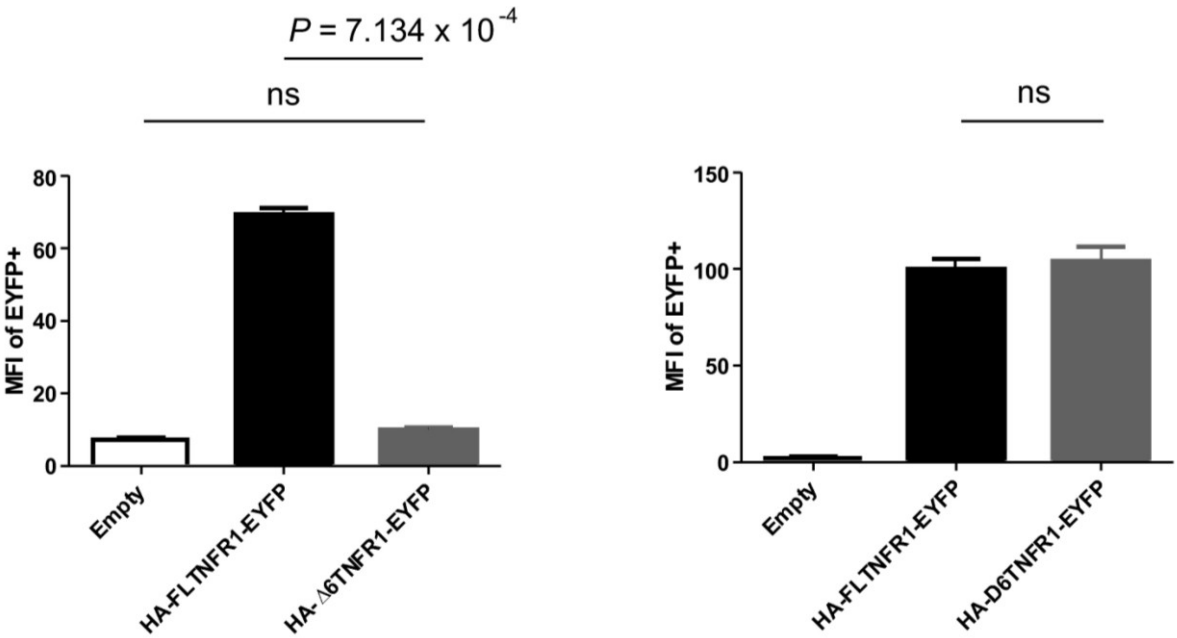
construct empty pEYFP-N1 vector and analysed at 48 h for anti-TNFR1 staining. **(a)** Graphs of Mean Fluorescence Intensity (MFI) of anti-TNFR1 staining in $EYFP^+$ **(left panel)** non-permeabilised and **(right panel)** permeabilised cells. **(b)** Analysis of sTNFR1 production in cell culture supernatants at 72 h of HEK 293T cells transfected with the indicated the indicated TNFR1-EYFP fusion protein construct or empty pEYFP-N1 vector by R&D systems sTNFR1 ELISA. Error bars represent mean ± SEM; *P* values are indicated; ns = non-significant.

All manner of properties of wildtype and naturally-occurring/experimentally generated TNFR1 mutants have been investigated using N-terminal peptide tags, which allows their unbiased detection (D'Alessio *et al.*, 2010; Lobito *et al.*, 2006; Yang *et al.*, 2006). Moreover, removal of exon 6 partially truncates the extracellular domain of the receptor which could potentially influence anti-TNFR1 antibody binding, as has been observed for certain TRAPS mutants (Todd *et al.*, 2007) (Figure 4.1). We therefore generated N-terminally HA-tagged, FLTNFR1- and Δ6TNFR1-EYFP fusion cDNA constructs by cloning and used them to investigate TNFR1 expression in a transient transfection system. Anti-HA staining was analysed in EYFP positive cells by flow cytometry; surface expression was only observed in cells transfected with HA-FLTNFR1-EYFP, whilst similar total levels of HA staining were observed between HA-FLTNFR1-EYFP and HA-Δ6TNFR1-EYFP transfected cells upon permeabilisation (Figure 4.6). Transfected cells were also stained with anti-TNFR1 as a control; similar staining was observed as when cells were transduced with TNFR1 lentiviruses (Figure 4.2). These results suggest that Δ6TNFR1 is either defective in trafficking to or anchoring at the cell surface.

a


Surface
Surface + Intracellular
Anti-HA
Empty EYFP-N1 vector
HA-FLTNFR1-EYFP
HA-Δ6TNFR1-EYFP

b


Surface
Surface + Intracellular
P = 7.134 x 10-4
ns
ns
MFI of EYFP+
80
60
40
20
0
150
100
50
0
Empty
HA-FLTNFR1-EYFP
HA-Δ6TNFR1-EYFP
HA-D6TNFR1-EYFP

C

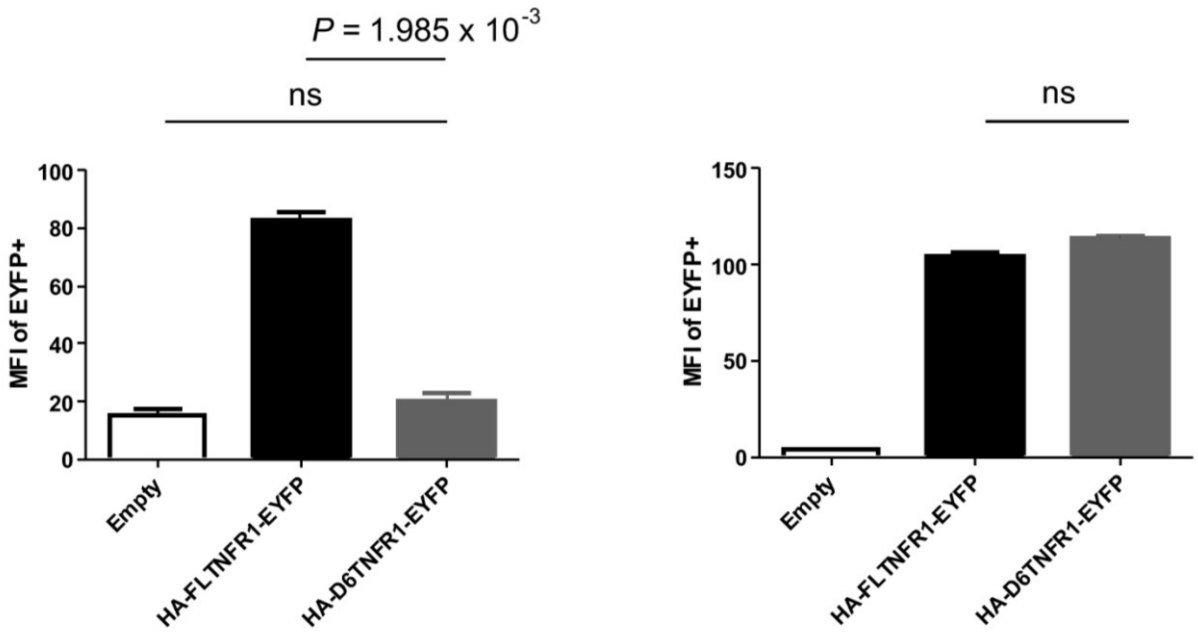


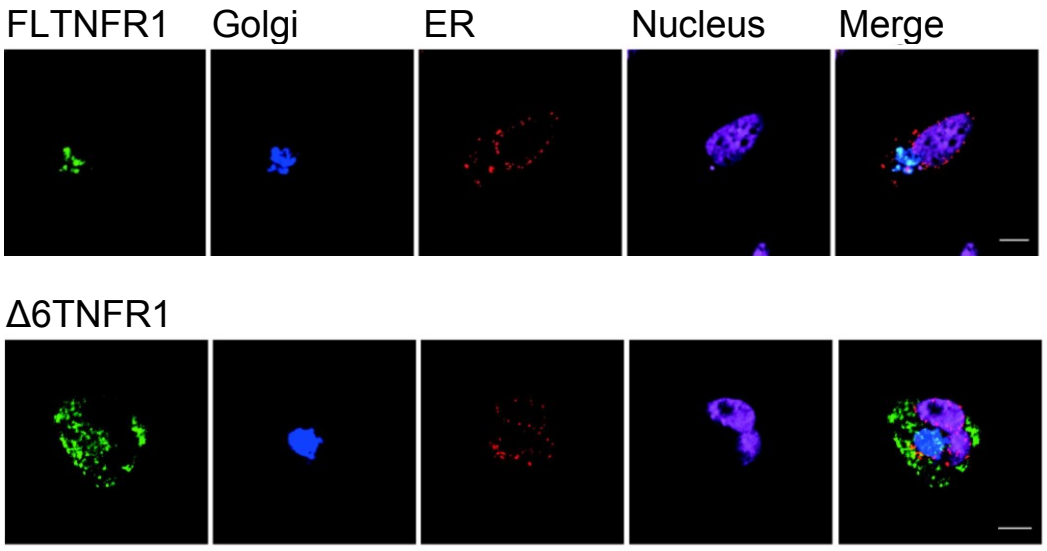
Figure 4.6: Expression and localisation HA-tagged FLTNFR1 and Δ6TNFR1 EYFP fusion proteins. Cells were transfected with the indicated HA-TNFR1-EYFP construct or empty EYFP-N1 vector and EYFP$^+$ cells analysed at 72 h for **(a)** & **(b)** anti-HA staining or **(c)** anti-TNFR1 staining. **(a)** Overlays of representative histograms of cells expressing the indicated HA-TNFR1-EYFP fusion proteins stained with anti-HA **(b & c)** Graphs of Mean Fluorescence Intensity (MFI) of **(b)** anti-HA and **(c)** anti-TNFR1 staining in EYFP$^+$ cells. Error bars represent mean ± SEM; *P* values are indicated; ns = non-significant.

4.3.3 Subcellular localisation of intracellular Δ6TNFR1 compared with FLTNFR1

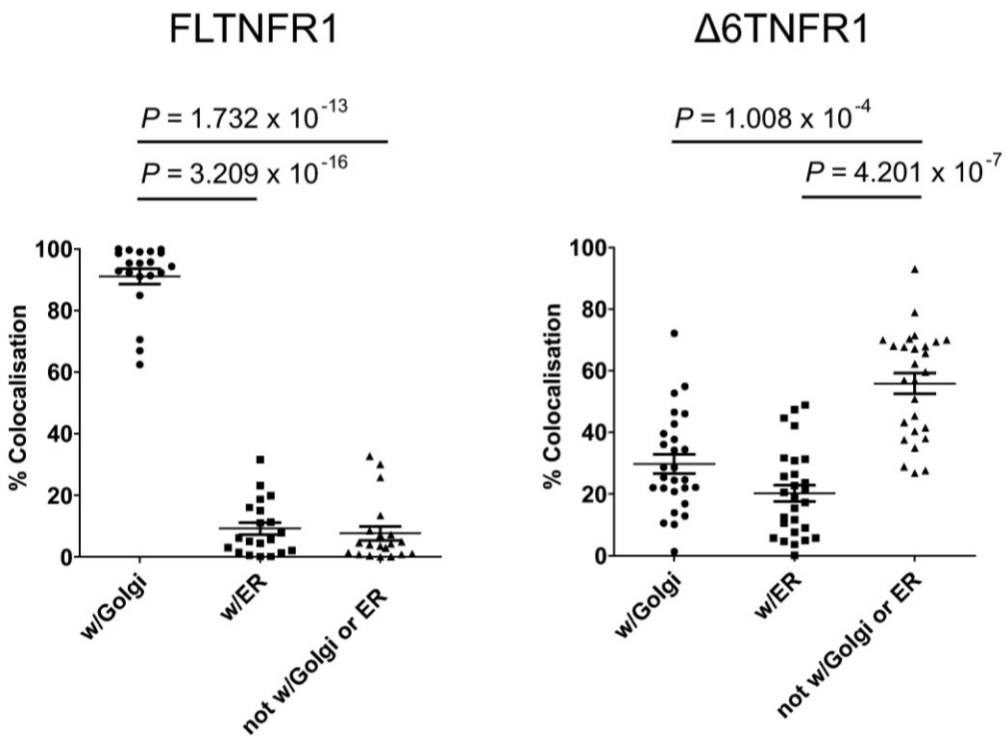
The subcellular localisation of Δ6TNFR1 compared to FLTNFR1 was investigated using fluorescent fusions of organelle-resident proteins by confocal microscopy (Figure 4.7). Quantification of colocalisation was performed on the indicated number of images, and this demonstrated that whilst FLTNFR1 localised primarily to the Golgi apparatus – in agreement with the literature – the

intracellular distribution of Δ6TNFR1 was found to be more diffuse, with the majority of expression localised neither to the Golgi nor the ER (Figure 4.7b).

a



b



C

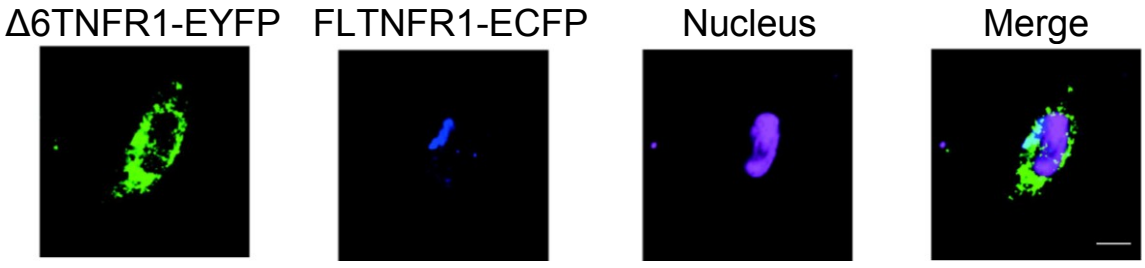


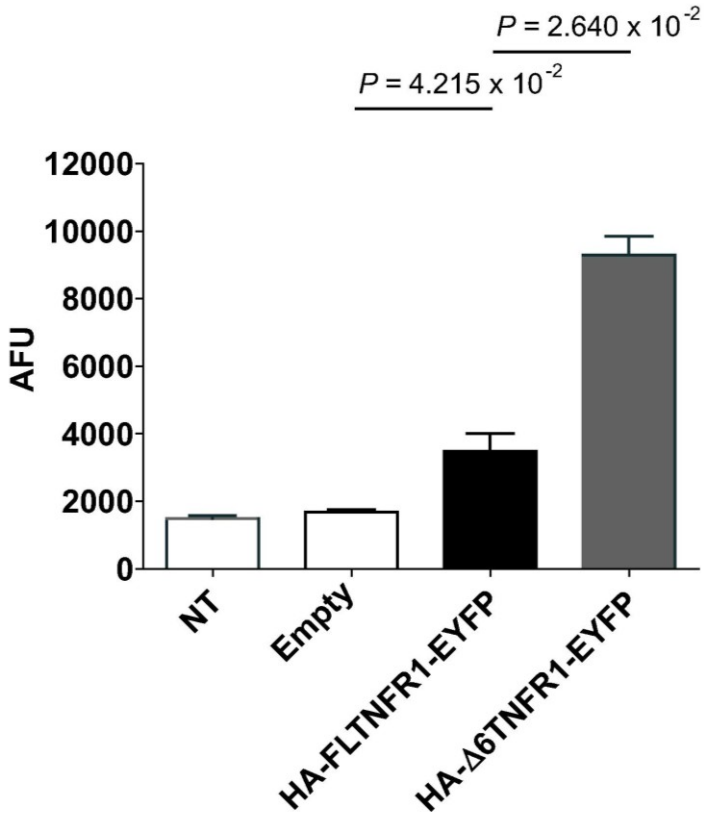
Figure 4.7: Subcellular localisation of FLTNFR1 and Δ6TNFR1 fusion proteins by confocal microscopy. **(a-c)** HeLa cells were co-transfected with the indicated TNFR1-EYFP and organelle-resident protein fluorescent fusion constructs. 48 h later cells were stained with TO-PRO®-3 iodide and analysed by confocal microscopy. ER marker = SRβ-DsRed2. Golgi marker = GalNAcT2-ECFP. **(b)** Quantification of TNFR1 fusion protein colocalisation with organelle markers was performed using MetaMorph software. **(c)** HeLa cells were co-transfected with Δ6TNFR1-EYFP and FLTNFR1-ECFP constructs,

stained at 48 h post-transfection with TO-PRO®-3 iodide and analysed by confocal microscopy. Error bars represent SEM; FLTNFR1 *n* = 20, Δ6TNFR1 *n* = 27 cells; *P* values are indicated. Scale bar = 10 µm.

4.3.4 Further analysis of soluble expression of Δ6TNFR1 compared with FLTNFR1 *in vitro*

The R&D ELISA antibody pair is designed to detect full-length and cleaved, shed TNFR1 by binding distinct epitopes on the extracellular portion of the receptor. Recognition by one or both of these antibodies might be compromised in the case of binding to Δ6TNFR1 and so an alternative ELISA was developed, in which proteins in the cell culture supernatant were coated directly to ELISA wells and an anti-HA antibody was used to quantify HA-tagged species. Figure 4.8a shows that in stark contrast to the results of the R&D sTNFR1 ELISA, more than twice the amount of soluble receptor was detected in culture supernatant of cells transfected with HA-Δ6TNFR1-EYFP than those transfected with HA-FLTNFR1-EYFP (*P* = 0.0264). To confirm this, anti-HA western blots were performed on whole cell lysates and concentrated supernatants, and once again considerably more anti-HA signal was seen in the supernatant of HA-Δ6TNFR1-EYFP transfected cells (Figure 4.8b, lower panel). This suggests that the Δ6TNFR1 transcript encodes a stable protein that, lacking the necessary hydrophobic transmembrane domain, cannot translocate into the cell membrane and so is released into the extracellular space.

a


P = 2.640 x 10-2
P = 4.215 x 10-2
12000
10000
8000
6000
4000
2000
0
AFU
NT
Empty
HA-FLTNFR1-EYFP
HA-Δ6TNFR1-EYFP

b

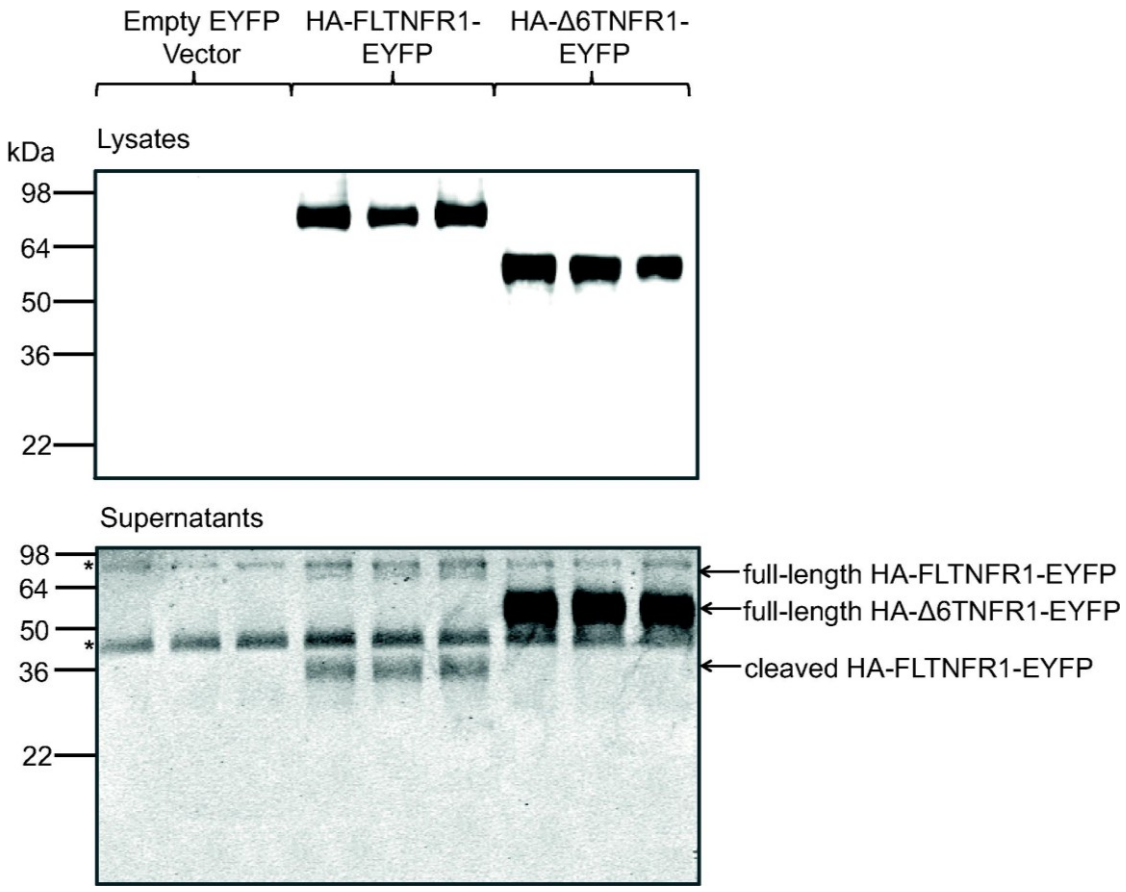


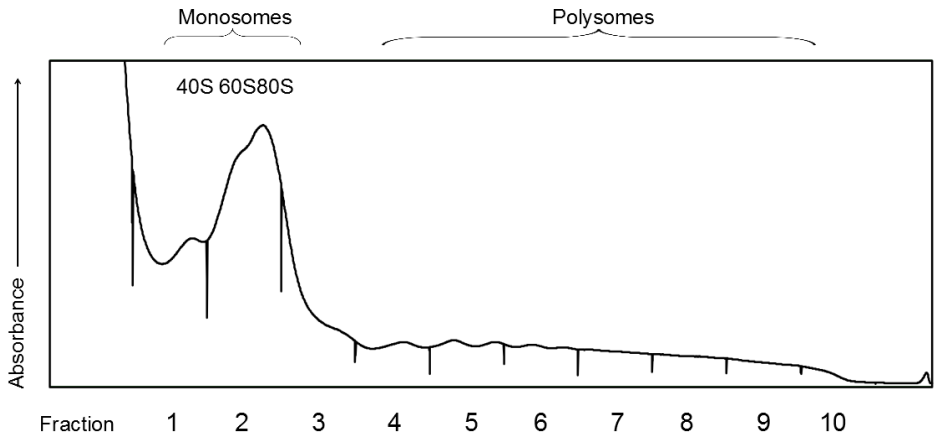
Figure 4.8: Soluble TNFR1 production from cells expressing HA-tagged FLTNFR1 and Δ6TNFR1 EYFP fusion proteins. 48 h cell culture supernatants from cells transfected with empty pEYFP-N1 (Empty), HA-FLTNFR1-EYFP or HA-Δ6TNFR1-EYFP constructs were analysed for soluble expression of HA by **(a)** anti-HA ELISA and **(b)** an anti-HA western blot. Error bars represent mean ± SEM; *P* values are indicated. AFU = Arbitrary Fluorescence Units.

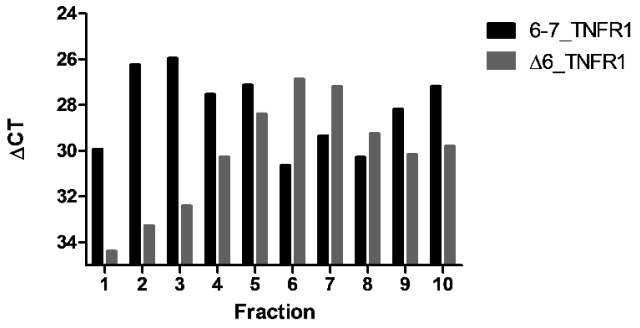
4.3.5 Analysis Δ6_TNFR1 mRNA distribution across ribosome fractions

We next sought to determine if Δ6_TNFR1 transcripts are translated by demonstrating an association with polysome fractions. In the first instance, lysates from the monocytic U937 and T cell

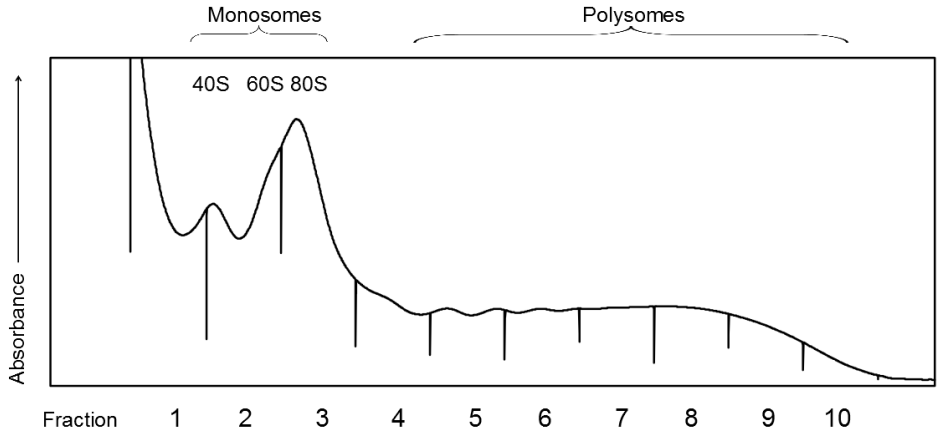
Jurkat cell lines were centrifuged through sucrose gradients to fractionate ribosomal RNA, and transcripts lacking or containing *TNFRSF1A* exon 6 were quantified in each fraction by qRT-PCR (Figure 4.9a and b).

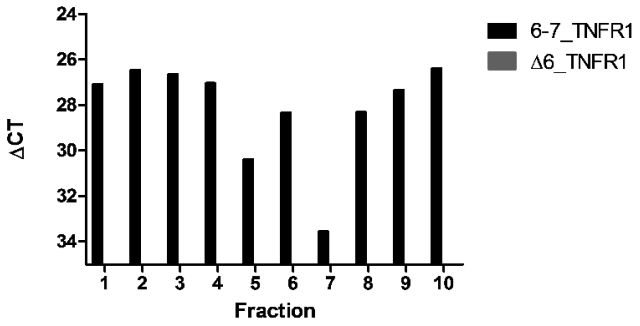
a


Monosomes
Polysomes
40S 60S80S
Absorbance
Fraction 1 2 3 4 5 6 7 8 9 10


6-7_TNFR1
Δ6_TNFR1
ΔCT
24
26
28
30
32
34
1 2 3 4 5 6 7 8 9 10
Fraction

b


Monosomes
Polysomes
40S 60S 80S
Absorbance
Fraction 1 2 3 4 5 6 7 8 9 10


6-7_TNFR1
Δ6_TNFR1
ΔCT
24
26
28
30
32
34
1 2 3 4 5 6 7 8 9 10
Fraction

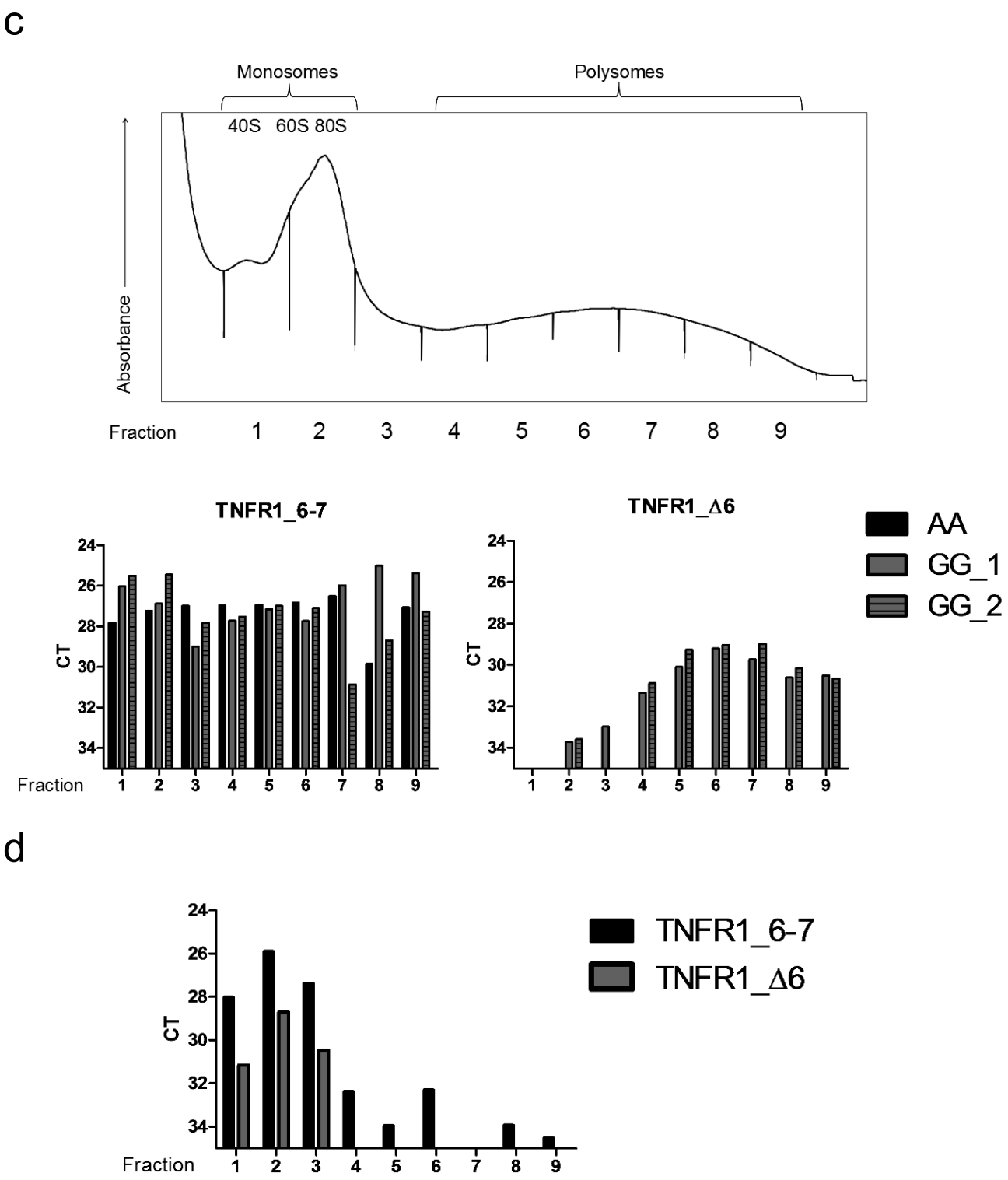


Figure 4.9: qRT-PCR analysis of ribosome-associated *TNFRSF1A* transcripts. Chromatograms show representative A_{260} sedimentation profiles obtained from post-nuclear lysate supernatants centrifuged through linear 20-47% sucrose gradients. Monosome and polysome fractions are

indicated. Graphs show expression levels of *TNFRSF1A* transcripts lacking or containing exon 6 in the indicated fractions **(a)** U937 and **(b)** Jurkat cells. **(c)** PBMCs from rs1800693^{G} and rs1800693^{A} homozygote donors **(d)** PBMCs from a rs1800693^{G} homozygote donor subjected to a gradient containing 10 mM EDTA. CT = cycle threshold.

U937 cells are homozygous for the rs1800693^{G} allele and Δ6_TNFR1 mRNA could be detected across polysome and monosome fractions (Figure 4.9a), whilst no Δ6_TNFR1 transcript was observed in any Jurkat fractions, in accordance with their homozygous rs1800693^{A} genotype (Figure 4.9b). We next sought to obtain similar evidence for the active translation of Δ_6TNFR1 mRNA in primary immune cells isolated from the peripheral blood of healthy donors. Figure 4.9c shows that Δ6_TNFR1 mRNA was found to be associated with polysome fractions obtained from PBMCs of two rs1800693^{G} homozygotes, whilst none was found in fractions obtained from PBMCs of an rs1800693^{A} homozygote. These results suggest that Δ6_TNFR1 mRNA is actively translated into protein in PBMCs of rs1800693^{G} homozygotes. Moreover, Figure 4.9d shows that Δ_6TNFR1 transcripts are released from the polysome fractions and found in the monosome fractions following incubation with EDTA, demonstrating that the transcript is simply not forming aggregates in the polysome fractions (del Prete *et al.*, 2007; Nielsen *et al.*, 1995).

4.3.6 Developing an ELISA system for the analysis of soluble expression of Δ6TNFR1 in human samples

Having demonstrated that translated into a soluble protein (Figures 4.8 and 4.9), we next sought to demonstrate the existence of Δ6TNFR1 at the protein level in primary samples. As no antibody exists that is able to specifically detect Δ6TNFR1 over FLTNFR1 or cleaved sTNFR1, we trialled a series of antibody pairs in an attempt to develop an assay that could recognise all three soluble TNFR1

species equally. This would give the potential to be able to identify differences in total soluble TNFR1 species in the serum or cell culture supernatant of samples by rs1800693 genotype. Several ELISA antibody pairs were trialled using biotinylated BAF225 as a detection antibody, following capture with one of several anti-TNFR1 antibodies that are known to recognise epitopes in the extracellular domain of TNFR1. None of the ELISA antibody pairs trialled on supernatant from cells transiently transfected with HA-TNFR1-EYFP constructs gave results that mirrored those using the anti-HA ELISA and western blot (Figure 4.10).

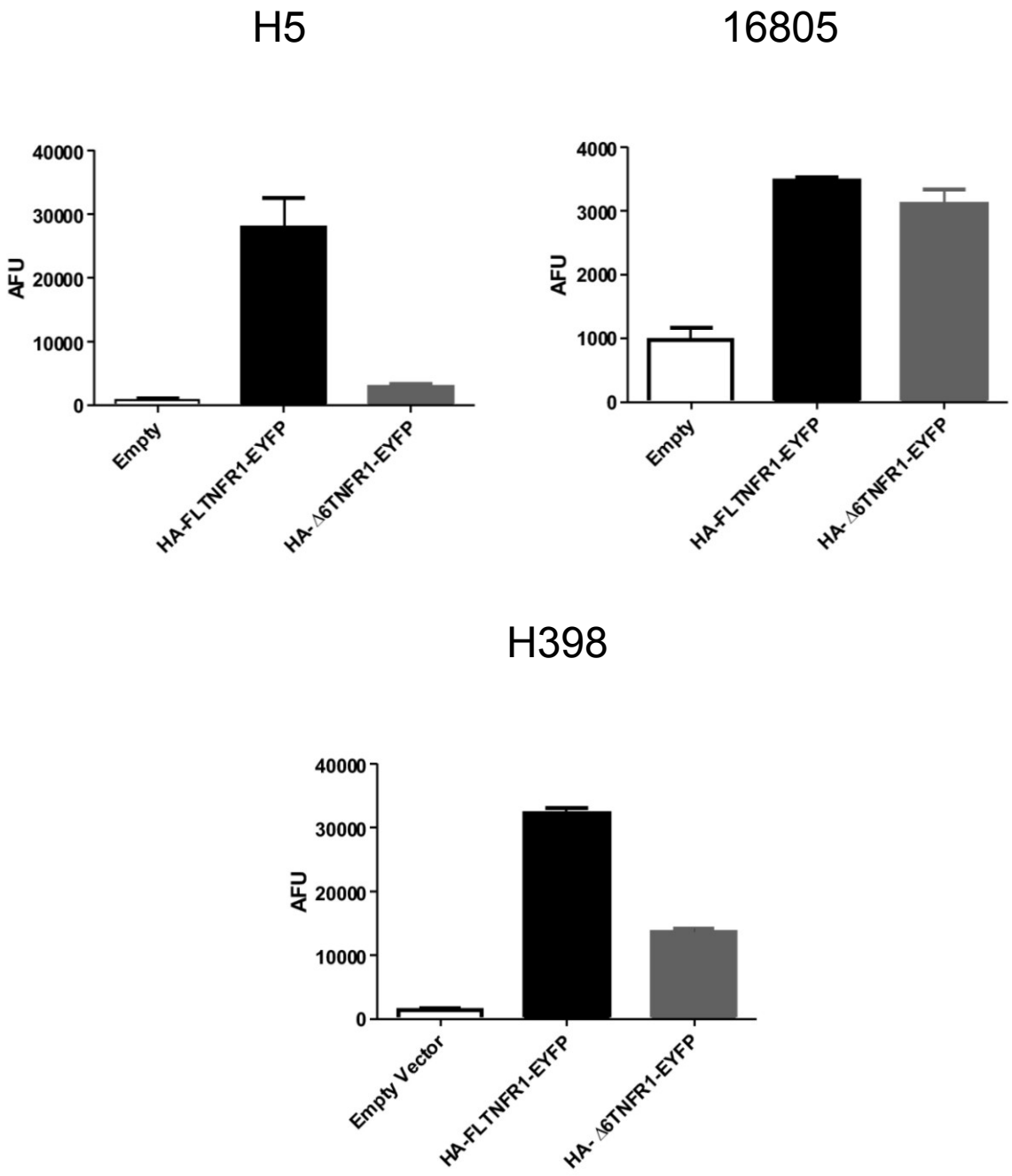
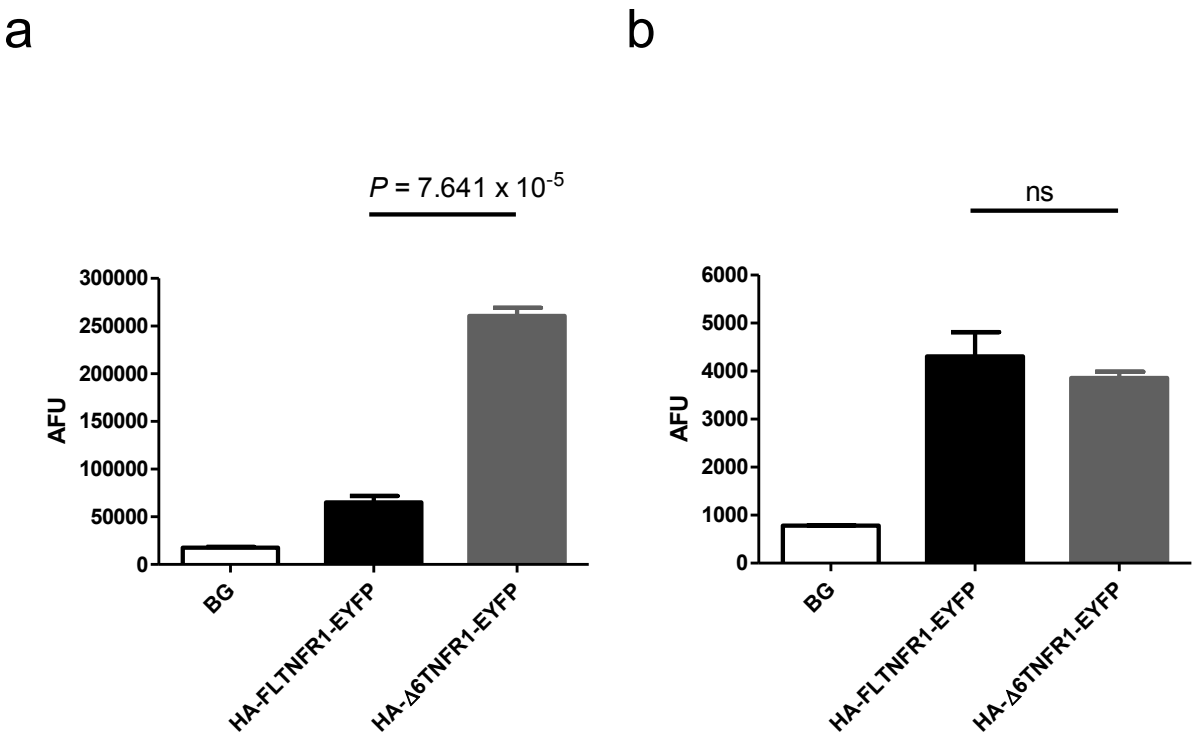
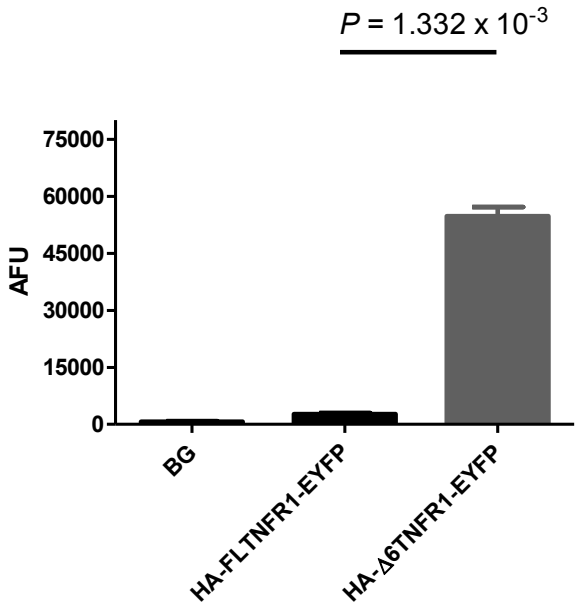


Figure 4.10: Analysis of ability of anti-TNFR1 ELISA antibody pairs to recognise FLTNFR1 and Δ6TNFR1. 48 h cell culture supernatants from cells transfected with empty pEYFP-N1, HA-FLTNFR1-EYFP or HA-Δ6TNFR1-EYFP constructs were analysed for soluble TNFR1 expression by ELISA. Capture antibody clones are indicated. Error bars represent mean ± SEM. AFU = Arbitrary Fluorescence Units.

As we were unable to identify a pair of antibodies that were equally able to detect FLTNFR1 and Δ6TNFR1 in a sandwich ELISA, we next tried to develop an alternative assay making use of a single antibody to the extracellular domain of TNFR1. Figure 4.11a shows the results of an assay using the capture antibody from the R&D systems ELISA antibody pair, clone 16805, followed by biotinylated anti-mouse IgG1 and Europium-labelled streptavidin to detect total soluble TNFR1 species directly coated to ELISA plate wells from cell culture supernatant of cells transfected with HA-Δ6TNFR1-EYFP or HA-FLTNFR1-EYFP. The results gave very strong signal above background levels detected in cell culture supernatant using mouse IgG1 isotype control (Figure 4.11b), and displayed a similar trend in soluble TNFR1 species to an anti-HA ELISA performed on the same cell culture supernatants (Figure 4.11c). We therefore investigated if we could observe a trend towards increased total soluble TNFR1 species in the plasma isolated from blood samples of healthy donors by genotype using this assay. Figure 4.11d shows that no genotype-dependant trends were detected.



c



d

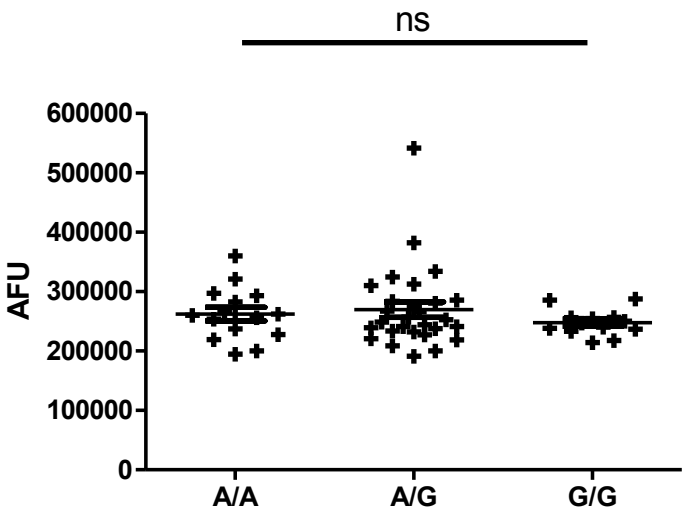


Figure 4.11: Analysis of soluble TNFR1 levels in cell culture supernatants and plasma. 48 h cell culture supernatants from cells transfected with HA-FLTNFR1-EYFP or HA-Δ6TNFR1-EYFP constructs or background (BG) levels of soluble TNFR1 species were analysed by ELISA using **(a)** 16805 followed by biotinylated anti-mouse IgG1 and Eu-streptavidin, **(b)** mouse IgG1 isotype control followed by

biotinylated anti-mouse IgG1 and Eu-streptavidin and **(c)** biotinylated anti-HA.11. **(d)** Total soluble TNFR1 levels in donor plasma samples were determined by performing ELISA assays as in **(a)** and **(b)** and subtracting values for isotype control assays from values for anti-TNFR1 clone 16805 assays. Error bars represent mean ± SEM; rs1800693^{GG} *n* = 13, rs1800693^{AG} *n* = 28, rs1800693^{AA} *n* = 15; *P* values are indicated; ns = non-significant. AFU = Arbitrary Fluorescence Units.

Finally, we had a monoclonal antibody made commercially to purified, recombinant Δ6TNFR1-Fc, screening against sTNFR1-Fc to ensure no cross reactivity with soluble, cleaved sTNFR1 (Supplementary Figure 5; for details about protein expression and purification, see sections 5.2.7 and 5.3.5). This was then used to capture Δ6TNFR1, which was subsequently detected with 16805 (as this antibody clone best recognises Δ6TNFR1 (Figure 4.10)) in a sandwich ELISA. Figure 4.12 shows the results of ELISAs performed on serum samples from healthy donors and MS patients. Using purified, recombinant Δ6TNFR1-Fc as a standard we were able to determine the detection limit of this assay to be ~ 1.25 ng/ml, and clear signal was seen in samples both from healthy controls and MS patients. Significantly higher levels of Δ6TNFR1 were present in the sera of MS patients than controls (Figure 4.12).

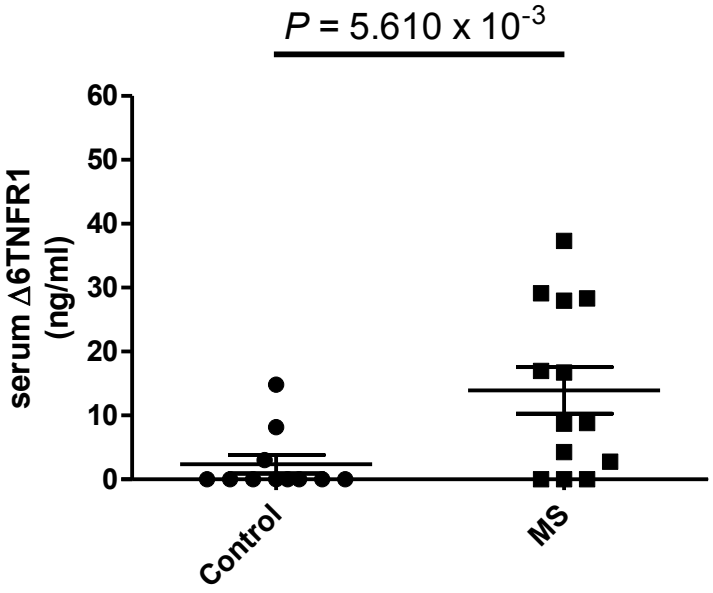


Figure 4.12: Serum Δ6TNFR1 levels in controls and MS patients. Sera obtained from healthy donors (Controls) and MS patients (MS) was analysed by ELISA for Δ6TNFR1. Detection limit = 1.25 ng/ml; values below this threshold were given a zero value. Error bars represent mean ± SEM; Controls *n* = 11, MS *n* = 13; The *P* value is indicated.

4.3.7 Surface, cellular and soluble expression of TNFR1 species in human immune cells by rs1800693 genotype

As Δ6TNFR1 cannot be detected at the surface of cells transduced with lentivirus or transfected with Δ6TNFR1 constructs, anti-TNFR1 staining of peripheral blood immune cell subsets was compared to that of an isotype control to see if reduced surface TNFR1 expression could be detected in individuals harbouring the rs1800693^{G} allele. Whole blood multiplex immunostaining and flow cytometry was used to delineate immune cell populations, in which TNFR1 or isotype control staining was analysed (Figure 4.13). In agreement with qRT-PCR data that showed no detectable decrease in the number of transcripts containing exon 6 by genotype (Figure 3.3c and e), no

genotype-dependent trends were observed. This suggests that the increase in transcripts lacking exon 6 does not result in a significant reciprocal decrease in the surface expression of FLTNFR1.

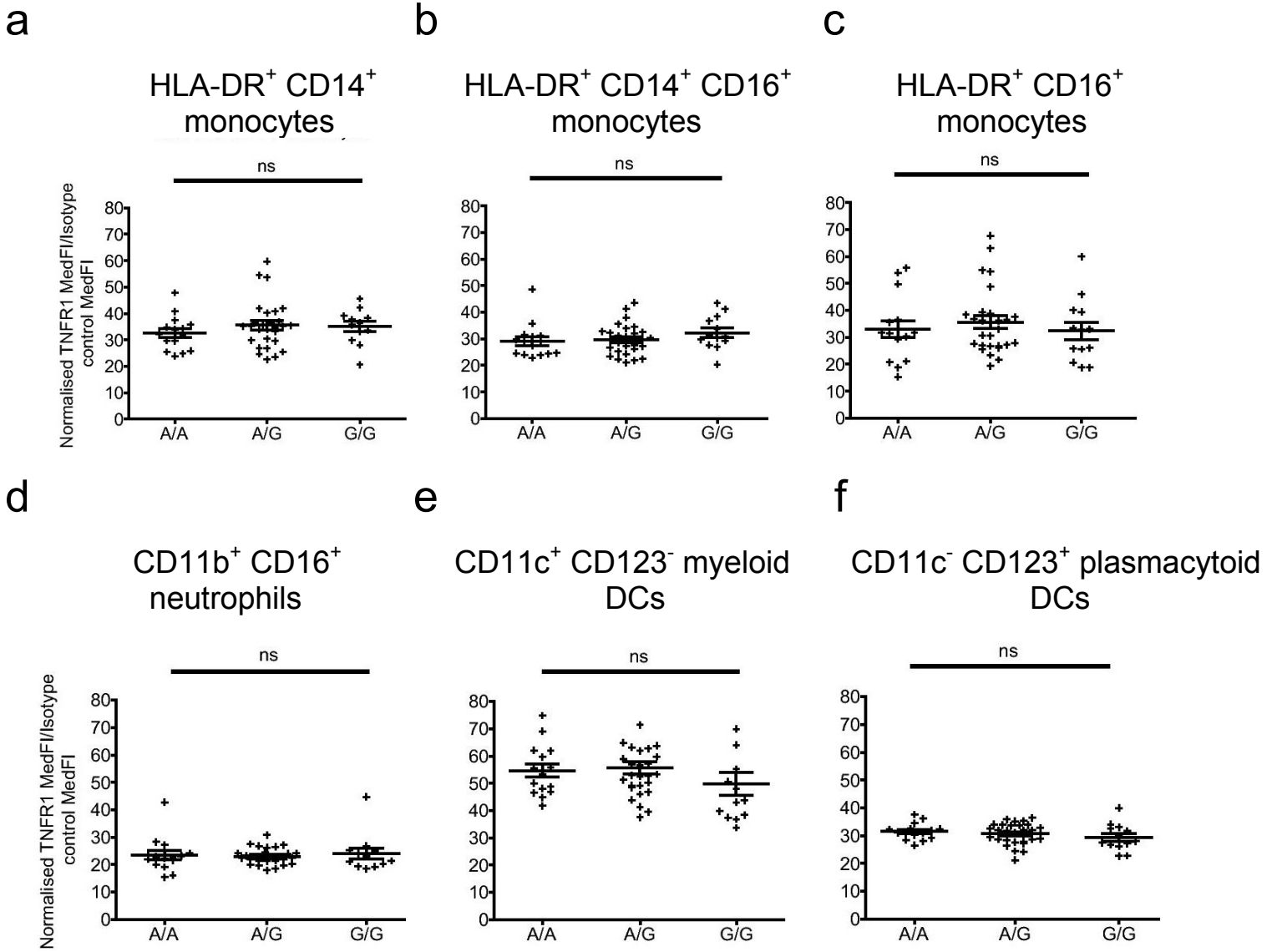

a
HLA-DR+ CD14+ monocytes
b
HLA-DR+ CD14+ CD16+ monocytes
c
HLA-DR+ CD16+ monocytes
d
CD11b+ CD16+ neutrophils
e
CD11c+ CD123- myeloid DCs
f
CD11c- CD123+ plasmacytoid DCs
Normalised TNFR1 MedFI/Isotype control MedFI
ns
A/A
A/G
G/G

Figure 4.13: TNFR1 surface expression by donor genotype at rs1800693 in human peripheral blood immune cell subsets. TNFR1 cell surface levels were measured by flow cytometry on (**a**) HLA-DR^{+} CD14+, (**b**) CD14^{+} CD16^{+}, and (**c**) CD16^{+} monocytes, (**d**) CD11b^{+} CD16^{+} neutrophils, and (**e**) CD11c^{+} CD123^{-} myeloid and (**f**) CD11c^{-} CD123^{+} plasmacytoid dendritic cells (DCs). Graphs show ratios of Median fluorescence intensity (MedFI) values of anti-TNFR1 staining normalised to control for day-to-day variation, to MedFI of normalised isotype control values. 1-d.f. Error bars represent mean ± SEM; rs1800693^{GG} *n* = 13, rs1800693^{AG} *n* = 28, rs1800693^{AA}; ns = non-significant.

4.4 Discussion

4.4.1 Δ6TNFR1 is not detected at the cell surface, has diffuse intracellular expression and is a secreted protein

The 272 amino acid truncation associated with skipping of *TNFRSF1A* exon 6 removes several well characterised functional domains of TNFR1 (Figure 4.1). Exon 6 encodes both the C-terminal portion of the fourth cysteine-rich domain (CRD) of TNFR1 and the metalloprotease cleavage site utilised by TNF Cleaving Enzyme (TACE) to generate soluble (28 kDa) TNFR1 from the full-length, membrane-bound protein (Gullberg *et al.*, 1992; Marsters *et al.*, 1992; Reddy *et al.*, 2000). Downstream, the frameshift removes the transmembrane domain required to anchor the full-length protein at the cell surface and the intracellular death domain, which has been demonstrated to be essential for all signalling functions of FLTNFR1 (Brakebusch *et al.*, 1992; Rothe *et al.*, 1992; Tartaglia *et al.*, 1993). The cytoplasmic portion of the receptor also contains regions important for determining the subcellular localisation of TNFR1, such as *trans*-Golgi-retention and surface expression regulation motifs (Cottin *et al.*, 2002; Fielding *et al.*, 2004; Storey *et al.*, 2002). *In silico* analysis predicted the novel 45 amino acid sequence not to have any recognised domains or regions of striking hydrophobicity/hydrophilicity (Supplementary Figure 2), and so we hypothesised that this part of the protein would be non-functional.

Equal detection of control exons 3-4 by qRT-PCR in cells transduced with Δ6TNFR1 lentivirus qRT-PCR data (Figure 4.4a) and expression of Δ6TNFR1 protein from constructs that were not modified to remove the non-coding cDNA downstream of the stop codon introduced by the frameshift associated with the skipping of exon 6 (Figure 4.2) demonstrated that the Δ6_TNFR1 mRNA is not degraded by nonsense mediated decay (Shyu *et al.*, 2008), in agreement with similar levels of control *TNFRSF1A* exon expression across rs1800693 genotypes in donor PBMCs (Figure 3.3f). Studies in the lentiviral transduction and transient transfection systems demonstrated that whilst

levels of total TNFR1 expression are not significantly different from one another, in cells expressing FLTNFR1 a significant proportion of this is at the cell surface, whilst cells expressing Δ6TNFR1 display surface staining that is not significantly different from background levels. These results are consistent with Δ6TNFR1 having lost the series of non-polar amino acids that form the 25 aa hydrophobic transmembrane domain encoded by *TNFRSF1A* exon 7, which have been demonstrated in previous studies to be necessary for insertion into and anchoring of the receptor at the cell membrane (Rothe *et al.*, 1992).

The similarity between stainings obtained with the anti-TNFR1 antibody clone H398 and the anti-HA (Figures 4.2 and 4.5 cf. Figure 4.6a) suggest that H398 recognises a domain of the extracellular portion of TNFR1 that is unperturbed by the frameshift associated with removal of *TNFRSF1A* exon 6. Furthermore, as anti-TNFR1 staining of untagged TNFR1 proteins (Figures 4.2 and 4.5) is comparable with that obtained using HA-tagged species (Figure 4.6b), it is unlikely that this tag interferes with the normal functioning of the receptor. The concordance of results in using lentiviral and transient transfection expression systems additionally suggest that C terminal fluorescent fusions of TNFR1 do not interfere with the normal trafficking of the protein, in agreement with previous studies (Chan *et al.*, 2000; Lobito *et al.*, 2006).

Fluorescent fusions of TNFR1 have also been used to investigate intracellular distributions of wildtype and mutant TNFR1 proteins in transiently transfected cells using confocal microscopy by co-transfecting cells with fluorescent fusions of organelle-resident proteins (Lobito *et al.*, 2006). The use of fluorescent fusions of proteins of interest and organelle-resident proteins removes the need for staining with antibodies and organelle-markers. The β chain of the Signal Recognition Particle Receptor (SRβ) is a transmembrane protein has been shown to be associated exclusively with the

rough ER, whilst N-acetylgalactosaminyltransferase 2 (GalNAc-T2) is an enzyme involved in post-translational modifications that occur in the *trans*-Golgi (Rottger *et al.*, 1998; Schwartz and Blobel, 2003). Analysis of TNFR1 distribution using this technique necessitates the use of cell lines that have not been transformed with the SV40 T antigen such as HEK293T cells, as the receptor proteins expressed under the control of the CMV promoter are over-expressed in these cell lines, and constitutively accumulate in the ER (the site of over-expressed and unfolded proteins). HeLa cells were therefore used to study subcellular localisation of FLTNFR1 and Δ6TNFR1, which were found to have distinct intracellular distributions (Figure 4.7). FLTNFR1-EYFP was found to be concentrated in the *trans*-Golgi, as evidenced by colocalisation of EYFP fluorescence with that of a fluorescent fusion of GalNAc-T2 (Figure 4.7a and b); significantly more than FLTNFR1-EYFP localised to the ER or to neither the Golgi nor the ER (Figure 4.7b). Δ6TNFR1, however, was found to be more diffuse, with no proclivity for the *trans*-Golgi (Figure 4.7a and b), and significantly more localising neither to the Golgi nor the ER Figure 4.7b). Outside of the *trans*-Golgi and the small ER-resident pool, FLTNFR1 fusions formed foci of high intensity (Figure 4.7a). These were thought to be the localised pools of surface-expressed TNFR1 described in the literature (Cottin *et al.*, 2002; Fielding *et al.*, 2004). The diffuse intracellular distribution of Δ6TNFR1 within the endomembrane system is consistent with the removal of the surface expression regulation and C-terminal, 23 amino acid *trans*-Golgi retention motifs (Figure 4.1). Moreover, the failure of Δ6TNFR1 to form high intensity foci may also be an indication that the protein is unable to self-associate to form multimers.

Initial studies using a commercially-available ELISA antibody pair for the detection of soluble TNFR1 (ie. the extracellular domain of the FLTNFR1 protein) in the supernatant of cells expressing FLTNFR1 and Δ6TNFR1 through both the lentiviral transduction and transient transfection systems revealed significantly more to be produced from cells expressing FLTNFR1 (Figures 4.3 and 4.5). In conjunction with the inability of this protein to be expressed at the cell surface, this led us to hypothesise that

Δ6TNFR1 was a misfolded protein that was therefore being retained intracellularly. However, misfolded TNFR1 mutant proteins have previously been demonstrated to accumulate in the ER (Lobito *et al.*, 2006; Todd *et al.*, 2004), and only a very small proportion of Δ6TNFR1 colocalised with an ER-resident protein by confocal microscopy (Figure 4.7). Furthermore, sTNFR1 levels in cell culture supernatant of cells expressing Δ6TNFR1, whilst much lower than levels for cells expressing FLTNFR1, were significantly higher than background levels (Figures 4.3 and 4.5). If Δ6TNFR1 is unable to traffick to the cell surface and is therefore retained intracellularly and/or degraded, sTNFR1 levels in cell culture supernatant should be comparable to background. Subsequent studies making use of the HA tag for the unbiased detection of TNFR1 species in cell culture supernatant revealed that in stark contrast with the results of the R&D systems sTNFR1 ELISA, more than twice as much Δ6TNFR1 was detected as exosomally-released FLTNFR1 plus cleaved, shed extracellular domain of FLTNFR1 (Figure 4.8). Due to the use of a single antibody to detect antigen from samples coated directly to ELISA plate wells, the direct anti-HA ELISA is less sensitive and specific than the R&D systems sandwich ELISA. Nevertheless, significant HA signal above background was reproducibly detected in the cell culture supernatants of cells expressing HA-FLTNFR1-EYFP or HA-Δ6TNFR1-EYFP. Moreover anti-HA ELISA results were supported by western blots performed on concentrated supernatants, demonstrating that ELISA results were not due to a bias in the ability of HA-Δ6TNFR1-EYFP to coat the base of ELISA plate wells (Figure 4.8).

4.4.2 Transcripts lacking *TNFRSF1A* exon 6 are translated in cells homozygous for rs1800693^{G}

Figure 4.9 demonstrates that Δ6_TNFR1 mRNA was detected in the polysome fractions obtained from a monocytic cell line and from PBMCs of rs1800693^{G} homozygous individuals, and so is translated into protein. The profile of 6-7_TNFR1 transcript distribution across ribosome fractions is consistent between samples, suggesting that differences are not artefacts of sample preparation or processing. Furthermore, the higher levels of 6-7_TNFR1 mRNA associated with heavier polysome

fractions compared with Δ6_TNFR1 mRNA is in agreement with the larger size of the full-length TNFR1 transcript; ie. more ribosomes are able to associate per transcript for simultaneous translation (Figure 4.9c). The higher levels of Δ6_TNFR1 mRNA detected across all fractions from U937 cells compared with those from PBMCs of rs1800693^{G} homozygote donors may be due to this being a monocytic cell line; this cell type had previously been demonstrated to express the highest levels of Δ6_TNFR1 mRNA (Figure 3.3a).

Whilst we had previously demonstrated the existence of the Δ6_TNFR1 transcript in immune cells isolated from blood of rs1800693^{A} homozygotes (Figure 3.3d), the very low levels observed may be below a threshold required for the initiation of translation, or the signal may be diluted across ribosome fractions such that the methods used are not sensitive enough to detect signal in any single fraction. Indeed, in the homozygous rs1800693^{A} Jurkat cell line low levels of polysome-associated Δ6_TNFR1 transcript are detected (Figure 4.9b).

4.4.3 Δ6TNFR1 is detected in sera and is increased in MS patients compared to controls

The above data suggest that rs1800693^{G} results in the production of a secreted TNFR1 isoform, and that serum and/or *ex vivo* cell culture supernatant of individuals harbouring one or more copies of the rs1800693^{G} allele should have increased levels of soluble TNFR1 species. The paucity of information available as to the specific epitopes of the extracellular domain of TNFR1 that commercially available anti-TNFR1 antibodies recognise led us to adopt a speculative approach to identify an appropriate ELISA antibody pair. Of the several different anti-TNFR1 capture antibodies that were trialled on the same cell culture supernatant that so convincingly demonstrated Δ6TNFR1 to be a secreted protein none were able to reproduce the result achieved using the HA tag, and all

appeared compromised in their ability to detect Δ6TNFR1 compared to sTNFR1/FLTNFR1 (Figure 4.10).

The R&D Systems human sTNFR1 ELISA antibody pair uses a capture antibody (16805) that is capable of neutralising the TNF binding activity of TNFR1. This suggests that it binds the ligand binding domains of the protein (CRDs 2 and 3), which are retained in full in Δ6TNFR1 ((Banner *et al.*, 1993; Marsters *et al.*, 1992) Figure 4.1). We previously demonstrated the clone H398 anti-TNFR1 antibody to be able to recognise FLTNFR1 and Δ6TNFR1 with similar affinity (Figure 4.6), giving a staining pattern similar to that obtained when cells transiently expressing HA-tagged receptors stained with an anti-HA antibody. Results for the H398 capture, BAF225 detection ELISA antibody pair show a similar trend to those obtained with the R&D Systems ELISA antibody pair, which is in agreement with H398 having also been demonstrated to neutralise TNF binding by TNFR1 (Kruppa *et al.*, 1992). Finally, clone H5 was used as a capture antibody in combination with BAF225 as a detection antibody. This ELISA antibody pair gave equally poor detection of soluble TNFR1 species in supernatants of cells expressing HA-FLTNFR1-EYFP and HA-Δ6TNFR1-EYFP. The biotinylated secondary antibody BAF225 may recognise an epitope that is removed or altered by the frameshift associated with removal of *TNFRSF1A* exon 6.

Using 16805 followed by biotinylated anti-mouse IgG and Europium-labelled streptavidin we were able to detect HA-Δ6TNFR1-EYFP in cell culture supernatants at high levels (Figure 4.11a). However, this assay appeared to preferentially detect HA-FLTNFR1-EYFP, as only ~ 4 times more total soluble TNFR1 was detected in cell culture supernatants of cells transfected with HA-Δ6TNFR1-EYFP compared to HA-FLTNFR1-EYFP using this assay, in contrast to the ~ 20 times more detected by anti-HA ELISA on the same cell culture supernatants (Figure 4.11c). We reasoned that we still might be

able to detect an increase in total soluble TNFR1 species in plasma samples of donors using this assay; although Figure 4.11d shows that no trends were subsequently observed by donor genotype. The observed reduction in the capacity to detect Δ6TNFR1 compared to FLTNFR1 might preclude the recognition of any trend using this assay.

A Δ6TNFR1-specific monoclonal capture antibody was able to detect Δ6TNFR1 protein in the serum of controls, and increased levels in the serum of MS patients by sandwich ELISA (Figure 4.12). Serum samples generally give reduced background levels in ELISAs when compared to plasma, as serum is devoid of clotting factors, and may have facilitated detection of Δ6TNFR1. The MS patients from which the samples were obtained had RRMS, and whilst it might be interesting to know if and how serum Δ6TNFR1 levels vary during different stages of disease, this would require a large-scale analysis. Access to hundreds of patient serum samples would be necessary to attain the statistical power to thoroughly and accurately quantify differences in serum isoform levels whilst taking into account genotype, age, sex, disease course, treatment, and serum storage duration dependent effects, to name just some of the variables that have been shown to influence soluble cytokine receptor levels (Maier *et al.*, 2009). Moreover, as Δ6TNFR1 may mainly be produced and be acting in the localized environment of the site of pathology in CNS, an assessment of serum isoform levels in MS patients may not accurately reflect changes in the CNS during different stages of disease.

Serum samples were not available for the cohort of healthy individuals genotyped for rs1800693 so we could not look for by-genotype differences in serum Δ6TNFR1 levels. In any case, for the reasons described above, a very large sample size would be likely to be required to attain the appropriate statistical power. Similarly, whilst there appears to be significantly more Δ6TNFR1 in MS patient sera

the very small sample size should be noted. If this observation can be confirmed in a larger study it would raise the possibility of using serum Δ6TNFR1 levels for diagnostic and/or prognostic purposes.

4.4.4 No rs1800693 genotype-dependent differences are observed in surface TNFR1 levels

In light of results demonstrating no significant difference between the levels of *TNFRSF1A* transcripts containing exon 6 in various immune cell subsets by rs1800693 genotype (Fig.3.3c and e), it is not surprising that no decrease in the median fluorescence intensity (MedFI) of anti-TNFR1 surface staining was detected on monocytes, neutrophils and dendritic cell populations isolated from individuals harbouring the rs1800693^{G} allele was detected (Figure 4.13). Taken together, these data suggest that the mechanism by which rs1800693^{G} confers susceptibility to MS is not by reduction of the surface expression of, and thereby downregulation of signalling through, TNFR1. Even if a decrease in FLTNFR1 mRNA expression had been detected, this might not have translated to a decrease in surface expression, as the majority of cellular TNFR1 is found in the Golgi, where it acts as a pool to constantly replenish surface TNFR1 levels ((Wang *et al.*, 2003) Figure 4.7). It is important to consider that the number of individuals of each genotype analysed in this study and/or the sensitivity of the assay to detect surface TNFR1 expression may be insufficient to detect a difference by genotype. Even so, a change in surface expression that is so modest that it is undetectable by flow cytometry in a study of this size would seem unlikely to be the main means by which the variant predisposes to MS. This led us to hypothesise that the mechanism by which rs1800693^{G} confers MS susceptibility is through a property of secreted Δ6TNFR1, a function or cellular consequence of the protein when expressed intracellularly or some combination of the two.

5.0 Functional characterisation of Δ6TNFR1

5.1 Introduction

Having demonstrated the existence of Δ6TNFR1 as a protein we sought to investigate how the functional properties of this isoform departed from those of the full-length protein in terms of signalling, receptor oligomerisation and ligand binding.

5.1.1 Functional properties of TNFR1

TNFR1 lacks intrinsic enzymatic activity, and the 80 amino acid death domain located within its cytoplasmic portion has been demonstrated to be essential for all signalling functions of the receptor; TNFR1 in which the death domain has been experimentally deleted or mutated are non-functional (Brakebusch *et al.*, 1992; Rothe *et al.*, 1992). The DD is composed of six alpha helices, and is required for the recruitment of adaptor proteins such as TRADD, FADD and RIPK1, that interact through homotypic associations with their own death domains (Liu *et al.*, 1996; Micheau and Tschopp, 2003). Through associations between TNFR1 DD and the DDs of adaptor proteins both complex I, required for NF-κB-mediated signalling, and the DISC, required for induction of apoptosis, are formed (Kelliher *et al.*, 1998; Micheau and Tschopp, 2003; Tartaglia *et al.*, 1993). The signalling capabilities of various TRAPS-associated TNFR1 mutants have been investigated in transient transfection and inducible expression systems; spontaneous apoptosis has been assessed by analysis of DNA fragmentation and mitochondrial membrane potential, whilst spontaneous NF-κB-mediated signalling has been investigated using NF-κB luciferase reporter constructs, and downstream by analysis of levels of NF-κB targets, such as IL-8, by ELISA (Lobito *et al.*, 2006; Rebelo *et al.*, 2006; Siebert *et al.*, 2005; Todd *et al.*, 2004).

Misfolding of mutant proteins in the ER can lead to their accumulation and bring about ER stress responses such as the unfolded protein response (UPR) and the ER overload response (EOR) (Pahl and Baeuerle, 1997; Schroder and Kaufman, 2005). These responses upregulate the transcription and activity of proteins involved in folding and glycosylation of proteins in the ER, slow or stop translation processes and can induce apoptosis in cells with irrecoverable levels of ER stress.

5.1.2 ER stress responses

Protein misfolding can contribute to autoimmunity through exposure of ordinarily cryptic epitopes, and through impaired function of cells required for the proper establishment or maintenance of tolerance mechanisms (Todd *et al.*, 2008). Furthermore, cells with active ER stress responses are less susceptible to the induction of programmed cell death, and so this may represent a mechanism by which autoreactive cells escape central and peripheral tolerance (Todd *et al.*, 2008).

Under normal conditions, immunoglobulin-heavy-chain binding protein (BIP) binds to and inhibits the transmembrane activating transcription factor 6 (ATF6), inositol-requiring transmembrane kinase/endonuclease 1 (IRE1) and pancreatic ER kinase (PERK). When misfolded proteins accumulate in the ER lumen, BIP is recruited away from ATF6, IRE1 and PERK and the UPR is initiated (Schroder and Kaufman, 2005). ATF6 moves to the Golgi where it is cleaved to yield the ATF6f transcription factor, which initiates the transcription of BIP, CCAAT/enhancer-binding protein homologous protein (CHOP) and X-box binding protein 1 (XBP1); CHOP is capable of initiating the apoptotic cascade in cells with irrevocable levels of stress (Ma *et al.*, 2002; Schroder and Kaufman, 2005). Release of BIP from IRE1 allows its homo-dimerisation and activation through phosphorylation. Activated IRE1 acts as an endoribonuclease to splice a 26 bp intron from *XBP1* mRNA, yielding a more stable and potent isoform of XBP1 that acts as a transcription factor for genes important for secretory function (Calfon

et al., 2002; Yoshida *et al.*, 2001). IRE1 can also activate JNK through TRAF and apoptosis signal regulating kinase 1 (ASK1), promoting cell survival or apoptosis. PERK is activated by phosphorylation following BIP release, and activates eukaryotic translation initiation factor 2α (EIF2α), which arrests the translation of most proteins (Schroder and Kaufman, 2005). Certain proteins such as ATF3 are capable of escaping EIF2α inhibition of translation, and translocate to the nucleus to upregulate the transcription of additional UPR target genes, including growth-arrest DNA damage gene 34 (GADD34), which can inhibit *CHOP* expression (Schroder and Kaufman, 2005). The EOR occurs as the result of Ca^{2+} leakage and the production of ROS in response to membrane stress in the overloaded ER, and leads to the activation of NF-κB and ultimately to the expression of genes promoting cell survival (Kuang *et al.*, 2005; Pahl and Baeuerle, 1997).

5.1.3 Assessing receptor oligomerisation by resonance energy transfer

Several members of the TNFR superfamily have disease-associated dominant-negative signalling mutants (Lobito *et al.*, 2011). For example, an autoimmune disorder that occurs as the result of uncontrolled proliferation of autoreactive lymphocytes known as autoimmune lymphoproliferative syndrome (ALPS) occurs due to ineffective Fas-FasL mediated deletion of autoagressive lymphocytes in the periphery, due to mutations in the Fas receptor. Two-thirds of ALPS mutations occur in the cytoplasmic domain of Fas, resulting in its truncation or alteration of the DD, rendering the receptor unable to recruit for example FADD for the initiation of apoptosis (Worth *et al.*, 2006). The majority of ALPS-associated Fas mutants display a dominant pattern of inheritance as mutant, non-functional Fas molecules associate with wildtype receptor to form functionally compromised receptor complexes (Wang *et al.*, 2010). Furthermore, experimentally generated TNFR1 mutants that have analogous DD inactivating or cytoplasmic domain truncating mutations display similar dominant negative inhibition of signalling, by associating with full-length TNFR1 through their intact PLADs (Chan *et al.*, 2000; Lobito *et al.*, 2006).

Resonance energy transfer (RET) techniques are used to investigate potential protein-protein interactions (Stryer and Haugland, 1967). They make use of the overlapping emission frequencies of excited donor chromophores and excitation frequencies of acceptor chromophores, such that excitation of a donor will cause emission from an acceptor by resonance energy transfer if the chromophores are within 10 nm of one another (Banning *et al.*, 2010). For example, fluorescence resonance energy transfer (FRET) will occur between closely interacting CFP and YFP fluorophores upon excitation with light of a wavelength of ~ 440 nm (Chan *et al.*, 2001). This wavelength will greatly excite CFP but not YFP, which has an excitation peak of ~ 480 nm. However, as peak emission of CFP is in the range of ~ 480 nm, emission from YFP at ~ 540 nm is nevertheless observed (Chan *et al.*, 2001). FRET has previously analysed by flow cytometry to investigate self-association of wildtype Fas and TNFR1 receptors, self-association of experimental or disease-associated mutants, and hetero-association between wildtype and mutant receptors, using C terminal YFP and CFP fusions (Chan *et al.*, 2000; Siegel *et al.*, 2000). In their 2000 Nature paper, Chan *et al.* used this technique to demonstrate the function of CRD1 as the PLAD of full-length TNFR1, by demonstrating that mutants with an experimentally deleted PLAD were unable to self-associate or associate with full-length TNFR1 (Chan *et al.*, 2000). Furthermore, Lobito *et al.* 2006 showed dramatically reduced capacity of several structural TRAPS mutant receptors to self-associate, and near complete inability to associate with full-length TNFR1 (Lobito *et al.*, 2006).

Bioluminescence resonance energy transfer (BRET) is a related technique based on the same principle, but with less background excitation of the acceptor fluorophore (due to less spectral overlap) than is observed with FRET, reducing noise and allowing more sensitive detection of associations between proteins (Xu *et al.*, 1999). In BRET^2, bioluminescence (395 nm) from the oxidation of a coelenterazine derivative by *Renilla* luciferase (Rluc) is used to excite a GFP variant,

GFP^2, which emits at 510 nm (James *et al.*, 2006). Energy transfer efficiencies can thereafter be determined ratiometrically by dividing the acceptor emission (GFP^2 fluorescence) intensity by the donor emission (luminescence) intensity, and this reflects the proximity of Rluc to GFP^2 (James *et al.*, 2006).

5.1.4 Analysing TNF binding and neutralisation

Co-immunoprecipitation assays are a useful starting point in the study of protein-protein binding interactions, allowing their absolute and qualitative determination. Typically, binding partners for a protein of interest are 'pulled' out of solution using an antibody recognising a non-interacting part of the protein. Binding partners are then resolved by SDS-PAGE, and visualised and identified using downstream applications. Co-immunoprecipitation assays using TNF-FLAG and TRAPS mutant TNFR1-Fc fusions have previously demonstrated that structural TRAPS mutants fail to bind TNF, whilst sTNFR1-Fc and the R92Q TRAPS mutant are capable of binding TNF (Lobito *et al.*, 2006). Additionally, Todd *et al.* 2004 analysed the ability of several TNFR1 mutants to bind TNF in an *in vitro* assay, in which cells expressing the TRAPS mutant of interest where incubated with TNF and analysed by flow cytometry using an anti-TNF antibody (Todd *et al.*, 2004).

Both cell membrane-associated and soluble TNFR1 species (full-length and cleaved, shed receptor) are capable of binding TNF (Hawari *et al.*, 2004). Equilibrium binding studies with ^{125}I-labelled TNF and the extracellular domain of TNFR1 fused to human IgG have estimated the affinity of TNFR1 for soluble TNF to be in the range of 20-60 pM (Grell *et al.*, 1998b). The very high affinity of the receptor for its ligand allows cells to respond to very small amounts of TNF to bring about functional consequences.

Analysis of surface plasmon resonance (SPR) by Biacore is a technique that allows the very sensitive detection of interactions between molecules (reviewed by (Schuck, 1997). Polarised light is internally refracted from the gold surface of a Biacore chip, through which an electric current is passed. This generates an electric field density which interacts with free electrons in the gold layer, causing the production of electromagnetic waves called surface plasmons from the external surface of the gold chip. The angle of internal refraction is sensitive to changes in the refractive index of this region, such that even a very weak interaction between a molecule immobilised to the surface of the gold chip and a putative binding partner passed over the surface of the chip can be detected. The change in refractive index is measured in real time to yield sensograms which can then be used to quantitatively characterise associations, through the calculation of association and dissociation constants. The relative binding of the extracellular domain of the wildtype and TRAPS mutant TNFR1 proteins to TNF has previously been investigated SPR by Biacore, where investigators were able to demonstrate significant reduction in binding due to structural changes as the result of TRAPS mutations (Lobito *et al.*, 2006).

The relative ability of putative TNF inhibitors to neutralise the biological effects of the cytokine have been assessed *in vitro* using either reporter cell lines that give an enzymatic readout upon TNF signalling through TNFR1 to upregulate NF-κB activity, or cells that are sensitive to TNF-induced cell death (Nesbitt *et al.*, 2007). Percentage inhibition is determined by comparison to NF-κB induction or apoptosis in cells untreated with TNF inhibitor (0% inhibition) and those not treated with TNF (no TNF-induced signalling), and can be plotted against the concentration of the inhibitor used to generate a dose-response curve. Dose-responsive curves can then be used to quantitatively determine the ability of inhibitors to interfere with TNF function, through calculation of the half maximal inhibitory concentration (IC50) of an inhibitor; the concentration at which 50% inhibition of TNF-mediated signalling function is inhibited.

5.2 Methods

5.2.1 Constructs for transient transfections

The construction of EYFP and ECFP fluorescent fusion protein constructs for FLTNFR1 and Δ6TNFR1 are described in 4.2.3.1. An EYFP fusion protein construct for the extracellular domain of human Fas (FAS180) was constructed in the same way, using a insert integrating a 3' *KpnI* and 5' *BamHI* restriction sites, amplified by PCR (2.2.1) from a construct encoding the full-length human Fas cDNA sequence (clone 6172538; Open Biosystems, Thermo Scientific) using FAS180fluor_F (5'-ATGGTACCGCCACCATGCTGGGCATCTGGACCCTCC-3') and FAS180fluor_R (5'-CGCGGATCCGTGACCAAGCTTTGGATTTCATTTCTGAAG-3') primers.

5.2.2 Analysis of apoptosis

5.2.2.1 DNA fragmentation

Spontaneous apoptosis was analysed in HEK 293T cells transiently transduced with lentivirus as follows. HEK 293T cells were seeded in 6 well plates and subsequently transduced (4.2.1) with empty lentivirus or the indicated TNFR1 lentivirus at an MOI of 50. 72 h post-transduction cells were harvested by trypsinisation (2.3.2) and pelleted by centrifugation in wells of a V-bottomed, 96-well plate at 300 x *g* for 2 min at 4°C. Supernatant was discarded and cells were washed by resuspension in 200 µl of PBS, 2% FBS followed by centrifugation at 300 x *g* for 2 min at 4°C. The supernatant was discarded, and cells were permeabilised by resuspension in 200 µl of ice-cold 70% EtOH for 30 min at 4°C. At the end of this incubation period cells were pelleted by centrifugation at 300 x *g* for 2 min at 4°C, the supernatant was discarded and then cells were washed with 200 µl of PBS, 2% FBS as above. Cells were subsequently stained in a solution containing 50 µg/ml Propidium Iodide (PI; Sigma) and 1 µg/ml of DNAse-free RNAse A (Sigma) for 30 min at room temperature. Finally, cells were pelleted by centrifugation, resuspended in 200 µl of PBS, 2% FBS and passed through a 40 µm cell strainer

(Partrics) to ensure a single cell suspension. Cells were then analysed for PI staining by flow cytometry. Events were gated to exclude debris (low forward-scatter, low side-scatter) and doublets (high PI, high pulse-width). Cells with a PI fluorescence intensity below that of the G_0/G_1 diploid content peak were defined as apoptotic.

5.2.2.2 Mitochondrial membrane integrity

HeLa or HT1080 cells were seeded in 12 well cell culture dishes and transfected (2.3.3) 24 h later with the empty pECFP-N1 vector or the indicated TNFR1-ECFP construct. In the indicated conditions, the pan caspase inhibitor zVAD.fmk was added to a final concentration of 50 µM as a broad-spectrum inhibitor of spontaneous apoptosis, as a control. After 18 h, mitochondrial membrane potential ($\Delta\psi_M$) was analysed by staining cells with the mitochondrion-selective potentiometric dye tetramethylrhodamine methyl ester (TMRM) at a final concentration of 200 nM, for 20 min at 37°C. As a positive control for mitochondrial membrane depolarisation, a condition in which non-transfected cells were incubated with 5 mM H_2O_2 (Sigma) at 37°C for 1 h before addition of TMRM was included. Cells were subsequently washed by resuspension in 200 µl of PBS, 2% FBS and centrifugation at 300 x *g* for 2 min at 4°C, resuspended in 200 µl of PBS, 2% FBS and analysed by flow cytometry. For all conditions except those with non-transfected cells, TMRM signal from 1 x 10^4 events in an $ECFP^+$ gate was analysed.

5.2.3 Analysis of NF-κB-mediated signalling

5.2.3.1 NF-κB induction

NF-κB-mediated transcriptional activation was assayed using the NF-κB response element firefly luciferase reporter construct (pGL4.74 [luc2P/NF-κB-RE/Hygro]; Promega) as follows. HEK 293T or HT1080 cells were seeded in 12 well culture dishes and subsequently co-transfected with 0.3 µg of

the empty pEYFP-N1 vector, the indicated TNFR1-EYFP or FAS180-EYFP construct along with 0.25 µg of the NF-κB-RE luciferase reporter construct, and 0.05 µg of a vector constitutively expressing *Renilla* luciferase under the control of the minimal thymidine kinase (TK) promoter (pG4.32[hRluc/TK]; Promega) as a transfection efficiency and viability control (2.3.3 and 2.1.2). For titration experiments or experiments in which the total amount of receptor-encoding cDNA transfected was reduced, pcDNA3.1 (Invitrogen) was used to maintain a constant total amount of DNA in each transfection. 50 µM zVAD.fmk was added to all conditions to prevent spontaneous apoptosis. After 24 h incubation at 37°C, 5% CO_2 cells were sequentially analysed for firefly and *Renilla* luciferase activity using the Dual Luciferase Reporter Assay System (Promega) according to the manufacturer's instructions. Cell culture medium was removed and cells were rinsed with 1 ml of PBS warmed to 37°C. PBS was aspirated, 250 µl of 1 X passive lysis buffer (PLB; Promega) and cells were allowed to lyse with gentle rocking at room temperature for 15 min. Cell lysates were mixed by pipetting, and 20 µl aliquots of each lysate were added to separate 100 µl aliquots of luciferase assay reagent II (LAR II) in wells of a flat-bottomed 96-well plate (BD Falcon). Firefly luciferase activity in lysates was then measured using a Fusion Microplate Reader (Packard). 100 µl of 1 X Stop&Glo® Reagent (Promega) was then added to each well and mixed by pipetting, and *Renilla* luciferase activity was measured on the Fusion Microplate Reader. Relative induction of NF-κB was determined by dividing firefly luciferase readings by *Renilla* luciferase readings.

5.2.3.2 IL-8 production

HEK 293T cells were transduced with lentiviruses as described in 4.2.1 and cultured for 72 h at 37°C in 5% CO_2. Supernatants were then harvested and cleared of cells and debris by centrifugation for 10 min at 16,200 x *g* in a microcentrifuge. IL-8 levels were then analysed by ELISA (2.2.12) using the Human CXCL8/IL-8 DuoSet® ELISA kit (R&D Systems), using capture (part 890804) and detection (part 890805) antibodies at the recommended concentrations (4 µg/ml and 20 ng/ml, respectively).

5.2.4 Flow cytometry

Constructs expressing FLTNFR1 and Δ6TNFR1 in the pECFP-N1 vector with the ECFP removed were generated by cloning (2.1.1), using *KpnI* and *NotI* restriction sites. Inserts incorporating the appropriate 5' and 3' restriction sites were generated by PCR amplification (2.2.1) from existing FLTNFR1-EYFP and Δ6TNFR1-EYFP constructs (4.2.3.1) using the primers indicated in Table 5.1.

Name	***Sequence***
TNFR1fluor_F	5'-TAGGTACCGCCACCATGGGCCTCTCCACCGT-3'
FLTNFR1nofus_R	5'-AGTGCGGCCGCCTATCTGAGAAGACTGGGCGCGG-3'
Δ6TNFR1nofus_R	5'-CATGCGGCCGCCTAGGTGTCGATTTCCCACAAACAATGGA-3'

Table 5.1: Primers for the construction of non-fluorescently-tagged receptor constructs in the pECFP-N1 vector backbone.

HEK 293T cells were seeded and co-transfected (2.3.3) 24 h later with the amounts of FLTNFR1-ECFP, Δ6TNFR1 and FAS180 constructs. 48 h post-transfection, cells were analysed on a FACS Calibur by flow cytometry for ECFP signal by excitation with a 405 nm laser, emission collected in a channel with a 450/40 filter.

5.2.5 Analysis of the UPR

5.2.5.1 XBP1 splicing

HT1080 cells were seeded in 12 well plates and transfected (2.3.3) with the empty pEYFP-N1 vector of the indicated TNFR1-EYFP constructs. Cells were incubated at 37°C in 5% CO_2 for 48 h and were

then harvested by trypsinisation (2.3.2) and total RNA was extracted as described in 2.2.3. As a positive control for UPR induction, non-transfected cells were incubated with 0.5 µM Thapsigargin for 6 h prior to RNA isolation. cDNA was subsequently synthesised as described in 2.2.4, and PCR (2.2.1) was performed with XBP1sp_F (5'- TTACGAGAGAAAACTCATGGCC-3') and XBP1sp_R (5'-GGGTCCAAGTTGTCCAGAATGC-3') primers, flanking the 26 bp intron of human *XBP1* that is removed by IRE1 in response to ER stress (Samali *et al.*, 2010). PCR products were resolved in 6% TBE polyacrylamide (2.2.6.2) and bands were visualised using SYBR® Gold Nucleic Acid Gel Stain as described in 2.2.6.2.

5.2.5.2 XBP1 induction

An XBP1 firefly Luciferase reporter construct was derived from pGL4.74 by cloning (2.1.1) four tandem XBP1 consensus binding sites (TGGATGACGTGTACA) (Lee *et al.*, 2003) in place of the NF-κB response element using *KpnI* and *BglII* (AGATCT) restriction sites, using XBP1rep_F (5'-ATGGTACCTGAGCTCGCTAGCTGGATGACGTGTACATGGATGACGTGTACATGGATGACG-3') and XBP1rep_R (5'-ATAGATCTTGTACACGTCATCCATGTACACGTCATCCATGTACACGTCATCCATGTACACGTC-3') primers by PCR (2.2.1). This construct was then used in luciferase reporter assays in which HT1080 cells were seeded in 12 well culture dishes, co-transfected with 0.3 µg of the empty pEYFP-N1 vector and the indicated TNFR1-EYFP construct along with 0.25 µg of the XBP1-RE luciferase reporter construct, and 0.05 µg of the pG4.32[hRluc/TK] vector (2.3.3 and 2.1.2). After 24 h incubation at 37°C in 5% CO_2 firefly and *Renilla* luciferase activities were measured, and XBP1 induction was determined as described above (5.2.3.1).

5.2.6 Analysis of association

5.2.6.1 Fluorescence resonance energy transfer

Fluorescence resonance energy transfer (FRET) analysis was performed by flow cytometry as described by Chan *et al.* 2000 (Chan *et al.*, 2000). HEK 293T cells were seeded and co-transfected (2.3.3) 24 h later with equal amounts of the indicated ECFP and EYFP fusion protein constructs. Following a further 24 h incubation at 37°C in 5% CO_2 cells were harvested and ECFP signal was analysed by flow cytometry by excitation with a 405 nm laser and collection in a channel with a 450/40 filter, and EYFP signal was analysed by excitation at 488 nm and collection in a channel with a 529/24 filter. Finally, FRET signal was analysed by excitation at 405 nm and collection of emission in a channel with a 529/24 filter. FRET signal was analysed in 2 x 10^4 in cells within a live, $ECFP^+EYFP^+$ cell gate. Background FRET signal from non-interacting proteins was determined as that detected in cells co-expressing FLTNFR1-ECFP and FAS180-EYFP; signal in the FRET channel (excitation at 405 nm, emission at 529/24 nm) above this background level was considered to be evidence of association between ECFP and EYFP fusion proteins.

5.2.6.2 Bioluminescence resonance energy transfer

FLTNFR1 and Δ6TNFR1 C-terminal Rluc and GFP^2 fusion protein constructs were generated by cloning in-frame into the pRluc-N3 and $pGFP^2$-N3 vectors (both BioSignal Packard), respectively (2.1.2). Inserts were amplified by PCR (2.2.1) from TNFR1-EYFP cDNA constructs using the primers in Table 5.2, to incorporate *KpnI* and *BamHI* restriction sites at the 5' and 3' ends of the insert for cloning (2.1.1).

Name	*Sequence*
TNFR1_BRET_F	5'-ATGGTACCGCCACCATGGGCCTCTCCACCGTGCCTGACC-3'
FL_BRET_R	5'-TGAGGATCCGTTCTGAGAAGACTGGGCGCGGGCGGGAG-3'
Δ6_BRET_R	5'-ATGGATCCGTGGTGTCGATTTCCCACAAACAATGGAGTAGAGCTTGGACTTCCACCGT-3'

Table 5.2: Primers for the generation of TNFR1 constructs for use in $BRET^2$ assays.

Bioluminescence resonance energy transfer ($BRET^2$) assays were performed and analysed as described by James *et al.* 2006 (James *et al.*, 2006). HEK 293T cells were seeded in 6 well cell culture dishes 24 h prior to transfection. For Type I $BRET^2$ assays, cells were transiently co-transfected (2.3.3) with the ratios of the indicated GFP^2 and Rluc fusion protein constructs as shown in Table 5.3, to a total amount of 1 µg DNA per well/condition. Non-transfected cells were included as a negative control, and a condition in which cells are transfected with a construct expressing hRluc fused to GFP^2 was included as a positive control for $BRET^2$. After 24 h incubation at 37°C in 5% CO_2, cell culture medium was removed, cells were washed once with 1 ml of PBS at 37°C and then harvested in 1 ml of ice-cold PBS by pipetting and transferred to 1.5 ml eppendorf tubes. Cells were pelleted by centrifugation in a microcentrifuge at 900 x *g* for 2 min at room temperature. The supernatant was discarded and pellets were resuspended at ~ 1.5 x 10^6 cells/ml in cold PBS. 100 µl aliquots were the transferred to wells of a 96-well OptiPlate™ (Perkin Elmer) and analysed for BRET signal immediately after addition of 10 µM Coelenterazine 400A (DeepBlueC™; Perkin Elmer) in a Fusion Microplate Analyser following excitation at 410±40 nm, detected using a photomultiplier tube (PMT) with 410±40 nm (RLU-*A*) and 515±15 nm (RLU-*B*) filters, voltage at 1100 V and gain at 50. Separate 100 µl aliquots of cells were then analysed for GFP^2 fluorescence by excitation at 425±10 nm and detection using a PMT with a 515±15 nm filter, 500 V and gain at 1. Finally, coelenterazine-*h* (Biotium) was added to this aliquot of cells to 10 µM and incubated for 2 min in the dark before *Renilla* luciferase

activity (luminescence) was measured with a PMT at 550V and gain 1. All BRET, fluorescence and luminescence values were the average of 3, 1 second reads.

GFP² ***construct***	***Rluc construct***
2	1
1	1
1	3
1	6
1	9
1	12
1	15
1	39

Table 5.3: Ratios of GFP^2:Rluc constructs transfected into HEK 293T cells for Type I $BRET^2$ assays. Total amount of DNA per transfection = 1 µg.

$BRET_{eff}$ was subsequently calculated by subtracting background (values obtained from non-transfected cells) dividing RLU-*A* by RLU-*B*, correcting for luciferase expression alone, and normalising to values obtained from the fused Rluc-GFP^2, so that $BRET_{eff}$ for this positive control = 1. $BRET_{eff}$ values were then plotted against the donor:acceptor ratio (GFP^2/Rluc) and the function of the BRET model for oligomers ($BRET_{eff}/BRET_{max} = 1 - 1/((1+f)^{n-1})$) that best fitted the data (ie. minimised the residuals), or the model for random interactions between non-interacting proteins was used to represent the relationship between $BRET_{eff}$ and GFP^2/Rluc for the indicated BRET pairs.

Type II $BRET^2$ assays were performed in the same way, except that cells were transfected at a constant GFP^2:Rluc ration of 12:1 and taken for analysis of BRET, fluorescence and luminescence at hourly intervals from 10 h post-transfection, to allow analysis of $BRET_{eff}$ at varying levels of

expression. $BRET_{eff}$ was calculated as above and plotted against Rluc activity (as an indicator of total BRET pair expression), and linear regression analysis of $BRET_{eff}$ vs. Rluc activity was performed.

5.2.7 Recombinant Protein Expression and Purification

Constructs in pCDM.7 encoding the extracellular domain of TNFR1 and the first CRD of the death receptor family member DR5 cloned in-frame with an upstream CD5 leader sequence and a downstream human IgG1 sequence (sTNFR1-Fc and DR5-CRD1-Fc, respectively), and the human cDNA sequence for TNF cloned in-frame with an upstream FLAG tag (DYKDDDDK) sequence (TNF-FLAG) were kind gifts of Prof. Richard Siegel with permission from Prof. Gavin Screaton (Imperial College London, UK). An equivalent Δ6TNFR1-Fc construct was generated using *KpnI* and *BamHI* restriction sites; the insert was generated from the existing the Δ6TNFR1-EYFP construct by PCR (2.2.1) using Δ6Fc_F (5'-ACTGATATCTATATACCCCTCAGGGGTTATTGG-3') and Δ6Fc_R (5'-AACCATGGAGGTGTCGATTTCCCACAAAC-3') primers.

HEK 293T cells were seeded in T175 flasks and transiently transfected (2.3.3) with Fc fusion or TNF-FLAG constructs. 24 h post transfection, cell culture medium was removed, cells were washed with 20 ml PBS at 37°C and 15 ml of GIBCO® FreeStyle™ Expression Medium (Invitrogen) supplemented with 100 U/ml Penicillin-Streptomycin Solution and 2 mM L-Glutamine was added. Cells were cultured for a further 72 h, at which point supernatant was harvested and centrifuged at 10 000 g for 30 min to remove cells and debris. Cell culture supernatant containing TNF-FLAG was aliquoted and stored at -80°C for future use in co-immunoprecipitation and SPR studies. Fc fusion proteins were purified from culture supernatant using protein A Sepharose (Sigma). Cell culture supernatant was diluted with 2 volumes of PBS, 0.5 M NaCl (pH 7.4). 0.25 g of lyophilised protein A Sepharose beads per 500 ml of diluted cell culture supernatant were swelled in PBS, 0.5M NaCl at room temperature

for 30 min. Beads were washed twice with 50 ml of PBS, 0.5M NaCl, pelleting by centrifugation at 3,450 x *g* at room temperature for 5 min. The beads were then resuspended in 3 ml of ice-cold PBS, 0.5 M NaCl, loaded into 10 ml Poly-Prep® columns (BioRad) and the diluted cell culture supernatant containing the Fc fusion protein was flowed through the column at a rate of ~ 1 ml/min at 4°C. After 3, 10 ml washes with PBS, 0.5 M NaCl bound proteins were eluted in 2 ml fractions from protein A Sepharose beads with 0.1 M citric acid, pH 3.0. The solution of eluted protein and 0.1 M citric acid was neutralised with 2.75 M Tris HCl, pH 8.5. The concentration of eluted proteins was quantified by measuring A260/280 nm with a NanoDrop spectrophotometer in triplicate, and protein quality and purity was analysed by resolving 15 µg of reduced and non-reduced proteins by 12.5% SDS-PAGE (2.2.8).

5.2.8 Co-immunoprecipitations

5.2.8.1 Using protein A Sepharose

10 µg of the indicated Fc-fusion proteins was mixed by rotation with 500 µl of cell culture supernatant containing TNF-FLAG in 1.5 ml eppendorfs for 2 h at 4°C. 0.05 g of protein A Sepharose was then added and the mixture was rotated at 4°C overnight. Tubes were centrifuged at 1,500 x *g* for 5 min to pellet the protein A Sepharose beads, the supernatant was discarded and the beads with bound proteins were washed 3 times with 1 ml of PBS, 0.5 M NaCl. Immunoprecipitated proteins were eluted by boiling samples under reducing conditions in Laemmli buffer. Eluted proteins were subsequently resolved by 12.5% SDS-PAGE (2.2.8) and bands were visualised using SimplyBlue™ SafeStain (2.2.9). Rough quantification of intensity of TNFR1-Fc and TNF-FLAG bands was performed using ImageJ software, and was used to calculate the amount of TNF-FLAG immunoprecipitated as a fraction of the TNFR1-Fc pulled out.

5.2.8.2 Using anti-FLAG-M2 agarose

60 µg of the indicated Fc-fusion proteins was receptor was mixed by rotation with 200 µl of cell culture supernatant containing TNF-FLAG in 1.5 ml eppendorfs for 2 h at 4°C. 100 µl anti-FLAG M2 agarose beads (Sigma) were then added and the mixture was rotated at 4°C overnight. anti-FLAG M2 agarose beads were then pelleted and washed, and proteins were eluted, resolved and visualised as above.

5.2.9 Cell-based TNF binding assay

HEK 293T cells were seeded and transfected (2.3.3) 24 h later with empty pEYFP-N1 vector, HA-FLTNFR1-EYFP or HA-Δ6TNFR1-EYFP constructs. At 30 h post-transfection, cells were harvested by trypsinisation (2.3.2), washed once with 200 µl PBS and permeabilised by being resuspended in 200 µl of ice-cold 70% EtOH in PBS and incubated at 4°C for 30 min. Cells were then washed twice with 200 µl PBS, 2% FBS, resuspended in PBS at 4 x 10^5 cells/ml and separated into aliquots for total anti-HA staining and assaying TNF binding. Anti-HA staining was performed as described in 4.2.5.1. For analysis of TNF binding, permeabilised cells were incubated with biotinylated recombinant human TNF (R&D Systems) at 10 µl per 1 x 10^4 cells, at 4°C for 45 min. Alexa-Fluor® 647-conjugated Streptavidin (Molecular Probes, Invitrogen) was then added at 0.1 µg/1 x 10^4 cells, cells were incubated for a further 30 min at 4°C, cells were washed twice by centrifugation at 300 x *g* for 2 min at 4°C and resuspension in 200 µl of PBS, 2% FBS, and cells were finally resuspended in 200 µl of PBS, 2% FBS and analysed by flow cytometry on a FACS-Calibur.

5.2.10 Surface Plasmon Resonance

Surface Plasmon resonance spectroscopy was performed using the Biacore T100 system (GE), at 25°C. Anti-FLAG M2 monoclonal antibody (Sigma; 10 µg/ml in 10 mM sodium acetate, pH 5.0) was amine-coupled to a CM-5 chip and unreacted carboxymethyl sites were capped thereafter using 1 M

ethanolamine HCl pH 8.0. TNF-FLAG was directly immobilised on anti-FLAG-coated chips from tissue culture supernatant. Experiments were carried out using serial dilutions of the indicated purified Fc-fusion proteins in HEPES-EP (10 mM HEPES pH 7.4, 150 mM NaCl, 3.4 mM EDTA, 0.005% Tween 20). Between experiments, anti-FLAG surfaces were regenerated with a 30 s pulse of 10 mM glycine-HCl pH 2.0. Receptors were passed over the sensor ship at the indicated concentrations at a constant flow rate of 60 µl/min for 1 min, and dissociation was measured over 10 min. After subtraction of blank bulk refraction, binding curves were analysed using Biacore T100 Evaluation software to obtain fittings of the data and determine dissociation constants (K_d), assuming 1:1 binding.

5.2.11 Constructs and concentrated cell culture supernatants for use in neutralisation assays

The HA-DR5.CRD1-EYFP construct was generated by PCR (2.2.1) using the DR5.CRD1-Fc construct as a template and the primers indicated in Table 5.4. The HA-sTNFR1-EYFP construct was generated by PCR (2.2.1) using the sTNFR1-Fc construct to yield the extracellular portion of TNFR1, minus the 21 amino acid signal peptide using the primers indicated in Table 5.4. Both inserts integrated *XhoI* and *KpnI* restriction enzyme sites at 5' and 3' ends, respectively. These sites were then used to clone the insert (2.1.1) in-frame with upstream TNFR2 leader-HA and downstream EYFP sequences into the TNFR2 leader-HA-EYFP vector (2.1.2).

Name	***Sequence***
HAsTNFR1_F	5'-ATCTCGAGATATACCCCTCAGGGGTTATTGG-3'
HAsTNFR1_R	5'-ATGGTACCGTGCCTGAGTCCTCAGTGC-3'
HADR5_F	5'-ATCTCGAGCCCCAACAAGACCTAGCTC-3'
HADR5_F	5'-ATGGTACCCCTGATTCTTTGTGGACACATTCG-3'

Table 5.4: Primers for the generation of constructs for analysis of soluble receptor expression.

Concentrated cell culture supernatants containing control or putative TNF-neutralising species were prepared for use in neutralisation assays as follows. HEK 293T cells were seeded in cell culture vessels and transfected (2.3.3) 24 h later with the appropriate construct. At 24 h post-transfection cell culture medium was removed, cells were washed with PBS warmed to 37°C and then cultured for a further 72 h in FreeStyle™ Expression Medium. Cell culture supernatants were then centrifuged at 10 000 g for 30 min to remove cells and debris before being concentrated 45 X using Amicon Ultra-15 Centrifugal Filter Units (Ultracel-10 membrane; Millipore) by centrifugation at 4000 x g at 4°C. Protein concentration was determined by BioRad Protein Assay (BioRad) as described in 2.2.10.

5.2.12 Comparison of HA-tagged protein expression by anti-HA ELISA

60 µl of concentrated supernatants from cells expressing HA-sTNFR1-EYFP, HA-Δ6TNFR1-EYFP and HA-DR5.CRD1-EYFP were analysed for HA by performing an anti-HA ELISA as described in 2.2.12 and 4.2.6.

5.2.13 Neutralisation assays

5 x 10^4 HEK-Blue™ TNFα/IL-1β cells were seeded per well of a 96 well plate in cell culture medium, in the presence of 25 ng/ml of TNF. The indicated amounts of purified Fc fusion proteins, or concentrated cell culture supernatants containing expressed soluble proteins were added, and the cells and proteins were incubated for 24 h at 37°C in 5% CO_2. Conditions in which TNF was not added and no Fc fusion protein/cell culture supernatant was added were included as controls. 100 µl aliquots of the SEAP 1 X QUANTI-Blue™ (Invivogen) were prepared in 96 well plates, and 20 µl of 24 h cell culture supernatant was added and mixed by pipetting. The solution was then incubated at 37°C for 15 min before the OD of samples at 655 nm was read using a Fusion Microplate Reader to determine SEAP activity. Percentage neutralisation was calculated by dividing the OD for each

sample by the average OD for cells not incubated with Fc fusion protein/cell culture supernatant, subtracting this number from 1 and multiplying by 100. Percentage neutralisation was then plotted against the amount of Fc fusion protein/cell culture supernatant added to the sample. For studies using purified Fc fusion proteins, dose-response curves were fitted to sTNFR1-Fc and Δ6TNFR1-Fc data by performing a least squares non-linear regression of log(Fc fusion protein) vs. response. Dose-response curves were then used to derive IC50 values.

5.3 Results

5.3.1 Analysis of the ability of Δ6TNFR1 to induce spontaneous apoptosis *in vitro* compared with FLTNFR1

As the frameshift caused by splicing out of exon 6 is predicted to remove the DD which is required for apoptotic and NF-κB-mediated signalling through TNFR1 (Figure 4.1), we decided to investigate the ability of Δ6TNFR1 to engage these pathways relative to FLTNFR1.

To evaluate apoptotic signalling, HEK 293T cells were transiently transduced with FLTNFR1 and Δ6TNFR1 lentivirus and analysed for cellular DNA content. During apoptosis, caspases and DNAses cleave and fragment the DNA, which is subsequently lost from the nucleus (Riccardi and Nicoletti, 2006). Cells with apoptotic nuclei can therefore be identified as those with a sub-diploid DNA content (Riccardi and Nicoletti, 2006) (Figure 5.1b). Figure 5.1a shows that approximately 50% of FLTNFR1-transduced cells were apoptotic 24 h post-transduction, more than double the amount than in those transduced with Δ6TNFR1, which was found to induce apoptosis to a similar extent as transducing cells with empty lentivirus.

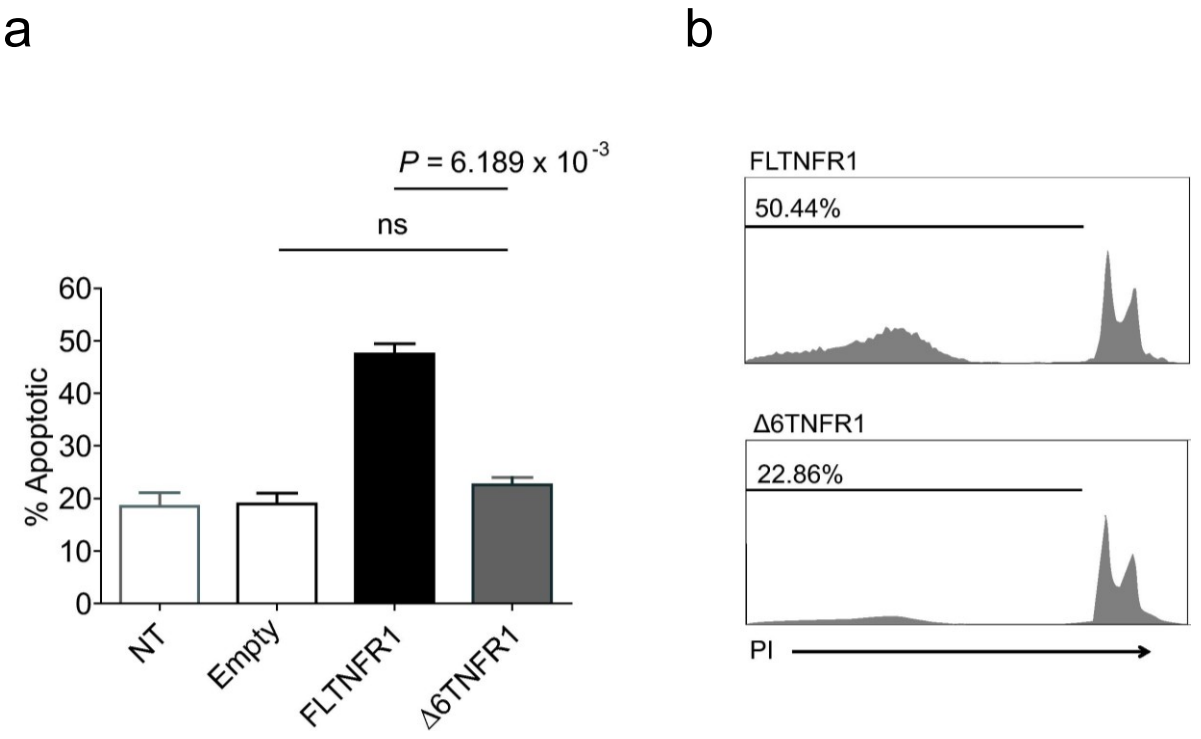


Figure 5.1: Spontaneous apoptosis of HEK 293T cells expressing TNFR1 proteins following lentiviral transduction by DNA fragmentation analysis. Cells were transduced with empty or the indicated TNFR1 lentivirus at an MOI of 50. 72 h post-transduction, cells were harvested, washed and permeabilised. Cells were subsequently stained in buffer containing 50 µg/ml PI and 1 µg/ml of RNAse A, washed and analysed by flow cytometry for DNA staining. After gating to exclude debris and doublets, cells with a sub-diploid (G_0/G_1) DNA content were deemed apoptotic. **(a)** Graph showing percentage of events that were apoptotic. **(b)** Representative histograms of PI fluorescence from FLTNFR1- and Δ6TNFR1-transduced cells. zVAD.fmk = broad-spectrum caspase inhibitor. NT = non-transduced. Error bars represent mean ± SEM; *P* value is indicated; ns = non-significant.

An early consequence of apoptotic signalling through TNFR1 is mitochondrial membrane depolarisation; caspase-8 in the DISC cleaves Bid, resulting in Bax/Bak insertion into the mitochondrial membrane and loss of mitochondrial membrane potential ($\Delta\psi_M$) (Luo *et al.*, 1998). TMRM is a potentiometric, cationic, fluorescent dye that accumulates in the negatively-charged

mitochondria of healthy cells. When $\Delta\psi_M$ collapses during apoptosis the dye becomes more evenly distributed throughout the cytoplasm of the cell, resulting in a drop in overall fluorescence intensity (Rasola and Geuna, 2001). Figure 5.2 shows that almost three times as many cells expressing FLTNFR1-ECFP were apoptotic ($TMRM^{low}$) as cells expressing Δ6TNFR1-ECFP; the use of TNFR1-ECFP fusion protein constructs allowed apoptosis to be assessed specifically in cells expressing the receptor without the need for compensation due to spectral overlap. Taken together, these data demonstrate that Δ6TNFR1 cannot induce spontaneous apoptosis.

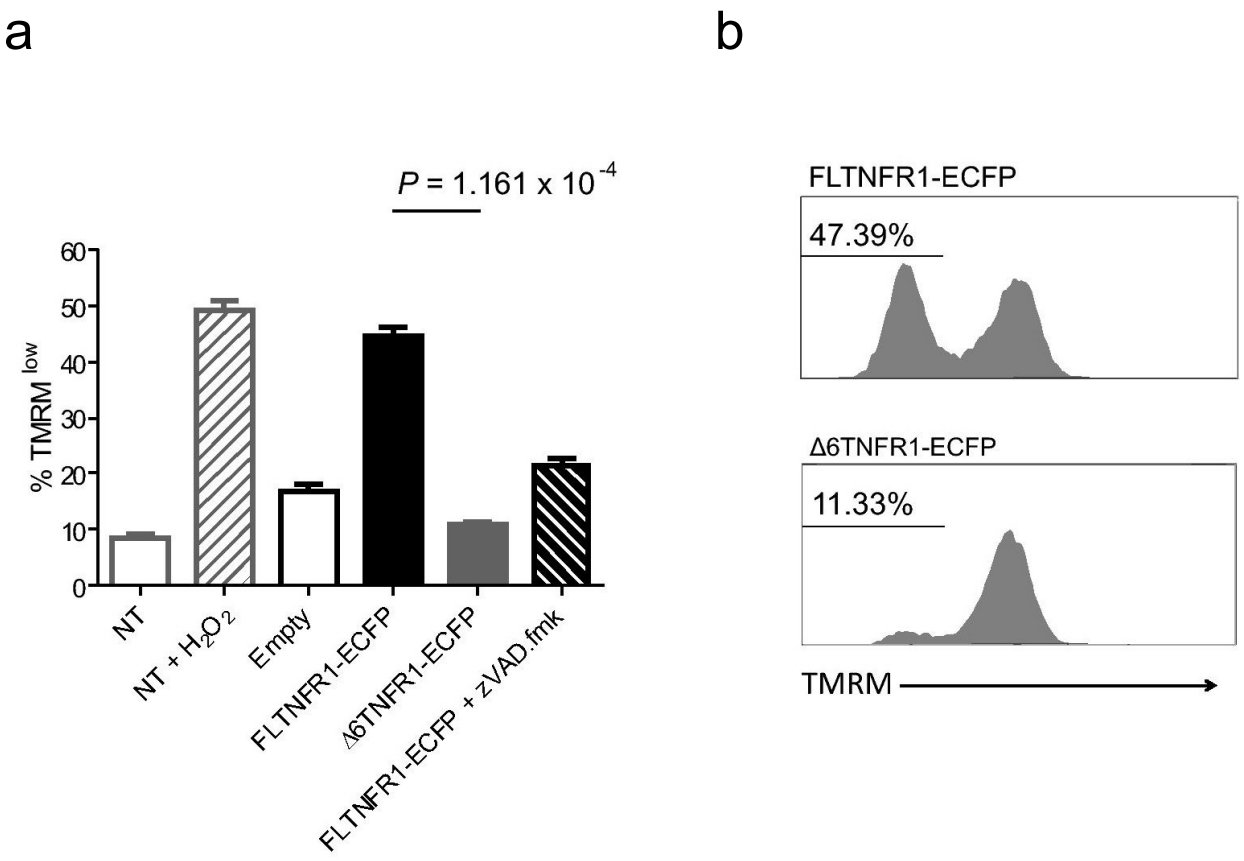


Figure 5.2: Spontaneous apoptosis of HEK 293T cells expressing TNFR1-ECFP fusion proteins by analysis of mitochondrial integrity. HeLa cells were transfected with the empty pECFP-N1 vector or the indicated TNFR1-ECFP construct. At 18 h post-transfection, mitochondrial membrane potentials ($\Delta\psi_M$) were analysed by staining cells with the mitochondrion-selective probe

tetramethylrhodamine methyl ester (TMRM) (Gross *et al.*, 1999; Rasola and Geuna, 2001). Cells were subsequently washed and the TMRM signal was analysed in $ECFP^+$ cells (except for non-transfected (NT) cells) by flow cytometry. As positive and negative controls for apoptosis, non-transfected cells were incubated with 5 mM H_2O_2 and 50 µM of the pan caspase inhibitor zVAD.fmk respectively (Garcia-Calvo *et al.*, 1998; Rasola and Geuna, 2001). **(a)** Graph showing percentage of events that were apoptotic ($TMRM^{low}$). **(b)** Representative histograms of TMRM fluorescence from cells expressing FLTNFR1-ECFP and Δ6TNFR1-ECFP. Error bars represent mean ± SEM; *P* value is indicated.

5.3.2 Analysis of the ability of Δ6TNFR1 to induce spontaneous NF-κB-mediated signalling *in vitro* compared with FLTNFR1

To investigate NF-κB-mediated signalling, HEK 293T cells were transiently co-transfected with either FLTNFR1-EYFP or Δ6TNFR1-EYFP along with firefly luciferase under the control of an NF-κB response element, and *Renilla* luciferase under the control of the minimal thymidine kinase (TK) promoter. NF-κB induction was assessed by measuring firefly luciferase activity, normalised to *Renilla* luciferase to control for transfection efficiency and the viability of transfected cells. FLTNFR1-EYFP transfected cells upregulated NF-κB significantly more than those transfected with Δ6TNFR1-EYFP (*P* = <0.0001), which had NF-κB/RLTK values that were not significantly different to those from cells transfected with the empty EYFP vector (*P* = 0.8209; Figure 5.3a). This same pattern was observed when the assay was performed in the HT1080 cell line (Figure 5.3b). To ensure that the EYFP tag was not interfering with the NF-κB signalling capacity of either FLTNFR1 or Δ6TNFR1 control experiments were performed in which cells were transduced with TNFR1 lentiviruses (Figure 5.4a), and in a separate assay NF-κB/RLTK values were compared between cells transiently transfected with untagged versus EYFP-tagged receptors (Figure 5.4b).

a b

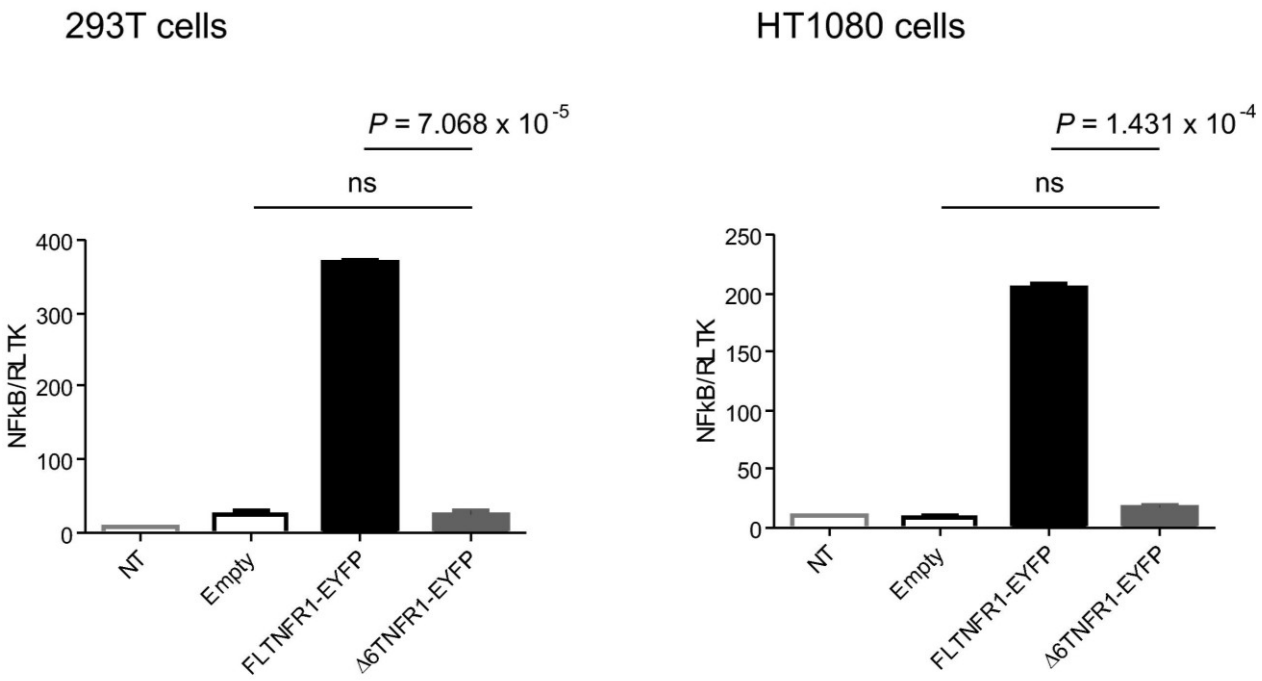


Figure 5.3: Analysis of spontaneous NF-κB induction signaling in cells expressing FLTNFR1-EYFP and Δ6TNFR1-EYFP. **(a)** HEK 293T cells or **(b)** HT1080 cells were analysed for firefly luciferase NF-κB reporter activity 24 h after co-transfection with the indicated TNFR1-EYFP construct or empty pEYFP-N1 vector. Firefly luciferase activity was normalised to *Renilla* luciferase (RLTK), a transfection efficiency and viability control. NT = non-transfected. Error bars represent mean ± SEM; *P* values are indicated; ns = non-significant.

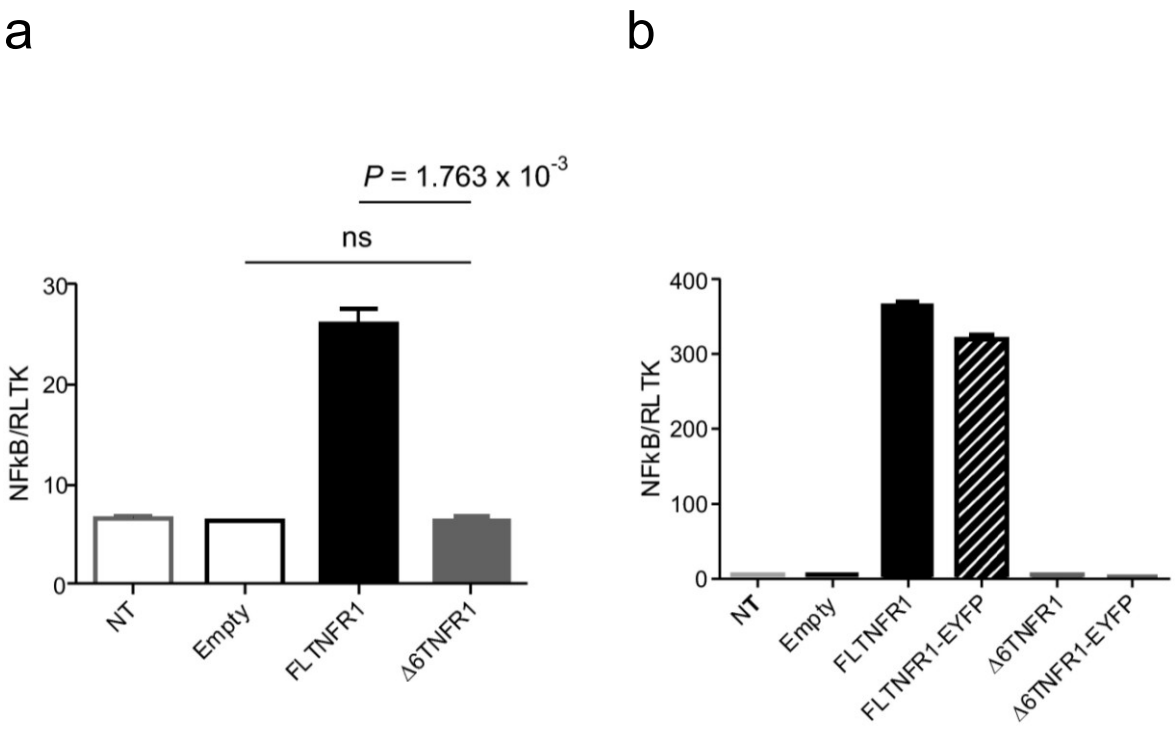


Figure 5.4: Analysis of spontaneous NF-κB induction signaling in cells expressing FLTNFR1 and Δ6TNFR1 compared with EYFP fusion proteins. **(a)** HEK 293T cells were transduced with empty lentivirus (Empty) or the indicated TNFR1 lentivirus, transfected at 72 h post-transduction with NF-κB reporter and RLTK constructs and analysed for reporter activities 24 h later. **(b)** HEK 293T cells were analysed for firefly luciferase NF-κB reporter activity 24 h after transient co-transfection with the indicated TNFR1 or TNFR1-EYFP construct, or empty pEYFP-N1 vector. Firefly luciferase activity was normalised to *Renilla* luciferase (RLTK). NT = non-transfected/non-transduced. Error bars represent mean ± SEM; *P* value is indicated; ns = non-significant.

Spontaneous NF-κB in HEK 293T cells has previously been shown to result in the upregulation of IL-8, and so cell culture supernatants of cells transduced with FLTNFR1 and Δ6TNFR1 lentivirus were analysed for this proinflammatory chemokine (Figure 5.5). Cells expressing FLTNFR1 were shown to have secreted much more IL-8 than Δ6TNFR1-transduced cells (p = <0.0001), which had secreted

similar levels to those transduced with empty lentivirus (p = 0.6516). Together, these results demonstrate that, as expected, Δ6TNFR1 is unable engage spontaneous NF-κB-mediated signalling.

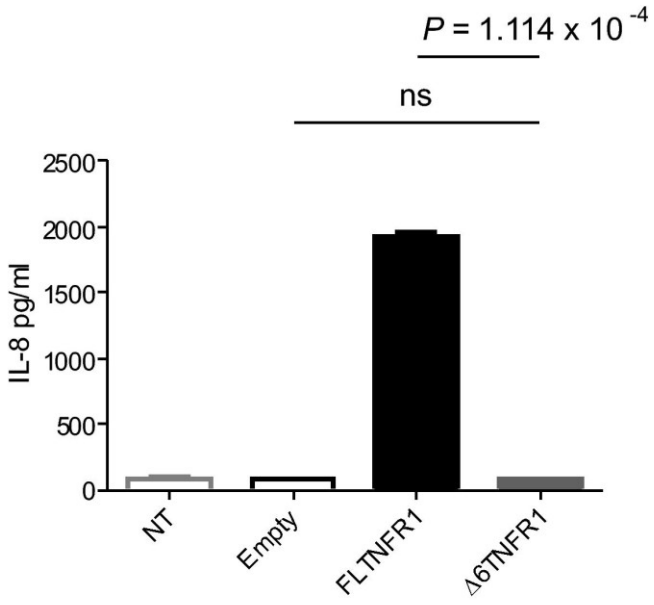


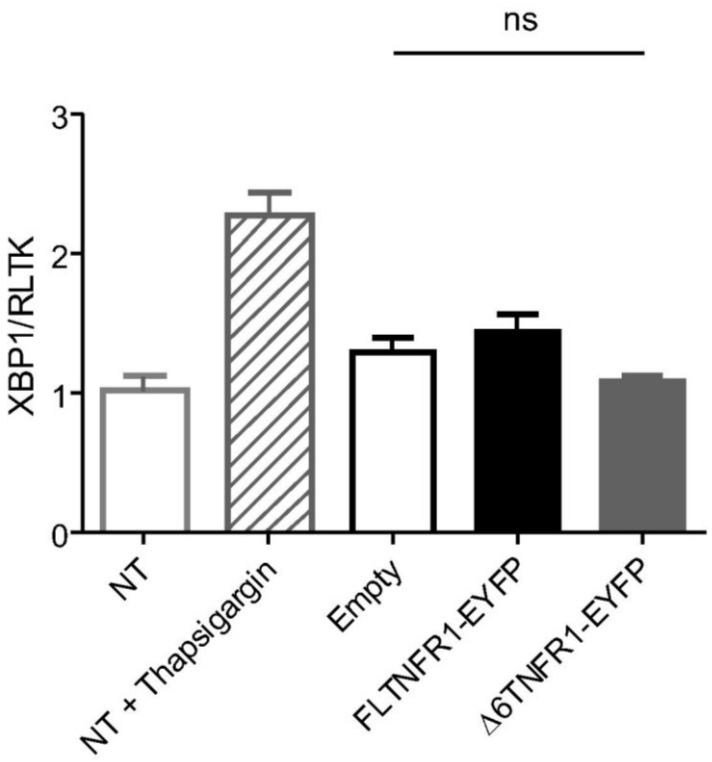
Figure 5.5: Analysis of IL-8 levels in cell culture supernatant of TNFR1-transduced cells. IL-8 levels were detected by sandwich ELISA in 72 h cell culture supernatants of cells transduced with the indicated TNFR1 lentivirus or empty lentivirus. NT = non-transduced. Error bars represent mean ± SEM; *P* value is indicated; ns = non-significant.

5.3.3 Analysis of the ability of Δ6TNFR1 and FLTFNR1 to spontaneously induce ER stress responses *in vitro*

The lack of any NF-κB signalling above background levels also suggested that Δ6TNFR1 does not exert any of its functional consequences through induction of the ER overload response (EOR) which engages NF-κB signalling as the result of the accumulation of proteins in the ER (Pahl and Baeuerle, 1997). As significant levels of Δ6TNFR1 were found to be localised to the ER by confocal microscopy

(Figure 4.8), accumulation of this potentially misfolded mutant protein might have invoked this or other ER stress responses, such as the unfolded protein response (UPR) (Schroder and Kaufman, 2005). Induction of the regulator chaperone for protein folding XBP1 was analysed in TNFR1-EYFP transfected HT1080 cells using an XBP1 luciferase reporter construct (Lee *et al.*, 2003). Thapsigargin, a constitutive inducer of the UPR was included as a positive control. XBP1 luciferase reporter activity was found to be comparable across cells transfected with all constructs (Figure 5.6a). Furthermore, induction of the UPR-associated splice isoform of XBP1 was observed only in Thapsigargin-treated cells (Figure 5.6b) (Samali *et al.*, 2010). Together, these results demonstrate that Δ6TNFR1 does not invoke ER stress responses.

a



b

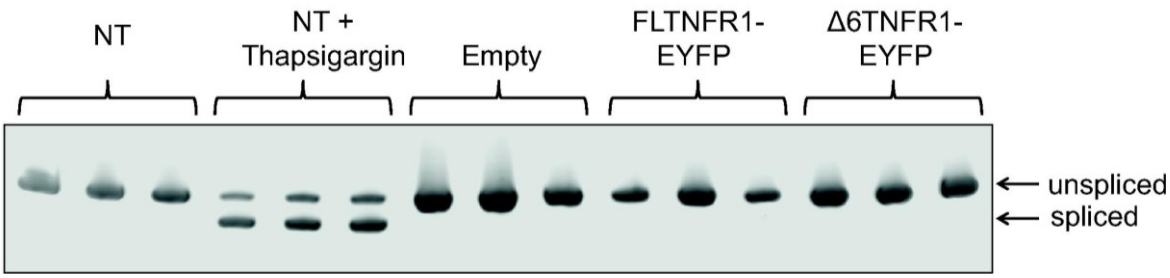


Figure 5.6: Analysis of the unfolded protein response in cells expressing FLTNFR1 and Δ6TNFR1. (**a**) HT1080 cells were co-transfected with an XBP1 firefly luciferase reporter construct, RLTK and the indicated TNFR1-EYFP constructs or pEYFP-N1. 24 h later cells were analysed for firefly luciferase activity, which was then normalised to *Renilla* luciferase. (**b**) HT1080 cells were transfected with the indicated TNFR1-EYFP constructs or pEYFP-N1 and 24 h later RNA was isolated, cDNA was made and

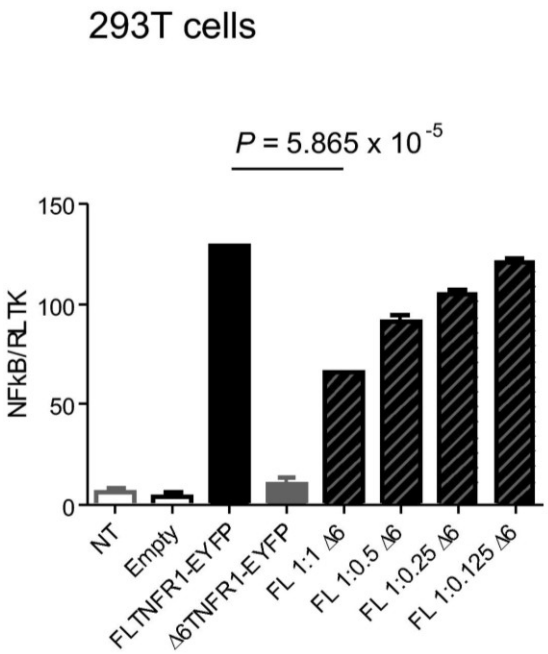
XBP1 splicing was analysed by PCR with primers flanking the alternatively spliced 26 bp region. Bands corresponding to spliced and unspliced XBP1 mRNA are indicated. Thapsigargin = positive inducer of UPR. NT = non-transfected. Error bars represent mean ± SEM; ns = non-significant.

5.3.4 Analysis of the capacity of Δ6TNFR1 to interact and interfere with FLTFNR1 and signalling *in vitro*

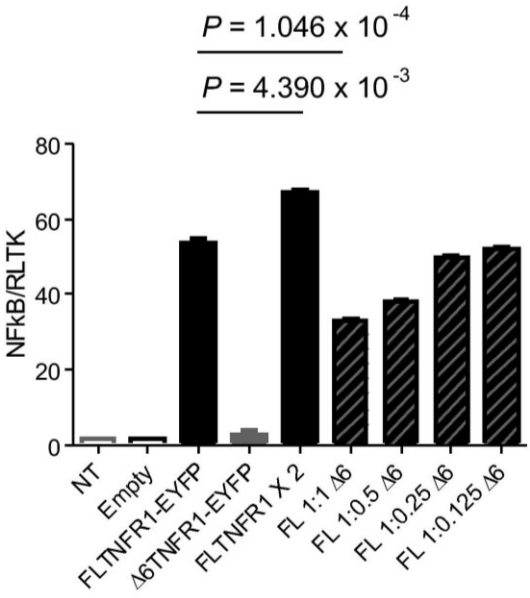
Having convincingly demonstrated Δ6TNFR1 to be unable to engage any signalling pathways associated with TNFR1, and seeing as it retains the PLAD of the full-length receptor we investigated if it could potentially associate with FLTNFR1 to form functionally compromised receptor complexes (Chan *et al.*, 2000). The results of NF-κB reporter assays in which the Δ6TNFR1-ECFP construct was titrated into transfections along with constant amounts of FLTNFR1-ECFP construct DNA in HEK 293T and HT1080 cells are shown in Figures 5.7a and 5.7b, respectively. Although these studies seemed to indicate that Δ6TNFR1 had the capacity to inhibit FLTNFR1 signalling, subsequent studies found the pattern of decreased NF-κB induction to also be the case when a construct encoding a control protein known not to interact with FLTNFR1 – the extracellular portion of FAS (FAS180) – was titrated into transfections (Figure 5.7c) (Chan *et al.*, 2000; Lobito *et al.*, 2006). Figure 5.7d shows that titrating in unlabelled Δ6TNFR1 with FLTNFR1-ECFP resulted in a decrease in ECFP fluorescence that mirrored the reduction in NF-κB induction. This suggested that rather than inhibition of signalling function of the FLTNFR1 protein, simply less FLTNFR1 protein is made in the presence of cDNA encoding another protein. In an attempt to reduce the total amount of protein being made to levels such that constant levels of FLTNFR1 could be maintained and allowing additional titration of Δ6TNFR1, an experiment was performed in which cells were transfected with a constant amount of total DNA and decreasing amounts of the FLTNFR1-ECFP construct DNA. Whilst the number of ECFP positive cells gradually decreased, the level of fluorescence from ECFP-positive cells remained consistent, suggesting similar levels of protein expression (Figure 5.7e). Finally, a titration NF-κB

reporter experiment was performed using one third of the amount of protein encoding cDNA in HT1080 cells, which are not transformed with the SV40 T antigen and so express receptor proteins at much more physiological levels (Figure 5.7f). The same pattern of decreased NF-κB induction with increasing Δ6TNFR1-ECFP construct DNA was observed.

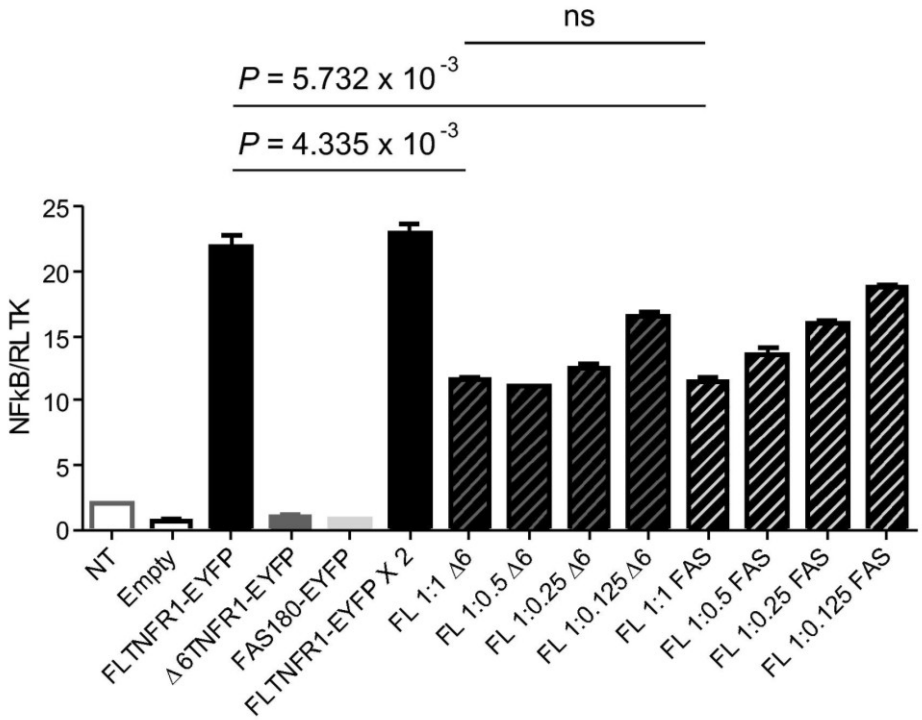
a


293T cells
P = 5.865 x 10 -5
NFkB/RLTK
150
100
50
0
NT
Empty
FLTNFR1-EYFP
Δ6TNFR1-EYFP
FL 1:1 Δ6
FL 1:0.5 Δ6
FL 1:0.25 Δ6
FL 1:0.125 Δ6

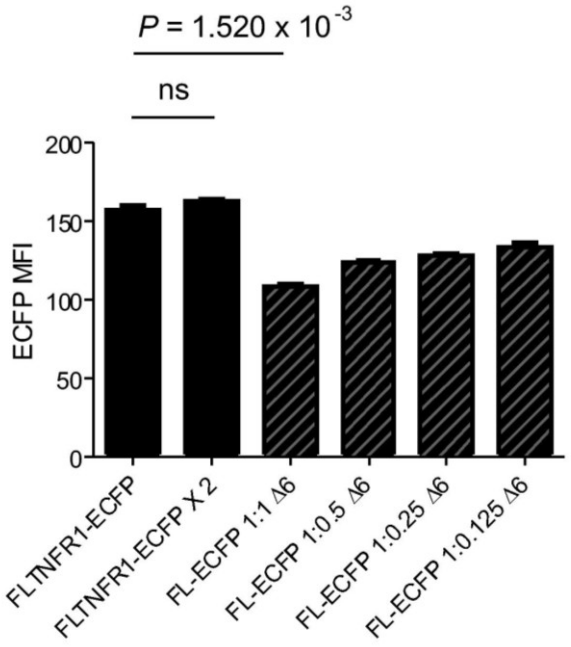
b


HT1080 cells
P = 1.046 x 10 -4
P = 4.390 x 10 -3
NFkB/RLTK
80
60
40
20
0
NT
Empty
FLTNFR1-EYFP
Δ6TNFR1-EYFP
FLTNFR1 X 2
FL 1:1 Δ6
FL 1:0.5 Δ6
FL 1:0.25 Δ6
FL 1:0.125 Δ6

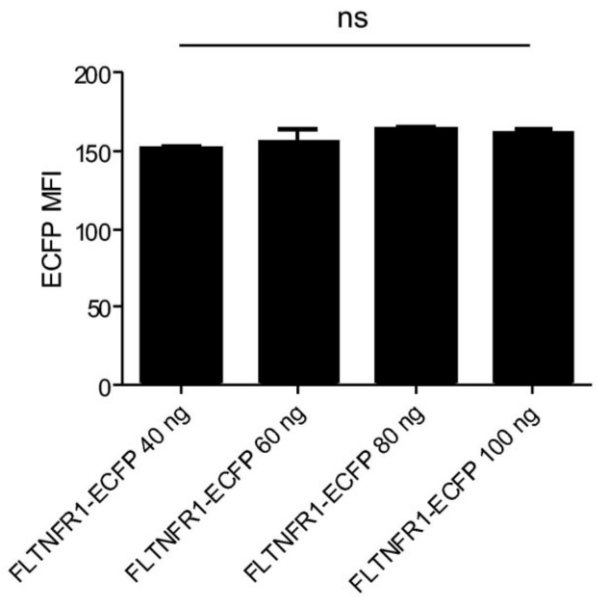
c


ns
P = 5.732 x 10 -3
P = 4.335 x 10 -3
NFkB/RLTK
25
20
15
10
5
0
NT
Empty
FLTNFR1-EYFP
Δ6TNFR1-EYFP
FAS180-EYFP
FLTNFR1-EYFP X 2
FL 1:1 Δ6
FL 1:0.5 Δ6
FL 1:0.25 Δ6
FL 1:0.125 Δ6
FL 1:1 FAS
FL 1:0.5 FAS
FL 1:0.25 FAS
FL 1:0.125 FAS

d


P = 1.520 x 10-3
ns
ECFP MFI
200
150
100
50
0
FLTNFR1-ECFP
FLTNFR1-ECFP X 2
FL-ECFP 1:1 Δ6
FL-ECFP 1:0.5 Δ6
FL-ECFP 1:0.25 Δ6
FL-ECFP 1:0.125 Δ6

e


ns
ECFP MFI
200
150
100
50
0
FLTNFR1-ECFP 40 ng
FLTNFR1-ECFP 60 ng
FLTNFR1-ECFP 80 ng
FLTNFR1-ECFP 100 ng

f

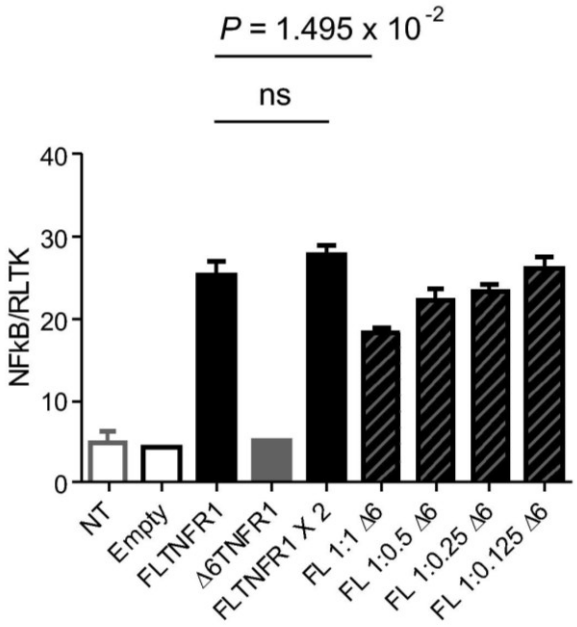

P = 1.495 x 10-2
ns
NFkB/RLTK
40
30
20
10
0
NT
Empty
FLTNFR1
Δ6TNFR1
FLTNFR1 X 2
FL 1:1 Δ6
FL 1:0.5 Δ6
FL 1:0.25 Δ6
FL 1:0.125 Δ6

Figure 5.7: Analysis of spontaneous NF-κB induction signaling in cells co-expressing FLTNFR1-EYFP and Δ6TNFR1-EYFP. **(a & c)** HEK 293T cells or **(b, c & f)** HT1080 cells were co-transfected with the indicated ratios of FLTNFR1-EYFP to Δ6TNFR1-EYFP, or **(c)** FLTNFR1-EYFP to FAS180-EYFP constructs. Cells were analysed for firefly luciferase NF-κB reporter activity 24 h after co-transfection. Firefly luciferase activity was normalised to *Renilla* luciferase (RLTK). **(d & e)** HEK 293T cells were transiently co-transfected with the indicated amounts of **(d)** FLTNFR1-ECFP and Δ6TNFR1 FAS180 constructs, or **(e)** FLTNFR1-ECFP construct and analysed for ECFP expression by flow cytometry after 48 h. For all experiments pcDNA3.1 was used to maintain a constant total level of DNA being transfected. NT = non-transfected. Error bars represent mean ± SEM; *P* values are indicated; ns = non-significant.

To confirm that Δ6TNFR1 doesn't interact with FLTNFR1 to form mixed receptor complexes with altered functional properties, we investigated the ability of Δ6TNFR1 to associate with FLTNFR1, and to self-associate using fluorescence resonance energy transfer (FRET) and bioluminescence resonance energy transfer (BRET) techniques. C-terminal ECFP and EYFP fusions of FLTNFR1, Δ6TNFR1 and FAS180 were made and co-transfected in various combinations into HEK 293T cells, and FRET signal (excitation at 405 nm, emission at 529 nm) was analysed in CFP^+YFP^+ double positive cells by flow cytometry (Figure 5.8). FAS180 has previously been demonstrated not to associate with FLTNFR1, and has been used as a negative control in FRET analysis of TNFR1 association by flow cytometry (Lobito *et al.*, 2006). We therefore used FLTNFR1-ECFP + FAS180-EYFP co-transfected cells to define background FRET from non-interacting proteins (Figure 5.8, upper right panel); signal in the FRET channel above this intensity was taken to be evidence of association. Whilst FLTNFR1 displayed strong self-association (49.40-50.76% FRET-positive), in agreement with previous studies of this kind (Chan *et al.*, 2000; Lobito *et al.*, 2006), Δ6TNFR1 was found neither to associate with FLTNFR1 (0.46-0.57%) nor with itself (0.07-0.10%).

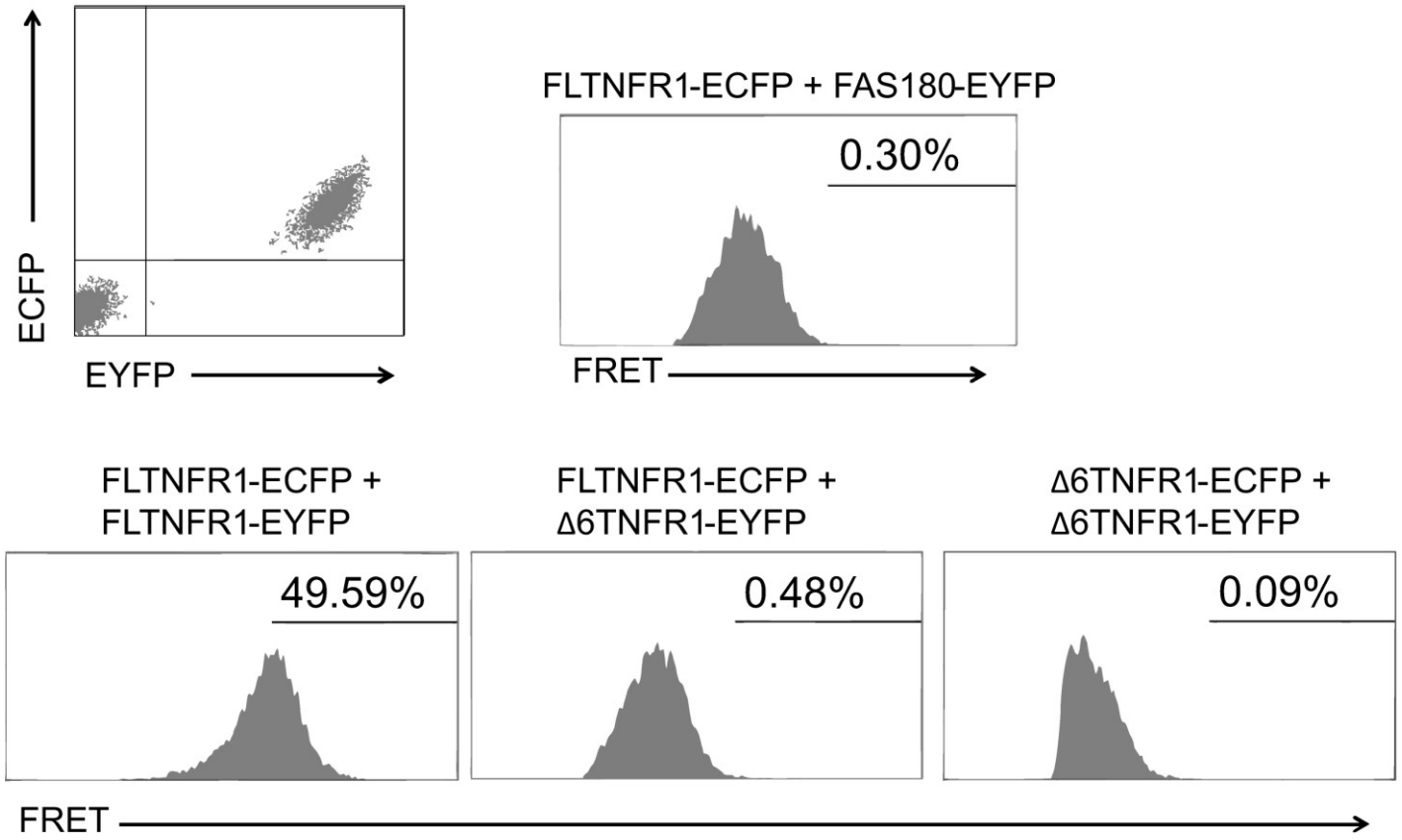


Figure 5.8: Analysis of FLTNFR1 and Δ6TNFR1 associations by FRET. HEK 293T cells were co-transfected with the indicated TNFR1-ECFP and –EYFP, or FAS180-EYFP fusion protein constructs. ECFP, EYFP Double-positive cells **(top left panel)** were analysed 24 h later for FRET by flow cytometry. FRET signals from FLTNFR1-ECFP + FAS180-EYFP co-transfected cells were used to define background signal arising from random interaction between non-associating proteins **(top right panel)**. Percentages of FRET-positive events are indicated. Histograms are representative of five samples for each condition.

Hetero-oligomerisation of FLTNFR1 and Δ6TNFR1 was next assessed using the more sensitive BRET^2 technique in a Type II assay. FLTNFR1-GFP^2 and Δ6TNFR1-Rluc were co-transfected into 293T cells at a constant ratio of 12:1, and harvested for analysis at hourly time points from 10 h post-transfection. At a constant acceptor/donor ratio, BRET$_{eff}$ for non-interacting proteins is dependent on the expression level; at high expression levels, random interactions will result in BRET signal, but this will fall to zero at low expression levels (James *et al.*, 2006; Kenworthy and Edidin, 1998). For oligomers, however, BRET$_{eff}$ will remain above zero even at very low levels of expression, as complexes are formed at all densities (James *et al.*, 2006; Kenworthy and Edidin, 1998). Figure 5.9 demonstrates that FLTNFR1 and Δ6TNFR1 do not associate to form hetero-oligomers.

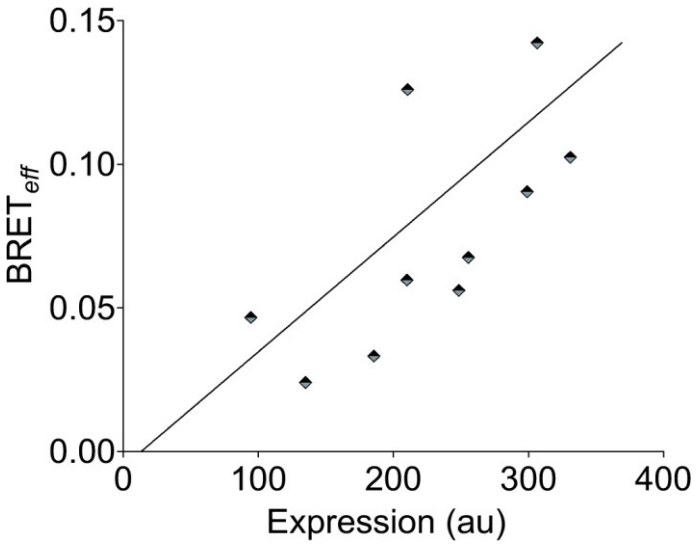


Figure 5.9: Analysis of hetero-association of FLTNFR1 with Δ6TNFR1 by Type II BRET^2. HEK 293T cells were co-transfected with FLTNFR1-GFP^2 and Δ6TNFR1-Rluc at a ratio of 12:1. GFP2 expression, luciferase activity and BRET*eff* were measured in cells taken at hourly time-points from 10 h post-transfection. au = arbitrary units.

Finally, self-association of TNFR1 proteins was analysed by $BRET^2$ in a Type I assay. C-terminal GFP^2 and Rluc TNFR1 fusion constructs were co-transfected into 293T cells at varying GFP^2: Rluc ratios and subsequently analysed for GFP^2 fluorescence, Rluc activity and BRET. For oligomers, the relative donor (Rluc) concentration is predicted to strongly influence the GFP^2/Rluc ratio, as donors self-associate, reducing BRET efficiency ($BRET_{eff}$) (James *et al.*, 2006). In this instance, the GFP^2/Rluc ratio (*f*) plotted against $BRET_{eff}$ should follow a hyperbola dependent on the stoichiometry of the oligomer (*n*); as the relative concentration of donors decreases, $BRET_{eff}$ approaches saturation (James *et al.*, 2006; Veatch and Stryer, 1977).

$$\frac{BRET_{eff}}{BRET_{max}} = 1 - \frac{1}{(1 + f)^{n-1}}$$

For non-interacting BRET pairs, $BRET_{eff}$ above a threshold is predicted to be independent of the GFP^2/Rluc ratio, as donors "experience" the same acceptor environment, as long as GFP^2/Rluc ratios are high enough to prevent competition between donors for acceptors (Fung and Stryer, 1978; James *et al.*, 2006; Kenworthy and Edidin, 1998; Wolber and Hudson, 1979). Figure 5.10 shows $BRET_{eff}$ plotted against GFP/Rluc values; the FLTNFR1 data best fitted the BRET equation for trimers (*n* = 3; solid line), and the dotted line shows the fit of Δ6TNFR1 data (for [GFP]/[Rluc] > 2) to a constant value, as predicted for random interactions between monomers. The data are consistent with FLTNFR1 forming trimeric complexes and Δ6TNFR1 existing as monomers.

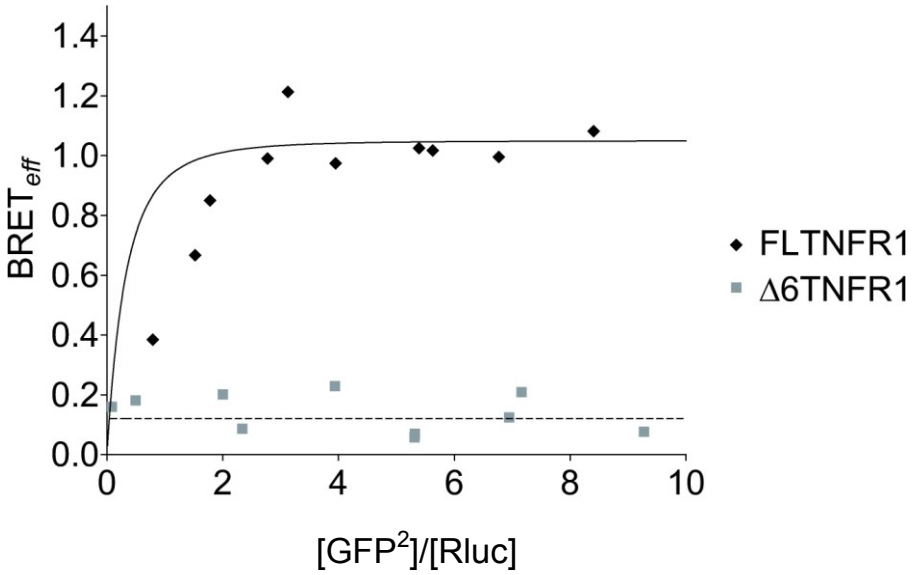


Figure 5.10: Analysis of homotypic associations of FLTNFR1 and Δ6TNFR1 by Type I BRET^2. Varying ratios of FLTNFR1-GFP^2:FLTNFR1-Rluc and Δ6TNFR1-GFP^2:Δ6TNFR1-Rluc were transfected into HEK 293T cells to analyse the self-association of FLTNFR1 and Δ6TNFR1 respectively. GFP^2 fluorescence, luciferase activity and BRET*eff* were measured at 24 h post-transfection. Data for FLTNFR1 approximate to the BRET equation for a trimer (solid line), and of Δ6TNFR1 data (for [GFP^2]/[Rluc] > 2) to a constant value, as predicted for non-interacting monomers (dotted line).

Taken together, FRET and BRET studies strongly suggest that Δ6TNFR1 is neither able to self-associate, nor associate with FLTNFR1 to form mixed receptor complexes.

5.3.5 Analysis of the capacity of Δ6TNFR1 to bind and neutralise TNF compared with TFNR1 *in vitro*

Having demonstrated that Δ6TNFR1 is a secreted protein, and in light of the fact that Δ6TNFR1 retains the ligand binding domains on the full-length protein (Figure 4.1) (Marsters *et al.*, 1992), we next investigated its ability to bind TNF. A construct in which Δ6TNFR1 was fused to human IgG1 (Δ6TNFR1-Fc) was made from a construct encoding the extracellular portion of full-length TNFR1

(sTNFR1-Fc), which was obtained along with a construct encoding a negative control Fc fusion for TNF binding, the first cysteine-rich domain of DR5 (DR5.CRD1-Fc), kindly provided by Prof. Richard Siegel (Lobito *et al.*, 2006). Recombinant proteins were expressed by transient transfection and purified from cell culture supernatant. Figure 5.11a shows a Coomassie-stained SDS polyacrylamide gel of the reduced and non-reduced products of purification. A construct encoding TNF fused to a FLAG tag (TNF-FLAG) was also obtained from our collaborators, and was similarly expressed in cell culture. Figure 5.11b shows the results of a western blot with an anti-FLAG antibody, demonstrating expression of TNF-FLAG in the cell culture supernatant.

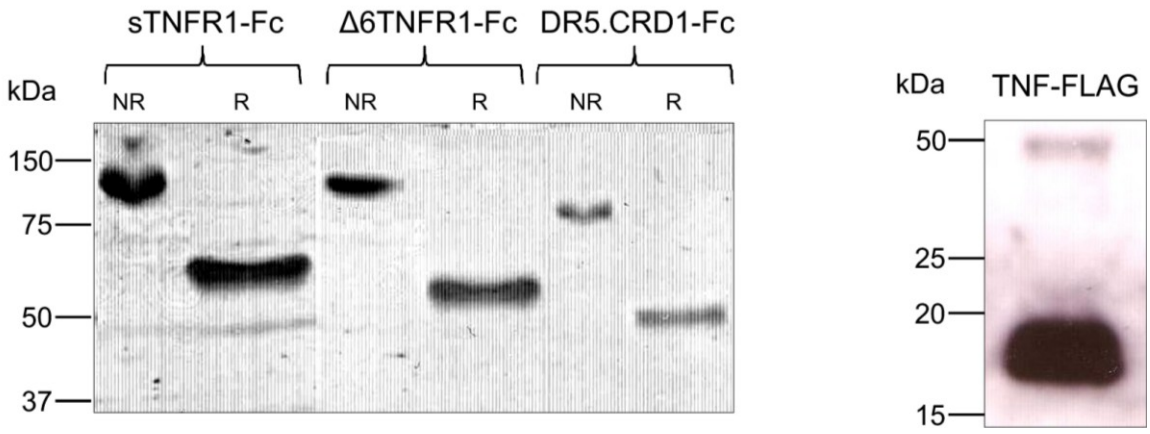
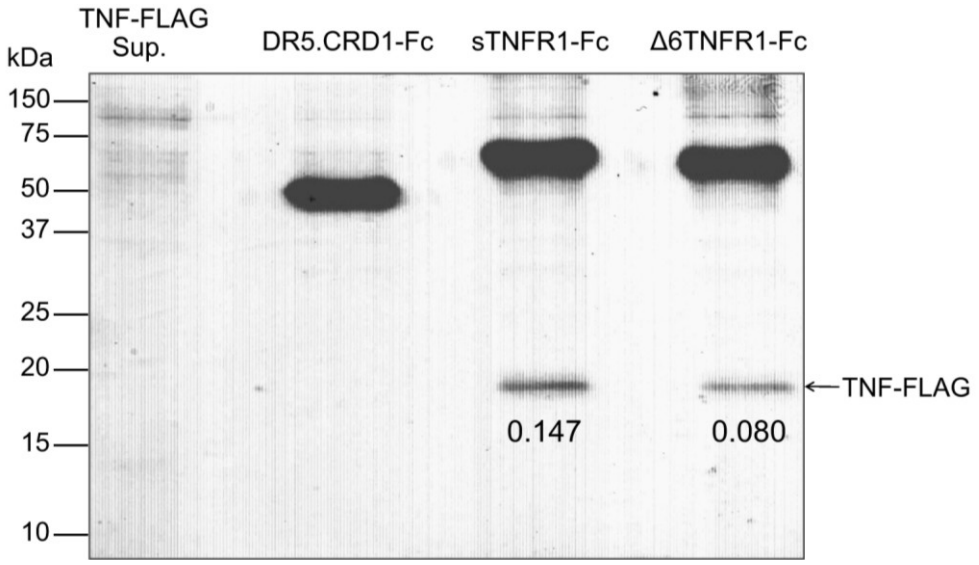


Figure 5.11: Expressed receptor and ligand proteins for use in binding analysis assays. **(a)** sTNFR1, Δ6TNFR1 and DR5.CRD1 Fc fusion proteins were expressed by transient transfection in HEK 293T cells and purified from 72 h cell culture supernatant using protein A Sepharose. 15 µg of reduced (R) and non-reduced (NR) proteins were then resolved by 12.5% SDS-PAGE and visualised using SimplyBlue™ SafeStain. **(b)** HEK 293T cells were transiently transfected with the TNF-FLAG construct and a western blot was performed on 20 µl of 72 h cell culture supernatant resolved by 12.5% SDS-PAGE, using an anti-FLAG antibody.

Immunoprecipitation experiments were performed in which the indicated Fc fusion proteins were incubated with cell culture supernatant containing TNF-FLAG, and Fc fusion protein-binding partner complexes were immunoprecipitated using protein A Sepharose. Figure 5.12a shows that a clear band at the molecular weight of TNF-FLAG (17.5 kDa) was seen in both sTNFR1-Fc and Δ6TNFR1-Fc lanes, but not in DR5.CRD1-Fc or TNF-FLAG supernatant only lanes. Approximate quantification of the relative intensity of TNF-FLAG and TNFR1-Fc bands revealed that sTNFR1-Fc was more efficient at immunoprecipitating TNF-FLAG, suggesting a higher affinity for TNF than Δ6TNFR1-Fc. A further series of experiments were performed in which protein complexes were immunoprecipitated with anti-FLAG antibody conjugated to agarose beads (Figure 5.12b). The presence of a non-specific band at ~ 50 kDa obscured the visualisation of Fc fusion proteins, potentially interfering with detection of DR5.CRD1-Fc. However, co-immunoprecipitation studies using protein A Sepharose (Figure 5.12a) and SPR analysis below (Figure 5.14) convincingly demonstrate that DR5.CRD1-Fc does not bind TNF-FLAG.

a



b

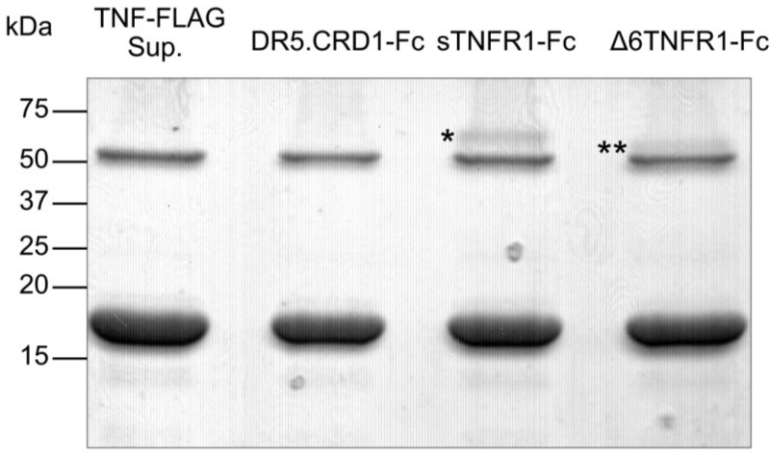
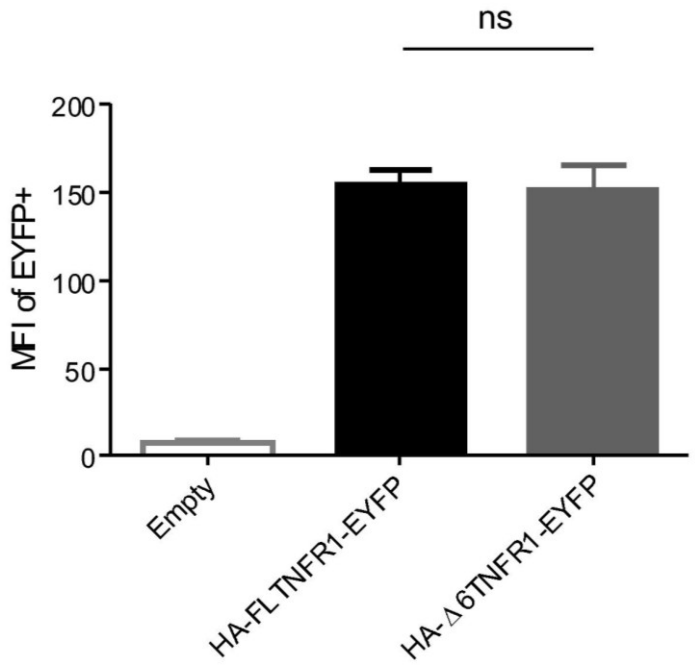


Figure 5.12: Immunoprecipitation of TNFR1-TNF complexes. The indicated purified TNFR1-Fc or DR5.CRD1-Fc fusion proteins were incubated with supernatant containing TNF-FLAG and complexes were immunoprecipitated using **(a)** protein A Sepharose or **(b)** anti-FLAG-M2 agarose beads. Immunoprecipitated proteins were subsequently eluted from beads, resolved by SDS-PAGE and visualised using SimplyBlue™ SafeStain. Quantification of TNFR1-Fc and TNF-FLAG bands in **(a)** was performed using ImageJ software; intensity of TNF-FLAG band as a proportion of TNFR1-Fc band intensity is shown. * = sTNFR1-Fc; ** = Δ6TNFR1-Fc.

To investigate binding of TNF in a different setting, cells that were transfected with HA-FLTNFR1-EYFP and HA-Δ6TNFR1-EYFP constructs were permeabilised and incubated with TNF, and analysed by flow cytometry. Figure 5.13 shows that cells expressing HA-Δ6TNFR1-EYFP bound significantly more TNF that those transfected with the empty EYFP vector. Taken together these results indicate that Δ6TNFR1 is capable of binding to TNF. Despite similar levels total levels of intracellular TNFR1 expression between HA-FLTNFR1-EYFP and HA-Δ6TNFR1-EYFP transfected cells the former bound significantly more TNF-biotin (Figure 5.13b). Furthermore, crude quantification of intensity of the

TNF-FLAG band relative to that of the sTNFR1-Fc band in Figure 5.12a suggests that whilst Δ6TNFR1 has the capacity to bind TNF, it is reduced when compared to that of the full-length protein.

a



b

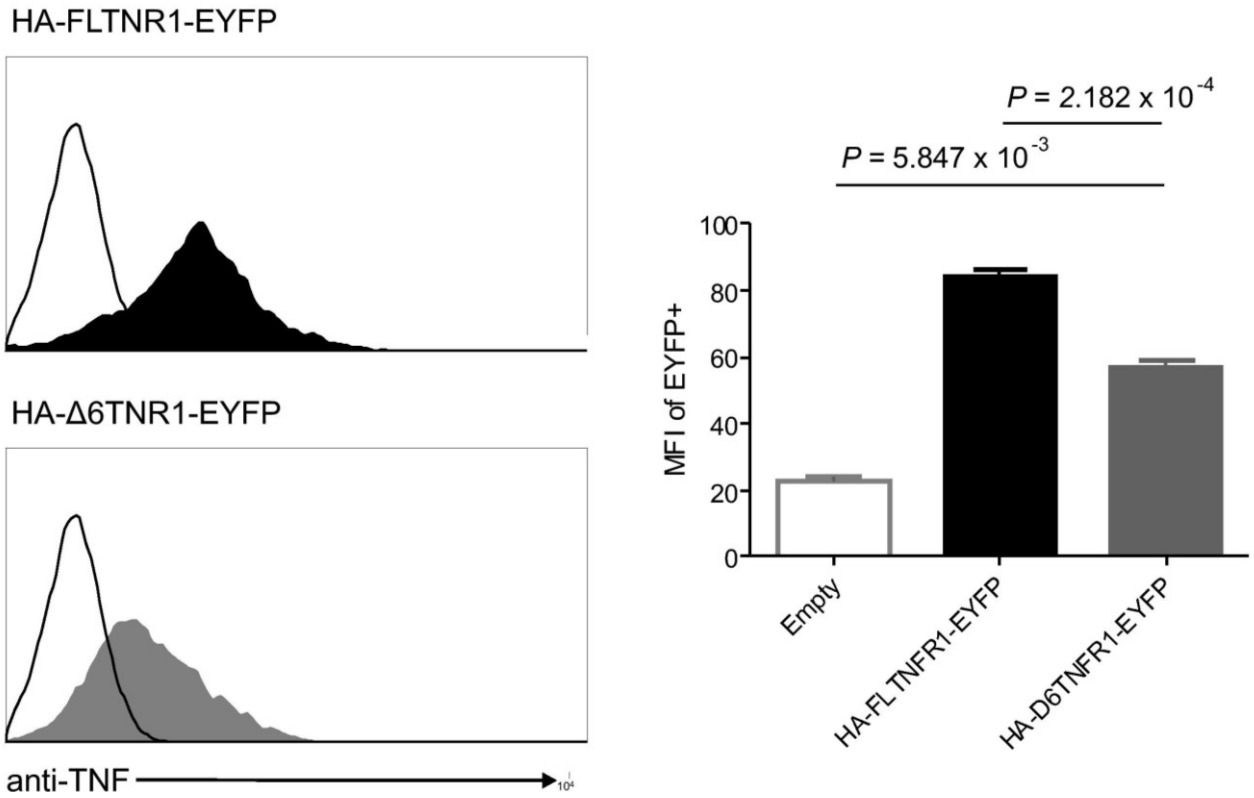


Figure 5.13: TNF binding of cells expressing HA-FLTNFR1-EYFP and HA-Δ6TNFR1-EYFP. HEK293T cells were transfected with the indicated HA-TNFR1-EYFP fusion protein constructs, harvested 48 h post-transfection and cells expressing proteins ($EYFP^+$) were analysed either for **(a)** HA-staining or **(b)** ability to bind TNF, using TNF-biotin followed by Alexa-Fluor® 647-conjugated-streptavidin, by flow cytometry. **(b, left panel)** Representative histograms of TNF binding of cells expressing the indicated HA-TNFR1-EYFP fusion proteins; **(b, right panel)** Graph of histograms of anti-TNF MFI from cells expressing the indicated HA-TNFR1-EYFP fusion proteins. Empty = EYFP vector. Error bars represent mean ± SEM; *P* values are indicated; ns = non-significant.

To investigate the comparative ability of Δ6TNFR1 to bind TNF further, Surface Plasmon Resonance (SPR) was performed. Serial dilutions of the indicated Fc fusion proteins were passed over a chip

coated with TNF and fits of dissociation curves were used to calculate dissociation constants (K_d). The affinity of Δ6TNFR1-Fc for TNF (K_d = 1.56 x 10^{-8}) was found to be approximately 20 times lower than that of sTNFR1-Fc (K_d = 7.19 x 10^{-10}; Figure 5.14), suggesting that whilst Δ6TNFR1 retains the ability to bind TNF it does so with much lower affinity than FLTNFR1.

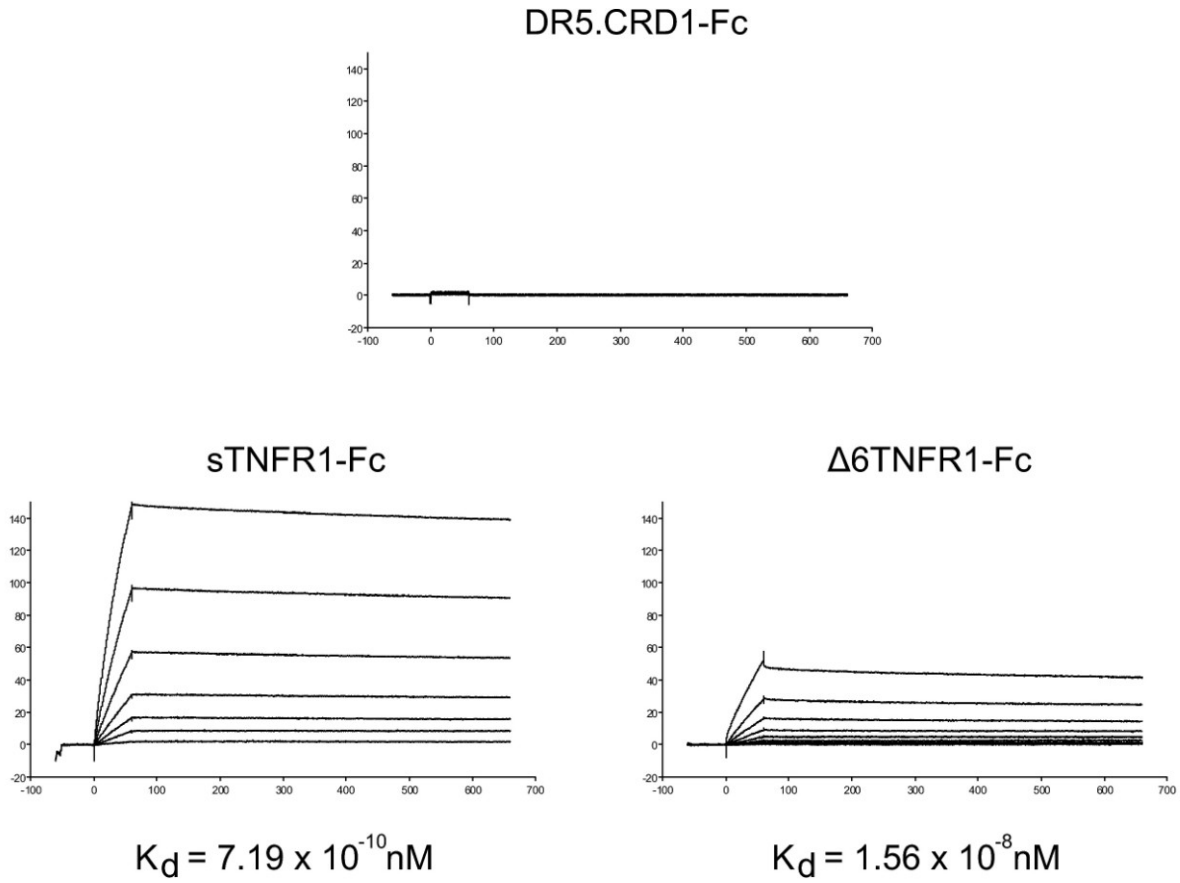
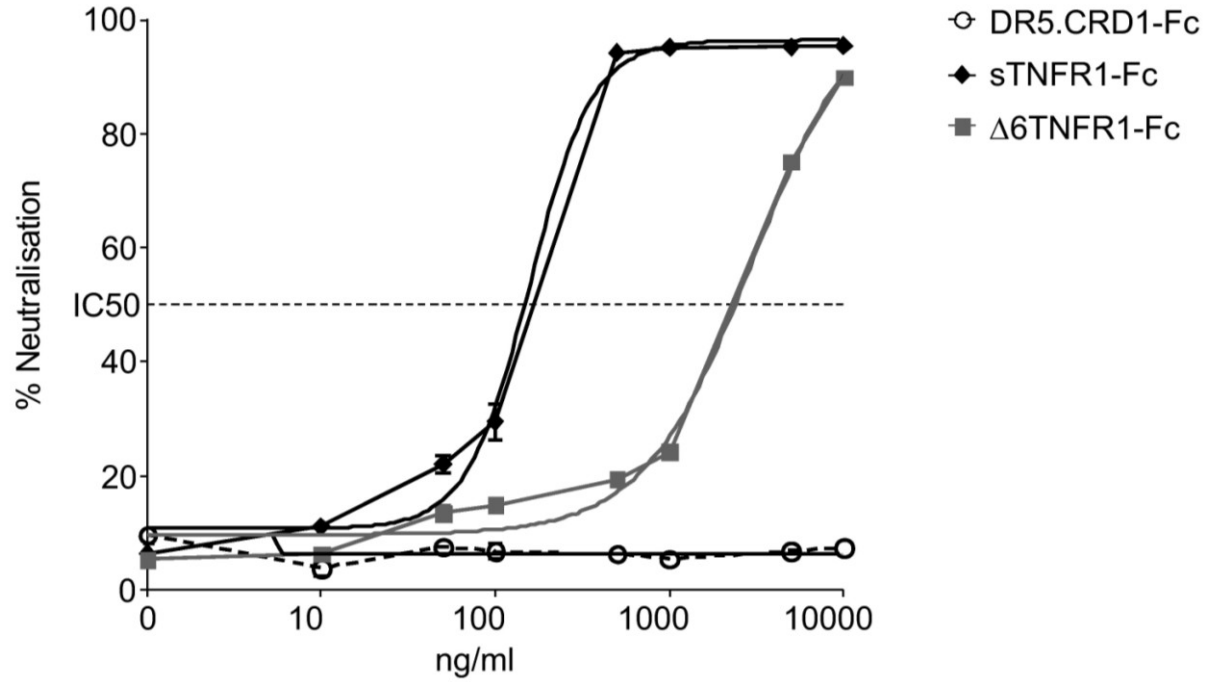


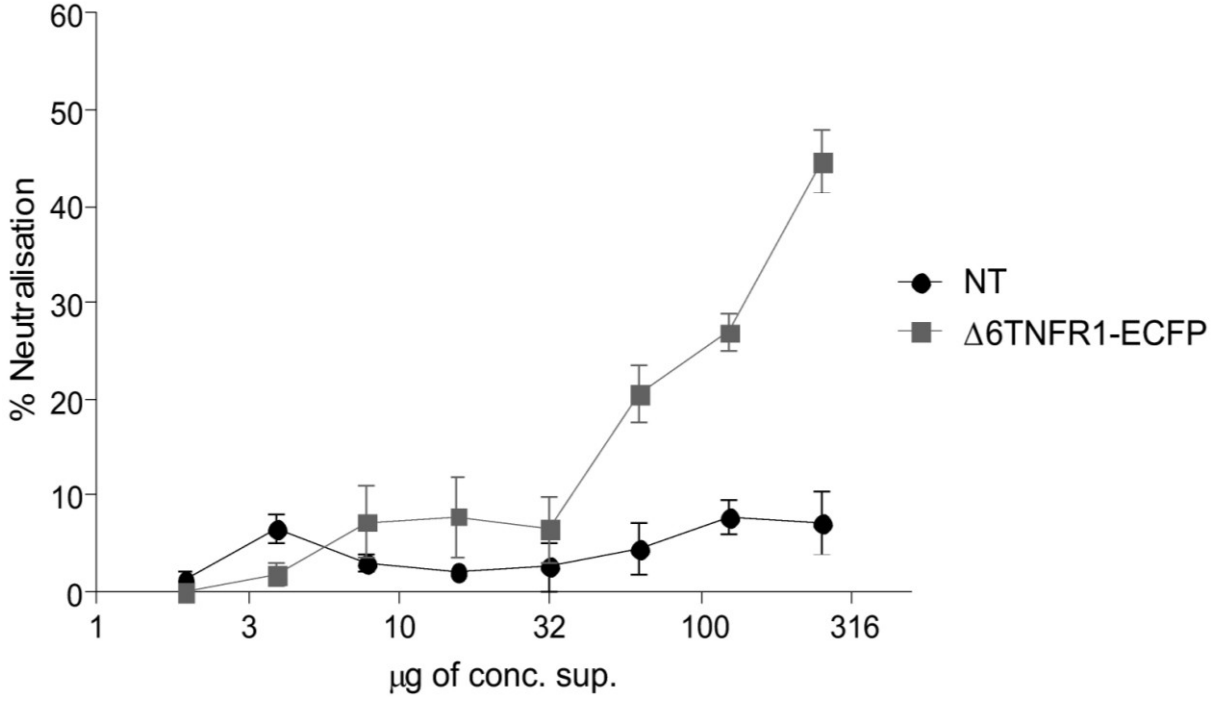
Figure 5.14: Analysis of TNFR1-Fc fusion protein binding to TNF by Surface Plasmon Resonance. Serial dilutions of the indicated purified TNFR1-Fc fusion proteins or DR5.CRD1-Fc were passed over CM5 sensor chips coated with TNF-FLAG and dissociation was measured over 10 min. Sensorgrams show resonance units (RU) over time and the fit of models used to derive the indicated dissociation constants (K_d), assuming 1:1 binding.

Soluble cleaved and exosomally released TNFR1 and TNFR2 species have previously been demonstrated to be able to bind and neutralise the effects of TNF (Hawari *et al.*, 2004). We used an *in vitro* reporter cell line assay to investigate if Δ6TNFR1 could neutralise the ability of TNF in cell culture supernatant. The HEK-Blue™ TNFα/IL1β reporter cell line expresses Secreted Embryonic Alkaline Phosphatase (SEAP) under the control of an NF-κB response element. Upon treatment with TNF, signalling through TNFR1 upregulates NF-κB, causing SEAP production which can then be quantified by addition of QUANTI-Blue™, a SEAP substrate that gives a colorimetric readout upon dephosphorylation. In agreement with SPR data, Δ6TNFR1-Fc and sTNFR1-Fc were both found to be able to neutralise the effects of TNF, but the IC50 for Δ6TNFR1-Fc (3034 ng/ml) is approximately 20 times higher than that of sTNFR1-Fc (157.8 ng/ml; Figure 5.15a). Fc fusion proteins are constrained by disulphide bonds between IgG domains to be dimeric; seeing as we have demonstrated that Δ6TNFR1 does not self-associate we sought to investigate if the monomeric receptor could neutralise TNF. As a pilot for this study, cell culture supernatant from cells transfected with Δ6TNFR1-ECFP was concentrated 45 times and compared with similarly treated concentrated supernatant from non-transfected cells in a neutralisation assay. Figure 5.15b shows that Δ6TNFR1-ECFP culture supernatant was able to inhibit TNF significantly more than non-transfected supernatant. Following this result, N-terminally HA-tagged sTNFR1-EYFP and DR5.CRD1-EYFP constructs were made to be compared alongside HA-Δ6TNFR1-EYFP in an inhibition assay. Figure 5.15c shows the results of an anti-HA ELISA, in which similar levels of HA-DR5.CRD1-EYFP, HA-sTNFR1-EYFP and HA-Δ6TNFR1-EYFP are shown to be present in the concentrated supernatants that were used in the neutralisation assay shown in Figure 5.15d. Monomeric Δ6TNFR1 shows similar properties to dimeric Δ6TNFR1-Fc in its ability to bind a neutralise TNF.

a


100
80
60
IC50
40
20
0
% Neutralisation
0
10
100
1000
10000
ng/ml
DR5.CRD1-Fc
sTNFR1-Fc
Δ6TNFR1-Fc

b


60
50
40
30
20
10
0
% Neutralisation
1
3
10
32
100
316
μg of conc. sup.
NT
Δ6TNFR1-ECFP

C

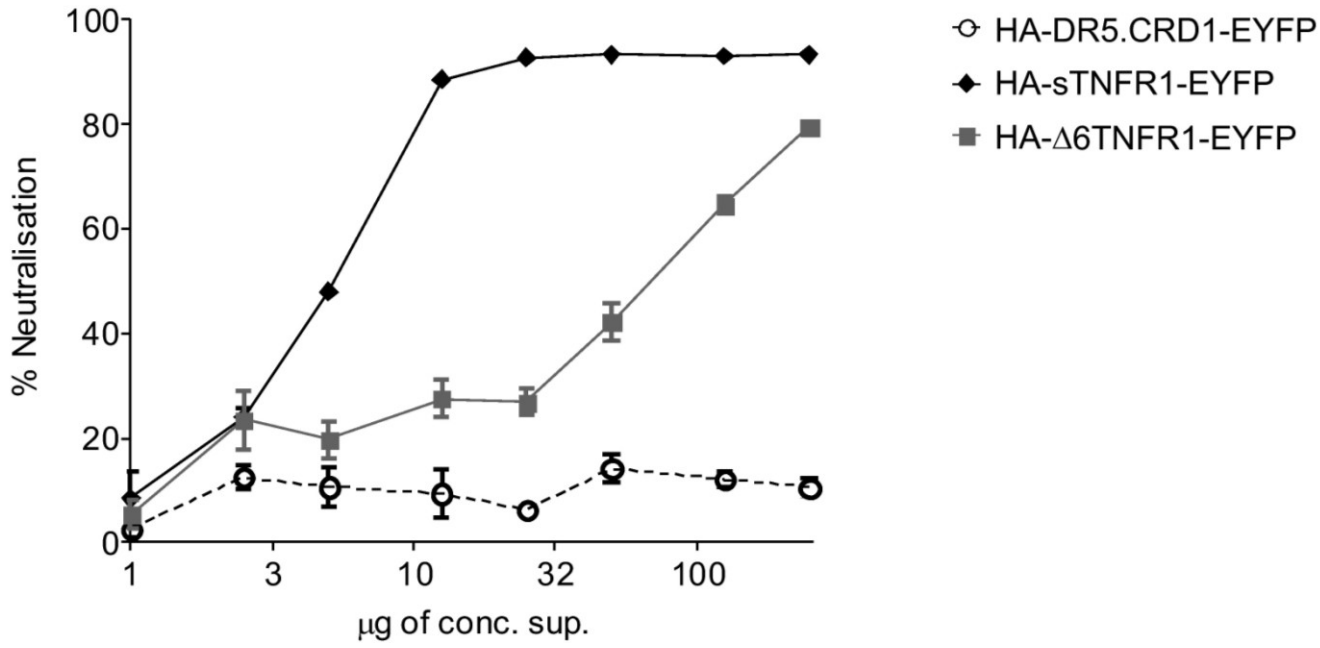


Figure 5.15: Comparative analysis of TNF neutralisation by sTNFR1 and Δ6TNFR1. HEK-Blue™ TNFα/IL1β SEAP reporter cells were incubated with recombinant human TNF in the presence of **(a)** the indicated amount of purified TNFR1-Fc fusion proteins or DR5.CRD1-Fc, **(b)** the indicated amount of concentrated 72 h cell culture supernatant from cells expressing Δ6TNFR1-ECFP or DR5.CRD1-ECFP, or **(d)** the indicated amount of concentrated 72 h cell culture supernatant from cells expressing HA-sTNFR1-EYFP, HA-Δ6TNFR1-EYFP or HA-DR5.CRD1-EYFP. **(c)** The levels of expression of the recombinant HA-tagged sTNFR1, Δ6TNFR1 and DR5.CRD1 EYFP fusion proteins in concentrated cell culture supernatant were analysed by ELISA. Error bars represent mean ± SEM.

5.4 Discussion

5.4.1 Δ6TNFR1 is devoid of all signalling properties of the full-length receptor

The Intracellular death domain (DD) of TNFR1 has previously been shown to be necessary for the recruitment of adaptor proteins that subsequently initiate downstream prosurvival and apoptotic signalling (Kelliher *et al.*, 1998; Liu *et al.*, 1996; Tartaglia *et al.*, 1993). Moreover, TNFR1 must associate into functional trimers or larger-order complexes at the cell surface to initiate signalling (Chan *et al.*, 2000; Lobito *et al.*, 2011). As the frameshift associated with removal of exon 6 from the mature *TNFRSF1A* transcript is predicted to remove the DD from Δ6TNFR1, and we also had demonstrated that Δ6TNFR1 is not expressed at the cell surface (Figures 4.3, 4.6 and 4.7), we hypothesised that Δ6TNFR1 would be unable to engage NF-κB and apoptotic signalling pathways.

In two separate expression systems, and using two distinct assays for apoptotic signalling, Δ6TNFR1 was demonstrated to be incapable of spontaneously inducing programmed cell death, which occurred at a level not significantly different than that observed in cells transduced with empty lentivirus, or transfected with empty vector (Figure 5.1). Only twice the amount of apoptosing cells were detected amongst cells expressing FLTNFR1 compared with Δ6TNFR1 by cell cycle analysis/DNA content using PI, whilst analysis of $\Delta\psi_M$ revealed more than four times as many cells to be apoptotic in cells expressing FLTNFR1-ECFP compared with those expressing FLTNFR1-ECFP (Figure 5.2). This may be explained by differences between the assays. Analysis of the % of cells with sub-diploid DNA content gives high background levels for apoptosis, as evidenced by ~ 20 % of non-transduced cells being apoptotic (Figure 5.1). In contrast, only ~ 10% of non-transfected cells analysed for $\Delta\psi_M$ by staining with TMRM were found to be apoptotic (Figure 5.1). Furthermore, the use of ECFP fluorescence as an indicator of cellular expression of TNFR1 proteins allowed noise from non-transfected, dying/dead cells to be eliminated in the TMRM assay. The almost complete inhibition of loss of $\Delta\psi_M$ to background levels by treatment of FLTNFR1-ECFP transfected cells with the pan-

caspase inhibitor zVAD.fmk demonstrated the loss of $\Delta\psi_M$ associated with FLTNFR1-ECFP expression to be a result of caspase-mediated apoptosis.

Similarly, spontaneous NF-κB-mediated signalling was observed in cells expressing with FLTNFR1, but not in those expressing Δ6TNFR1 (Figures 5.3 and 5.4). Activation of NF-κB as the result of signalling through TNFR1 increases levels of the soluble chemokine IL-8 by binding response elements in its promoter region and upregulation of its transcription (Matsusaka *et al.*, 1993). Accordingly, spontaneous expression of FLTNFR1 was able to induce production of IL-8 that could be detected in the cell culture supernatant of transduced cells, whilst expression of Δ6TNFR1 did not result in IL-8 secretion (Figure 5.5). Altogether, the above demonstrates that Δ6TNFR1 cannot induce spontaneous apoptotic or NF-κB-mediated signalling.

5.4.2 *In vitro* expression of Δ6TNFR1 does not evoke ER stress responses

Trafficking mutants of soluble and membrane-bound proteins that are nevertheless expressed intracellularly may evoke cellular signalling, even if not by classical means. Following translation mutant proteins are often misfolded and so cannot traffick beyond the ER, where they are retained and accumulate, before being retro-transported to the cytosol for degradation by the proteasome, through ER-associated degradation (Vembar and Brodsky, 2008). ER accumulation can trigger stress responses such as the EOR and UPR, leading either to cell survival signalling or the triggering of apoptosis (Pahl and Baeuerle, 1997; Schroder and Kaufman, 2005). Confocal microscopy identified a significant proportion of Δ6TNFR1 to be localised to the ER (Figure 4.8). ER-associated Δ6TNFR1 does not cause the EOR as NF-κB signalling, which is upregulated by the EOR (Pahl and Baeuerle, 1997), was not significantly different from background levels in cells expressing Δ6TNFR1 (Figures 5.3 and 5.4). Similarly, as discussed above, Δ6TNFR1 does not induce apoptosis above background levels

(Figures 5.1 and 5.2). Moreover, analysis of XBP1 activation and splicing provided no evidence for the induction of ER stress responses by Δ6TNFR1 (Figure 5.6).

It is perhaps not surprising that no induction of the UPR could be detected in cells expressing Δ6TNFR1 above background levels. Whilst Δ6TNFR1 cannot insert into the cell membrane it is not retained intracellularly, with significant amounts being secreted; it is therefore unlikely to accumulate in the ER to a level to be able to bring about stress responses. That Δ6TNFR1 is secreted demonstrates that it is not a misfolded TNFR1 mutant, and Δ6TNFR1 does not appear to be targeted for degradation any more than FLTNFR1, as evidenced by the similar total levels of cellular TNFR1 expression observed in cells transiently expressing Δ6TNFR1 or FLTNFR1 (Figures 4.3, 4.6 and 4.7). The most important steps for proper protein folding in the ER are N-linked glycosylation and the formation of disulphide bonds (Vembar and Brodsky, 2008). Δ6TNFR1 retains the three N-glycosylation sites of FLTNFR1 (Gray *et al.*, 1990), and recombinant Δ6TNFR1-Fc resolves by SDS-PAGE such that it appears to be a glycosylated protein (Figures 5.11a and 5.12). The frameshift induced by the removal of exon 6 occurs downstream of intramolecular disulphide bond-forming cysteine residues that when mutated have been demonstrated to result in TNFR1 misfolding (Churchman *et al.*, 2008; Lobito *et al.*, 2006), but does truncate CRD4, removing 3 of its 6 cysteine residues (Banner *et al.*, 1993). Studies have shown that the first two cysteine residues in CRD4 form a disulphide bond and that the third forms a disulphide bond with residue 6 (Banner *et al.*, 1993). Δ6TNFR1 may therefore have a single unpaired cysteine, or this may form a disulphide bond with the single cysteine residue in the novel 45 amino acid sequence induced by the frameshift (Figure 4.1). In any case, the disruption caused by the Δ6TNFR1 frameshift to the normal disulphide bonding of TNFR1 is not sufficient to render the protein unable to traffick through the endomembrane system and be secreted (Figure 4.9). Previous studies with TRAPS-associated TNFR1 mutants that are misfolded due to mutations disrupting disulphide bonds in the extracellular domain of TNFR1 and

fail to traffick beyond the ER show much higher levels in the ER by confocal microscopy, and yet these proteins do not evoke the UPR or EOR. Simon *et al.* recently demonstrated that certain TRAPS mutant receptors that are retained in the ER are able to activate MAPKs and upregulate the production of proinflammatory cytokines in response to LPS stimulation (Simon *et al.*, 2010). However, this activity relies on their being able to recruit adaptor proteins to their functionally-competent DDs to initiate signalling, so Δ6TNFR1 is highly unlikely to be able to initiate pro-inflammatory signalling through a similar mechanism.

5.4.3 Δ6TNFR1 cannot associate with FLTNFR1 to influence signalling, nor can it self-associate

A cytoplasmic domain-deleted TNFR1 has previously been demonstrated to significantly interfere with the function of FLTNFR1 *in vitro* (Chan *et al.*, 2000; Lobito *et al.*, 2006), and several dominant-negative signalling mutants and decoy receptors of TNFR superfamily members have been identified, with altered or truncated cytoplasmic domains (Kuehn *et al.*; Lobito *et al.*, 2011; Shimomura *et al.*, 2004; Siegel *et al.*, 2000). These alterations render the receptors unable or impaired in their ability to recruit the necessary adaptor proteins for the initiation of signalling cascades. As discussed earlier, the mutant receptors are thought to associate with wildtype receptors through their unperturbed PLAD domains, forming functionally compromised receptor complexes. As Δ6TNFR1 retains the PLAD domain (Figure 4.1) and was shown by confocal microscopy to colocalise with FLTNFR1 in the ER and Golgi (Figure 4.8), we sought to investigate the receptors could physically associate.

Titration experiments performed with FLTNFR1 and Δ6TNFR1 constructs in the NF-κB reporter assay system highlight the problems associated with the use of artificial expression systems to analyse subtle interactions, and the importance of appropriate controls (Figure 5.7). Perhaps if stable

FLTNFR1 transfectants were to be made from HeLa or HT1080 cells (ie. lines not transformed with the SV40 T antigen), the influence of transient transfection of Δ6TNFR1 and FAS180 on NF-κB signalling upon treatment with TNF could be compared. Complications relating to the presence of Δ6TNFR1 as a soluble protein could be overcome by using a large excess of TNF to stimulate TNFR1 signalling.

FRET analysis confirmed that Δ6TNFR1 is no more able to form mixed receptor complexes with FLTNFR1 than the extracellular domain of another member of the TNFR superfamily, Fas (Figure 5.8), which has been used by others as negative control for flow-cytometry FRET assays of TNFR1 associations. As the contribution of rs1800693^{G} to disease susceptibility is small (OR = 1.12 (95% C.I. = 1.11-1.14)), even very low levels of association between non-functional Δ6TNFR1 and FLTNFR1 might be sufficient to explain the functional effect of the SNP. We therefore investigated association further with BRET^2, a technique that has been estimated to be up to 20 times more sensitive than FRET, and again there was no evidence for hetero-association (Figure 5.9).

Studies have shown that TNFR1 associates into trimers and higher-order multimers at the cell surface (Lobito *et al.*, 2011), and the fact that residuals for the data from the analysis of homotypic association of FLTNFR1 using a Type I BRET^2 assay were minimised by being fitted to the BRET equation for trimeric associations is a validation of the investigation of interactions of TNFR1 proteins using this technique, and suggests it could be used to study the interactions of other mutant TNFR1 proteins (Figure 5.10).

As Δ6TNFR1 cannot be anchored at the cell surface it may not have the opportunity to associate with FLTNFR1 through its PLAD domain. Colocalisation of Δ6TNFR1 and FLTNFR1 (Figure 4.8c) suggests that there may be the capacity for the proteins to interact upstream of the cell surface, but as Δ6TNFR1 lacks the transmembrane domain of the full-length protein and therefore cannot be membrane-anchored, it may be that whilst FLTNFR1 resides in the ER and Golgi membranes, Δ6TNFR1 is lumenal and so the proteins cannot interact.

Δ6TNFR1 was also convincingly demonstrated not to be able to self-associate (Figures 5.8 and 5.10). Previous studies have shown that low-level self-association can occur for TNFR1 TRAPS mutant proteins that are unable to traffick beyond the ER (Lobito *et al.*, 2006). In these cases association is thought to be result of the formation of intermolecular disulphide bonds between unpaired cysteine residues on mutant TNFR1 monomers, as the result of a mutation that removes a cysteine residue or otherwise results in misfolding of the protein such that multiple unpaired cysteines are exposed (Churchman *et al.*, 2008; Lobito *et al.*, 2006). The unpaired cysteine residue created by the frameshift in Δ6TNFR1 does not appear to confer the ability for association in this way. The aforementioned TRAPS mutants retain transmembrane domains; it may be that intermolecular associations are unable to occur unless receptor proteins are concentrated in membranes. Alternatively, the truncation and/or novel 45 amino acid sequence associated with Δ6TNFR1 may cause conformational changes that render it unable to associate via its PLAD domain.

As rs1800693^{G} is a common variant (allele frequency = 0.45 (De Jager *et al.*, 2009b)) it is perhaps not surprising that it doesn't result in the production of a dominant negative TNFR1 mutant. As the TNF-TNFR1 signalling axis is so important in a wide variety of fundamental biological processes it is likely that such a detrimental variant would have been strongly selected against or even abortive, and

would not be maintained at such a high frequency in the population. Indeed, whilst there are naturally-occurring signalling domain mutants of Fas, ectodysplasin A receptor (EDAR) and transmembrane activator and CAML interactor (TACI) members of the TNFR superfamily, of the myriad of disease-associated TNFR1 mutations catalogued to date, no dominant-negative mutants have been identified (Lobito *et al.*, 2011).

5.4.4 Δ6TNFR1 retains the ability to bind and neutralise TNF, but with a reduced affinity and capacity compared to TNFR1

Δ6TNFR1 retains in full the CRDs 2 and 3 that are thought to be most important in ligand binding (Banner *et al.*, 1993), and was demonstrated in several *in vitro* assays to be capable of binding TNF, providing further evidence that it is a properly folded protein (Figures 5.12, 5.13, 5.14 and 5.15). The cell-based assay for analysis of TNF binding using HA-tagged TNFR1 proteins (Figure 5.13), whilst informative in demonstrating absolutely that Δ6TNFR1 could bind TNF, may not allow accurate inference of relative affinity of FLTNFR1 and Δ6TNFR1 for TNF. Binding of TNF-biotin in this instance takes places in a highly artificial setting, and having demonstrated the differences in the intracellular trafficking and subcellular localisation of the two proteins (Figure 4.8), the relative permeabilisation of organelles/accessibility of TNF-biotin to receptors might not be fair and equal, potentially biasing the comparison.

Interactions between the TNFR1 Fc fusion proteins and immobilised TNF-FLAG were found by SPR to be very strong – in agreement with previous studies (Lobito *et al.*, 2006) – such that dissociation was minimal upon cessation of injection of Fc fusion proteins. Affinities were therefore calculated as dissociation constants using association rates of TNFR1 Fc fusions injected at a variety of concentrations, by analysing the trajectory of the binding curves to equilibrium binding. The affinity of TNFR1 for TNF reported here (K_d = 7.19 x 10^{-10}) is similar to that reported in studies in which

equilibrium binding of cloned and native receptors to ^{125}I-labelled TNF was analysed (K_d = 1.9-6 x 10^{-11}) (Grell *et al.*, 1998a). Modest differences may be attributable to differences between the assays and temperatures used to analyse binding. The kinetics of TNF binding of full-length TNFR1 were similar to those observed in a study that analysed relative binding of several TNFR1 mutants using the same Fc fusion binding to TNF-FLAG captured using amine-coupled anti-FLAG M2 system used in this study (Lobito *et al.*, 2006). It is important to note that as Fc fusions constrain both sTNFR1 and Δ6TNFR1 to be dimeric that the K_ds calculated here might not reflect their *in vivo* affinities. Nevertheless, they allow inference of the relative affinities of sTNFR1 and Δ6TNFR1 in a controlled fashion.

TNF binding by Δ6TNFR1 was reproducibly found to occur with an affinity roughly 20 times lower than that of FLTNFR1 (Figure 5.14). Some studies have previously shown CRD4 to be dispensable for binding of TNF by FLTNFR1, and in any case Δ6TNFR1 retains the A1 module of CRD4 that has more recently been suggested to play a role in TNF binding (Banner *et al.*, 1993; Cao *et al.*, 2009). Other studies have, however, demonstrated a ~ 10-fold reduction in affinity for TNF upon deletion of CRD4 (Marsters *et al.*, 1992). In any case, it is unexpected that Δ6TNFR1 would display such a reduced affinity for TNF compared with FLTNFR1. This may be explained by conformational changes as a result of the partial deletion of CRD4 (Figure 4.1 and Supplementary Figure 6), which may sterically inhibit ligand access to key TNF-binding residues in CRDs 2 and 3 (Banner *et al.*, 1993; Takasaki *et al.*, 1997).

Both recombinant, purified Δ6TNFR1-Fc and Δ6TNFR1-ECFP and HA-Δ6TNFR1-EYFP expressed in cell culture supernatant were demonstrated to bind and neutralise TNF-TNFR1 signalling (Figure 5.15). Moreover, IC50 values derived from fitted dose-response curves estimated Δ6TNFR1-Fc to be ~ 20 times less able to neutralise TNF than sTNFR1-Fc, corroborating the results of SPR studies (Figure

5.15a). Neutralisation assays using HA-TNFR1-EYFP proteins in concentrated cell culture supernatants were such that even at maximal concentrations of concentrated supernatant, neutralisation of TNF signalling by HA-Δ6TNFR1-EYFP had not plateaued. This precluded the possibility of plotting dose-response curves and deriving IC50s to compare relative ability of HA-sTNFR1-EYFP and HA-Δ6TNFR1-EYFP to bind and neutralise TNF, and then comparing this with SPR data and the difference between IC50s calculated using Fc fusion proteins. However, once again, approximately 20 times more HA-Δ6TNFR1-EYFP supernatant was required to neutralise ~ 50% of TNF signalling compared to HA-sTNFR1-EYFP supernatant.

6.0 Concluding remarks

This study has demonstrated that the MS-associated G allele of the rs1800693 SNP in the gene encoding the principle receptor for TNF results in an alternative splicing event, causing truncation of the translated protein and ultimately to the production of a functional, secreted protein with the capacity to bind and neutralise TNF signalling. These findings are striking in light of the results of clinical trials in MS patients for anti-TNF therapies and reported side-effects of their use in the treatment of immune-mediated inflammatory disorders.

The amelioration of clinical symptoms through treatment with TNF antagonists in animal models and subsequent successful clinical trials in patients led to the licensing of several neutralising anti-TNF antibodies (infliximab, adalimumab, golimumab and certolizumab pegol) and a soluble TNFR2 receptor chimera (etanercept) in the treatment of a range of inflammatory autoimmune diseases, including Rheumatoid Arthritis, Crohn's Disease, Ankylosing Spondylitis (AS) and Psoriasis (reviewed in (Caminero *et al.*, 2011) and (Tracey *et al.*, 2008)).

Trials for anti-TNF therapy in MS patients were partly based on correlations with TNF levels and disease severity, progression, relapses and detection of the cytokine in active lesions (Caminero *et al.*, 2011). Furthermore, results of studies in EAE had shown that genetic knockout of TNF or antagonism with neutralising antibodies and recombinant soluble receptors could prevent or delay disease onset (reviewed by (Probert *et al.*, 2000; Selmaj and Raine, 1995).

Despite these observations, trials for two anti-TNF biologics in MS patients resulted in increased frequency of relapses, numbers of lesions and the worsening of symptoms (The Lenercept Multiple

Sclerosis Study Group, 1999; van Oosten *et al.*, 1996). Perhaps of greatest relevance to the findings of this study, one of these agents, lenercept, is the extracellular domain of TNFR1 fused to human IgG1, for which a dose-dependent increase in relapse frequency and severity was observed (The Lenercept Multiple Sclerosis Study Group, 1999). Moreover, demyelinating episodes and MS-like symptoms such as optic neuritis are rare, but significant side effects of treatment with licensed anti-TNF therapies in the treatment of other autoimmune diseases (reviewed by (Bosch *et al.*, 2011).

Several mechanisms have been proposed to explain the development of demyelinating disease as a side effect of TNF antagonism and the negative results of trials in MS patients. As a key regulator in an elaborate and finely-tuned network of cytokines, TNF dysregulation could result in significant departures from the normal production of a variety of pro- and anti-inflammatory soluble mediators, with disease-exacerbating consequences (Evangelidou *et al.*, 2010; Prinz, 2011). Autoimmunity may be promoted by the impaired clearance of apoptotic material in conjunction with increased TCR signalling and decreased apoptosis of autoreactive T cells (Ernandez and Mayadas, 2009; Kodama *et al.*, 2005; Prinz, 2011). Inhibition of TNF signalling may also facilitate the dissemination of viral or bacterial infections that may subsequently trigger or worsen autoimmune reactions through molecular mimicry, epitope spreading or bystander activation (Fujinami *et al.*, 2006). Following CNS insult TNF-TNFR1 signalling has been proposed to be neuroprotective, upregulating ROS scavengers and having a role in maintaining Ca^{2+} homeostasis (Figiel, 2008); neutralisation of TNF may therefore sensitise neurons to axonal degeneration, with consequent exacerbation of clinical symptoms.

As Δ6TNFR1 is expressed intracellularly, a further mechanism by which it might downregulate TNF signalling is through binding and consequently making unavailable intracellular TNF, as has been observed for a splice variant of TNFR2 (Scherubl *et al.*, 2005). The net effect of Δ6TNFR1-TNF

interactions is complicated further by the observation that at low levels, soluble TNF receptors have been demonstrated to be able to act as agonists of TNF signalling, through stabilising TNF structure and thereby increasing its bioavailability (Aderka *et al.*, 1992). Whilst this would not be able to account for the disease-exacerbating consequences of treatment with lenercept in MS patients, which was administered at high levels, it represents a potential mechanism by which Δ6TNFR1, which is likely to be present at low levels, could predispose individuals to MS by propagating inflammatory processes.

As mentioned previously, transgenic TNFR2 knockout mice develop more severe EAE, and several studies have suggested that tmTNF-TNFR2 signalling may be important for limiting CNS pathology, and that sTNF-TNFR1 signalling alone may be responsible for the disease-exacerbating effects of TNF. Kassiotis and Kollias demonstrated that whilst TNF is proinflammatory immediately after disease initiation, it appears to be required for remission, and that in its absence myelin-specific T cells accumulate and contribute to the development of a late chronic form of EAE (Kassiotis and Kollias, 2001). Moreover, they showed TNF-mediated immunosuppression did not require TNFR1, but that this receptor was required for the acute proinflammatory effects of TNF (Kassiotis and Kollias, 2001). Furthermore, Alexopoulou *et al.* 2006 made use of the differing affinities of TNFR1 and TNFR2 for sTNF and tmTNF to demonstrate suppression of EAE onset and progression in transgenic mice expressing a non-sheddable tmTNF, which was therefore only able to signal through TNFR2 (Alexopoulou *et al.*, 2006). More recently, Taoufik *et al.* demonstrated that selective inhibition of sTNF protected mice from developing EAE (Taoufik *et al.*, 2011), and Brambilla *et al.* showed that treatment of EAE mice with a specific sTNF inhibitor was associated with axon preservation and remyelination (Brambilla *et al.*, 2011). Selective inhibition of sTNF-TNFR1 signalling may therefore be an alternative therapeutic strategy in the treatment of MS.

The immunomodulatory effects of tmTNF signalling through TNFR2 may be as a result of the consequent reversion of activated myelin-specific T cells to T_{reg}s, and in T_{reg}-mediated regulation of T_H1 and T_H17 expansion (Bilate and Lafaille, 2010; Chee *et al.*, 2011; Suvannavejh *et al.*, 2000). TNF-TNFR2 signalling has also been shown to promote the development and maturation of oligodendrocytes, and so may be important for remyelination and clinical remission (Arnett *et al.*, 2001; Kassiotis and Kollias, 2001).

The findings of the above studies may provide an explanation for the clinical experience with TNF antagonists in MS patients. They show that broad-spectrum inhibition of TNF signalling delays disease onset and limits the extent of initial CNS pathology; however, the MS patients in anti-TNF therapy trials already had established disease. In these individuals inhibition of tmTNF-TNFR2 signalling through the use of pan-TNF antagonists may have released autoreactive T cell populations from their normal regulation, resulting in the increased frequency of relapses and exacerbation of clinical symptoms. Ultimately, the contrast between the effects of TNF antagonism observed in animal models with those in MS patients remains unexplained and is still an active area of research.

In agreement with the successful use of anti-TNF agents in the treatment of a variety of autoimmune diseases, no associations have been identified to date for the *TNFRSF1A* gene region with any of these conditions (Franke *et al.*, 2010; Stahl *et al.*, 2010; Strange *et al.*, 2010), except for AS, which has an independently associated SNP compared to MS (Evans *et al.*, 2011). This suggests that the Δ6TNFR1 isoform described here is unlikely to influence predisposition to the development of any of these diseases. Interestingly, rs1800693^G has also been found to be associated with primary biliary cirrhosis (PBC)(Mells *et al.*, 2011), but to date there is no clinical experience with TNF antagonists in

the treatment of this disease. The results of this study would suggest that anti-TNF therapy should not be trialled in PBC patients, and that it might lead to the worsening of symptoms.

As the side effects demyelinating episodes and MS-like symptoms associated TNF-antagonism are very rare, they may only arise in individuals with a pre-existing sensitivity or predisposition to the development of demyelinating disease, which may be unmasked upon treatment with anti-TNF agents.

The results of this study are also of significance in that they address a common criticism of GWAS; that they have little clinical value, as they typically identify disease-associated variants that have modest functional consequences and contribution to disease, which is reflected in their modest odds ratios (Goldstein, 2009). This position does not take into account that drugs designed to target the pathogenic pathways identified through the associations of component variants through GWAS are likely to have a much larger impact on these pathways than the disease-associated variants (Altshuler *et al.*, 2008). This is exemplified by this study, in which ~ 20 times greater neutralisation was observed with sTNFR1-Fc (equivalent to lenercept) than with naturally occurring Δ6TNFR1 at equal concentrations. Moreover, levels of TNF antagonists during treatment are likely to be much, much higher than endogenous levels of Δ6TNFR1.

This study has therefore, through investigating the functional effect of the MS-associated rs1800693^{G} allele, revealed how the administration of TNF antagonists could precipitate, unmask or worsen demyelinating diseases such as MS. It uncovers a previously unidentified use for GWAS, in that they may serve to directly inform and direct therapeutic strategy in the treatment of common

diseases with complex inheritance.

7.0 References

Aartsma-Rus A, van Ommen GJ. Antisense-mediated exon skipping: a versatile tool with therapeutic and research applications. RNA 2007; 13: 1609-24.

Aderka D, Engelmann H, Maor Y, Brakebusch C, Wallach D. Stabilization of the bioactivity of tumor necrosis factor by its soluble receptors. J Exp Med 1992; 175: 323-9.

Albert LJ, Inman RD. Molecular mimicry and autoimmunity. N Engl J Med 1999; 341: 2068-74.

Alberts B. Molecular biology of the cell. New York ; Abingdon: Garland Science, 2008.

Alexopoulou L, Kranidioti K, Xanthoulea S, Denis M, Kotanidou A, Douni E, et al. Transmembrane TNF protects mutant mice against intracellular bacterial infections, chronic inflammation and autoimmunity. Eur J Immunol 2006; 36: 2768-80.

Altshuler D, Daly MJ, Lander ES. Genetic mapping in human disease. Science 2008; 322: 881-8.

Arnett HA, Mason J, Marino M, Suzuki K, Matsushima GK, Ting JP. TNF alpha promotes proliferation of oligodendrocyte progenitors and remyelination. Nat Neurosci 2001; 4: 1116-22.

Australia and New Zealand Multiple Sclerosis Genetics Consortium. Genome-wide association study identifies new multiple sclerosis susceptibility loci on chromosomes 12 and 20. Nat Genet 2009; 41: 824-8.

Bailey SL, Schreiner B, McMahon EJ, Miller SD. CNS myeloid DCs presenting endogenous myelin peptides 'preferentially' polarize CD4+ T(H)-17 cells in relapsing EAE. Nat Immunol 2007; 8: 172-80.

Banner DW, D'Arcy A, Janes W, Gentz R, Schoenfeld HJ, Broger C, et al. Crystal structure of the soluble human 55 kd TNF receptor-human TNF beta complex: implications for TNF receptor activation. Cell 1993; 73: 431-45.

Banning C, Votteler J, Hoffmann D, Koppensteiner H, Warmer M, Reimer R, et al. A flow cytometry-based FRET assay to identify and analyse protein-protein interactions in living cells. PLoS One 2010; 5: e9344.

Bar-Or A, Fawaz L, Fan B, Darlington PJ, Rieger A, Ghorayeb C, et al. Abnormal B-cell cytokine responses a trigger of T-cell-mediated disease in MS? Ann Neurol 2010; 67: 452-61.

Baralle D, Baralle M. Splicing in action: assessing disease causing sequence changes. J Med Genet 2005; 42: 737-48.

Baralle D, Lucassen A, Buratti E. Missed threads. The impact of pre-mRNA splicing defects on clinical practice. EMBO Rep 2009; 10: 810-6.

Barry M, Bleackley RC. Cytotoxic T lymphocytes: all roads lead to death. Nat Rev Immunol 2002; 2: 401-9.

Bauman J, Jearawiriyapaisarn N, Kole R. Therapeutic potential of splice-switching oligonucleotides. Oligonucleotides 2009; 19: 1-13.

Benoist C, Mathis D. Autoimmunity provoked by infection: how good is the case for T cell epitope mimicry? Nat Immunol 2001; 2: 797-801.

Bianchi K, Meier P. A tangled web of ubiquitin chains: breaking news in TNF-R1 signaling. Mol Cell 2009; 36: 736-42.

Bielekova B, Sung MH, Kadom N, Simon R, McFarland H, Martin R. Expansion and functional relevance of high-avidity myelin-specific CD4+ T cells in multiple sclerosis. J Immunol 2004; 172: 3893-904.

Bilate AM, Lafaille JJ. Can TNF-alpha boost regulatory T cells? J Clin Invest 2010; 120: 4190-2.

Black DL. Mechanisms of alternative pre-messenger RNA splicing. Annu Rev Biochem 2003; 72: 291-336.

Blencowe BJ. Alternative splicing: new insights from global analyses. Cell 2006; 126: 37-47.

Bosch X, Saiz A, Ramos-Casals M. Monoclonal antibody therapy-associated neurological disorders. Nat Rev Neurol 2011; 7: 165-72.

Brakebusch C, Nophar Y, Kemper O, Engelmann H, Wallach D. Cytoplasmic truncation of the p55 tumour necrosis factor (TNF) receptor abolishes signalling, but not induced shedding of the receptor. EMBO J 1992; 11: 943-50.

Brambilla R, Ashbaugh JJ, Magliozzi R, Dellarole A, Karmally S, Szymkowski DE, et al. Inhibition of soluble tumour necrosis factor is therapeutic in experimental autoimmune encephalomyelitis and promotes axon preservation and remyelination. Brain 2011; 134: 2736-54.

Brett D, Pospisil H, Valcarcel J, Reich J, Bork P. Alternative splicing and genome complexity. Nat Genet 2002; 30: 29-30.

Bronnum-Hansen H, Koch-Henriksen N, Stenager E. Trends in survival and cause of death in Danish patients with multiple sclerosis. Brain 2004; 127: 844-50.

Brynedal B, Duvefelt K, Jonasdottir G, Roos IM, Akesson E, Palmgren J, et al. HLA-A confers an HLA-DRB1 independent influence on the risk of multiple sclerosis. PLoS One 2007; 2: e664.

Bulua AC, Simon A, Maddipati R, Pelletier M, Park H, Kim KY, et al. Mitochondrial reactive oxygen species promote production of proinflammatory cytokines and are elevated in TNFR1-associated periodic syndrome (TRAPS). J Exp Med 2011; 208: 519-33.

Buratti E, Baralle M, De Conti L, Baralle D, Romano M, Ayala YM, et al. hnRNP H binding at the 5' splice site correlates with the pathological effect of two intronic mutations in the NF-1 and TSHbeta genes. Nucleic Acids Res 2004; 32: 4224-36.

Burton PR, Clayton DG, Cardon LR, Craddock N, Deloukas P, Duncanson A, et al. Association scan of 14,500 nonsynonymous SNPs in four diseases identifies autoimmunity variants. Nat Genet 2007; 39: 1329-37.

Calfon M, Zeng H, Urano F, Till JH, Hubbard SR, Harding HP, et al. IRE1 couples endoplasmic reticulum load to secretory capacity by processing the XBP-1 mRNA. Nature 2002; 415: 92-6.

Caminero A, Comabella M, Montalban X. Tumor necrosis factor alpha (TNF-alpha), anti-TNF-alpha and demyelination revisited: an ongoing story. J Neuroimmunol 2011; 234: 1-6.

Cao Y, Wang Z, Bu X, Tang S, Mei Z, Liu P. A synthetic peptide derived from A1 module in CRD4 of human TNF receptor-1 inhibits binding and proinflammatory effect of human TNF-alpha. Inflammation 2009; 32: 139-45.

Cartegni L, Krainer AR. Correction of disease-associated exon skipping by synthetic exon-specific activators. Nat Struct Biol 2003; 10: 120-5.

Chan FK, Chun HJ, Zheng L, Siegel RM, Bui KL, Lenardo MJ. A domain in TNF receptors that mediates ligand-independent receptor assembly and signaling. Science 2000; 288: 2351-4.

Chan FK, Siegel RM, Zacharias D, Swofford R, Holmes KL, Tsien RY, et al. Fluorescence resonance energy transfer analysis of cell surface receptor interactions and signaling using spectral variants of the green fluorescent protein. Cytometry 2001; 44: 361-8.

Chee J, Angstetra E, Mariana L, Graham KL, Carrington EM, Bluethmann H, et al. TNF receptor 1 deficiency increases regulatory T cell function in nonobese diabetic mice. J Immunol 2011; 187: 1702-12.

Chen G, Goeddel DV. TNF-R1 signaling: a beautiful pathway. Science 2002; 296: 1634-5.

Chen M, Manley JL. Mechanisms of alternative splicing regulation: insights from molecular and genomics approaches. Nat Rev Mol Cell Biol 2009; 10: 741-54.

Christy AL, Brown MA. The multitasking mast cell: positive and negative roles in the progression of autoimmunity. J Immunol 2007; 179: 2673-9.

Churchman SM, Church LD, Savic S, Coulthard LR, Hayward B, Nedjai B, et al. A novel TNFRSF1A splice mutation associated with increased nuclear factor kappaB (NF-kappaB) transcription factor activation in patients with tumour necrosis factor receptor associated periodic syndrome (TRAPS). Ann Rheum Dis 2008; 67: 1589-95.

Colombo M, Dono M, Gazzola P, Roncella S, Valetto A, Chiorazzi N, et al. Accumulation of clonally related B lymphocytes in the cerebrospinal fluid of multiple sclerosis patients. J Immunol 2000; 164: 2782-9.

Compston A, Coles A. Multiple sclerosis. Lancet 2008; 372: 1502-17.

Cooper TA. Use of minigene systems to dissect alternative splicing elements. Methods 2005; 37: 331-40.

Corpet F. Multiple sequence alignment with hierarchical clustering. Nucleic Acids Res 1988; 16: 10881-90.

Cottin V, Doan JE, Riches DW. Restricted localization of the TNF receptor CD120a to lipid rafts: a novel role for the death domain. J Immunol 2002; 168: 4095-102.

Coulombe-Huntington J, Lam KC, Dias C, Majewski J. Fine-scale variation and genetic determinants of alternative splicing across individuals. PLoS Genet 2009; 5: e1000766.

Couturier N, Bucciarelli F, Nurtdinov RN, Debouverie M, Lebrun-Frenay C, Defer G, et al. Tyrosine kinase 2 variant influences T lymphocyte polarization and multiple sclerosis susceptibility. Brain 2011; 134: 693-703.

Croxford AL, Kurschus FC, Waisman A. Mouse models for multiple sclerosis: historical facts and future implications. Biochim Biophys Acta 2010; 1812: 177-83.

D'Alessio A, Kluger MS, Li JH, Al-Lamki R, Bradley JR, Pober JS. Targeting of tumor necrosis factor receptor 1 to low density plasma membrane domains in human endothelial cells. J Biol Chem 2010; 285: 23868-79.

De Jager PL, Baecher-Allan C, Maier LM, Arthur AT, Ottoboni L, Barcellos L, et al. The role of the CD58 locus in multiple sclerosis. Proc Natl Acad Sci U S A 2009a; 106: 5264-9.

De Jager PL, Jia X, Wang J, de Bakker PI, Ottoboni L, Aggarwal NT, et al. Meta-analysis of genome scans and replication identify CD6, IRF8 and TNFRSF1A as new multiple sclerosis susceptibility loci. Nat Genet 2009b; 41: 776-82.

Deb C, Lafrance-Corey RG, Schmalstieg WF, Sauer BM, Wang H, German CL, et al. CD8+ T cells cause disability and axon loss in a mouse model of multiple sclerosis. PLoS One 2010; 5: e12478.

del Prete MJ, Vernal R, Dolznig H, Mullner EW, Garcia-Sanz JA. Isolation of polysome-bound mRNA from solid tissues amenable for RT-PCR and profiling experiments. RNA 2007; 13: 414-21.

Della Chiesa M, Romagnani C, Thiel A, Moretta L, Moretta A. Multidirectional interactions are bridging human NK cells with plasmacytoid and monocyte-derived dendritic cells during innate immune responses. Blood 2006; 108: 3851-8.

Dendrou CA, Plagnol V, Fung E, Yang JH, Downes K, Cooper JD, et al. Cell-specific protein phenotypes for the autoimmune locus IL2RA using a genotype-selectable human bioresource. Nat Genet 2009; 41: 1011-5.

Dogan RI, Getoor L, Wilbur WJ, Mount SM. SplicePort--an interactive splice-site analysis tool. Nucleic Acids Res 2007; 35: W285-91.

Donnelly P. Progress and challenges in genome-wide association studies in humans. Nature 2008; 456: 728-31.

Dri P, Gasparini C, Menegazzi R, Cramer R, Alberi L, Presani G, et al. TNF-Induced shedding of TNF receptors in human polymorphonuclear leukocytes: role of the 55-kDa TNF receptor and involvement of a membrane-bound and non-matrix metalloproteinase. J Immunol 2000; 165: 2165-72.

Du K, Peng Y, Greenbaum LE, Haber BA, Taub R. HRS/SRp40-mediated inclusion of the fibronectin EIIIB exon, a possible cause of increased EIIIB expression in proliferating liver. Mol Cell Biol 1997; 17: 4096-104.

Duddy M, Niino M, Adatia F, Hebert S, Freedman M, Atkins H, et al. Distinct effector cytokine profiles of memory and naive human B cell subsets and implication in multiple sclerosis. J Immunol 2007; 178: 6092-9.

Eikelenboom MJ, Killestein J, Izeboud T, Kalkers NF, van Lier RA, Barkhof F, et al. Chemokine receptor expression on T cells is related to new lesion development in multiple sclerosis. J Neuroimmunol 2002; 133: 225-32.

Ernandez T, Mayadas TN. Immunoregulatory role of TNFalpha in inflammatory kidney diseases. Kidney Int 2009; 76: 262-76.

Etzensperger R, McMahon RM, Jones EY, Fugger L. Dissection of the multiple sclerosis associated DR2 haplotype. J Autoimmun 2008; 31: 201-7.

Eugster HP, Frei K, Bachmann R, Bluethmann H, Lassmann H, Fontana A. Severity of symptoms and demyelination in MOG-induced EAE depends on TNFR1. Eur J Immunol 1999; 29: 626-32.

Evangelidou M, Tseveleki V, Vamvakas SS, Probert L. TNFRI is a positive T-cell costimulatory molecule important for the timing of cytokine responses. Immunol Cell Biol 2010; 88: 586-95.

Evans DM, Spencer CC, Pointon JJ, Su Z, Harvey D, Kochan G, et al. Interaction between ERAP1 and HLA-B27 in ankylosing spondylitis implicates peptide handling in the mechanism for HLA-B27 in disease susceptibility. Nat Genet 2011; 43: 761-7.

Evsyukova I, Somarelli JA, Gregory SG, Garcia-Blanco MA. Alternative splicing in multiple sclerosis and other autoimmune diseases. RNA Biol 2010; 7: 462-73.

Fabriek BO, Zwemmer JN, Teunissen CE, Dijkstra CD, Polman CH, Laman JD, et al. In vivo detection of myelin proteins in cervical lymph nodes of MS patients using ultrasound-guided fine-needle aspiration cytology. J Neuroimmunol 2005; 161: 190-4.

Fielding CA, Siebert S, Rowe M, Brennan P. Analysis of human tumour necrosis factor receptor 1 dominant-negative mutants reveals a major region controlling cell surface expression. FEBS Lett 2004; 570: 138-42.

Figiel I. Pro-inflammatory cytokine TNF-alpha as a neuroprotective agent in the brain. Acta Neurobiol Exp (Wars) 2008; 68: 526-34.

Fletcher JM, Lalor SJ, Sweeney CM, Tubridy N, Mills KH. T cells in multiple sclerosis and experimental autoimmune encephalomyelitis. Clin Exp Immunol 2010; 162: 1-11.

Fox EJ. Management of worsening multiple sclerosis with mitoxantrone: a review. Clin Ther 2006; 28: 461-74.

Franciotta D, Salvetti M, Lolli F, Serafini B, Aloisi F. B cells and multiple sclerosis. Lancet Neurol 2008; 7: 852-8.

Franke A, McGovern DPB, Barrett JC, Wang K, Radford-Smith GL, Ahmad T, et al. Genome-wide meta-analysis increases to 71 the number of confirmed Crohn's disease susceptibility loci. Nat Genet 2010; 42: 1118-1125.

Friese MA, Fugger L. Autoreactive CD8+ T cells in multiple sclerosis: a new target for therapy? Brain 2005; 128: 1747-63.

Friese MA, Fugger L. Pathogenic CD8(+) T cells in multiple sclerosis. Ann Neurol 2009; 66: 132-41.

Friese MA, Jakobsen KB, Friis L, Etzensperger R, Craner MJ, McMahon RM, et al. Opposing effects of HLA class I molecules in tuning autoreactive CD8+ T cells in multiple sclerosis. Nat Med 2008; 14: 1227-35.

Fugger L, Friese MA, Bell JI. From genes to function: the next challenge to understanding multiple sclerosis. Nat Rev Immunol 2009; 9: 408-17.

Fujinami RS, von Herrath MG, Christen U, Whitton JL. Molecular mimicry, bystander activation, or viral persistence: infections and autoimmune disease. Clin Microbiol Rev 2006; 19: 80-94.

Fujita K, Srinivasula SM. Ubiquitination and TNFR1 signaling. Results Probl Cell Differ 2009; 49: 87-114.

Fung BK, Stryer L. Surface density determination in membranes by fluorescence energy transfer. Biochemistry 1978; 17: 5241-8.

Gandhi R, Laroni A, Weiner HL. Role of the innate immune system in the pathogenesis of multiple sclerosis. J Neuroimmunol 2010; 221: 7-14.

Garcia-Calvo M, Peterson EP, Leiting B, Ruel R, Nicholson DW, Thornberry NA. Inhibition of human caspases by peptide-based and macromolecular inhibitors. J Biol Chem 1998; 273: 32608-13.
Garcia-Sanz JA, Lenig D. Translational control of interleukin 2 messenger RNA as a molecular mechanism of T cell anergy. J Exp Med 1996; 184: 159-64.
Gilden DH. Infectious causes of multiple sclerosis. Lancet Neurol 2005; 4: 195-202.
Gimenez MA, Sim JE, Russell JH. TNFR1-dependent VCAM-1 expression by astrocytes exposes the CNS to destructive inflammation. J Neuroimmunol 2004; 151: 116-25.
Glass CK, Saijo K, Winner B, Marchetto MC, Gage FH. Mechanisms underlying inflammation in neurodegeneration. Cell 2010; 140: 918-34.
Gold R, Linington C, Lassmann H. Understanding pathogenesis and therapy of multiple sclerosis via animal models: 70 years of merits and culprits in experimental autoimmune encephalomyelitis research. Brain 2006; 129: 1953-71.
Goldstein DB. Common genetic variation and human traits. N Engl J Med 2009; 360: 1696-8.
Goodwin RG, Anderson D, Jerzy R, Davis T, Brannan CI, Copeland NG, et al. Molecular cloning and expression of the type 1 and type 2 murine receptors for tumor necrosis factor. Mol Cell Biol 1991; 11: 3020-6.
Goodwin RG, Friend D, Ziegler SF, Jerzy R, Falk BA, Gimpel S, et al. Cloning of the human and murine interleukin-7 receptors: demonstration of a soluble form and homology to a new receptor superfamily. Cell 1990; 60: 941-51.
Goverman J. Autoimmune T cell responses in the central nervous system. Nat Rev Immunol 2009; 9: 393-407.
Goyenvalle A, Davies KE. Challenges to oligonucleotides-based therapeutics for Duchenne muscular dystrophy. Skelet Muscle 2011; 1: 8.
Graveley BR, Hertel KJ, Maniatis T. SR proteins are 'locators' of the RNA splicing machinery. Curr Biol 1999; 9: R6-7.
Gray E, Thomas TL, Betmouni S, Scolding N, Love S. Elevated activity and microglial expression of myeloperoxidase in demyelinated cerebral cortex in multiple sclerosis. Brain Pathol 2008; 18: 86-95.
Gray PW, Barrett K, Chantry D, Turner M, Feldmann M. Cloning of human tumor necrosis factor (TNF) receptor cDNA and expression of recombinant soluble TNF-binding protein. Proc Natl Acad Sci U S A 1990; 87: 7380-4.
Graziewicz MA, Tarrant TK, Buckley B, Roberts J, Fulton L, Hansen H, et al. An endogenous TNF-alpha antagonist induced by splice-switching oligonucleotides reduces inflammation in hepatitis and arthritis mouse models. Mol Ther 2008; 16: 1316-22.
Gregersen JW, Kranc KR, Ke X, Svendsen P, Madsen LS, Thomsen AR, et al. Functional epistasis on a common MHC haplotype associated with multiple sclerosis. Nature 2006; 443: 574-7.
Gregory SG, Schmidt S, Seth P, Oksenberg JR, Hart J, Prokop A, et al. Interleukin 7 receptor alpha chain (IL7R) shows allelic and functional association with multiple sclerosis. Nat Genet 2007; 39: 1083-91.
Grell M, Becke FM, Wajant H, Mannel DN, Scheurich P. TNF receptor type 2 mediates thymocyte proliferation independently of TNF receptor type 1. Eur J Immunol 1998a; 28: 257-63.
Grell M, Wajant H, Zimmermann G, Scheurich P. The type 1 receptor (CD120a) is the high-affinity receptor for soluble tumor necrosis factor. Proc Natl Acad Sci U S A 1998b; 95: 570-5.
Gross A, Yin XM, Wang K, Wei MC, Jockel J, Milliman C, et al. Caspase cleaved BID targets mitochondria and is required for cytochrome c release, while BCL-XL prevents this release but not tumor necrosis factor-R1/Fas death. J Biol Chem 1999; 274: 1156-63.
Gullberg U, Lantz M, Lindvall L, Olsson I, Himmler A. Involvement of an Asn/Val cleavage site in the production of a soluble form of a human tumor necrosis factor (TNF) receptor. Site-directed mutagenesis of a putative cleavage site in the p55 TNF receptor chain. Eur J Cell Biol 1992; 58: 307-12.

Hafler DA, Compston A, Sawcer S, Lander ES, Daly MJ, De Jager PL, et al. Risk alleles for multiple sclerosis identified by a genomewide study. N Engl J Med 2007; 357: 851-62.
Hammond SM, Wood MJ. Genetic therapies for RNA mis-splicing diseases. Trends Genet 2011; 27: 196-205.
Harkiolaki M, Holmes SL, Svendsen P, Gregersen JW, Jensen LT, McMahon R, et al. T cell-mediated autoimmune disease due to low-affinity crossreactivity to common microbial peptides. Immunity 2009; 30: 348-57.
Hart PH, Gorman S, Finlay-Jones JJ. Modulation of the immune system by UV radiation: more than just the effects of vitamin D? Nat Rev Immunol 2011; 11: 584-96.
Hauser SL, Waubant E, Arnold DL, Vollmer T, Antel J, Fox RJ, et al. B-cell depletion with rituximab in relapsing-remitting multiple sclerosis. N Engl J Med 2008; 358: 676-88.
Hawari FI, Rouhani FN, Cui X, Yu ZX, Buckley C, Kaler M, et al. Release of full-length 55-kDa TNF receptor 1 in exosome-like vesicles: a mechanism for generation of soluble cytokine receptors. Proc Natl Acad Sci U S A 2004; 101: 1297-302.
Hehlgans T, Pfeffer K. The intriguing biology of the tumour necrosis factor/tumour necrosis factor receptor superfamily: players, rules and the games. Immunology 2005; 115: 1-20.
Hillert J, Olerup O. HLA and MS. Neurology 1993; 43: 2426-7.
Hofman FM, Hinton DR, Johnson K, Merrill JE. Tumor necrosis factor identified in multiple sclerosis brain. J Exp Med 1989; 170: 607-12.
Hogquist KA, Baldwin TA, Jameson SC. Central tolerance: learning self-control in the thymus. Nat Rev Immunol 2005; 5: 772-82.
Houdayer C, Dehainault C, Mattler C, Michaux D, Caux-Moncoutier V, Pages-Berhouet S, et al. Evaluation of in silico splice tools for decision-making in molecular diagnosis. Hum Mutat 2008; 29: 975-82.
Huang YM, Xiao BG, Ozenci V, Kouwenhoven M, Teleshova N, Fredrikson S, et al. Multiple sclerosis is associated with high levels of circulating dendritic cells secreting pro-inflammatory cytokines. J Neuroimmunol 1999; 99: 82-90.
Hutchinson WM, Haire M. Measles-virus-specific IgG in optic neuritis and in multiple sclerosis after optic neuritis. Br Med J 1976; 1: 64-6.
Iioka H, Loiselle D, Haystead TA, Macara IG. Efficient detection of RNA-protein interactions using tethered RNAs. Nucleic Acids Res 2011; 39: e53.
Jack C, Ruffini F, Bar-Or A, Antel JP. Microglia and multiple sclerosis. J Neurosci Res 2005; 81: 363-73.
Jagodic M, Colacios C, Nohra R, Dejean AS, Beyeen AD, Khademi M, et al. A role for VAV1 in experimental autoimmune encephalomyelitis and multiple sclerosis. Sci Transl Med 2009; 1: 10ra21.
James JR, Oliveira MI, Carmo AM, Iaboni A, Davis SJ. A rigorous experimental framework for detecting protein oligomerization using bioluminescence resonance energy transfer. Nat Methods 2006; 3: 1001-6.
Jersild C, Svejgaard A, Fog T. HL-A antigens and multiple sclerosis. Lancet 1972; 1: 1240-1.
Ji Q, Perchellet A, Goverman JM. Viral infection triggers central nervous system autoimmunity via activation of CD8+ T cells expressing dual TCRs. Nat Immunol 2010; 11: 628-34.
Johnson JM, Castle J, Garrett-Engele P, Kan Z, Loerch PM, Armour CD, et al. Genome-wide survey of human alternative pre-mRNA splicing with exon junction microarrays. Science 2003; 302: 2141-4.
Kalbfuss B, Mabon SA, Misteli T. Correction of alternative splicing of tau in frontotemporal dementia and parkinsonism linked to chromosome 17. J Biol Chem 2001; 276: 42986-93.
Kampa D, Cheng J, Kapranov P, Yamanaka M, Brubaker S, Cawley S, et al. Novel RNAs identified from an in-depth analysis of the transcriptome of human chromosomes 21 and 22. Genome Res 2004; 14: 331-42.

Kandel ER, Schwartz JH, Jessell TM. Principles of neural science. New York, NY ; London: McGraw-Hill, 2000.

Kassiotis G, Kollias G. Uncoupling the proinflammatory from the immunosuppressive properties of tumor necrosis factor (TNF) at the p55 TNF receptor level: implications for pathogenesis and therapy of autoimmune demyelination. J Exp Med 2001; 193: 427-34.

Kebir H, Kreymborg K, Ifergan I, Dodelet-Devillers A, Cayrol R, Bernard M, et al. Human TH17 lymphocytes promote blood-brain barrier disruption and central nervous system inflammation. Nat Med 2007; 13: 1173-5.

Kelliher MA, Grimm S, Ishida Y, Kuo F, Stanger BZ, Leder P. The death domain kinase RIP mediates the TNF-induced NF-kappaB signal. Immunity 1998; 8: 297-303.

Kenworthy AK, Edidin M. Distribution of a glycosylphosphatidylinositol-anchored protein at the apical surface of MDCK cells examined at a resolution of <100 A using imaging fluorescence resonance energy transfer. J Cell Biol 1998; 142: 69-84.

Kimberley FC, Lobito AA, Siegel RM, Screaton GR. Falling into TRAPS--receptor misfolding in the TNF receptor 1-associated periodic fever syndrome. Arthritis Res Ther 2007; 9: 217.

Kodama S, Davis M, Faustman DL. The therapeutic potential of tumor necrosis factor for autoimmune disease: a mechanistically based hypothesis. Cell Mol Life Sci 2005; 62: 1850-62.

Kofler DM, Severson CA, Mousissian N, De Jager PL, Hafler DA. The CD6 multiple sclerosis susceptibility allele is associated with alterations in CD4+ T cell proliferation. J Immunol 2011; 187: 3286-91.

Korner H, Lemckert FA, Chaudhri G, Etteldorf S, Sedgwick JD. Tumor necrosis factor blockade in actively induced experimental autoimmune encephalomyelitis prevents clinical disease despite activated T cell infiltration to the central nervous system. Eur J Immunol 1997a; 27: 1973-81.

Korner H, Riminton DS, Strickland DH, Lemckert FA, Pollard JD, Sedgwick JD. Critical points of tumor necrosis factor action in central nervous system autoimmune inflammation defined by gene targeting. J Exp Med 1997b; 186: 1585-90.

Korte A, Kochling J, Badiali L, Eckert C, Andreae J, Geilen W, et al. Expression analysis and characterization of alternatively spliced transcripts of human IL-7Ralpha chain encoding two truncated receptor proteins in relapsed childhood all. Cytokine 2000; 12: 1597-608.

Kouwenhoven M, Teleshova N, Ozenci V, Press R, Link H. Monocytes in multiple sclerosis: phenotype and cytokine profile. J Neuroimmunol 2001; 112: 197-205.

Kraus J, Voigt K, Schuller AM, Scholz M, Kim KS, Schilling M, et al. Interferon-beta stabilizes barrier characteristics of the blood-brain barrier in four different species in vitro. Mult Scler 2008; 14: 843-52.

Kruppa G, Thoma B, Machleidt T, Wiegmann K, Kronke M. Inhibition of tumor necrosis factor (TNF)-mediated NF-kappa B activation by selective blockade of the human 55-kDa TNF receptor. J Immunol 1992; 148: 3152-7.

Kuang E, Wan Q, Li X, Xu H, Liu Q, Qi Y. ER Ca2+ depletion triggers apoptotic signals for endoplasmic reticulum (ER) overload response induced by overexpressed reticulon 3 (RTN3/HAP). J Cell Physiol 2005; 204: 549-59.

Kuehn HS, Caminha I, Niemela JE, Rao VK, Davis J, Fleisher TA, et al. FAS haploinsufficiency is a common disease mechanism in the human autoimmune lymphoproliferative syndrome. J Immunol; 186: 6035-43.

Kyewski B, Klein L. A central role for central tolerance. Annu Rev Immunol 2006; 24: 571-606.

Lang HL, Jacobsen H, Ikemizu S, Andersson C, Harlos K, Madsen L, et al. A functional and structural basis for TCR cross-reactivity in multiple sclerosis. Nat Immunol 2002; 3: 940-3.

Lanzavecchia A. How can cryptic epitopes trigger autoimmunity? J Exp Med 1995; 181: 1945-8.

Lee AH, Iwakoshi NN, Glimcher LH. XBP-1 regulates a subset of endoplasmic reticulum resident chaperone genes in the unfolded protein response. Mol Cell Biol 2003; 23: 7448-59.

Lee BP, Imhof BA. Lymphocyte transmigration in the brain: a new way of thinking. Nat Immunol 2008; 9: 117-8.

Leray E, Yaouanq J, Le Page E, Coustans M, Laplaud D, Oger J, et al. Evidence for a two-stage disability progression in multiple sclerosis. Brain 2010; 133: 1900-13.

Levin LI, Munger KL, Rubertone MV, Peck CA, Lennette ET, Spiegelman D, et al. Multiple sclerosis and Epstein-Barr virus. JAMA 2003; 289: 1533-6.

Liu ZG, Hsu H, Goeddel DV, Karin M. Dissection of TNF receptor 1 effector functions: JNK activation is not linked to apoptosis while NF-kappaB activation prevents cell death. Cell 1996; 87: 565-76.

Lobito AA, Gabriel TL, Medema JP, Kimberley FC. Disease causing mutations in the TNF and TNFR superfamilies: Focus on molecular mechanisms driving disease. Trends Mol Med 2011; 17: 494-505.

Lobito AA, Kimberley FC, Muppidi JR, Komarow H, Jackson AJ, Hull KM, et al. Abnormal disulfide-linked oligomerization results in ER retention and altered signaling by TNFR1 mutants in TNFR1-associated periodic fever syndrome (TRAPS). Blood 2006; 108: 1320-7.

Locksley RM, Killeen N, Lenardo MJ. The TNF and TNF receptor superfamilies: integrating mammalian biology. Cell 2001; 104: 487-501.

Long JC, Caceres JF. The SR protein family of splicing factors: master regulators of gene expression. Biochem J 2009; 417: 15-27.

Lopez-Bigas N, Audit B, Ouzounis C, Parra G, Guigo R. Are splicing mutations the most frequent cause of hereditary disease? FEBS Lett 2005; 579: 1900-3.

Lopez-Diego RS, Weiner HL. Novel therapeutic strategies for multiple sclerosis--a multifaceted adversary. Nat Rev Drug Discov 2008; 7: 909-25.

Lublin FD, Reingold SC. Defining the clinical course of multiple sclerosis: results of an international survey. National Multiple Sclerosis Society (USA) Advisory Committee on Clinical Trials of New Agents in Multiple Sclerosis. Neurology 1996; 46: 907-11.

Lukong KE, Chang KW, Khandjian EW, Richard S. RNA-binding proteins in human genetic disease. Trends Genet 2008; 24: 416-25.

Lunemann JD, Tintore M, Messmer B, Strowig T, Rovira A, Perkal H, et al. Elevated Epstein-Barr virus-encoded nuclear antigen-1 immune responses predict conversion to multiple sclerosis. Ann Neurol 2010; 67: 159-69.

Luo X, Budihardjo I, Zou H, Slaughter C, Wang X. Bid, a Bcl2 interacting protein, mediates cytochrome c release from mitochondria in response to activation of cell surface death receptors. Cell 1998; 94: 481-90.

Ma Y, Brewer JW, Diehl JA, Hendershot LM. Two distinct stress signaling pathways converge upon the CHOP promoter during the mammalian unfolded protein response. J Mol Biol 2002; 318: 1351-65.

Maier LM, Lowe CE, Cooper J, Downes K, Anderson DE, Severson C, et al. IL2RA genetic heterogeneity in multiple sclerosis and type 1 diabetes susceptibility and soluble interleukin-2 receptor production. PLoS Genet 2009; 5: e1000322.

Majewski J, Ott J. Distribution and characterization of regulatory elements in the human genome. Genome Res 2002; 12: 1827-36.

Manki A, Nishikomori R, Nakata-Hizume M, Kunitomi T, Takei S, Urakami T, et al. Tumor necrosis factor receptor-associated periodic syndrome mimicking systemic juvenile idiopathic arthritis. Allergol Int 2006; 55: 337-41.

Marsters SA, Frutkin AD, Simpson NJ, Fendly BM, Ashkenazi A. Identification of cysteine-rich domains of the type 1 tumor necrosis factor receptor involved in ligand binding. J Biol Chem 1992; 267: 5747-50.

Martyn CN, Cruddas M, Compston DA. Symptomatic Epstein-Barr virus infection and multiple sclerosis. J Neurol Neurosurg Psychiatry 1993; 56: 167-8.
Matlin AJ, Clark F, Smith CW. Understanding alternative splicing: towards a cellular code. Nat Rev Mol Cell Biol 2005; 6: 386-98.
Matsusaka T, Fujikawa K, Nishio Y, Mukaida N, Matsushima K, Kishimoto T, et al. Transcription factors NF-IL6 and NF-kappa B synergistically activate transcription of the inflammatory cytokines, interleukin 6 and interleukin 8. Proc Natl Acad Sci U S A 1993; 90: 10193-7.
Mazzucchelli R, Durum SK. Interleukin-7 receptor expression: intelligent design. Nat Rev Immunol 2007; 7: 144-54.
McKay FC, Swain LI, Schibeci SD, Rubio JP, Kilpatrick TJ, Heard RN, et al. Haplotypes of the interleukin 7 receptor alpha gene are correlated with altered expression in whole blood cells in multiple sclerosis. Genes Immun 2008; 9: 1-6.
Mells GF, Floyd JA, Morley KI, Cordell HJ, Franklin CS, Shin SY, et al. Genome-wide association study identifies 12 new susceptibility loci for primary biliary cirrhosis. Nat Genet 2011; 43: 329-32.
Micheau O, Tschopp J. Induction of TNF receptor I-mediated apoptosis via two sequential signaling complexes. Cell 2003; 114: 181-90.
Mikulits W, Pradet-Balade B, Habermann B, Beug H, Garcia-Sanz JA, Mullner EW. Isolation of translationally controlled mRNAs by differential screening. FASEB J 2000; 14: 1641-52.
Milatovich A, Song K, Heller RA, Francke U. Tumor necrosis factor receptor genes, TNFR1 and TNFR2, on human chromosomes 12 and 1. Somat Cell Mol Genet 1991; 17: 519-23.
Mueller DL. Mechanisms maintaining peripheral tolerance. Nat Immunol 2010; 11: 21-7.
Murphy CA, Hoek RM, Wiekowski MT, Lira SA, Sedgwick JD. Interactions between hemopoietically derived TNF and central nervous system-resident glial chemokines underlie initiation of autoimmune inflammation in the brain. J Immunol 2002; 169: 7054-62.
Murphy KP, Travers P, Walport M, Ehrenstein M, Janeway CA. Janeway's immunobiology. New York ; London: Garland Science, 2008.
Napoli I, Neumann H. Protective effects of microglia in multiple sclerosis. Exp Neurol 2009; 225: 24-8.
Nave KA, Trapp BD. Axon-glial signaling and the glial support of axon function. Annu Rev Neurosci 2008; 31: 535-61.
Nesbitt A, Fossati G, Bergin M, Stephens P, Stephens S, Foulkes R, et al. Mechanism of action of certolizumab pegol (CDP870): in vitro comparison with other anti-tumor necrosis factor alpha agents. Inflamm Bowel Dis 2007; 13: 1323-32.
Neugebauer KM, Stolk JA, Roth MB. A conserved epitope on a subset of SR proteins defines a larger family of Pre-mRNA splicing factors. J Cell Biol 1995; 129: 899-908.
Nielsen FC, Ostergaard L, Nielsen J, Christiansen J. Growth-dependent translation of IGF-II mRNA by a rapamycin-sensitive pathway. Nature 1995; 377: 358-62.
Oksenberg JR, Baranzini SE. Multiple sclerosis genetics--is the glass half full, or half empty? Nat Rev Neurol 2010; 6: 429-37.
Oksenberg JR, Baranzini SE, Sawcer S, Hauser SL. The genetics of multiple sclerosis: SNPs to pathways to pathogenesis. Nat Rev Genet 2008; 9: 516-26.
Pagani F, Buratti E, Stuani C, Baralle FE. Missense, nonsense, and neutral mutations define juxtaposed regulatory elements of splicing in cystic fibrosis transmembrane regulator exon 9. J Biol Chem 2003; 278: 26580-8.
Pahl HL, Baeuerle PA. The ER-overload response: activation of NF-kappa B. Trends Biochem Sci 1997; 22: 63-7.
Patsopoulos NA, de Bakker PI, Esposito F, Reischl J, Lehr S, Bauer D, et al. Genome-wide meta-analysis identifies novel multiple sclerosis susceptibility loci. Ann Neurol 2011; 70: 897-912.
Pelletier D, Hafler DA. Fingolimod for multiple sclerosis. N Engl J Med 2012; 366: 339-47.

Perera D, Stankovich J, Butzkueven H, Taylor BV, Foote SJ, Kilpatrick TJ, et al. Fine mapping of multiple sclerosis susceptibility genes provides evidence of allelic heterogeneity at the IL2RA locus. J Neuroimmunol 2009; 211: 105-9.

Powell MB, Mitchell D, Lederman J, Buckmeier J, Zamvil SS, Graham M, et al. Lymphotoxin and tumor necrosis factor-alpha production by myelin basic protein-specific T cell clones correlates with encephalitogenicity. Int Immunol 1990; 2: 539-44.

Prinz JC. Autoimmune-like syndromes during TNF blockade: does infection have a role? Nat Rev Rheumatol 2011; 7: 429-34.

Probert L, Eugster HP, Akassoglou K, Bauer J, Frei K, Lassmann H, et al. TNFR1 signalling is critical for the development of demyelination and the limitation of T-cell responses during immune-mediated CNS disease. Brain 2000; 123 (Pt 10): 2005-19.

Ramagopalan SV, Dyment DA, Cader MZ, Morrison KM, Disanto G, Morahan JM, et al. Rare variants in the CYP27B1 gene are associated with multiple sclerosis. Ann Neurol 2011; 70: 881-6.

Ransohoff RM. Natalizumab for multiple sclerosis. N Engl J Med 2007; 356: 2622-9.

Rasola A, Geuna M. A flow cytometry assay simultaneously detects independent apoptotic parameters. Cytometry 2001; 45: 151-7.

Rebelo SL, Bainbridge SE, Amel-Kashipaz MR, Radford PM, Powell RJ, Todd I, et al. Modeling of tumor necrosis factor receptor superfamily 1A mutants associated with tumor necrosis factor receptor-associated periodic syndrome indicates misfolding consistent with abnormal function. Arthritis Rheum 2006; 54: 2674-87.

Reddy P, Slack JL, Davis R, Cerretti DP, Kozlosky CJ, Blanton RA, et al. Functional analysis of the domain structure of tumor necrosis factor-alpha converting enzyme. J Biol Chem 2000; 275: 14608-14.

Riccardi C, Nicoletti I. Analysis of apoptosis by propidium iodide staining and flow cytometry. Nat Protoc 2006; 1: 1458-61.

Rice GP, Hartung HP, Calabresi PA. Anti-alpha4 integrin therapy for multiple sclerosis: mechanisms and rationale. Neurology 2005; 64: 1336-42.

Rieckmann P, Albrecht M, Kitze B, Weber T, Tumani H, Broocks A, et al. Tumor necrosis factor-alpha messenger RNA expression in patients with relapsing-remitting multiple sclerosis is associated with disease activity. Ann Neurol 1995; 37: 82-8.

Roberts J, Palma E, Sazani P, Orum H, Cho M, Kole R. Efficient and persistent splice switching by systemically delivered LNA oligonucleotides in mice. Mol Ther 2006; 14: 471-5.

Rosati G. The prevalence of multiple sclerosis in the world: an update. Neurol Sci 2001; 22: 117-39.

Rothe J, Gehr G, Loetscher H, Lesslauer W. Tumor necrosis factor receptors--structure and function. Immunol Res 1992; 11: 81-90.

Rottger S, White J, Wandall HH, Olivo JC, Stark A, Bennett EP, et al. Localization of three human polypeptide GalNAc-transferases in HeLa cells suggests initiation of O-linked glycosylation throughout the Golgi apparatus. J Cell Sci 1998; 111 (Pt 1): 45-60.

Ruddle NH, Bergman CM, McGrath KM, Lingenheld EG, Grunnet ML, Padula SJ, et al. An antibody to lymphotoxin and tumor necrosis factor prevents transfer of experimental allergic encephalomyelitis. J Exp Med 1990; 172: 1193-200.

Samali A, Fitzgerald U, Deegan S, Gupta S. Methods for monitoring endoplasmic reticulum stress and the unfolded protein response. Int J Cell Biol 2010; 2010: 830307.

Sawcer S, Ban M, Maranian M, Yeo TW, Compston A, Kirby A, et al. A high-density screen for linkage in multiple sclerosis. Am J Hum Genet 2005; 77: 454-67.

Sawcer S, Hellenthal G, Pirinen M, Spencer CC, Patsopoulos NA, Moutsianas L, et al. Genetic risk and a primary role for cell-mediated immune mechanisms in multiple sclerosis. Nature 2011; 476: 214-9.

Scherubl C, Schneider-Brachert W, Schutze S, Hehlgans T, Mannel DN. Colocalization of endogenous TNF with a functional intracellular splice form of human TNF receptor type 2. J Inflamm (Lond) 2005; 2: 7.

Schmid-Schonbein GW. Analysis of inflammation. Annu Rev Biomed Eng 2006; 8: 93-131.

Schneider-Brachert W, Tchikov V, Neumeyer J, Jakob M, Winoto-Morbach S, Held-Feindt J, et al. Compartmentalization of TNF receptor 1 signaling: internalized TNF receptosomes as death signaling vesicles. Immunity 2004; 21: 415-28.

Schroder M, Kaufman RJ. The mammalian unfolded protein response. Annu Rev Biochem 2005; 74: 739-89.

Schuck P. Use of surface plasmon resonance to probe the equilibrium and dynamic aspects of interactions between biological macromolecules. Annu Rev Biophys Biomol Struct 1997; 26: 541-66.

Schutze S, Tchikov V, Schneider-Brachert W. Regulation of TNFR1 and CD95 signalling by receptor compartmentalization. Nat Rev Mol Cell Biol 2008; 9: 655-62.

Schwartz T, Blobel G. Structural basis for the function of the beta subunit of the eukaryotic signal recognition particle receptor. Cell 2003; 112: 793-803.

Sean Riminton D, Korner H, Strickland DH, Lemckert FA, Pollard JD, Sedgwick JD. Challenging cytokine redundancy: inflammatory cell movement and clinical course of experimental autoimmune encephalomyelitis are normal in lymphotoxin-deficient, but not tumor necrosis factor-deficient, mice. J Exp Med 1998; 187: 1517-28.

Selmaj K, Papierz W, Glabinski A, Kohno T. Prevention of chronic relapsing experimental autoimmune encephalomyelitis by soluble tumor necrosis factor receptor I. J Neuroimmunol 1995; 56: 135-41.

Selmaj K, Raine CS, Cross AH. Anti-tumor necrosis factor therapy abrogates autoimmune demyelination. Ann Neurol 1991; 30: 694-700.

Selmaj KW, Raine CS. Experimental autoimmune encephalomyelitis: immunotherapy with anti-tumor necrosis factor antibodies and soluble tumor necrosis factor receptors. Neurology 1995; 45: S44-9.

Serafini B, Rosicarelli B, Franciotta D, Magliozzi R, Reynolds R, Cinque P, et al. Dysregulated Epstein-Barr virus infection in the multiple sclerosis brain. J Exp Med 2007; 204: 2899-912.

Sharief MK, Hentges R. Association between tumor necrosis factor-alpha and disease progression in patients with multiple sclerosis. N Engl J Med 1991; 325: 467-72.

Shimomura Y, Sato N, Miyashita A, Hashimoto T, Ito M, Kuwano R. A rare case of hypohidrotic ectodermal dysplasia caused by compound heterozygous mutations in the EDAR gene. J Invest Dermatol 2004; 123: 649-55.

Shyu AB, Wilkinson MF, van Hoof A. Messenger RNA regulation: to translate or to degrade. EMBO J 2008; 27: 471-81.

Siebert S, Fielding CA, Williams BD, Brennan P. Mutation of the extracellular domain of tumour necrosis factor receptor 1 causes reduced NF-kappaB activation due to decreased surface expression. FEBS Lett 2005; 579: 5193-8.

Siegel RM, Frederiksen JK, Zacharias DA, Chan FK, Johnson M, Lynch D, et al. Fas preassociation required for apoptosis signaling and dominant inhibition by pathogenic mutations. Science 2000; 288: 2354-7.

Simon A, Park H, Maddipati R, Lobito AA, Bulua AC, Jackson AJ, et al. Concerted action of wild-type and mutant TNF receptors enhances inflammation in TNF receptor 1-associated periodic fever syndrome. Proc Natl Acad Sci U S A 2010; 107: 9801-6.

Skoko N, Baralle M, Buratti E, Baralle FE. The pathological splicing mutation c.6792C>G in NF1 exon 37 causes a change of tenancy between antagonistic splicing factors. FEBS Lett 2008; 582: 2231-6.

Stahl EA, Raychaudhuri S, Remmers EF, Xie G, Eyre S, Thomson BP, et al. Genome-wide association study meta-analysis identifies seven new rheumatoid arthritis risk loci. Nat Genet 2010; 42: 508-514.

Steinman L, Martin R, Bernard C, Conlon P, Oksenberg JR. Multiple sclerosis: deeper understanding of its pathogenesis reveals new targets for therapy. Annu Rev Neurosci 2002; 25: 491-505.

Storey H, Stewart A, Vandenabeele P, Luzio JP. The p55 tumour necrosis factor receptor TNFR1 contains a trans-Golgi network localization signal in the C-terminal region of its cytoplasmic tail. Biochem J 2002; 366: 15-22.

Strange A, Capon F, Spencer CCA, Knight J, Weale ME, Allen MH, et al. A genome-wide association study identifies new psoriasis susceptibility loci and an interaction between HLA-C and ERAP1. Nat Genet 2010; 42: 985-990.

Stryer L, Haugland RP. Energy transfer: a spectroscopic ruler. Proc Natl Acad Sci U S A 1967; 58: 719-26.

Suvannavejh GC, Lee HO, Padilla J, Dal Canto MC, Barrett TA, Miller SD. Divergent roles for p55 and p75 tumor necrosis factor receptors in the pathogenesis of MOG(35-55)-induced experimental autoimmune encephalomyelitis. Cell Immunol 2000; 205: 24-33.

Suzuki MG, Imanishi S, Dohmae N, Asanuma M, Matsumoto S. Identification of a male-specific RNA binding protein that regulates sex-specific splicing of Bmdsx by increasing RNA binding activity of BmPSI. Mol Cell Biol 2010; 30: 5776-86.

Swayze EE, Siwkowski AM, Wancewicz EV, Migawa MT, Wyrzykiewicz TK, Hung G, et al. Antisense oligonucleotides containing locked nucleic acid improve potency but cause significant hepatotoxicity in animals. Nucleic Acids Res 2007; 35: 687-700.

Tacke R, Chen Y, Manley JL. Sequence-specific RNA binding by an SR protein requires RS domain phosphorylation: creation of an SRp40-specific splicing enhancer. Proc Natl Acad Sci U S A 1997; 94: 1148-53.

Takada H, Chen NJ, Mirtsos C, Suzuki S, Suzuki N, Wakeham A, et al. Role of SODD in regulation of tumor necrosis factor responses. Mol Cell Biol 2003; 23: 4026-33.

Takahashi K, Aranami T, Endoh M, Miyake S, Yamamura T. The regulatory role of natural killer cells in multiple sclerosis. Brain 2004; 127: 1917-27.

Takasaki W, Kajino Y, Kajino K, Murali R, Greene MI. Structure-based design and characterization of exocyclic peptidomimetics that inhibit TNF alpha binding to its receptor. Nat Biotechnol 1997; 15: 1266-70.

Taoufik E, Tseveleki V, Chu SY, Tselios T, Karin M, Lassmann H, et al. Transmembrane tumour necrosis factor is neuroprotective and regulates experimental autoimmune encephalomyelitis via neuronal nuclear factor-{kappa}B. Brain 2011; 134: 2722-35.

Tartaglia LA, Ayres TM, Wong GH, Goeddel DV. A novel domain within the 55 kd TNF receptor signals cell death. Cell 1993; 74: 845-53.

The Lenercept Multiple Sclerosis Study Group. TNF neutralization in MS: results of a randomized, placebo-controlled multicenter study. The Lenercept Multiple Sclerosis Study Group and The University of British Columbia MS/MRI Analysis Group. Neurology 1999; 53: 457-65.

Todd DJ, Lee AH, Glimcher LH. The endoplasmic reticulum stress response in immunity and autoimmunity. Nat Rev Immunol 2008; 8: 663-74.

Todd I, Radford PM, Daffa N, Bainbridge SE, Powell RJ, Tighe PJ. Mutant tumor necrosis factor receptor associated with tumor necrosis factor receptor-associated periodic syndrome is altered antigenically and is retained within patients' leukocytes. Arthritis Rheum 2007; 56: 2765-73.

Todd I, Radford PM, Draper-Morgan KA, McIntosh R, Bainbridge S, Dickinson P, et al. Mutant forms of tumour necrosis factor receptor I that occur in TNF-receptor-associated periodic syndrome retain signalling functions but show abnormal behaviour. Immunology 2004; 113: 65-79.

Tracey D, Klareskog L, Sasso EH, Salfeld JG, Tak PP. Tumor necrosis factor antagonist mechanisms of action: a comprehensive review. Pharmacol Ther 2008; 117: 244-79.
Trapp BD, Nave KA. Multiple sclerosis: an immune or neurodegenerative disorder? Annu Rev Neurosci 2008; 31: 247-69.
Turner MD, Chaudhry A, Nedjai B. Tumour necrosis factor receptor trafficking dysfunction opens the TRAPS door to pro-inflammatory cytokine secretion. Biosci Rep 2012; 32: 105-12.
Tzartos JS, Friese MA, Craner MJ, Palace J, Newcombe J, Esiri MM, et al. Interleukin-17 production in central nervous system-infiltrating T cells and glial cells is associated with active disease in multiple sclerosis. Am J Pathol 2008; 172: 146-55.
Ueda H, Howson JM, Esposito L, Heward J, Snook H, Chamberlain G, et al. Association of the T-cell regulatory gene CTLA4 with susceptibility to autoimmune disease. Nature 2003; 423: 506-11.
Vaknin-Dembinsky A, Balashov K, Weiner HL. IL-23 is increased in dendritic cells in multiple sclerosis and down-regulation of IL-23 by antisense oligos increases dendritic cell IL-10 production. J Immunol 2006; 176: 7768-74.
van Deutekom JC, Janson AA, Ginjaar IB, Frankhuizen WS, Aartsma-Rus A, Bremmer-Bout M, et al. Local dystrophin restoration with antisense oligonucleotide PRO051. N Engl J Med 2007; 357: 2677-86.
van Horssen R, Rens JA, Schipper D, Eggermont AM, ten Hagen TL. EMAP-II facilitates TNF-R1 apoptotic signalling in endothelial cells and induces TRADD mobilization. Apoptosis 2006; 11: 2137-45.
van Oosten BW, Barkhof F, Truyen L, Boringa JB, Bertelsmann FW, von Blomberg BM, et al. Increased MRI activity and immune activation in two multiple sclerosis patients treated with the monoclonal anti-tumor necrosis factor antibody cA2. Neurology 1996; 47: 1531-4.
Vandenabeele P, Declercq W, Beyaert R, Fiers W. Two tumour necrosis factor receptors: structure and function. Trends Cell Biol 1995; 5: 392-9.
Vandenbroucke, II, Vandesompele J, Paepe AD, Messiaen L. Quantification of splice variants using real-time PCR. Nucleic Acids Res 2001; 29: E68-8.
Vanderlugt CL, Miller SD. Epitope spreading in immune-mediated diseases: implications for immunotherapy. Nat Rev Immunol 2002; 2: 85-95.
Veatch W, Stryer L. The dimeric nature of the gramicidin A transmembrane channel: conductance and fluorescence energy transfer studies of hybrid channels. J Mol Biol 1977; 113: 89-102.
Vembar SS, Brodsky JL. One step at a time: endoplasmic reticulum-associated degradation. Nat Rev Mol Cell Biol 2008; 9: 944-57.
Vieira PL, Heystek HC, Wormmeester J, Wierenga EA, Kapsenberg ML. Glatiramer acetate (copolymer-1, copaxone) promotes Th2 cell development and increased IL-10 production through modulation of dendritic cells. J Immunol 2003; 170: 4483-8.
Viglietta V, Baecher-Allan C, Weiner HL, Hafler DA. Loss of functional suppression by CD4+CD25+ regulatory T cells in patients with multiple sclerosis. J Exp Med 2004; 199: 971-9.
Voelker RB, Berglund JA. A comprehensive computational characterization of conserved mammalian intronic sequences reveals conserved motifs associated with constitutive and alternative splicing. Genome Res 2007; 17: 1023-33.
von Budingen HC, Bar-Or A, Zamvil SS. B cells in multiple sclerosis: connecting the dots. Curr Opin Immunol 2011; 23: 713-20.
Wallach D, Engelmann H, Nophar Y, Aderka D, Kemper O, Hornik V, et al. Soluble and cell surface receptors for tumor necrosis factor. Agents Actions Suppl 1991; 35: 51-7.
Wallach D, Varfolomeev EE, Malinin NL, Goltsev YV, Kovalenko AV, Boldin MP. Tumor necrosis factor receptor and Fas signaling mechanisms. Annu Rev Immunol 1999; 17: 331-67.
Wan YY. Multi-tasking of helper T cells. Immunology 2010; 130: 166-71.
Wang CY, Mayo MW, Baldwin AS, Jr. TNF- and cancer therapy-induced apoptosis: potentiation by inhibition of NF-kappaB. Science 1996; 274: 784-7.

Wang GS, Cooper TA. Splicing in disease: disruption of the splicing code and the decoding machinery. Nat Rev Genet 2007; 8: 749-61.

Wang J, Al-Lamki RS, Zhang H, Kirkiles-Smith N, Gaeta ML, Thiru S, et al. Histamine antagonizes tumor necrosis factor (TNF) signaling by stimulating TNF receptor shedding from the cell surface and Golgi storage pool. J Biol Chem 2003; 278: 21751-60.

Wang L, Yang JK, Kabaleeswaran V, Rice AJ, Cruz AC, Park AY, et al. The Fas-FADD death domain complex structure reveals the basis of DISC assembly and disease mutations. Nat Struct Mol Biol 2010; 17: 1324-9.

Watanuki T, Funato H, Uchida S, Matsubara T, Kobayashi A, Wakabayashi Y, et al. Increased expression of splicing factor SRp20 mRNA in bipolar disorder patients. J Affect Disord 2008; 110: 62-9.

Weber MS, Prod'homme T, Patarroyo JC, Molnarfi N, Karnezis T, Lehmann-Horn K, et al. B-cell activation influences T-cell polarization and outcome of anti-CD20 B-cell depletion in central nervous system autoimmunity. Ann Neurol 2010; 68: 369-83.

Wengel J, Petersen M, Nielsen KE, Jensen GA, Hakansson AE, Kumar R, et al. LNA (locked nucleic acid) and the diastereoisomeric alpha-L-LNA: conformational tuning and high-affinity recognition of DNA/RNA targets. Nucleosides Nucleotides Nucleic Acids 2001; 20: 389-96.

Wertz IE, Dixit VM. Regulation of death receptor signaling by the ubiquitin system. Cell Death Differ 2010; 17: 14-24.

Willer CJ, Dyment DA, Risch NJ, Sadovnick AD, Ebers GC. Twin concordance and sibling recurrence rates in multiple sclerosis. Proc Natl Acad Sci U S A 2003; 100: 12877-82.

Wolber PK, Hudson BS. An analytic solution to the Forster energy transfer problem in two dimensions. Biophys J 1979; 28: 197-210.

Wong GT. Speed congenics: applications for transgenic and knock-out mouse strains. Neuropeptides 2002; 36: 230-6.

Wood MJ, Gait MJ, Yin H. RNA-targeted splice-correction therapy for neuromuscular disease. Brain 2010; 133: 957-72.

Worth A, Thrasher AJ, Gaspar HB. Autoimmune lymphoproliferative syndrome: molecular basis of disease and clinical phenotype. Br J Haematol 2006; 133: 124-40.

Xu Y, Piston DW, Johnson CH. A bioluminescence resonance energy transfer (BRET) system: application to interacting circadian clock proteins. Proc Natl Acad Sci U S A 1999; 96: 151-6.

Yan XB, Tang CH, Huang Y, Fang H, Yu ZQ, Wu LM, et al. Alternative splicing in exon 9 of glucocorticoid receptor pre-mRNA is regulated by SRp40. Mol Biol Rep 2010; 37: 1427-33.

Yang Q, Kim YS, Lin Y, Lewis J, Neckers L, Liu ZG. Tumour necrosis factor receptor 1 mediates endoplasmic reticulum stress-induced activation of the MAP kinase JNK. EMBO Rep 2006; 7: 622-7.

Yoshida H, Matsui T, Yamamoto A, Okada T, Mori K. XBP1 mRNA is induced by ATF6 and spliced by IRE1 in response to ER stress to produce a highly active transcription factor. Cell 2001; 107: 881-91.

Zhang J, Hawari FI, Shamburek RD, Adamik B, Kaler M, Islam A, et al. Circulating TNFR1 exosome-like vesicles partition with the LDL fraction of human plasma. Biochem Biophys Res Commun 2008; 366: 579-84.

Zimmer J, Andres E, Hentges F. NK cells and Treg cells: a fascinating dance cheek to cheek. Eur J Immunol 2008; 38: 2942-5.

Zoledziewska M, Costa G, Pitzalis M, Cocco E, Melis C, Moi L, et al. Variation within the CLEC16A gene shows consistent disease association with both multiple sclerosis and type 1 diabetes in Sardinia. Genes Immun 2009; 10: 15-7.

Zozulya AL, Wiendl H. The role of regulatory T cells in multiple sclerosis. Nat Clin Pract Neurol 2008; 4: 384-98.

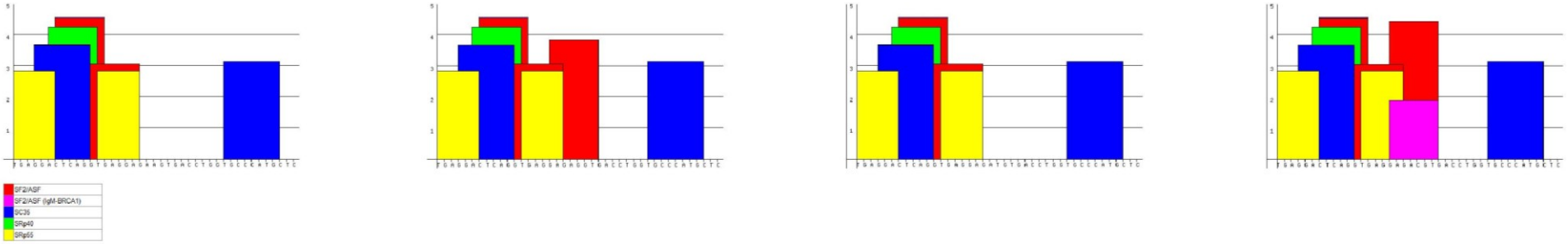
8.0 Supplementary figures

A G T C

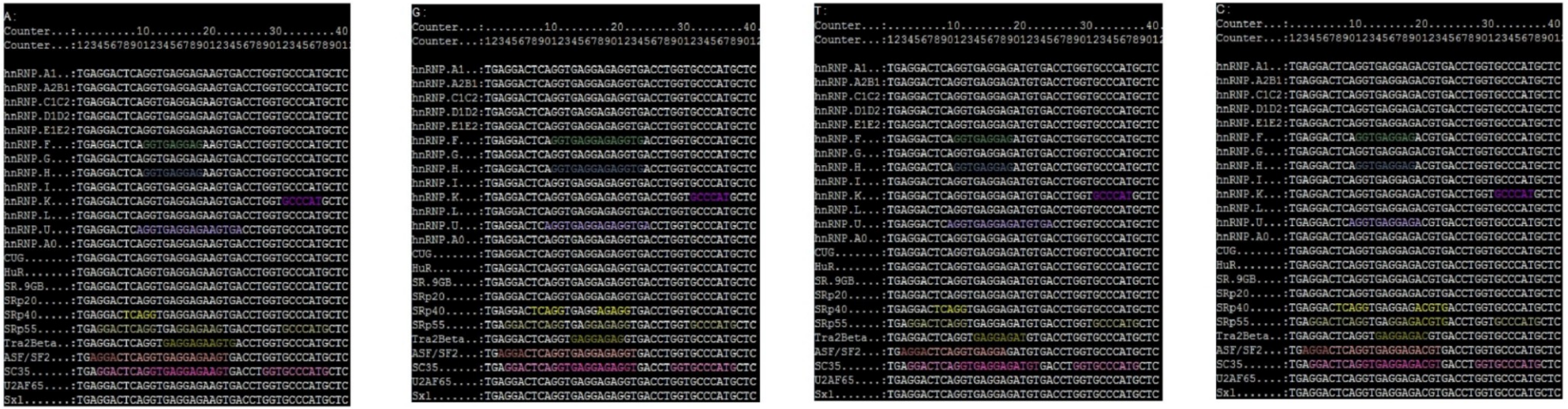
a



b



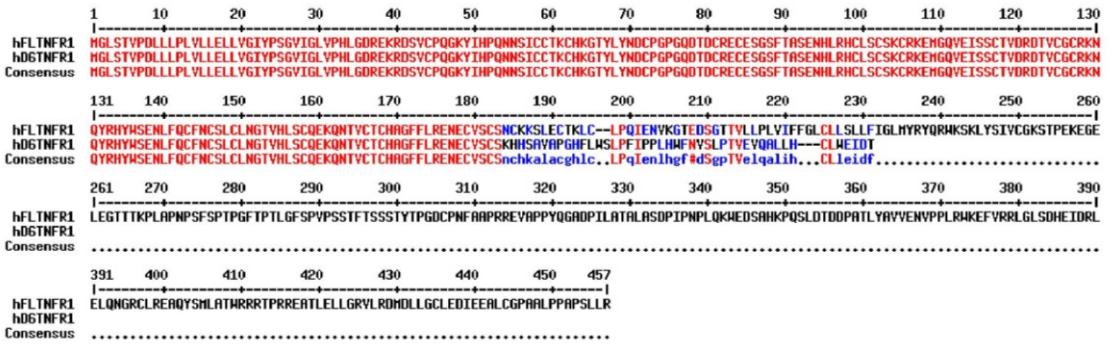
C



Supplementary Figure 1: *In silico* prediction of SR protein binding. Predicted binding sites in 41 nucleotide genomic DNA sequences, with rs1800693 A, G, T and C alleles in the middle position. Output from **(a)** SROOGLE **(b)** ESEfinder and **(c)** Splice Rainbow prediction programmes.

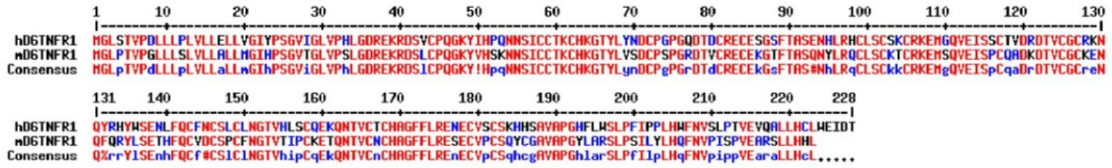
a

human FLTNFR1 vs. human Δ6TNFR1

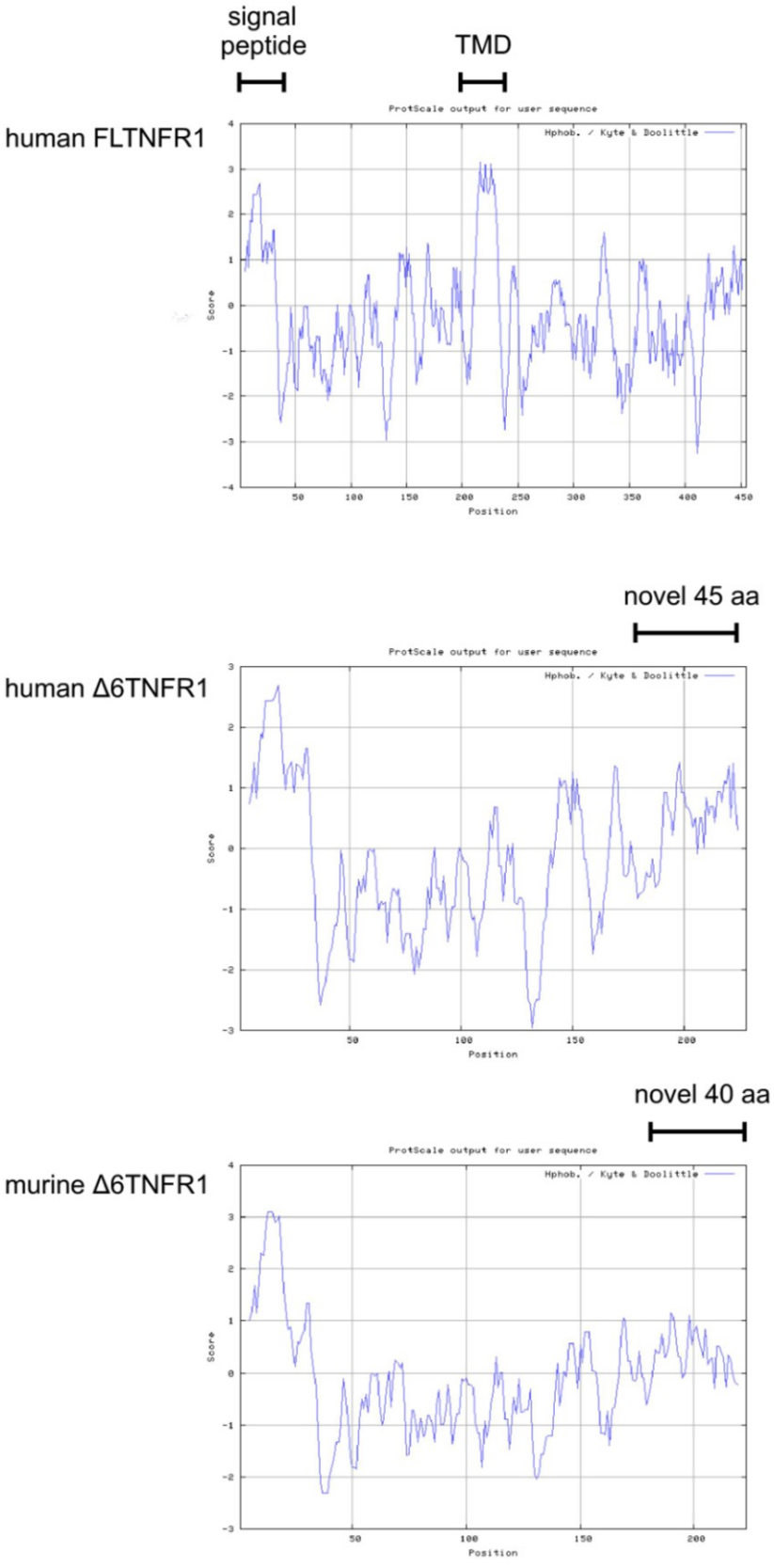


b

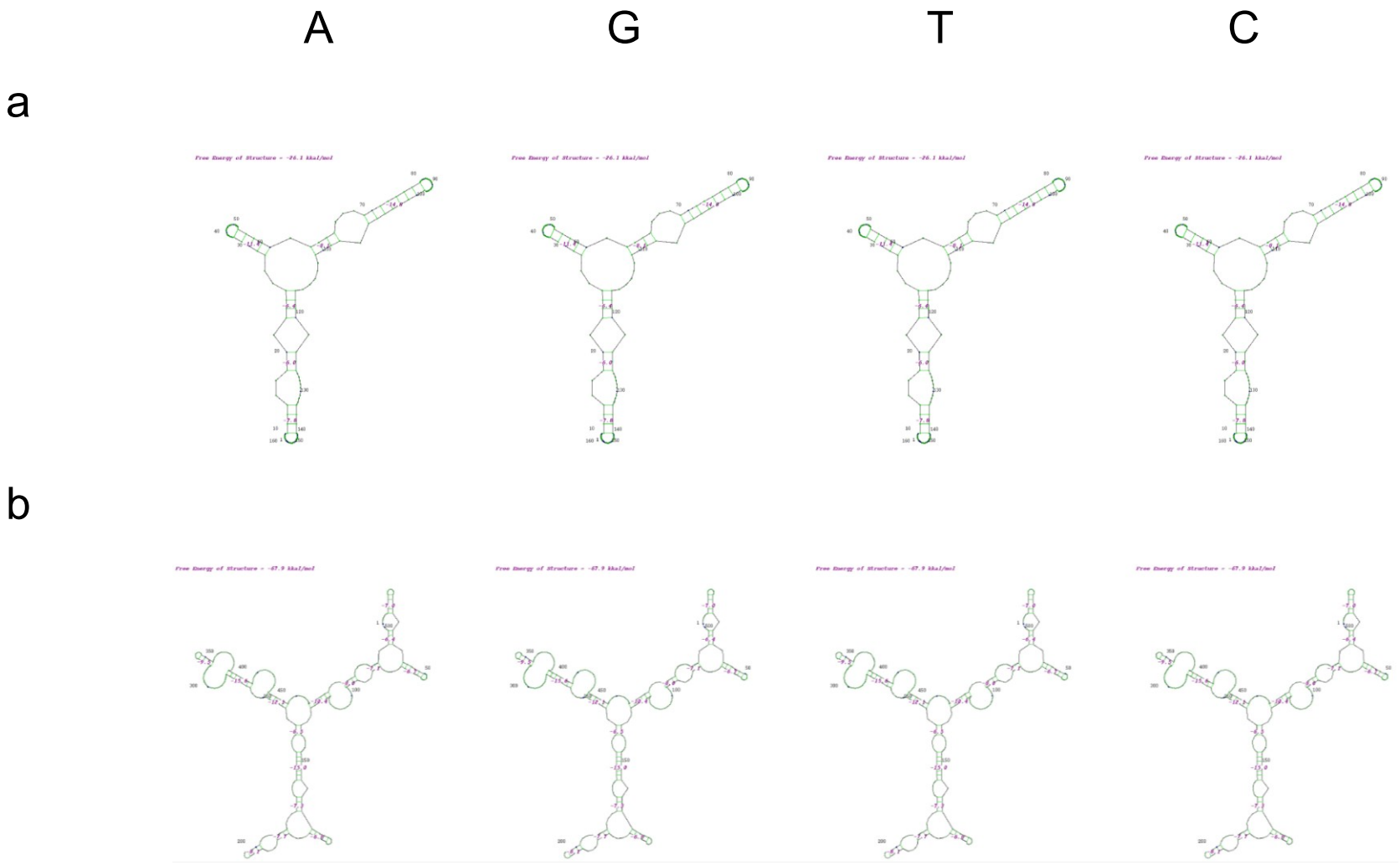
human Δ6TNFR1 vs. murine Δ6TNFR1



C


signal peptide
TMD
human FLTNFR1
ProtScale output for user sequence
Hphob. / Kyte & Doolittle
Score
Position
novel 45 aa
human Δ6TNFR1
ProtScale output for user sequence
Hphob. / Kyte & Doolittle
Score
Position
novel 40 aa
murine Δ6TNFR1
ProtScale output for user sequence
Hphob. / Kyte & Doolittle
Score
Position

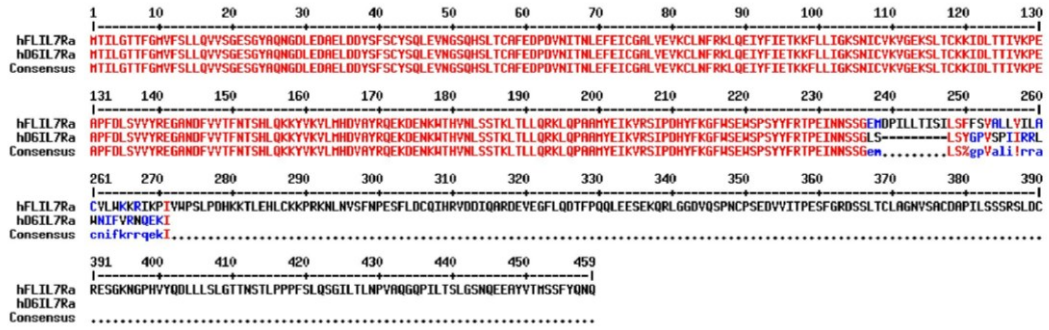
Supplementary Figure 2: Alignment of human and mouse TNFR1 isoform amino acid sequences, and *in silico* analysis of hydrophobicity. **(a)** Alignment of human FLTNFR1 with Δ6TNFR1. **(b)** Alignment of human Δ6TNFR1 with murine Δ6TNFR1. **(c)** Hydrophobicity plots of human FLTNFR1, Δ6TNFR1 and murine Δ6TNFR1. TMD = transmembrane domain.



Supplementary figure 3: Pfold prediction of RNA secondary structures based on rs1800693 allele. **(a)** 80 bases either side of the SNP. **(b)** 250 bases either side of the SNP.

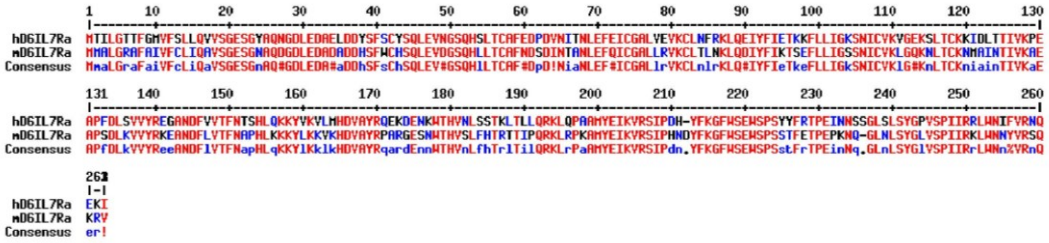
a

human FLIL7Rα vs. human Δ6IL7Rα

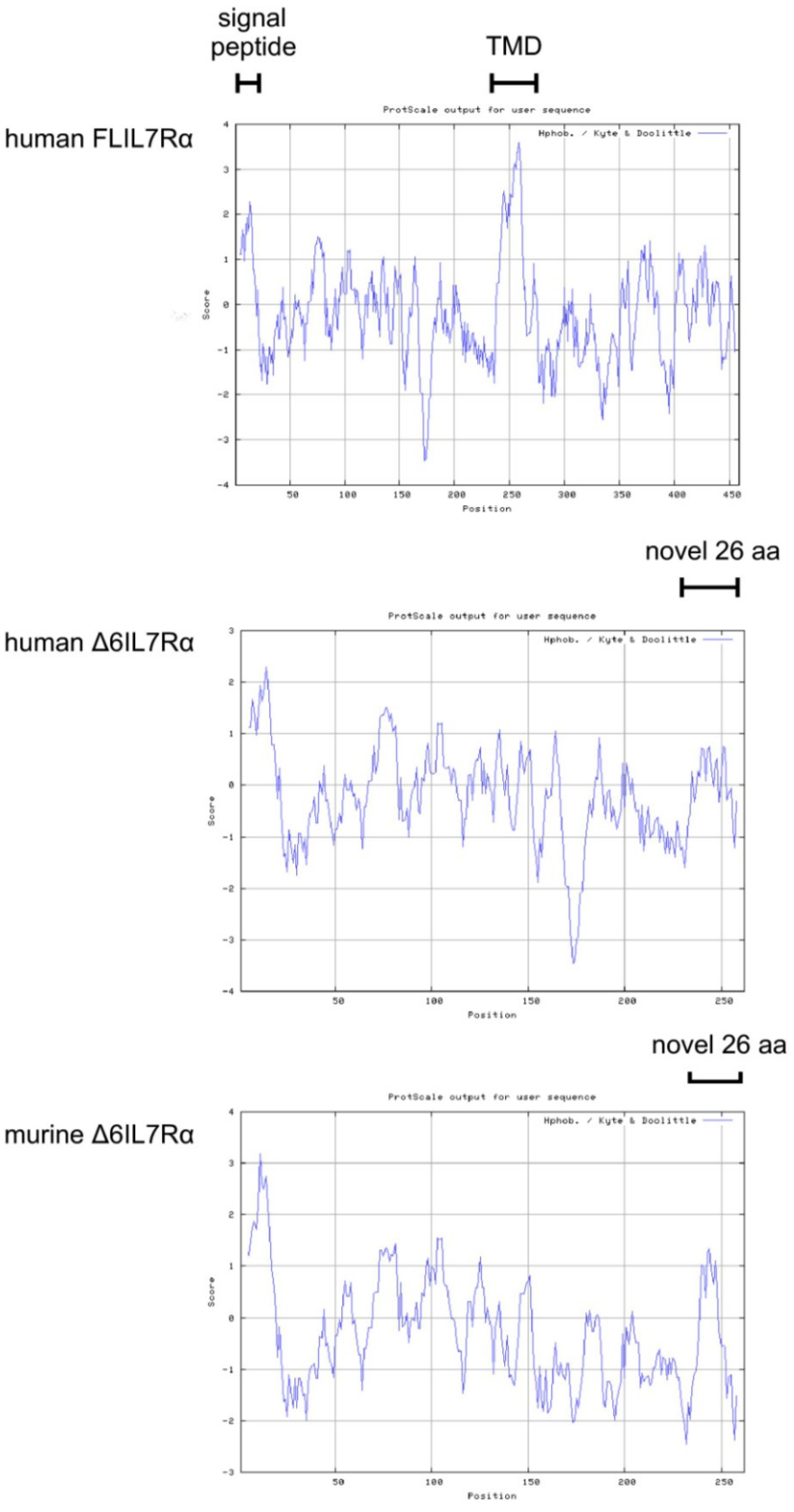


b

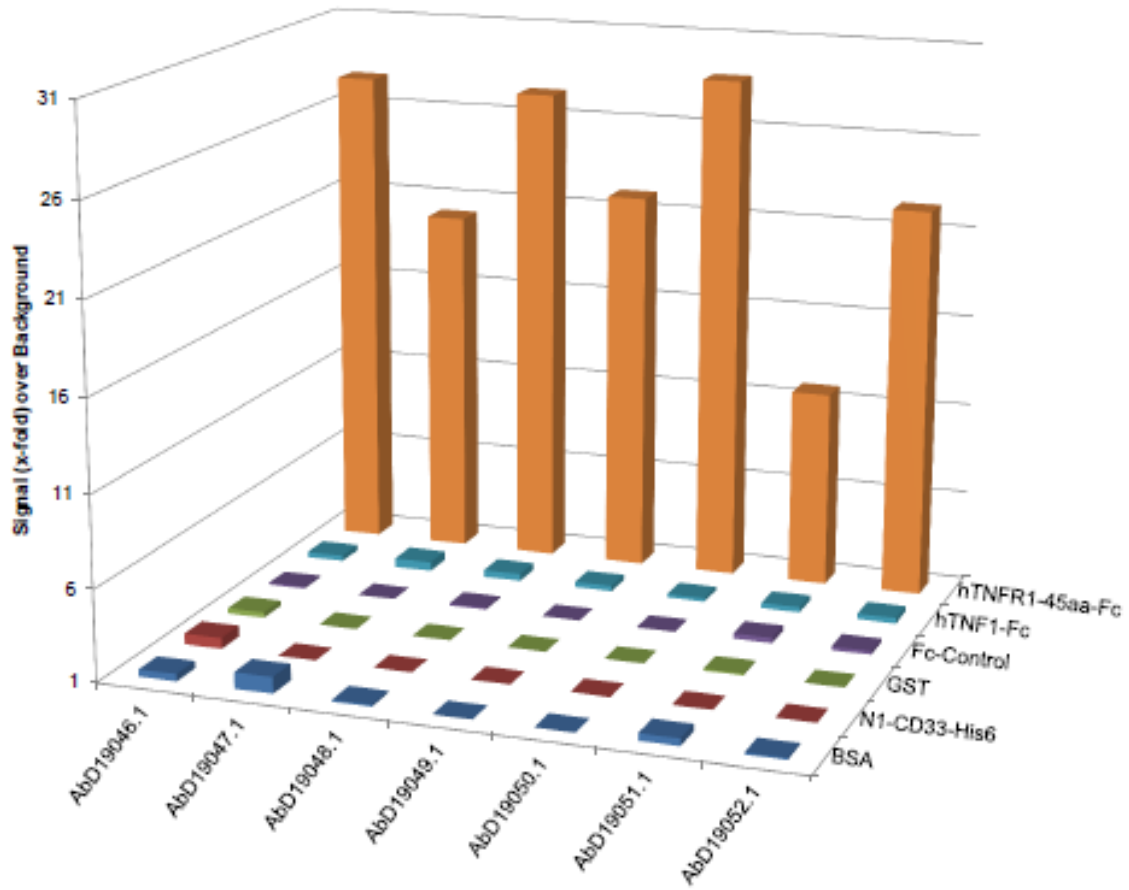
human Δ6IL7Rα vs. murine Δ6IL7Rα



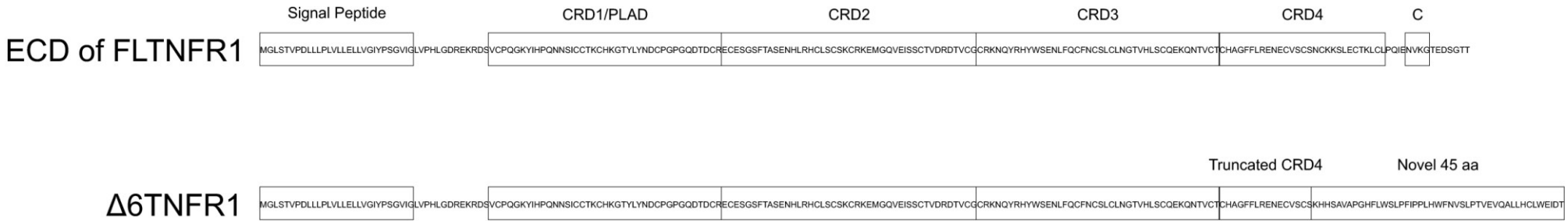
C


signal peptide
TMD
human FLIL7Rα
ProtScale output for user sequence
Hphob. / Kyte & Doolittle
Score
Position
novel 26 aa
human Δ6IL7Rα
ProtScale output for user sequence
Hphob. / Kyte & Doolittle
Score
Position
novel 26 aa
murine Δ6IL7Rα
ProtScale output for user sequence
Hphob. / Kyte & Doolittle
Score
Position

Supplementary Figure 4: Alignment of human and mouse IL7Rα isoform amino acid sequences, and *in silico* analysis of hydrophobicity. **(a)** Alignment of human FLIL7Rα with Δ6IL7Rα. **(b)** Alignment of human Δ6IL7Rα with murine Δ6IL7Rα. **(c)** Hydrophobicity plots of human FLIL7Rα, Δ6IL7Rα and murine Δ6IL7Rα. TMD = transmembrane domain.



Supplementary figure 5: ELISA performed by AbD Serotec to verify the specificity of anti-Δ6TNFR1 monoclonal antibodies (x-axis).Test substrates (z-axis) were coated on the plate. Clone AbD19050.1 showed the best binding and specificity to Δ6TNFR1 (hTNFR1-45aa-Fc), with no cross-reactivity to sTNFR1-Fc (hTNF1-Fc).



Supplementary figure 6: Schematic of Δ6TNFR1 and the extracellular domain of TNFR1. CRD = cysteine-rich domain; PLAD = Pre-Ligand Assembly Domain; C = Metalloprotease cleavage domain.